Since January 2020 Elsevier has created a COVID-19 resource centre with free information in English and Mandarin on the novel coronavirus COVID-19. The COVID-19 resource centre is hosted on Elsevier Connect, the company's public news and information website.

Journal of Infection 85 (2022) 702–769

Contents lists available at ScienceDirect

Journal of Infection

journal homepage: www.elsevier.com/locate/jinf

Letters to the Editor

Highly Pathogenic Avian Influenza outbreaks amongst bird populations in Europe - a view from China

Dear Editor,

A recent letter in this journal described an avian influenza virus of wild bird origin that is well adapted to a mammalian host, posing a potential threat to animal and human health.[1] This is reminiscent of the recent warnings about highly pathogenic avian influenza (HPAI) in Europe. HPAI, caused by highly pathogenic avian influenza virus (HPAIV), is a zoonotic disease that seriously endangers the poultry industry, human life, and public health. In October 2022, the European centre for Disease Prevention and Control (ECDC) issued an alert stating that the 2021–2022 HPAI epidemic season in Europe was the largest ever. The latest data (as of September 9, 2022) showed 3573 HPAI cases in wild birds and 2467 outbreaks in poultry, with 48 million birds culled.[2] The geographical extent of the outbreak was unprecedented, affecting 37 European countries from the Svalbard islands to southern Portugal and eastern Portugal to Ukraine.[3]

HPAI data from Europe (Fig. 1) showed both explosive growth and significant change in the epidemic strain over the past 3 years (Table 1). In 2018, the main epidemic strain was H5N6, whereas in 2019–2020, H5N8 was more prevalent. In 2021, the dominant strain changed again, and between September 2021 and September 2022, most cases were H5N1 (96.78%, 5311/5489). New strains of HPAIV constantly emerge through mutation, insertion, or recombination of the HA and NA genes.[4]

Long-distance migration of birds can spread HPAI. A study of the H5N8 HPAI outbreaks in Europe and Japan in 2015 showed that both originated from a single source population.[5] Bird migration also accelerates viral recombination. Although HPAIV is generally of low pathogenicity in wild birds, cross-species transmission to domestic poultry can be fatal. Dufour et al.[6] reported that an Asian passerine bird had completed an unusual route from Central Asia through Eurasia, which was related to the improved ecological suitability of southwestern Europe in winter. When transmission in wild birds increases, the risk of transmission from wild birds to domestic poultry also increases. The number of cases caused by wild birds in 2021 was four times higher than that in 2020 (2086 versus 513), which might be related to increased transmission among wild birds. Since some HPAIVs can infect humans, virus transmission in wild birds poses a public health threat.

Epidemiological data from the past 2 years show that although HPAI can occur year around, there is an obvious epidemic season in Europe, with relatively high levels in February–May and October–December, which might be climate related. Elsobky et al.[7] found that during the cold season, an increase in minimum temperature stimulated viral activity and increased the risk of disease, especially in the first quarter of the year (January, February, and March). Temperatures in the Northern Hemisphere were abnormally high this year, and as the global temperature warms, the minimum temperature increases, which may increase the risk of HPAI epidemics in Europe. Rising temperatures, increasing rainfall,

Table 1
HPAI outbreaks in Europe, 2018–2022. The table shows data for HPAI outbreaks reported by ECDC in the past 5 years. Domestic birds include poultry and captive birds. The main strain refers to the most prevalent HPAI strain reported during that period. (https://www.ecdc.europa.eu/en/publications-data/surveillance report avian influenza overview).

Number of HPAI infected birds				
Time period	Domestic	Wild	Total	Main strain (Number)
2017.11.16–2018.02.15	8	22	30	H5N6 (25)
2018.02.16–2018.05.15	16	55	71	H5N6 (59)
2018.05.16–2018.08.15	3	3	6	H5N6 (3) / H5N8 (3)
2018.08.16–2018.11.15	15	6	21	H5N8 (14)
2018.11.16–2019.02.15	2	2	4	H5N6 (2) / H5N8 (2)
2019.02.16–2019.08.15	5	0	5	H5N8 (5)
2019.08.16–2019.11.15	0	0	0	–
2019.11.16–2020.02.15	35	2	37	H5N8 (37)
2020.02.16–2020.05.15	289	1	290	H5N8 (287)
2020.05.16–2020.08.15	7	0	7	H5N8 (7)
2020.08.16–2020.12.07	51	510	561	H5N8 (510)
2020.12.08–2021.02.23	601	421	1022	H5N8 (917)
2021.02.24–2021.05.14	621	1051	1672	H5N8 (1492)
2021.05.15–2021.09.15	71	91	162	H5N8 (104)
2021.09.16–2021.12.08	344	523	867	H5N1 (811)
2021.12.09–2022.03.15	1263	1489	2652	H5N1 (2605)
2022.03.16–2022.06.10	772	410	1182	H5N1 (1130)
2022.06.11–2022.09.09	78	710	788	H5N1 (765)

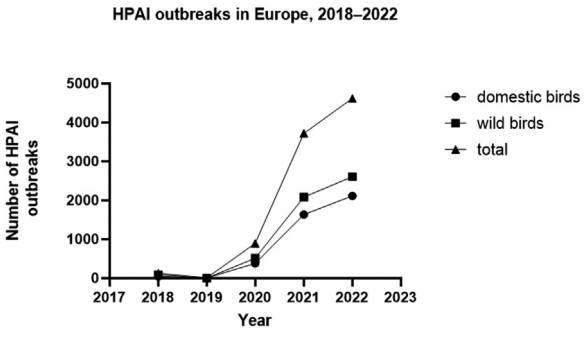

Fig. 1. HPAI outbreaks in Europe, 2018–2022. According to ECDC data on HPAI outbreaks in the past 5 years. The 2018 data include HPAI outbreaks reported from November 16, 2017 to November 15, 2018; 2019 data include outbreaks from November 16, 2018 to November 15, 2019; 2020 data include outbreaks from November 16, 2019 to December 27, 2020; 2021 data include outbreaks from December 8, 2020 to December 8, 2021; and 2022 data include outbreaks from December 9, 2021 to September 9, 2022.

https://doi.org/10.1016/j.jinf.2022.10.039

and summer droughts are likely to change the range and speed of pathogen spread, threatening humans, animals, and environmental ecosystems.[8] The HPAI epidemic in Europe might peak a second time, from October to December; therefore, more attention should be paid to epidemic prevention and control.

This year, the HPAI outbreaks in Europe were more serious, with more cases among wild birds. Europe's HPAI warning has alerted the rest of the world. As China has both the largest population and a large poultry industry with a high incidence of HPAI, greater HPAI prevention and control are required. In July 2022, the China Center for Animal Disease Control and Prevention reported the first HPAI cases of the year: an outbreak of H5N1 HPAI involving 273 wild birds. The punctate nature of the outbreak showed that they can be prevented and controlled.[9] In recent years, the rate of HPAI outbreaks in China has decreased significantly, which is closely related to their epidemic prevention and control measures. To control HPAIV, compulsory immunization and emergency culling measures are used, along with dynamic epidemic surveillance and timely vaccine updating. The mandatory HPAI immunization in China is regularly revised based on current strains; in the latest epidemic, a trivalent inactivated recombinant HPAIV vaccine (H5N6 H5-Re13 + H5N8 H5-Re14 + H7N9 H7-Re4) was used.[10] Strict biosecurity is another primary feature of HPAI prevention and control. In view of global warming and more extreme weather, it is even more important to regularly monitor wild birds carrying viruses. Based on the concept of "One Health," zoonotic diseases like HPAI should be paid attention to not only in Europe but worldwide.

Declaration of Competing Interest

None.

Acknowledgments

This work was supported by the Science and Technology Program of Guangdong Province (No. 2021B1212030015), Guangdong Provincial Special Fund for Modern Agriculture Industry Technology Innovation Teams (No. 2022KJ119), and the Special Project on Strategy for Rejuvenation of Guangdong Provincial Villages in 2022 (No. 5500-F22039).

References

1. Li Y., Li P., Xi J., et al. Wild bird-origin H_3N_8 avian influenza virus exhibit well adaptation in mammalian host. *J Infect* 2022;**84**(4):579–613.
2. European Centre for Disease Prevention and Control. 2021– 2022 data show largest avian flu epidemic in Europe ever.available at: https://www.ecdc.europa.eu/en/news-events/2021-2022.data show largest avian flu epidemic europe ever (accessed 3 October 2022).
3. European Centre for Disease Prevention and Control, 2022:avian influenza overview. Available at: https://www.ecdc.europa.eu/en/publications-data/surveillance.report.avian.influenza.overview (accessed 30 September 2022).
4. Lee D, Criado MF, Swayne DE. Pathobiological Origins and Evolutionary History of Highly Pathogenic Avian Influenza Viruses. *Csh Perspect Med* 2021;**11**(2).
5. Dalby A.R., Iqbal M.. The European and Japanese outbreaks of H5N8 derive from a single source population providing evidence for the dispersal along the long distance bird migratory flyways. *PeerJ* 2015;**3**:e934.
6. Dufour P., de Franceschi C., Doniol-Valcroze P., et al. A new westward migration route in an Asian passerine bird. *Curr Biol* 2021;**31**(24):5590–6.
7. Elsobky Y., El Afandi G., Abdalla E., et al. Possible ramifications of climate variability on HPAI-H5N1 outbreak occurrence: case study from the Menoufia, Egypt. *PloS One* 2020;**15**(10):e240442.
8. El-Sayed A., Kamel M.. Climatic changes and their role in emergence and re-emergence of diseases. *Environ Sci Pollut Res Int* 2020;**27**(18):22336–52.
9. Ministry of Agriculture and Rural Affairs of the People's Republic of China.,2022: H5N1HPAI was reported in wild birds in Gangcha and Gonghe counties of Qinghai Province. Available at: http://www.xmsyj.moa.gov.cn (accessed 22 July 2022).
10. China Institute of Veterinary Drug Control:recombinant avian influenza virus (H5+H7) trivalent inactivated vaccine (H5N6 H5 Re13 strains +H5N8 H5 Re14 strains +H7N9 H7 Re4 strains) and other veterinary drug products, 2022. Available at: http://www.cvda.org.cn/a/zhengjingban/zhengcefagui/jishuyaoqiuhebiaozhung/2022/0117/23592 (accessed 17 January 2022).

Yichun Chen[1], Lei Fan[1], Wenxuan Deng, Qiuyan Lin, Libin Chen*, Tao Ren*
College of Veterinary Medicine, South China Agricultural University, Guangzhou 510642, China
National and Regional Joint Engineering Laboratory for Medicament of Zoonosis Prevention and Control, Guangzhou, China
Key Laboratory of Animal Vaccine Development, Ministry of Agriculture, Guangzhou, China
Key Laboratory of Zoonosis Prevention and Control of Guangdong Province, Guangzhou, China

*Corresponding authors at: College of Veterinary Medicine, South China Agricultural University, 483 Wushan Road, Guangdong 510642, China.
E-mail addresses: chenlibin@scau.edu.cn (L. Chen), rentao6868@126.com (T. Ren)

[1] †These authors contributed equally to this work.
Accepted 30 October 2022
Available online 3 November 2022

https://doi.org/10.1016/j.jinf.2022.10.039

Development of monoclonal antibody-based antigens detection assays for orthopoxvirus and monkeypox virus

Dear Editor,

We read with great interest the paper by Yutong Sui et al., which developed a CRISPR-Cas12a-based detection assay for monkeypox virus (MPXV).[1] Nucleic acid detection and antigen detection are two important methods for the diagnosis of the infection of the viruses, the two methods complement each other. The CRISPR-based assay developed by Sui et al. provides a visual and fast alternative for the diagnosis of the monkeypox virus, this assay usually requires a nucleic acid enrichment process, and in this study, samples from authentic MPXV were not used for testing. Rapid antigen detection tests are highly valued in the detection of potentially infectious patients, as they can provide prompt results in a cost-effective manner. As a complement, we develop monoclonal antibody-based antigens detection assays for the rapid detection of Orthopoxvirus and MPXV.

MPXVis a zoonotic virus that was first discovered in monkeys in 1958 and in humans in 1970,[2] belongs to the orthopoxvirus, which also includes smallpox, cowpox, camelpox, and vaccinia viruses. Since May 2022, human cases of MPXV infection have been reported persistently in non-MPXV-endemic regions of Europe and North America and MPXV-endemic regions of Central and West Africa. As the number of human cases of MPXV infection continues to rise, the World Health Organization (WHO) declared on July 23, 2022, that monkeypox outbreaks in several countries and regions have amounted to a "Public Health Emergency of International Concern" (PHEIC), raising the MPXV epidemic to the same level as the COVID-19 pandemic. As of November 4, 2022, 109 countries and regions have reported cases of MPXV, bringing the total number of confirmed cases to 78,229.[3] The infection of MPXV can have a significant impact on multiple organ systems of the host, including the skin and mucosal barriers, lymphatic, lung, and gastrointestinal tract, the skin of an infected person can be severely exfoliated, and airway inflammation and bronchoppneumonitis re-

sulting from infection can limit air intake and reduce the willingness and/or ability to ingest food and water.[4] Of note, severe MPXV infection can result in death, with a mortality rate of 10.6% the for clade I virus and 3.6% the for clade II virus.[5] The proportion of asymptomatic MPXV infection is more than 13%, and the symptoms are often "atypical", which is easy to be misdiagnosed as other diseases, such as venereal diseases and COVID-19, therefore, the hidden transmission risk of MPXV is great.[6] Timely diagnosis of MPXV infection can prevent the wide spread of this virus and facilitate prompt treatment and recovery of infected persons. Although some monoclonal antibodies (mAbs) against poxviruses have been reported previously,[7–9] there are few studies on the specific diagnosis against the antigen of MPXV. In this study, three mouse mAbs against the A29L of MPXV were developed, using enzyme-linked immunosorbent assay (ELISA) and lateral flow immunoassay (LFIA), orthopoxvirus and MPXV can be sensitively and rapidly detected by two independent antibody pairs. These antibody-based A29L detection assays against MPXV only take 10–15 min and no specific equipment in a clinical laboratory is required.

We synthesized the expression sequence of A29L of clade II MPXV (Genbank number YP_010377135.1) and expressed and purified the A29L protein using E. coli prokaryotic expression system. Several MPXV A29L protein-specific mAbs were generated by immunization of 6-8-week-old BAL b/c mice with purified A29L using the murine hybridoma technique. The binding activity of all antibodies was preliminarily identified using the supernatant of hybridoma cells, and three of them were found to reveal good binding reactivity to A29L antigen, designated 3A1, 8F8 and 2D1, respectively. The three mAbs were produced in large quantities (Fig. 1A), and the variable region sequences of the antibodies were obtained by polymerase chain reaction using specific primers[10] (Fig. 1B). Then, we tested the binding reactivity of the three antibodies against MPXV A29L, camelpox virus A27L, and the corresponding membrane proteins of taterapox virus using the ELISA. 3A1 and 9F8 showed decent binding activity to the three distinct poxvirus antigens, the minimum reaction limits of 3A1 to the antigens of monkeypox, camelpox and taterapox were 256.00 pg/mL, 1280.00 pg/ ml and 1280.00 pg/ ml, respectively (Fig. C–E), the minimum reaction limits of 9F8 to the antigens of monkeypox, camelpox and taterapox were 1280.00, 1280.00 and 1280.00 pg/mL, respectively (Fig. F–H). 2D1 antibody showed good binding activity only to MPXV A29L, with a minimum reaction limit of 256.00 pg/mL (Fig. I), and weak binding activity against camelpox and taterapox antigen proteins, with the minimum reaction limits of 4 μg/mL (Fig. J and K). Next, we performed double antibody pairs sandwich-ELISA experiments base on the above three antibodies and found that one pair was sensitive for the detection of the antigens from all orpoxviruses, and the other pair specifically detected MPXV antigen only. Using 9F8 as capture antibody and 3A1 as detection antibody can detect all three orthopoxvirus antigens in a low concentration, the minimum detection limits for the antigens of monkeypox, camelpox and taterapox were 128.00, 640.00 and 3200.00 pg/mL, respectively (Fig. L–N). Using 3A1 as the capture antibody and 2D1 as the detection antibody, we can detect MPXV A29L in a low concentration, with the minimum detection limit of 128.00 pg/mL (Fig. O), this antibodies pair failed to detect antigens from camelpox and taterapox viruses (Fig. P and Q). Only vaccinia virus (Tiantan strain) has been successfully cultured in our laboratory, and authentic MPXV and related clinical infection samples have not been obtained. In a further experiment, we tested the detection activity of the above two antibody pairs against the authentic vaccinia virus and found that when using the pair of 9F8-3A1, the vaccinia virus could be detected at the level of 280 PFU (Fig. R), in contrast, when used the pair of 3A1-2D1, vaccinia virus could not be detected. This data was consistent with

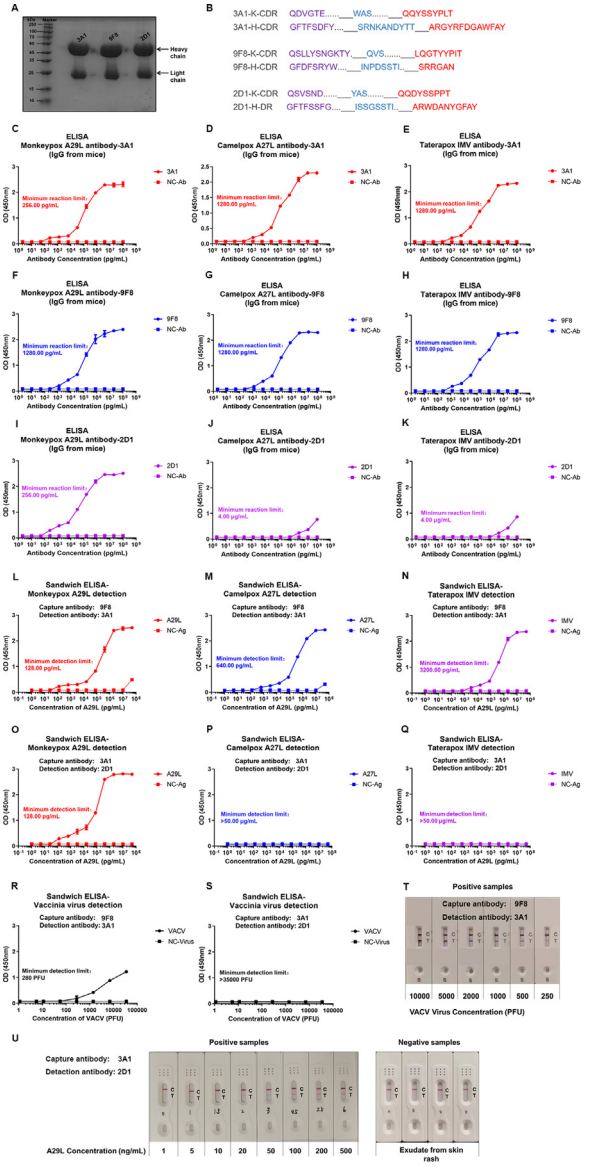

Fig. 1. Purifications, CDR sequences, antigen binding activities and double antibody sandwich antigen or virus detection activities of three monoclonal antibodies against A29L protein of MPXV. (**A**) SDS-PAGE analysis of purified 3A1, 9F8 and 2D1 antibodies which specific to A29L of MPXV. (**B**) CDR sequences of 3A1, 9F8 and 2D1 antibodies. (**C**) Reactivity of 3A1 with MPXV A29L protein in ELISA. (**D**) Reactivity of 3A1 with camelpox A27L protein in ELISA. (**E**) Reactivity of 3A1 with taterapox IMV protein in ELISA. (**F**) Reactivity of 9F8 with MPXV A29L protein in ELISA. (**G**) Reactivity of 9F8 with camelpox A27L protein in ELISA. (**H**) Reactivity of 9F8 with taterapox IMV protein in ELISA. (**I**) Reactivity of 2D1 with MPXV A29L protein in ELISA. (**J**) Reactivity of 2D1 with camelpox A27L protein in ELISA. (**K**) Reactivity of 2D1 with taterapox IMV protein in ELISA. (**L**) Detection of MPXV A29L protein using the 9F8-3A1 sandwich ELISA. (**M**) Detection of camelpox A27L protein using the 9F8-3A1 sandwich ELISA. (**N**) Detection of taterapox IMV protein using the 9F8-3A1 sandwich ELISA. (**O**) Detection of MPXV A29L protein using the 3A1-2D1 sandwich ELISA. (**P**) Detection of camelpox A27L protein using the 3A1-2D1 sandwich ELISA. (**Q**) Detection of taterapox IMV protein using the 3A1-2D1 sandwich ELISA. (**R**) Detection of authentic vaccinia virus using the 9F8-3A1 sandwich ELISA. (**S**) Detection of vaccinia virus using the 3A1-2D1 sandwich ELISA. (**T**) The rapid detection assay of a gradient concentration of vaccinia virus, in the format of LFIA, using LFIA test strip and two highly specific monoclonal antibodies against the A29L protein (9F8 for coating and 3A1 for conjugating). (**U**) The rapid detection assay of a gradient concentration of MPXV A29L protein, in the format of a LFIA, using LFIA test strip and two highly specific monoclonal antibodies against the A29L protein (3A1 for coating and 2D1 for conjugating). NC-Ab, a negative antibody which specific to SARS-CoV-2 generated by our laboratory. NC-Ag, a negative antigen (a receptor binding domain protein of SARS-CoV-2). NC-Virus, an influenza virus strain.

the result that pair of 9F8-3A1 could detect all poxvirus antigens, whereas pair of 3A1-2D1 could only specifically detect MPXV antigen in the ELISA assay (Fig. S). Finally, we used LFIA technology to develop a rapid detection kit for poxvirus based on 9F8-3A1 antibody pairing, which was still reactive to the vaccinia virus at a concentration of 250 PFU (Fig. T), and a specific rapid detection kit for monkeypox virus based on 3A1-2D1 antibody pairing, which is still reactive to A29L antigen at a concentration of 10 ng/mL (Fig. U). These two kits can get the detection result within 10–15 min, without professional equipment. The antibodies developed in this study can be applied to the rapid detection of orthopoxvirus and the rapid detection of MPXV specifically. MPXV is still prevalent worldwide and the epidemic area is still expanding at present, the findings in this study may provide a powerful tool for the prevention and control of MPXV epidemic. In the further study, we will try to contact the organizations where authentic MPXV was isolated and clinical samples from MPXV infection have been obtained, and test the reactivities of our diagnostic kits against these kinds of samples.

Declaration of Competing Interest

The authors declare no competing interests.

Funding

This work was supported by grants from National Natural Science Foundation of China (Grant number 81902058, 32170939 and 82111530302). Guangdong Basic and Applied Basic Research Foundation [Grant number 2020A1515010368 and 2022B1515020075]. Shenzhen Science and Technology Innovation Commission for Research and Development Project [Grant number JCYJ20190809183205622]. Guangdong Science and Technology Program key projects [No.2021B1212030014]. The Science and Technology Program of Guangzhou [202201011419]. The Basic Research Project of Key Laboratory of Guangzhou [No.202102100001]. Shenzhen Foundation of Science and Technology [No.JCYJ20180507182217748].

References

1. Sui Y., et al. CRISPR-Cas12a-based detection of monkeypox virus. *J Infect* 2022. doi:10.1016/j.jinf.2022.08.043.
2. Petersen E., et al. Human monkeypox: epidemiologic and clinical characteristics, diagnosis, and prevention. *Infect Dis Clin N Am* 2019;**33**:1027–43. doi:10.1016/j.idc.2019.03.001.
3. Centers for Disease Control and Prevention. 2022 Monkeypox Outbreak Global Map. Available at: https://www.cdc.gov/poxvirus/monkeypox/response/2022/world-map.html. (accessed November 6, 2022).
4. Reynolds M.G., McCollum A.M., Nguete B., Shongo Lushima R., Petersen B.W.. Improving the care and treatment of monkeypox patients in low-resource settings: applying evidence from contemporary biomedical and smallpox biodefense research. *Viruses* 2017;**9**. doi:10.3390/v9120380.
5. Bunge E.M., et al. The changing epidemiology of human monkeypox-A potential threat? A systematic review. *PLoS Negl Trop Diss* 2022;**16**:e0010141. doi:10.1371/journal.pntd.0010141.
6. Gispen R., Brand-Saathof B.. Three specific antigens produced in vaccinia, variola, and monkeypox infections. *J Infect Dis* 1974;**129**:289–95. doi:10.1093/infdis/129.3.289.
7. Gilchuk I., et al. Cross-neutralizing and protective human antibody specificities to poxvirus infections. *Cell* 2016;**167**:684–94 .e689. doi:10.1016/j.cell.2016.09.049.
8. Matho M.H., et al. Structural and functional characterization of Anti-A33 antibodies reveal a potent cross-species orthopoxviruses neutralizer. *PLoS Pathog* 2015;**11**:e1005148. doi:10.1371/journal.ppat.1005148.
9. Chen Z., et al. Chimpanzee/human mAbs to vaccinia virus B5 protein neutralize vaccinia and smallpox viruses and protect mice against vaccinia virus. *Proc Natl Acad Sci USA* 2006;**103**:1882–7. doi:10.1073/pnas.0510598103.
10. Shen C., et al. An IgM antibody targeting the receptor binding site of influenza B blocks viral infection with great breadth and potency. *Theranostics* 2019;**9**:210–31. doi:10.7150/thno.28434.

Mengjun Li[1], Yuelin Wang[1]
Guangdong Provincial Key Laboratory of Tropical Disease Research, School of Public Health, Southern Medical University, No.1023, South Shatai Road, Baiyun District, Guangzhou, Guangdong 510515, China

Chaohui Li[1]
Hoyotek Biomedical Co., Ltd., Floor 4, Zone C, Workshop No.1, China Civil Aviation Science and Technology Industrialization Base No. 225, Jinger Road, Tianjin Airport Economic Zone, Tianjin, China

Rui Xu[1]
Medical Laboratory Department, Guangdong Provincial Hospital of Chinese Medicine, Zhuhai, China

Jiayin Chen
Guangdong Provincial Key Laboratory of Tropical Disease Research, School of Public Health, Southern Medical University, No.1023, South Shatai Road, Baiyun District, Guangzhou, Guangdong 510515, China

Junfang Zhang
Shenzhen Research Institute of Xiamen University, China

Minghui Yang
Advanced Research Institute of Multidisciplinary Sciences, Beijing Institute of Technology, Beijing, China

Yushan Jiang, Yuqing Li
Guangdong Provincial Key Laboratory of Tropical Disease Research, School of Public Health, Southern Medical University, No.1023, South Shatai Road, Baiyun District, Guangzhou, Guangdong 510515, China

Zhujun Zeng
Guangdong Provincial Key Laboratory of Tropical Disease Research, School of Public Health, Southern Medical University, No.1023, South Shatai Road, Baiyun District, Guangzhou, Guangdong 510515, China
Medical Laboratory Department, Guangdong Provincial Hospital of Chinese Medicine, Zhuhai, China

Zhiguang Wu
Hoyotek Biomedical Co., Ltd., Floor 4, Zone C, Workshop No.1, China Civil Aviation Science and Technology Industrialization Base No. 225, Jinger Road, Tianjin Airport Economic Zone, Tianjin, China

Wei Zhao
Guangdong Provincial Key Laboratory of Tropical Disease Research, School of Public Health, Southern Medical University, No.1023, South Shatai Road, Baiyun District, Guangzhou, Guangdong 510515, China

Bo Wu*
Hoyotek Biomedical Co., Ltd., Floor 4, Zone C, Workshop No.1, China Civil Aviation Science and Technology Industrialization Base No. 225, Jinger Road, Tianjin Airport Economic Zone, Tianjin, China

Chenguang Shen*
Guangdong Provincial Key Laboratory of Tropical Disease Research, School of Public Health, Southern Medical University, No.1023, South Shatai Road, Baiyun District, Guangzhou, Guangdong 510515, China

*Corresponding authors.
E-mail addresses: wubotest@vip.sina.com (B. Wu), a124965468@smu.edu.cn (C. Shen)

[1] These authors contributed equally to this work.
Accepted 28 October 2022
Available online 2 November 2022

https://doi.org/10.1016/j.jinf.2022.10.036

Global differences in natural transmission rates of Monkeypox virus

Dear Editor,

In this journal, Usman Ayub Awan et al. highlighted the epidemiology of Monkeypox (MPX) and prompted public awareness of MPX as a zoonotic disease.[1] MPX has posed a serious public health threat worldwide since it was declared a Public Health Emergency of International Concern by the World Health Organization (WHO) on July 23, 2022. Monkeypox virus (MPXV) is characterized by complex transmission routes and concentrated on high-risk populations. Its effective reproduction number (R_{eff}) is still locally estimated to be greater than 1 (1.02–1.39) in people over 40 years old, even though the populations are partially vaccinated for smallpox, and already have some immunity.[2] As for the basic reproduction number (R_0), previous estimations did not eliminate the impact of existing coverage of the smallpox vaccine and coupled with the imperfection of the MPX surveillance system, which makes the derived R_0 likely underestimated.[3] Due to the varying distribution of exposed populations and high-risk populations, the region-wise R_0 is still unknown and requires a new round of estimation. Aimed to quantify the transmissibility of MPX for regions comprehensively and systematically, and provide evidence to explain the transmission characteristics and regional heterogeneity of MPX, this study estimates region-wise R_0, time-dependent reproduction number (R_t), explains the high values of estimations and emphasis the important means against MPX.

By September 20, 2022, the MPX outbreak has rapidly spread to 100 locations. The current MPX outbreak is most severe in Amer-

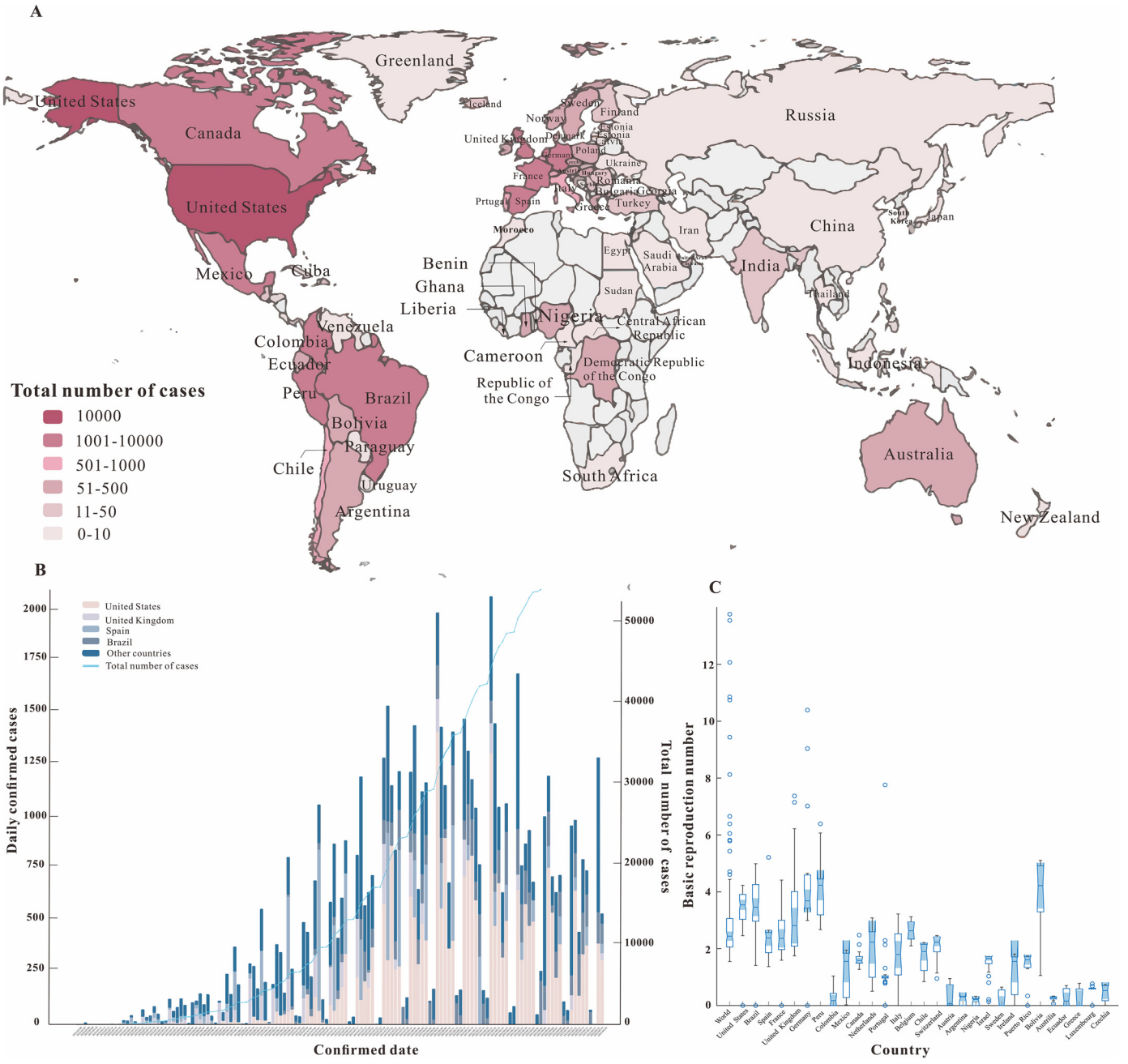

Fig. 1. Epidemic situation and calculation of transmissibility of monkeypox (A: The spatial distribution of monkeypox cases in different countries. B: Outbreak curve of confirmed monkeypox cases in global from 6 May, 2022, to 20 Sept, 2022. C: Box plots of basic reproduction numbers for global and multiple countries).

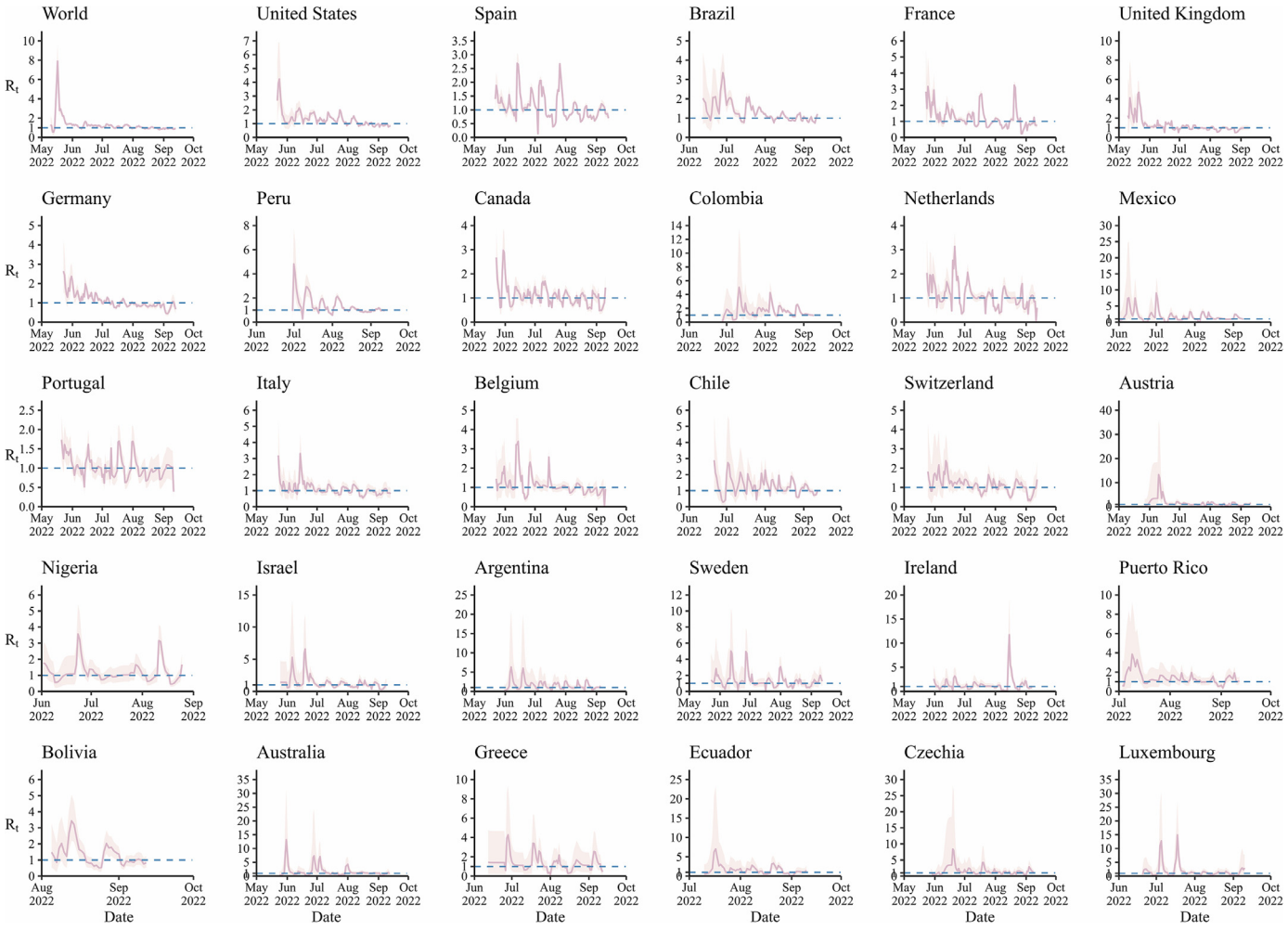

Fig. 2. Estimated time-dependent reproduction numbers from May 6, 2022, to September 20, 2022, globally and for 29 countries (The pink dash indicates the median R_t, the light pink interval indicates the 95% confidence interval, and the blue dashed line indicates R_t equal to 1. R_t calculated by the serial interval (mean: 4.0, standard deviation: 1.5)). (For interpretation of the references to colour in this figure legend, the reader is referred to the web version of this article.)

ica and Europe (Fig 1), where high risks are assessed by the WHO.[4] Among countries, the United States ranked first in the world with a total number of cases of 24,042, followed by Brazil (7115), Spain (7083), France (3898), and the United Kingdom (3591). Currently, the total number of cases of MPX worldwide has reached 64,208 (Fig 1). We selected 29 countries with a total number of MPX cases of more than 50 and stable case data to quantify the transmissibility of MPX. The uncertainties of R_0 due to data noise are quantified for each country using forward piecewise fitting, i.e. fitting in each time segment starting from the first observation gives one sample of R_0 in the specific region. The global median R_0 was 2.44 (interquartile range [IQR]: 2.06–3.06), with R_0 values of 3.54 (IQR: 3.04–3.91), 3.46 (IQR: 2.97–4.26), 2.38 (IQR: 1.86–2.57) for the United States, Brazil, and Spain, respectively. The median R_0 was highest in Peru (4.23 [IQR: 3.19–4.45]), and Greece was the lowest (3.77×10^{-4} [IQR: 3.56×10^{-4}–0.59]) (Fig 1). The global mean value of median R_t is 1.29 (standard deviation [SD]: 0.87), and the mean value of median R_t value of 1.31 (SD: 0.54), 1.33 (SD: 0.50), 1.11 (SD: 0.47) for the United States, Brazil, and Spain, respectively. The mean value of median R_t was highest in Luxembourg (1.81 [SD: 2.51]), and Portugal was the lowest (1.03 [SD: 0.28]). In specific scenarios of severe outbreaks, the maximal global R_t can reach 7.90, 4.23 in the United States, 3.36 and 2.69 in Brazil and Spain respectively (Fig 2).

The results showed the mean value of median R_t value for MPX of 1.36 (SD: 0.21) and the median R_0 value of 1.63 (IQR: 1.34–1.72) where the R_0 values we calculated were higher than the estimates listed on the WHO official website.[5] Several experts have made it clear that MPX will not be the next Corona Virus Disease 2019 (COVID-19), but why the calculated R_0 is close to COVID-19 (2.5 (range: 1.8–3.6)) or even higher than influenza (1.5)?[6] On one aspect, the most important transmission route of MPX is through close physical contact, along with relatively few transmission by droplets under prolonged face-to-face conditions, however, the respiratory diseases COVID-19 and influenza, are mainly transmitted by droplet transmission route. The physical contact mode of transmission is the main reason for limiting the spread of MPX. On the other aspect, our model considers and eliminates the effect of smallpox vaccination, and calculates the idealized transmissibility of MPX in a group with high-risk behaviors for men who have sex with men (MSM) without any interventions. The variation of high-risk social networks in fixed local contact patterns will undoubtedly amplify the transmissibility of MPX in the specific community; whereas the transmissibility of COVID-19 and influenza are estimated on an average mixed pattern of population. Other disease involving similar high-risk physical contact behaviors, like AcquiredImmune Deficiency Syndrome (AIDS), is often taken up for exploration alongside MPX. The popular question about which has

the higher reproduction number between MPX and AIDS means nothing because AIDS patients usually be infectious for their whole life, not as acute infectious disease as MPX is. The definition of reproduction number makes it not adequate for comparing the transmissibility between infectious and chronic diseases. Even if the transmission of MPX is unlikely to reach the same scale as COVID-19, the R_0 and R_t values derived from our study suggest an effective alert on the spread of MPX in high-risk population communities. The most important step against MPX is to raise public awareness of MPXV, especially in high-risk populations with high-risk behaviors, and to improve the case surveillance tracking system and vaccination strategies.

Ethical approval

The data we obtained are from the public database (Our world in data), therefore institutional review board approval and informed consent were not required. All data analyzed were anonymized.

Data availability

The data we obtained are from the public database (Our world in data, https://ourworldindata.org/monkeypox).

Competing interests

All authors declare no competing interests.

Acknowledgments

This study was partly supported by the Self-supporting Program of Guangzhou Laboratory (ZL-SRPG2200702), the Research Project on Education and Teaching Reform of Undergraduate Universities of Fujian Province (FBJG20210260), the Bill & Melinda Gates Foundation (INV-005834), and the National Key Research and Development Program of China (2021YFC2301604). The funders of the study had no role in study design, data collection, data analysis, data interpretation, or writing of the report.

Supplementary materials

Supplementary material associated with this article can be found, in the online version, at doi:10.1016/j.jinf.2022.10.032.

References

1. Awan U.A., Riasat S., Naeem W., Kamran S., Khattak A.A., Khan S.. Monkeypox: a new threat at our doorstep!. *J Infect* 2022;**85**(2) e47-e8.
2. Du Z., Shao Z., Bai Y., et al. Reproduction number of monkeypox in the early stage of the 2022 multi-country outbreak. *J Travel Med* 2022.
3. Schneider K.A., Eichner M. Does it matter who is spreading monkeypox? *Lancet Infect Dis* 2022;**22**(9):1266–7.
4. WHO. 2022 Monkeypox Outbreak: Global Trends. 2022. https://worldhealthorg.shinyapps.io/mpx_global/ (accessed September 25 2022).
5. WHO. Second meeting of the International Health Regulations (2005) (IHR) Emergency Committee regarding the multi-country outbreak of monkeypox. 2022. https://www.who.int/news/item/23-07-2022-second-meeting-of-the-international-health-regulations-(2005)-(ihr)-emergency-committee-regarding-the-multi-country-outbreak-of-monkeypox (accessed September 25 2022).
6. Petersen E., Koopmans M., Go U., et al. Comparing SARS-CoV-2 with SARS-CoV and influenza pandemics. *Lancet Infect Dis* 2020;**20**(9):e238–ee44.

Shiting Yang[1]
Xiaohao Guo[1]
Zeyu Zhao[1]
Yichao Guo
Kangguo Li
Guzainuer Abudurusuli
Tianmu Chen*
State Key Laboratory of Molecular Vaccinology and Molecular Diagnostics, School of Public Health, Xiamen University, Xiamen City, Fujian Province, China
*Corresponding author at: State Key Laboratory of Molecular Vaccinology and Molecular Diagnostics, School of Public Health, Xiamen University, 4221-117 South Xiang'an Road, Xiang'an District, Xiamen, Fujian Province, People's Republic of China.
E-mail address: chentianmu@xmu.edu.cn (T. Chen)
[1] These authors contributed equally to this study.
Accepted 23 October 2022
Available online 1 November 2022

https://doi.org/10.1016/j.jinf.2022.10.032

Initial SARS-CoV-2 RNA load in nasopharyngeal specimens is not associated with severity and midterm resolution of pneumonia in COVID-19 patients

Dear Editor,

Several studies aimed at evaluating the incidence of and delineating risk factors associated with post-acute COVID-19 syndrome have been published in *Journal of Infection*.[1-3] In this context, persistence of dyspnea, cough and chest pain, commonly associated with alterations in lung function tests and chest imaging have been reported in a non-negligible fraction of COVID-19 survivors up to 1 year after symptom onset.[4-5] To our best knowledge, limited information has been published on the potential impact of SARS-CoV-2 viral load at COVID-19 diagnosis on the time course of clinical and radiological resolution of SARS-CoV-2 pneumonia.[6] In the current retrospective, observational study we further assessed the potential link between viral load at the upper respiratory tract (URT) early after symptom onset, prior to hospitalization due to COVID-19 pneumonia, and recovery of lung function/resolution of lung abnormalities at medium term (median of 2 months) following hospital discharge.

A total of 131 adult COVID-19 patients (84 male/47 female; median age, 61 years; range, 19–85) presenting with pneumonia were enrolled. Patients were admitted to the Pneumology Service within two periods: between March 5 and December 4 2020, (n = 97), and between October 21 2021, and January 20 2022, (n = 34), during which COVID-19 in the Valencian Community was due (more than 97% of cases) to the ancestral Wuhan-Hu-1 (or Wuhan-Hu-1 G614) in the former and Omicron BA.1 in the latter period. The sample size was based on a convenience set of all available patients, without formal power calculations: only patients initially screened by the RT-PCR described below and who completed clinical, imaging and lung function evaluation by around 2 months after hospital discharge (median 57 days; IQR, 50–66) were included. Patient severity during hospital stay was stratified according to the WHO ordinary Outcomes Scale[7] as either mild disease (WHO score 3–4), or severe disease (WHO score 5–7. At follow-up residual dyspnea was evaluated using modified British Medical Research Council guidelines.[8] Patients also underwent lung function tests (spirometry) and chest X-ray (CXR). Unresolved cases were defined by Forced Vital Capacity (FVC) <80% (without Forced Expiratory Volume in 1 s-FEV1/FVC <70) and/or lung diffusion capacity (DLCO) <80% and/or persistent radiological alterations in the

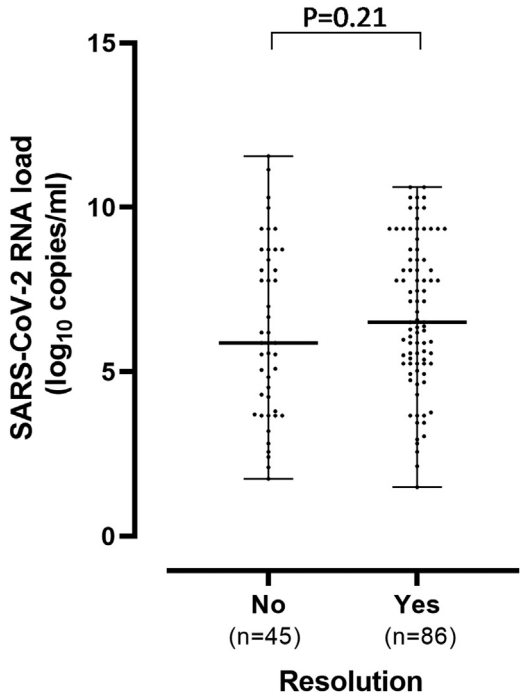

Fig. 1. SARS-CoV-2 RNA loads in nasopharyngeal specimens (NP) at diagnosis from COVID-19 patients who either recovered or not from pneumoniaa. *P* value for comparison of median values is shown.

CXR.[9] Persistence of residual lesions in the CXR was defined as any visible opacity on the CXR in the absence of prior history of pulmonary disease (except for asthma or sleep apnea) or uncontrolled cardiac or renal failure. Extent of radiological involvement after COVID-19 pneumonia was quantified using the adapted Radiographic Assessment of Lung Edema (RALE) score.[10] The study was approved by the INCLIVA Research Ethics Committee (June 2020), and informed consent was waived due to its retrospective nature. SARS-CoV-2 RNA loads in nasopharyngeal specimens (NP) were estimated using the TaqPath COVID-19 Combo Kit (Thermo Fisher Scientific, MS, USA) calibrated to the AMPLIRUN® TOTAL SARS-CoV-2 RNA Control (Vircell SA, Granada, Spain).[11] Across the Omicron BA.1 period, this variant was identified based on TaqPath S gene target failure (SGTF) and confirmed by whole-genome sequencing (not shown).

Medical records showed underlying pulmonary disease at the time of hospital admission (chronic obstructive pulmonary disease or asthma) in 20 patients. Importantly, all patients experiencing COVID-19 pneumonia presumably due to Omicron BA.1 had been fully vaccinated against COVID-19 with mRNA vaccines. Out of the 131 patients, 95 (72.5%) presented with mild COVID-19 pneumonia (WHO scale 4), while the remaining 36 patients had severe disease (WHO scale 5–7), requiring non-invasive ventilation ($n = 4$), high flow nasal oxygen cannula ($n = 11$) or respiratory support by invasive mechanical ventilation ($n = 21$). Median hospital stay was 10 days (range, 2–62). According to above-defined criteria, 45/131 patients (34.3%) were classified as not recovered by 2 months after hospital discharge (unresolved cases).

Initial SARS-CoV-2 RNA load in NP was quantified at a median of 6 days after symptom onset (IQR, 3–8). Median SARS-CoV-2 RNA loads did not differ significantly across the ancestral variant or Omicron BA.1-dominant study periods (6.2 $\log_{10}$ copies/ml vs. 7.1 $\log_{10}$ copies/ml, at equivalent sample collection times; $P = 0.07$). As shown in Fig. 1, patients displayed comparable ($P = 0.21$) viral loads in NP whether they recovered from pneumonia or not (median, 6.51 vs. 5.88 log10 copies/ml). NP specimens from patients in the two groups had been collected within a comparable time frame after symptom onset ($P = 0.39$).

We next conducted a subanalysis assessing the potential impact of SARS-CoV-2 RNA load in NP on resolution according to time elapsed since symptom onset. The following timeframes were arbitrarily defined: 0–2 days, 3–5 days, 6–8 days and 9–10 days. Patients with NP collected 11 or more days after symptom onset ($n = 27$) were excluded due to the lack of matching across comparison groups (not shown). SARS-CoV-2 RNA load was comparable across patients within all timeframes regardless or whether they recovered or not (Table 1). Regression logistic models (Supplementary Table 1) confirmed the apparent lack of impact of initial SARS-CoV-2 RNA load on this outcome (OR, 1.72; 95% CI, 0.83–3.58; $P = 0.14$); this observation stood regardless of the SARS-CoV-2 variant presumably involved in COVID-19 cases (Wuhan-Hu-1: OR, 1.74; 95% CI, 0.74–4.09; $P = 0.20$; Omicron BA.1: OR, 1.74; 95% CI, 0.42–7.28; $P = 0.44$). As expected, pneumonia severity was identified as a factor associated with unresolved pneumonia.

Our findings are in contrast to those of Lerum and colleagues who reported a negative association between viral load at baseline and the diffusion capacity of the lungs for carbon monoxide (DL_{CO}%) by 3 months after hospital discharge, the most frequently affected pulmonary function test variable in the study group (recruited prior to the availability of COVID-19 vaccines).[6] Nevertheless, no apparent association between viral load and resolution of computer tomography abnormal findings or other lung function parameters was observed. Of relevance, the study by Lerum et al.[6] and ours differ in several potentially critical factors such as the timing of URT specimen collection (median 8 vs. 6 days since symptom onset, respectively), and timing of clinical evaluation of patients after hospital discharge (median of 3 and 2 months, respectively).

The current study has several limitations that deserve comment, the first being the relatively small sample size (particularly during the Omicron BA.1 wave). Second, specimen collection may have been performed too late after SARS-CoV-2 infection (median of 6 days) to capture peak viral loads. Third, no viral cultures were performed to evaluate the content of viable viral particles in the specimens. Fourth, importantly, no sequential spec-

Table 1
Impact of SARS-CoV-2 RNA load in nasopharyngeal specimens at diagnosis on recovery from COVID-19 pneumonia 2 months after hospital discharge.

Days from symptom onset to time of specimen collection	Median (range) SARS-CoV-2 RNA viral load (in $\log_{10}$ copies/ml) according to recovery from pneumonia/no. of patients		*P* value[a]
	Resolved	Unresolved	
0–2	8.1 (2.9–10.6)/14	8.4 (1.7–11.2)/11	0.80
3–5	7.1 (3.4–10.3)/25	7.8 (5.5–11.6)/6	0.70
6–8	7.1 (2.1–9.4)/24	6.7 (4.8–10)/11	0.56
9–10	5.6 (3.8–8.1)/7	5.0 (3.2–8.7)/6	0.60

[a] Mann–Whitney U test. Two-sided exact *P* values are reported. A *P* value <0.05 was considered statistically significant. The analyses were performed using SPSS version 20.0 (SPSS, Chicago, IL, USA).

imens were available from participants, which hampered the assessment of SARS-CoV-2 RNA load kinetics in the URT at the individual level. Fifth, no computer tomography scans or lung function tests other than spirometry were systematically performed.

In summary, the data presented herein oppose the notion that SARS-CoV-2 at URT in patients eventually hospitalized with COVID-19 pneumonia has a major on the recovery rate, according to clinical, imaging and lung functional spirometry parameters by around 2 months after hospital discharge. In this context, our findings do not support prescribing new antivirals with potent intrinsic activity against SARS-CoV-2 based upon the magnitude of SARS-CoV-2 RNA load in the URT early after symptom onset. Nevertheless, given the above-highlighted limitations, further studies are warranted to clarify this issue.

Author contributions

RC, BO: methodology and data validation. JT, JS-C, NC, and MLB: data gathering and analysis. DN: conceptualization, data analysis and manuscript writing.

Funding

This work received no private or public funds.

Declaration of Competing Interest

The authors declare no conflicts of interest

Acknowledgements

We are grateful to residents and staff at the Microbiology Service of Hospital Clínico Universitario and medical and nursing staff at Hospital Clínico Universitario of Valencia.

Data availability statement

The data presented in the manuscript have not been made available, but can be shared upon request.

Supplementary materials

Supplementary material associated with this article can be found, in the online version, at doi:10.1016/j.jinf.2022.10.031.

References

1. Moreno-Pérez O., Merino E., Leon-Ramirez J.M., Andres M., Ramos J.M., Arenas-Jiménez J., et al. Post-acute COVID-19 syndrome. Incidence and risk factors: a Mediterranean cohort study. *J Infect* 2021;**82**:378–83.
2. Taboada M., Cariñena A., Moreno E., Rodríguez N., Domínguez M.J., Casal A., et al. Post-COVID-19 functional status six-months after hospitalization. *J Infect* 2021;**82**:e31–3.
3. Fernández-de-Las-Peñas C., Martín-Guerrero J.D., Cancela-Cilleruelo I., Moro-López-Menchero P., Rodríguez-Jiménez J., Navarro-Pardo E., et al. Exploring the recovery curves for long-term post-COVID functional limitations on daily living activities: the LONG-COVID-EXP-CM multicenter study. *J Infect* 2022;**84**:722–46.
4. Daines L., Zheng B., Pfeffer P., Hurst J.R., Sheikh A.. A clinical review of long-COVID with a focus on the respiratory system. *Curr Opin Pulm Med* 2022;**28**:174–9.
5. Huang C., Huang L., Wang Y., Li X., Ren L., Gu X., et al. 6-month consequences of COVID-19 in patients discharged from hospital: a cohort study. *Lancet* 2021;**397**:220–32.
6. Lerum T.V., Maltzahn N.N., Aukrust P., Trøseid M., Henriksen K.N., Kåsine T., et al. Persistent pulmonary pathology after COVID-19 is associated with high viral load, weak antibody response, and high levels of matrix metalloproteinase-9. *Sci Rep* 2021;**11**:23205.
7. WHO. Treatment Trial Design Master Protocol synopsis Final 18022020. www.who.int/blueprint/priority-diseases/key-action/COVID-19. Date last accessed: July 9 2022,.
8. Bestall J.C., Paul E.A., Garrod R., Garnham R., Jones P.W., Wedzicha J.A.. Usefulness of the Medical Research Council (MRC) dyspnoea scale as a measure of disability in patients with chronic obstructive pulmonary disease. *Thorax* 1999;**54**:581–6.
9. Sibila O., Molina-Molina M., Valenzuela C., Ríos-Cortés A., Arbillaga-Etxarrie A., Torralba García Y., et al. Spanish Society of Pulmonology and Thoracic Surgery (SEPAR) Consensus for post-COVID-19 Clinical Follow-up. *Open Resp Arch* 2020;**2**:278–83.
10. Wong H.Y.F., Lam H., Fong A.H., Leung S.T., Chin T.W., Lo C.S.Y., et al. Frequency and Distribution of Chest Radiographic Findings in COVID-19 Positive Patients. *Radiology* 2020;**296**:E72–8.
11. Albert E., Torres I., Bueno F., Huntley D., Molla E., Fernández-Fuentes M.Á., et al. Field evaluation of a rapid antigen test (Panbio™ COVID-19 Ag Rapid Test Device) for COVID-19 diagnosis in primary healthcare centres. *Clin Microbiol Infect* 2021;**27** 472.e7-472.e10.

Rosa Costa
Microbiology Service, Clinic University Hospital, INCLIVA Health Research Institute, Valencia, Spain

Jaime Signes-Costa
Pulmonary Department, Clinic University Hospital, INCLIVA Health Research Institute, Valencia, Spain

Beatriz Olea
Microbiology Service, Clinic University Hospital, INCLIVA Health Research Institute, Valencia, Spain

Julia Tarraso
Pulmonary Department, Clinic University Hospital, INCLIVA Health Research Institute, Valencia, Spain

Nieves Carbonell, María Luisa Blasco
Medical Intensive Care Unit, Clinic University Hospital, INCLIVA Health Research Institute, Valencia, Spain

David Navarro*
Microbiology Service, Clinic University Hospital, INCLIVA Health Research Institute, Valencia, Spain
Department of Microbiology, School of Medicine, University of Valencia, Valencia, Spain

*Corresponding author at: Microbiology Service, Hospital Clínico Universitario, Instituto de Investigación INCLIVA. *Av*. Blasco Ibáñez 17, 46010 Valencia, Spain.
E-mail address: david.navarro@uv.es (D. Navarro)

Accepted 23 October 2022
Available online 28 October 2022

https://doi.org/10.1016/j.jinf.2022.10.031

The changing epidemiology of PIMS-TS across COVID-19 waves: prospective national surveillance, January 2021 to July 2022, England

Dear Editor,

Author contributions

JS wrote the original draft, developed the modelling methodology, produced the figures, and performed all data analysis. HW helped to develop the modelling methodology. SL conceptualized the study and reviewed and edited the draft. TW-K curated all PIMS-TS data. SK, NG, MA, AP, and GO reviewed and edited the draft.

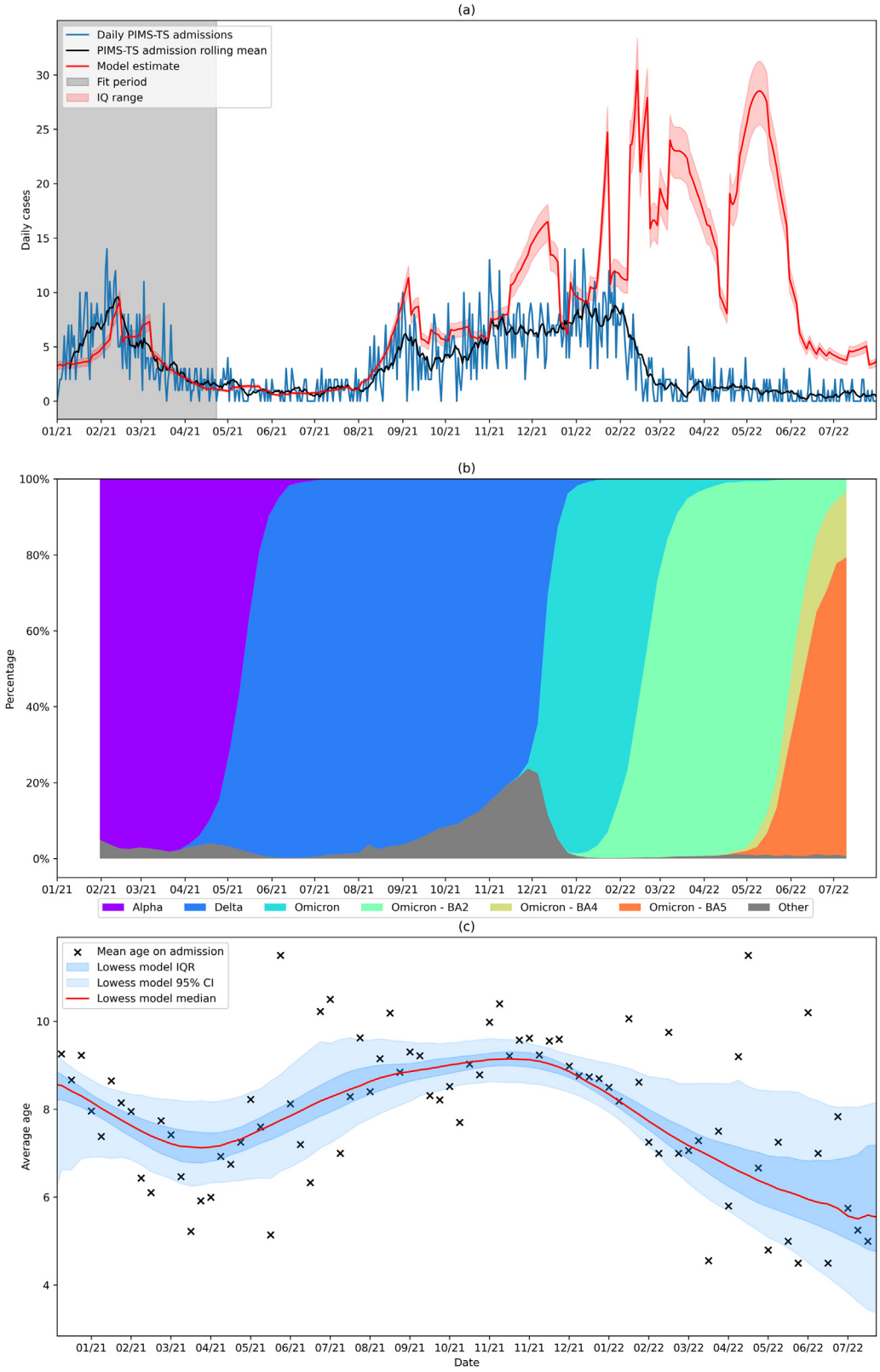

Fig. 1. (a) Forecasted PIMS-TS admissions based on a model fitted to the Alpha variant wave of COVID-19, alongside observed PIMS-TS admissions. (b) SARS-CoV-2 variant prevalence using available sequenced strains for England from 1 February 2021 as of 20 June 2022. [5] (c) Mean age of children with by week since December 2020. A Lowess filter with window size 1/3rd was fitted to identify the general trend in the data. Confidence intervals were produced by applying the filter 1000 times to a random subset of 50% of the data.

In April 2020, a rare but serious paediatric Multisystem Inflammatory Syndrome (PIMS-TS, also known as MIS-C) was identified, which was temporally and geographically associated with SARS-CoV-2. [1] In England, we estimated a PIMS-TS risk of 0·045% (95% credible interval, 0·035–0·068%) after SARS-CoV-2 infection in <15 year-olds, with a lag of 2–6 weeks. [2] These results were used to parameterise a model to predict new PIMS-TS cases based on estimated childhood SARS-CoV-2 infection. [2] SARS-CoV-2 infection rates were derived using the PHE-Cambridge real-time model, which uses multiple data sources to estimate national incidence in addition to laboratory-confirmed cases, which likely significantly underestimates true infection rates. [2] PIMS-TS cases during the first pandemic wave were derived from national surveillance, [1] and, from November 2020, using a new emergency ICD-10 code (U07.5, Multisystem inflammatory syndrome associated with COVID-19)in Secondary Uses Services (SUS, NHS Digital, Leeds, UK), a national administrative database used by National Health Service hospitals to record all admissions, emergency department attendances and outpatient appointments in England. [2] The outputs of this model were used to direct healthcare resources and inform policy during late 2020 and early 2021.

After the alpha wave in England (November 2020 to April 2021), the model's performance was re-parameterised using data over a longer time-period. The re-parameterisation estimated a slightly lower PIMS-TS risk after SARS-CoV-2 infection of 0·038% (95%CI, 0·037–0·041%). During the subsequent delta wave, the model significantly over-predicted the risk of PIMS-TS by 53%, with 450 (436–472) estimated versus 212 observed cases during June-October 2021 (median risk, 0·026%; 95%CI, 0·025–0·029%). These results and the modelling methodology are reported elsewhere. [2]

The emergence of the highly transmissible omicron in late 2021, which was able to evade natural and vaccine-induced immunity [3], raised concerns about further increases in PIMS-TS cases. Early reports, however, indicated an even lower risk of PIMS-TS with the new variant. [4]

Using the same methodology, [2] our model also identified further divergence between predicted and observed PIMS-TS with omicron compared to alpha. Between 15 December 2021, when omicron became dominant, and 01 August 2022, which encompassed infection waves due to omicron subvariants BA.1, BA.2, BA.4 and BA.5, [5] the model predicted 3165 (95%CI, 2855–3459) compared to 570 observed PIMS-TS cases, 82% (95%CI, 80–84%) lower (**Fig. 1a**). Notably, PIMS-TS cases declined rapidly after the BA.1 wave and have remained very low, despite large BA.2 waves from 15 February 2022 and BA.4/BA.5 waves since June 2022 (**Fig. 1b**). The model predicted 795 (717–867) compared to 446 observed cases (56% (51–62%) lower) during BA.1 (15 December 2021 to 14 February 2022), and 2352 (2122–2571) compared to 158 observed cases (93% (92- 94%) lower) during subsequent waves (15 February to 01 August 2022).

Using a combination of surveillance data, modelled estimates between the first pandemic and alpha waves and SUS coding, we estimated 2105 PIMS-TS cases since the start of the pandemic until 01 August 2022. The model trained on the Alpha wave predicted 6034 (95% CI, 5841–6234) cases over the same period.

Our findings add to the growing evidence of decreasing PIMS-TS risk with each SARS-CoV-2 wave. [4–6] Reasons for this decoupling include critical mutations in the virus superantigen motifs speculated to trigger the hyperinflammatory response. [2] Additionally, if, as is currently speculated, PIMS-TS is associated with an aberrant immune response to primary SARS-CoV-2 infection, then high immunity levels through infection and COVID-19 vaccination in children may be a significant contributing factor. By 24 July 2022, 10·6% of 5–11 and 58·3% of 12–15 year-olds had received ≥1 vaccine dose. [7] COVID-19 vaccination is currently not recommended for <5 year-olds in England, but this age-group had very high infection rates during the BA.1 wave. [8] Over time, PIMS-TS epidemiology could follow the related Kawasaki disease, with most cases occurring in infants and toddlers, the only age group likely to remain susceptible to the virus in the future. Our analysis shows a declining trend in the age of children diagnosed with PIMS-TS since the start of the pandemic, *albeit* with large confidence intervals in recent months because of low case numbers (**Fig. 1c**). In conclusion, the very low risk of PIMS-TS despite large rates of SARS-CoV-2 infections due to the BA.2, BA.4 and BA.5 subvariants in children will be reassuring to parents, clinicians and policy makers. On-going surveillance, however, is critical, particularly in the event of newly emerging variants.

References

[1]. Flood J., Shingleton J., Bennett E., Walker B.. Paediatric multisystem inflammatory syndrome temporally associated with SARS-CoV-2 (PIMS-TS): prospective, national surveillance, United Kingdom and Ireland. *Lancet Reg Health Eur* 2020;**3**:75–86 2021.

[2]. Shingleton J., Williams H., Burton L.. Risk of Paediatric Multisystem Inflammatory Syndrome (PIMS-TS) during the SARS-CoV-2 Alpha and Delta variant waves: national observational study, 2020-21, England,". *SSRN* 2022.

[3]. Moshin M., Mahmud S.. Omicron SARS-CoV-2 variant of concern: a review on its transmissibility, immune evasion, reinfection, and severity. *Medicine (Baltimore)* 2022;**101** e29165.

[4]. Cohen J.M., J C.M., Cheung R.C.. Lower risk of Multisystem Inflamatory Syndrome in Children (MIS-C) with the Delta and Omicron variants of SARS-CoV-2. *Clin Infect Dis* 2022.

[5]. UK Health Security Agency, "SARS-CoV-2 variants of concern and variant under investigation in England," UK Government, 2022.

[6]. Whittaker R., Greve-Isdahl M., Bøås H.. COVID-19 Hospitalization Among Children <18 Years by Variant Wave in Norway. *Pediatrics* 2022;**150**.

[7]. N.H.S. England, "COVID-19 Vaccination Statistics," 24 7 2022. [Online]. Available: https://www.england.nhs.uk/statistics/wp-content/uploads/sites/2/2022/07/COVID-19-weekly-announced-vaccinations-28-July-2022.pdf. [Accessed 6 9 2022].

[8]. UK Health Security Agency, "Weekly national influenze and COVI-19 surveillance report: week 13," UK Government, 2022.

Joseph Shingleton, Hannah Williams
Emergency Preparedness, Response and Resilience, UK Health Security Agency, Porton Down, UK
Joint Modelling Team (JMT), UK Health Security Agency, UK

Godwin Oligbu, Annabel Powell
Immunisation Division, UK Health Security Agency, 61 Colindale Avenue, London, NW9 5EQ, UK

Jonathan Cohen
Paediatric Immunology & Infectious Diseases, Evelina London Children's Hospital, London, UK

Moshe Arditi
Department of Pediatrics, Division of Infectious Diseases and Immunology, Cedars-Sinai Medical Center, Los Angeles, California, USA

Tiffany Watson-Koszel
NHS England and NHS Improvement, London, England

Simon Kenny
NHS England and NHS Improvement, London, England
Institute of Systems, Molecular and Integrative Biology, University of Liverpool, Liverpool, UK
Department of Paediatric Surgery, Alder Hey in the Park, Liverpool, UK

Nick Gent
Emergency Preparedness, Response and Resilience, UK Health Security Agency, Porton Down, UK
Joint Modelling Team (JMT), UK Health Security Agency, UK

Shamez N. Ladhani*
Immunisation Division, UK Health Security Agency, 61 Colindale Avenue, London, NW9 5EQ, UK
Paediatric Infectious Diseases Research Group, St George's University of London, UK

*Corresponding author: Dr Shamez Ladhani, Immunisation Division, UK Health Security Agency, 61 Colindale Avenue, London NW9 5EQ, UK.
E-mail address: shamez.ladhani@ukhsa.gov.uk (S.N. Ladhani)

Accepted 5 October 2022
Available online 20 October 2022

https://doi.org/10.1016/j.jinf.2022.10.017

Monkeypox virus productively infects human induced pluripotent stem cell-derived astrocytes and neural progenitor cells

Dear Editor,

Shortly after the outbreak of monkeypox virus (MPXV) in multiple countries in Europe and North America, Orviz and colleagues described confirmed MPX cases in Madrid, Spain, in a recent study published in this journal.[1] Aside from typical symptoms such as fever, lymph node enlargement, asthenia, and skin lesions, patients developed neurological signs including headaches and myalgia.[1] In addition, some groups reported MPX individuals with less typical neurological manifestations, such as seizures and encephalitis, who were more severely affected.[2] Studies in infected animals, such as rodents, suggested that the virus can also penetrate the brain.[3,4] However, it is unknown whether MPVX may infect cells in the central nervous system (CNS). We take advantage of our established human induced pluripotent stem cell (hiPSC) platform to address this knowledge gap.

Here, we investigated the susceptibility of hiPSC-derived neural progenitor cells (NPCs), neurons, and astrocytes to MPXV. An A.2 strain virus was isolated from an MPX patient in Thailand, propagated in Vero cells, and titered in HeLa cells. The derivation of human neural cells from hiPSCs has been described elsewhere.[5] Briefly, NPCs were derived from commercially available hiPSCs (ATCC, ACS-1019) using the dual SMAD inhibition protocol via embryoid bodies and rosette selection and maintained in N2B27 media supplemented with basic fibroblast growth factor (bFGF). Neurons were generated from NPCs by the removal of bFGF from the NPC culture media. Astrocytes were derived from NPCs in astrocyte differentiation and maturation media (STEMCELL Technologies). All derived neural cells expressed specific markers as expected. (**Supplementary Fig. S1**).

We initially assessed if MPXV infected hiPSC-derived neural cells by visual observation of the cultures over time and by immunofluorescence assays (IFA). hiPSC-derived NPCs, neurons, and astrocytes were infected with MPXV at multiplicities of infection (MOIs) of 0.0001, 0.001, and 0.1 in their corresponding media (N2B27 with bFGF, N2B27 and AM (Sciencell), respectively). Cell morphology was observed and imaged every 24 h (**Supplementary Fig. S2**). We noticed changes in the morphology of astrocytes 48 h post-infection (hpi), when they began to cluster (**Supplementary Fig. S2C**). At 96 hpi, cells were fixed for IFA as described in **Supplementary Fig. S1**. We found that MPXV-infected NPCs were less densely packed as compared to mock-infected NPCs (**Fig. 1A, top and Supplementary Fig. S1A**), likely due to an increase in cell detachment as a result of infection. Surprisingly, we found no cytopathic effect (CPE) in infected neurons at any MOI (**Fig. 1A, middle and Supplementary Fig. S1B**). In contrast, CPE is most pronounced in infected astrocytes, as indicated by the abundant formation of syncytia, larger cells with multiple nuclei (**Fig. 1A bottom and B).** As MOI rises, the occurrence of such CPE also increases (**Fig. 1A, bottom and Supplementary Fig. S2C**). Unfortunately, due to the unavailability of antibodies against MPXV proteins, we were unable to demonstrate co-labeling of cell type-specific markers and viral proteins. Instead, we assessed whether productive infection with MPXV occurs in these hiPSC-derived neural cells. Note that we have added 45-day-old hiPSC-derived neurons in this replication study in case the age of neurons might play a role in permissiveness to MPXV infection. NPCs, neurons (day 14 and day 45) and astrocytes, as well as Vero cells as positive controls, were infected with MPXV at an MOI of 1.0 for 1 h before being washed with PBS and replenished with the appropriate media. Supernatants were collected at 0, 24, 48, 72 and 96 hpi, the cells were imaged (**Supplementary Fig. S3**), and viral DNA was extracted from free virus for qPCR. Primers and conditions have been described elsewhere.[6] Cycle threshold (Ct) values of MPXV qPCR in NPCs and astrocytes as well as in Vero cells significantly decreased over time compared with the remaining input virus at 0 hpi (**Fig. 1C and Supplementary Table S1**), suggesting that MPXV could productively infect NPCs and astrocytes similar to Vero cells. On the other hand, such a change is not pronounced in 14-day-old and 45-day-old neurons (**Fig. 1C and Supplementary Table S1)**, suggesting that they are not permissive to MPXV. This supports our IFA findings. Intracellular viruses were not examined in this study, but the increased detection of viral genomic DNA in cell culture supernatants is a strong indicator of viral replication. It is also important to note that although the differences in Ct values between NPCs and astrocytes were relatively small, NPCs were seeded at a density four times higher than astrocytes, suggesting that among the three types of neural cells in this study, astrocytes may be the most permissive to or productive for MPXV infection.

Astrocytes play an important role in CNS homeostasis, such as maintenance of synapses, regulation of neurotransmitters, release of neurotrophic factors, and uptake of glutamate. Upon CNS injury or infection, they can become either neuroprotective for CNS repair or neurotoxic by promoting neuroinflammation.[7] These dynamic states have been reported to be associated with various neurodegenerative diseases such as Alzheimer's disease[8] and Parkinson's disease,[9] as well as infections.[10] Given the importance of astrocytes, it is logical to suppose that neurons in patients' brains would respond differently to MPXV infection than our findings, which demonstrated no change in the shape or distribution of hiPSC-derived neurons. They may be damaged not by the infection directly but by the changed properties of the infected astrocytes. More research employing more advanced models, such as co-culture of neurons and astrocytes or brain organoids more closely resembling the human brain, might provide more insight into the effects of MPXV infection on neurons in a more relevant setting.

In summary, we found that hiPSC-derived NPCs and astrocytes were susceptible to MPVX infection, causing dramatic changes in cell distribution and morphology, especially in astrocytes. Increased levels of viral DNA were detected in culture supernatants, suggesting productive replication. To our knowledge, this is the first study reporting differences in MPXV permissiveness between hiPSC-derived NPCs and astrocytes versus hiPSC-derived neurons, shedding light on the association between MPXV and reported neurological complications on a cellular level and guiding us

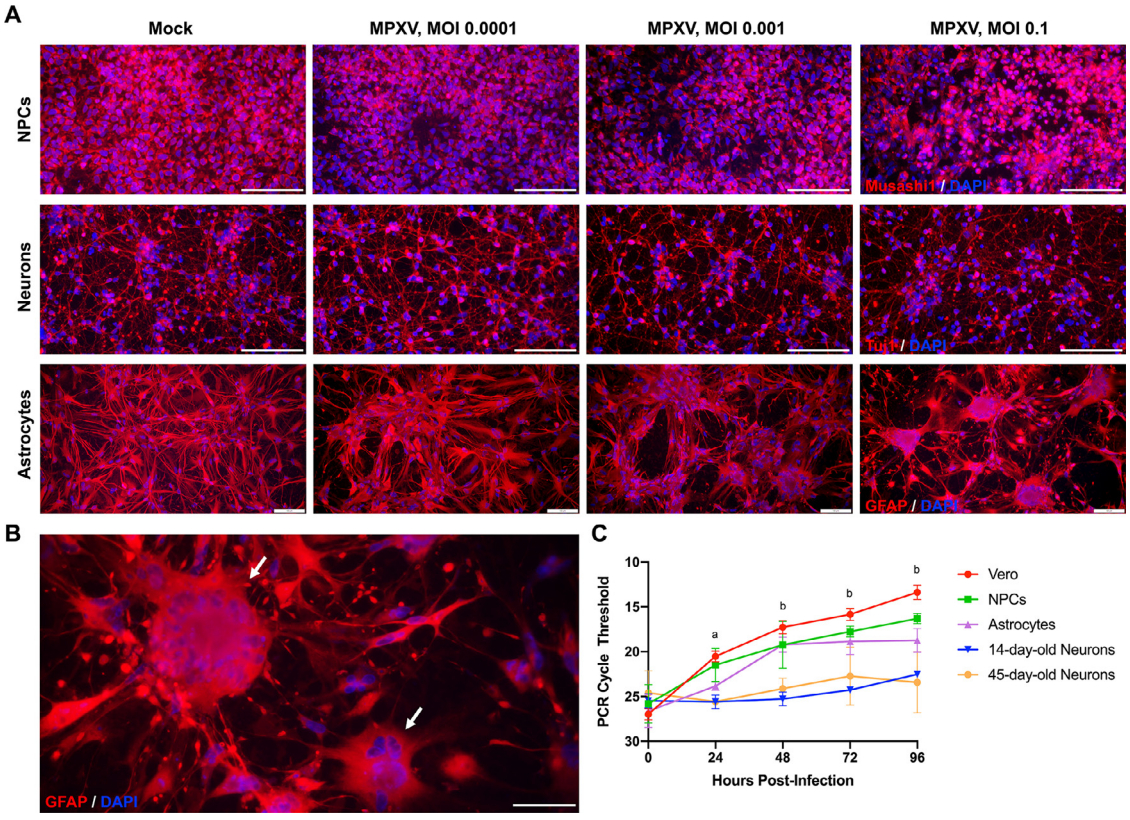

Fig. 1. MPXV infection in hiPSC-derived NPCs, neurons and astrocytes
(A) Representative images of NPCs (top), neurons (middle) and astrocytes (bottom) in MPXV and mock infections. Cells were seeded onto matrigel-coated 24-well plates at 4×10^5, 4.5×10^5, and 10^5 cells/well, respectively. Cells were then incubated with the virus at MOIs of 0.0001, 0.001 or 0.1. At 96 hpi, cells were fixed with 80% ice-cold acetone and immunofluorescently stained for cell-type specific markers (Musashi1, TuJ1 and GFAP, respectively) according to the protocol described in Supplementary Fig. S1. Bar, 100 μm. (B) Higher magnification of syncytia (white arrows) observed in MPXV-infected astrocyte culture. Bar, 50 μm. (C) PCR cycle threshold value of MPXV qPCR in NPCs, neurons (day 14 and day 45), and astrocytes as well as Vero cells at each timepoint. Cells were prepared as described above, infected with MPXV at an MOI of 1.0 for 1 h, washed, and fed with fresh culture media. Supernatants were collected at 0, 24, 48, 72, and 96 hpi. Viral DNA extraction was performed using the Viral Genome Extraction Kit II (Geneaid), and qPCR using primers specific for MPXV[6] was conducted. Statistical analyses were performed by two-way ANOVA. Multiple comparisons were performed within cell type, comparing cycle threshold at 24, 48, 72, and 96 hpi against 0 hpi. a, Vero and NPC values significantly different from 0 hpi, $p < 0.0001$; astrocyte values, $p = 0.0004$. b,Vero, NPC and astrocyte values significantly different from 0 hpi, $p < 0.0001$.

towards a deeper understanding of MPXV pathogenesis in the brain.

Funding

This work was supported by the National Center for Genetic Engineering and Biotechnology, Thailand (grant number P-18–50,193) and Program Management Unit for Human Resources and Institutional Development, Research and Innovation (PMU-B, grant number 78,027)

Declaration of Competing Interest

None.

Supplementary materials

Supplementary material associated with this article can be found, in the online version, at doi:10.1016/j.jinf.2022.10.016.

References

1. Orviz E., Negredo A., Ayerdi O., et al. Monkeypox outbreak in Madrid (Spain): clinical and virological aspects. *J Infect* 2022;**85**(4):412–17.
2. Sepehrinezhad A., Ashayeri Ahmadabad R., Sahab-Negah S.. Monkeypox virus from neurological complications to neuroinvasive properties: current status and future perspectives. *J Neurol* 2022. doi:10.1007/s00415-022-11339-w.
3. Kulesh D.A., Loveless B.M., Norwood D., et al. Monkeypox virus detection in rodents using real-time 3′-minor groove binder TaqMan assays on the Roche LightCycler. *Lab Invest* 2004;**84**(9):1200–8.
4. Hutson C.L., Lee K.N., Abel J., et al. Monkeypox zoonotic associations: insights from laboratory evaluation of animals associated with the multi-state US outbreak. *Am J Trop Med Hyg* 2007;**76**(4):757–68.
5. Chailangkarn T., Tanwattana N., Jaemthaworn T., et al. Establishment of human-induced pluripotent stem cell-derived neurons-A promising *in vitro* model for a molecular study of rabies virus and host interaction. *Int J Mol Sci* 2021;**22**(21):11986.
6. Li Y., Olson V.A., Laue T., Laker M.T., Damon I.K. Detection of monkeypox virus with real-time PCR assays. *J Clin Virol* 2006;**36**(3):194–203.
7. Fan Y.Y., Huo J.. A1/A2 astrocytes in central nervous system injuries and diseases: angels or devils? *Neurochem Int* 2021;**148**:105080.
8. King A., Szekely B., Calapkulu E., et al. The increased densities, but different distributions, of both C3 and S100A10 immunopositive astrocyte-like cells in Alzheimer's disease brains suggest possible roles for both A1 and A2 astrocytes in the disease pathogenesis. *Brain Sci* 2020;**10**(8):503.
9. Fujita A., Yamaguchi H., Yamasaki R., et al. Connexin 30 deficiency attenuates A2 astrocyte responses and induces severe neurodegeneration in a 1-methyl-4-phenyl-1,2,3,6-tetrahydropyridine hydrochloride Parkinson's disease animal model. *J Neuroinflammation* 2018;**15**(1):227.
10. Jin Y., Yao Y., El-Ashram S., Tian J., Shen J., Ji Y.. The neurotropic parasite toxoplasma gondii induces astrocyte polarization through NFkappaB pathway. *Front Med* 2019;**6**:267 (Lausanne).

Thanathom Chailangkarn, Samaporn Teeravechyan, Khemphitcha Attasombat, Theeradej Thaweerattanasinp
Virology and Cell Technology Research Team, National Center for Genetic Engineering and Biotechnology (BIOTEC), National Science and Technology Development Agency (NSTDA), 113 Thailand Science

Park, Phahonyothin Road, Khlong Nueng, Khlong Luang, Pathum Thani 12120, Thailand

Kitpong Sunchatawirul, Pawita Suwanwattana
Department of Disease Control, Ministry of Public Health, Bamrasnaradura Infectious Diseases Institute, Nonthaburi 11000, Thailand

Krit Pongpirul
Faculty of Medicine, Chulalongkorn University, Bangkok 10330, Thailand

Anan Jongkaewwattana
Virology and Cell Technology Research Team, National Center for Genetic Engineering and Biotechnology (BIOTEC), National Science and Technology Development Agency (NSTDA), 113 Thailand Science Park, Phahonyothin Road, Khlong Nueng, Khlong Luang, Pathum Thani 12120, Thailand

*Corresponding author.
E-mail address: thanathom.cha@biotec.or.th (T. Chailangkarn)

Accepted 13 October 2022
Available online 19 October 2022

https://doi.org/10.1016/j.jinf.2022.10.016

Germline variants of *IGHV3-53 / V3-66* are determinants of antibody responses to the BNT162b2 mRNA COVID-19 vaccine

Dear Editor,

While the effectiveness of COVID-19 vaccines has been established, there is low acquisition of neutralising antibodies (nAbs) after vaccination and waning of the antibody titre over time, along with an increased risk of breakthrough infection.[1,2] Despite the accumulation of information on the confounding factors of antibody titres after vaccination,[3,4] little is known about genetic factors.

It has been recognized that heavy chains of the nAbs against SARS-CoV-2 are frequently encoded by two paralogous immunoglobulin heavy variable (*IGHV*) genes, *IGHV3-53* and *IGHV3-66*.[5,6] We postulated that germline variants affecting the function or expression of these genes may influence antibody acquisition in recipients of COVID-19 vaccines designed to induce nAbs. To validate this hypothesis, we designed and conducted a two-part genetic analysis (Fig. 1). Samples and information from 2,015 healthcare workers at Chiba University Hospital who were going to receive the BNT162b2 mRNA COVID-19 vaccine (Pfizer and BioNTech) from 3 March to 9 April 2021 and had enrolled in our previous study [4] were obtained in this study. The Chiba University Hospital Ethics Committee approved the collection of samples and clinical information from the vaccine recipients (No. HS202101-03), and their genetic analyses (No. HS202105-01) in this study. All participants provided written informed consent for providing their clinical information and blood samples and were also given the opportunity to opt out of this study. First, single-nucleotide variants (SNVs) to be evaluated were determined. We narrowed down candidate SNVs surrounding *IGHV3-53* using expression quantitative loci and linkage disequilibrium information and selected rs11623191 as the most promising candidate. The procedure is detailed in Supplementary Figure 1. For *IGHV3-66*, we selected the SNV rs6423677 within the gene that has been reported to impact gene usage in *IGH* chains.[7] To avoid bias induced by clonal expansion in memory B cells, we assessed the influence of SNVs on the usage of *IGHV* genes in IgD heavy chains that are predominantly expressed in naïve B cells. We genotyped 96 participants for SNVs, performed next-generation sequencing of IgD heavy chains expressed by their peripheral blood mononuclear cells, and then conducted univariate linear regression analyses (see Supplementary Methods and Supplementary Table 1). As shown in Fig. 2A, rs6423677-C and rs11623191-T significantly increased the usage of *IGHV3-66* and *IGHV3-53*, respectively. In the second part, we evaluated the effects of these two SNVs on $\log_2$-transformed antibody

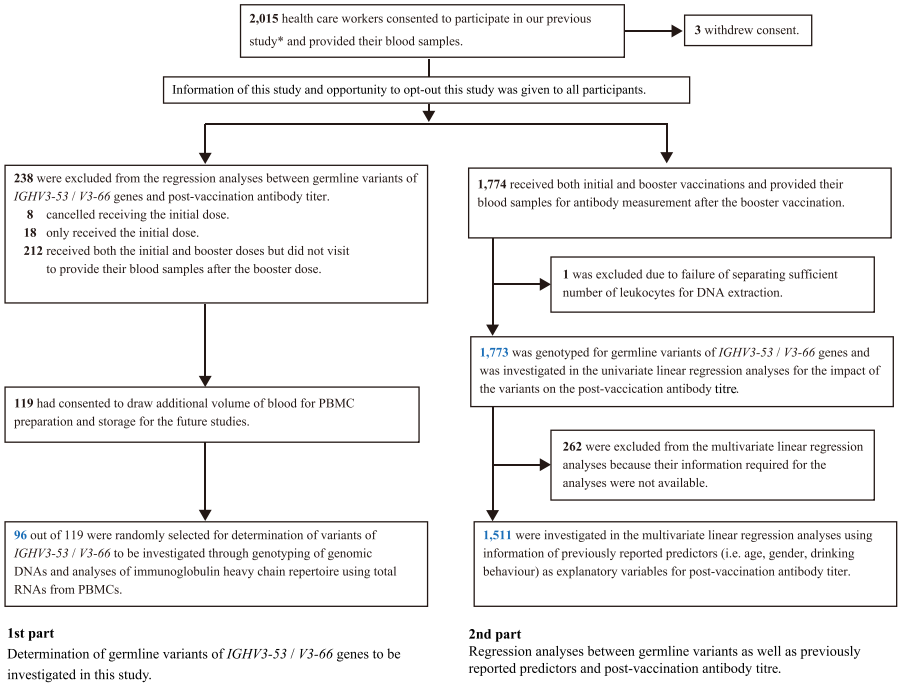

Fig. 1. Selection of the subjects in the two parts of the study. *Kageyama T. *et al.* [4].

A

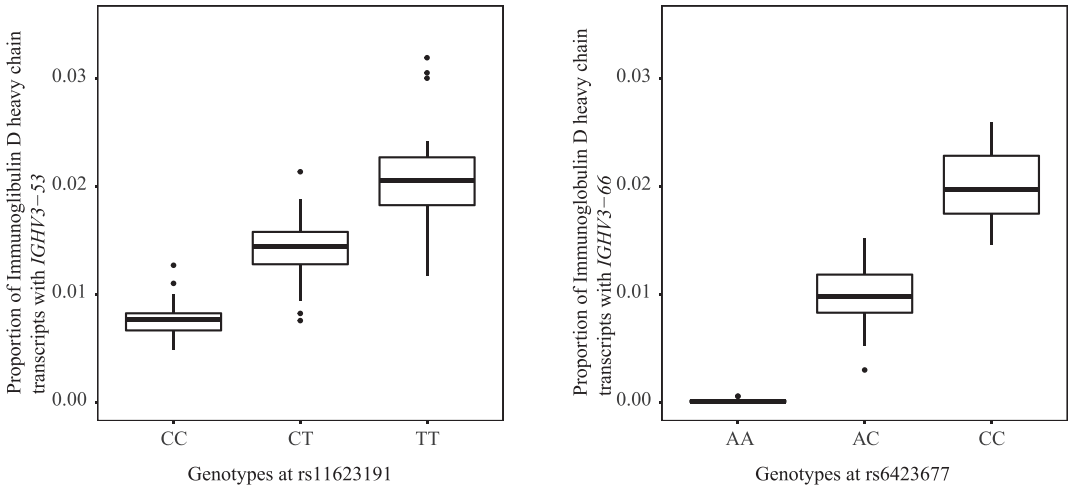

B

Variant	Genes	Alleles	Regression Coefficient [B]	95% confidence interval	*P* value
rs11623191	*IGHV3-53*	C/T	0.0021	-0.071– 0.075	0.96
rs6423677	*IGHV3-66*	A/C	0.080	0.0085– 0.15	0.028
2 SNVs[a]	*IGHV3-53/V3-66*	–	0.095	0.018– 0.17	0.015

C

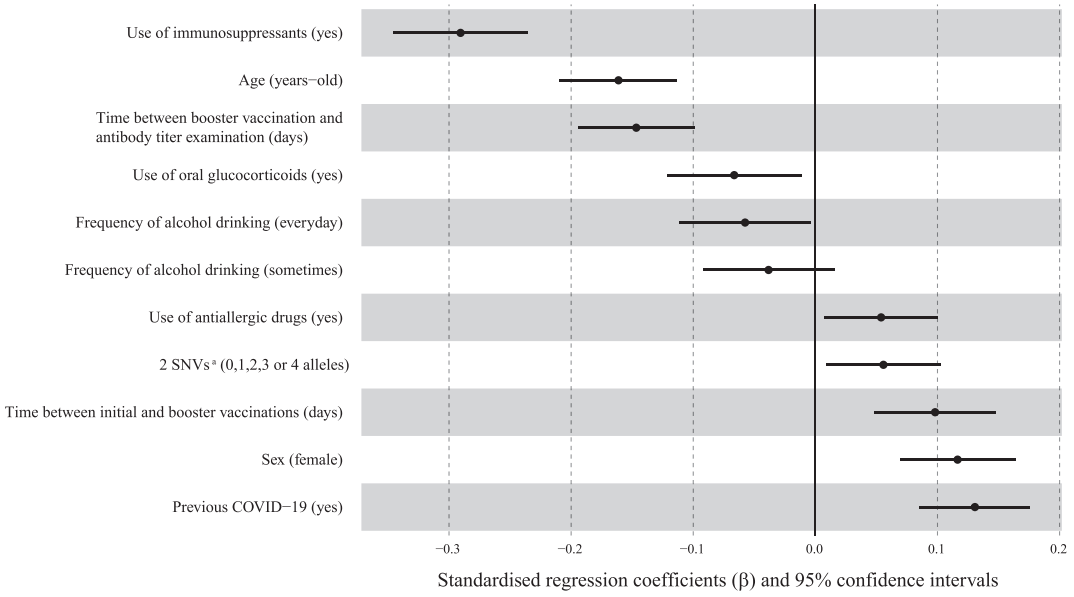

Fig. 2. A. Genotypes at single-nucleotide variants (SNVs) within immunoglobulin heavy variable (*IGHV*) genes and the usage of the genes in IgD heavy chain transcripts. Relationships between genotypes and gene usage in 96 subjects are shown for rs11623191 and *IGHV3-53* (left) and rs6423677 and *IGHV3-66* (right). Regression coefficients B, 95% confidence intervals, and *P* values in linear regression analyses were 0.010, (0.0093 – 0.011), and $<2.0 \times 10^{-16}$ for rs116231191 and 0.0065, (0.0056 – 0.0073), and $<2.0 \times 10^{-16}$ for rs6423677. B. Results of the univariate linear regression analysis for SNV alleles and the $\log_2$-transformed antibody titre against the severe acute respiratory syndrome-coronavirus 2 (SARS-CoV-2) spike (S) protein after booster vaccination with BNT162b2. For rs6423677 and rs11623191, the number of alleles associated with higher gene usage (C and T alleles, respectively) was used as the independent variable. The sum of the numbers of rs11623191-T and rs6423677-C alleles (0, 1, 2, 3, or 4) was used as the independent variable. C. Results of a multivariate linear regression analysis for various predictors of post-vaccination antibody titres against SARS-CoV-2 S protein. The sum of the number of rs6423677-C and rs11623191-T alleles as well as previously identified predictors of post-vaccination antibody titres (Kageyama T. *et al.*[4]) was used as explanatory variables. Dots and bars represent the standardised regression coefficient β and 95% confidence intervals for the variables, respectively.

titres against the anti-SARS-CoV-2 spike protein, which was correlated with the nAb titre [1] among 1,773 study participants after they received initial and booster vaccinations. As shown in Fig. 2B, rs6423677 had an impact on the antibody titre, and, as expected, the number of C alleles was a predictor of a higher value (regression coefficient [B] = 0.080, 95% confidence interval [CI], 0.0085–0.15). This relationship was not observed for rs11623191 (B = 0.0021, 95% CI, -0.071–0.075). Although not significant, the positive influence of the rs11623191-T allele on the antibody titre was consistently observed in subjects stratified by their genotypes at rs6423677 (Supplementary Table 2). Therefore, we evaluated the combined effects of these two SNVs. When the numbers of the rs6423677-C and rs11623191-T alleles were summed and used as independent variables, they appeared to predict a larger titre increase than rs6423677 alone (B = 0.095, 95% CI, 0.018–0.17; Fig. 2B).

A multivariate analysis was carried out for 1,511 (981 females and 530 males) out of 1,773 participants for whom information on predictive factors identified in our previous study,[4] including age, sex, and several factors such as medication and drinking behaviour, was also available. Again, a significant effect of the two SNV alleles on the antibody titre was observed (standardised coefficient [β] = 0.056, 95% CI, 0.0088–0.10; Fig. 2C). Interestingly, the influence of the two SNVs was not uniform among the participant subpopulations stratified by sex and/or age (Supplementary Figure 2 and Supplementary Table 3). The effect of the genotype of both *IGHV3-53* and *V3-66* on the usage of the genes in *IGH* transcripts was observed regardless of sex (Supplementary Figure 3). Therefore, we speculated that the difference in the genetic effect on the final antibody titre may have occurred after naïve B cells developed and matured.

Recently, it was reported that the plasma from BNT162b2 vaccine recipients has less neutralising ability against the Omicron variant compared to the ancestral strain.[8] Given the continuing pandemic and unpredictable breakthrough infections, refinement of preventive strategies for COVID-19, including the development of new vaccines against mutant strains and optimisation of vaccine programmes based on accurate risk prediction, is a public health issue. *IGHV3-53* has been found in potent candidates of broadly nAb (bnAb) for SARS-CoV-2 which are not affected by mutations in the receptor binding domain and cover circulating and emerging variants of SARS-CoV-2.[9] Thus, when the next-generation COVID-19 vaccine, which is designed using information on the epitopes of such bnAbs, becomes available, the significance of genotypes of *IGHV3-53* and its paralogue, *IGHV3-66*, might even increase.

Limitations regarding generalisability exist, because this was a single-site study of a single ethnic group. However, the low admixture of Japanese people and low cumulative incidence of COVID-19 (estimated to be as low as 0.36% - less than 0.45 million PCR confirmed cases in 125.8 million population) at the time of participant recruitment in Japan, might have contributed to the statistical power of detection. Considering the subsequent nationwide spread and progress of the pandemic vaccination program, future opportunities to study adult individuals who will be exposed to SARS-CoV-2 antigens for the first time in their lives will be limited.

This study is the first to reveal the influence of the germline variants of two *IGHV* genes on the antibody response against SARS-CoV-2 after BNT126b2 vaccination. As BNT126b2 is one of the first modified mRNA vaccines used in the real world, further investigations must be carried out to determine the genetic factors associated with the high efficacy of the vaccine or susceptibility to its side effects.

Author contributions

H.I., K. Yokote, H.N., and Y.O. conceived the study. Y.O. and Y.M. designed the study and wrote the main draft of the manuscript. Y.M., T.K., S.T., T.T., K.M., H.I., and H.H. collected samples and clinical information. Y.M. performed the next-generation sequencing and genotyping. Y.M., K. Yamazaki, and Y.O. performed statistical analyses. All authors contributed to and reviewed the final manuscript.

Data availability

The genotypes at rs6423677 and rs11623191, as well as post-vaccination antibody titres of the study participants, are available from the corresponding author upon request. There are restrictions on the availability of clinical information from the study participants for ethical reasons.

Declaration of Competing Interest

None.

Acknowledgements

We thank all the participants of this study. This study was supported by JSPS KAKENHI (grant number 22H03329 to Y. O.), the Chiba University IMO 2021 Support Program for KAKENHI (to Y. O.), and a donation to Chiba University Hospital and Future Medicine Funds at Chiba University.

Supplementary materials

Supplementary material associated with this article can be found, in the online version, at doi:10.1016/j.jinf.2022.10.015.

References

1. Vivaldi G, Jolliffe D A, Faustini S, Shields A M, Holt H, Perdek N, et al. Correlation between post-vaccination anti-spike antibody titres and protection against breakthrough SARS-CoV-2 infection: a population-based longitudinal study. *J Infect Dis* 2022 Online ahead of print.
2. Bergwerk M, Gonen T, Lustig Y, Amit S, Lipsitch M, Cohen C, et al. Covid-19 breakthrough infections in vaccinated health care workers. *N Engl J Med* 2021;**385**:1474–84.
3. Terpos E, Trougakos I P, Apostolakou F, Charitaki I, Sklirou A D, Mavrianou N, et al. Age-dependent and gender-dependent antibody responses against SARS-CoV-2 in health workers and octogenarians after vaccination with the BNT162b2 mRNA vaccine. *Am J Hematol* 2021;**96**:E257–9.
4. Kageyama T, Ikeda K, Tanaka S, Taniguchi T, Igari H, Onouchi Y, et al. Antibody responses to BNT162b2 mRNA COVID-19 vaccine and their predictors among healthcare workers in a tertiary referral hospital in Japan. *Clin Microbiol Infect* 2021;**27** 1861.e1-1861.e5. doi:10.1016/j.cmi.2021.07.042.
5. Barnes C O, West A P Jr., Huey-Tubman K E, Hoffmann M A G, Sharaf N G, Hoffman P R, et al. Structures of human antibodies bound to SARS–CoV-2 spike reveal common epitopes and recurrent features of antibodies. *Cell* 2020;**182**:828–42.
6. Zhang Q, Ju B, Ge J, Chan J F, Cheng L, Wang R, et al. Potent and protective IGHV3-53/3-66 public antibodies and their shared escape mutant on the spike of SARS-CoV-2. *Nat Commun* 2021;**12**:4210.
7. Johnson T A, Mashimo Y, Wu J Y, Yoon D, Hata A, Kubo M, et al. Association of an IGHV3-66 gene variant with Kawasaki disease. *J Hum Genet* 2021;**66**:475–89.
8. Cele S, Jackson L, Khoury D S, Khan K, Moyo-Gwete T, Tegally H, et al. Omicron extensively but incompletely escapes Pfizer BNT162b2 neutralization. *Nature* 2022;**602**:654–6.
9. Vanshylla K, Fan C, Wunsch M, Poopalasingam N, Meijers M, Kreer C, et al. Discovery of ultrapotent broadly neutralizing antibodies from SARS-CoV-2 elite neutralizers. *Cell Host Microbe* 2022;**30**:69–82.

Yoichi Mashimo, Keiko Yamazaki
Department of Public Health, Chiba University Graduate School of Medicine, 1-8-1 Inohana, Chuo, Chiba, Chiba 260-8670, Japan

Takahiro Kageyama, Shigeru Tanaka
Department of Allergy and Clinical Immunology, Chiba University Graduate School of Medicine, 1-8-1 Inohana, Chuo, Chiba, Chiba 260-8670, Japan

Toshibumi Taniguchi
Department of Infectious Diseases, Chiba University Hospital, 1-8-1 Inohana, Chuo, Chiba, Chiba 260-8670, Japan
Chiba University Hospital COVID-19 Vaccine Center, 1-8-1 Inohana, Chuo, Chiba, Chiba 260-8670, Japan

Kazuyuki Matsushita
Division of Laboratory Medicine, Chiba University Hospital, 1-8-1 Inohana, Chuo, Chiba, Chiba 260-8670, Japan

Hidetoshi Igari
Department of Infectious Diseases, Chiba University Hospital, 1-8-1 Inohana, Chuo, Chiba, Chiba 260-8670, Japan
Chiba University Hospital COVID-19 Vaccine Center, 1-8-1 Inohana, Chuo, Chiba, Chiba 260-8670, Japan

Hideki Hanaoka
Clinical Research Center, Chiba University Hospital, 1-8-1 Inohana, Chuo, Chiba, Chiba 260-8670, Japan

Koutaro Yokote
Department of Endocrinology, Hematology and Gerontology, Chiba University Graduate School of Medicine, 1-8-1 Inohana, Chuo, Chiba, Chiba 260-8670, Japan

Hiroshi Nakajima
Department of Allergy and Clinical Immunology, Chiba University Graduate School of Medicine, 1-8-1 Inohana, Chuo, Chiba, Chiba 260-8670, Japan
Chiba University Hospital COVID-19 Vaccine Center, 1-8-1 Inohana, Chuo, Chiba, Chiba 260-8670, Japan

Yoshihiro Onouchi*
Department of Public Health, Chiba University Graduate School of Medicine, 1-8-1 Inohana, Chuo, Chiba, Chiba 260-8670, Japan

*Corresponding author at: Department of Public Health, Chiba University Graduate School of Medicine, 1-8-1 Inohana, Chuo, Chiba, Chiba 260-8670, Japan.
E-mail address: onouchy@chiba-u.jp (Y. Onouchi)

Accepted 13 October 2022
Available online 2 November 2022

https://doi.org/10.1016/j.jinf.2022.10.015

Persistence of monkeypox virus DNA in clinical specimens

Dear Editor,

Recently, Orviz et al. [1] reported the monkeypox outbreak in Madrid of Spain which indicated accurate clinical and virological aspects of the disease outside endemic areas are needed, particularly for early diagnosis in clinic. In early May 2022, the re-emerging outbreak of a resting zoonotic virus, monkeypox virus (MPXV) (the genus *Orthopoxvirus*, the family *Poxviridae*) which was originally reported in humans in central Africa in 1970, attracts great concerns of global public authorities. As of August 29, 2022, MPXV has expanded to 99 countries, and over 48,000 confirmed cases recorded according to the latest CDC data. Clinically, monkeypox (MPX) cases are manifested mainly with skin/mucosal lesions at variable sites including genital, oropharyngeal or perianal areas. Men who have sex with men (MSM) are the mostly affected population. The confirmation of MPXV infection relies on detection of virus DNA in various body fluids. Recent studies reported the shedding of MPXV DNA in various samples [2,3]. However, the information of how frequently the MPXV DNA can be detected in variable clinical samples and how long it remains detectable are still very limited. To understand the dynamics of the early stages of MPXV infection is essential for clinical diagnostic testing and prevention interventions, in that, available observations evidence is only based on case reports.

In this study, we collected the laboratory detection data of MPX cases from the archived reports which included clear and consistent methods, and predict the duration of detecting MPXV DNA in various body fluids through mathematics model analysis. A total of 62 archived MPX cases (49 males, 13 females; median age 31y, range 0.4–50y) from 22 observation studies were included, of which 51 were non-HIV infected MPX cases (38 males, 13 females; median age 32y, range 0.4–49y), and remained 11 were HIV-infected MPX cases (11 males; median age 33y, range 26-50y) (Appendix Table 1). The main clinical manifestations of 62 MPX cases were rash (n=44, 70.97%), fever (n=28, 45.16%), lymphadenopathy (n=22, 35.48%), myalgia (n=11, 17.74%), headache (n=9, 14.52%), fatigue (n=4, 6.45%) and chills (n=4, 6.45%). Among the non-HIV infected MPX cases, skin rash were the most frequent clinical symptoms (n=34, 66.67%) (6-17 days, median 13d) followed by fever (n=23, 45.10%) (2-5d, median 3d), lymphadenopathy (n=19, 37.25%), myalgia (n=9, 17.65%), headache (n=9, 17.65%), chills (n=4, 7.84%) and fatigue (n=3, 5.88%). However, within the 11 HIV-infected MPX cases, the proportion of MPX with the symptoms of skin rash reach to 90.91%, no case with headache or chills (Appendix Table 1, Appendix Table 2).

We collected the molecular detection data of MPXV by PCR in 62 MPX cases. The parametric Weibull regression models (AFT) was employed to estimate the time until the loss of MPXV DNA detection in each body fluid and reported findings in medians and 95th percentiles using R software version 3.6.1 with flexsurv, survival, and survminer packages. Additional Lnorm and gamma models were used as to evaluate the sensitivity and stability of Weibull regression models. The time until loss of MPXV DNA detection in variable clinical samples was defined as the number of days after the first negative PCR result after the onset of symptoms. For the cases with intermittent results of MPXV detection, we used the date of the first negative result after the final recorded positive PCR results.

A total of 269 specimens of 62 MPX cases were included in this modeling analysis, including 23 urine samples (8.55%), 19 rash or skin lesions samples (7.06%), 17 nasopharyngeal swabs samples (6.32%),17 rectal swabs samples (6.32%), 16 semen samples (5.95%), 15 blood samples (5.58%), 14 fecal samples (5.20%) and 14 saliva samples (5.20%). The results of Weibull models showed that the median time of MPXV DNA persistence ranged from 5.7d to 13.5d in the nasopharynx swabs (8.6d, 95% CI 6.94-10.4d), feces (9.4d, 95% CI 7.15-12.4d), semen (11.4d, 95% CI 8.58-14.9d), urine (13.5d, 95% CI 10.3-17.5d), rash or skin lesions (5.7d, 95% CI 3.86-8.1d), saliva (8.9d, 95% CI 7.14-11.2d), blood (10.6d, 95% CI 6.37-16.9d), and rectal swabs (8.3d, 95% CI 6.58-10.7d) samples, while 11.3d (95% CI 9.88-13.1d) when using all samples data (Fig. 1, Appendix Figure 1). The additional comparisons of sensitivity and stability among Weibull, Lnorm, and gamma models showed no differences among them ($p<0.05$) (Appendix Table 3; Appendix Figure 2, 3).

Pettke et al. reported positive PCR results in semen samples from cases who recovered from MPXV infection for 54 d at maximum [3]. Nörz et al. found the prolonged presence of MPXV DNA in rash or skin lesions and blood samples [4]. In this study, we estimated the time for MPX cases to clear MPXV DNA in the acute phase of infection through an AFT-based modeling study. We found that the median time for semen samples from cases was 11.4d (95%

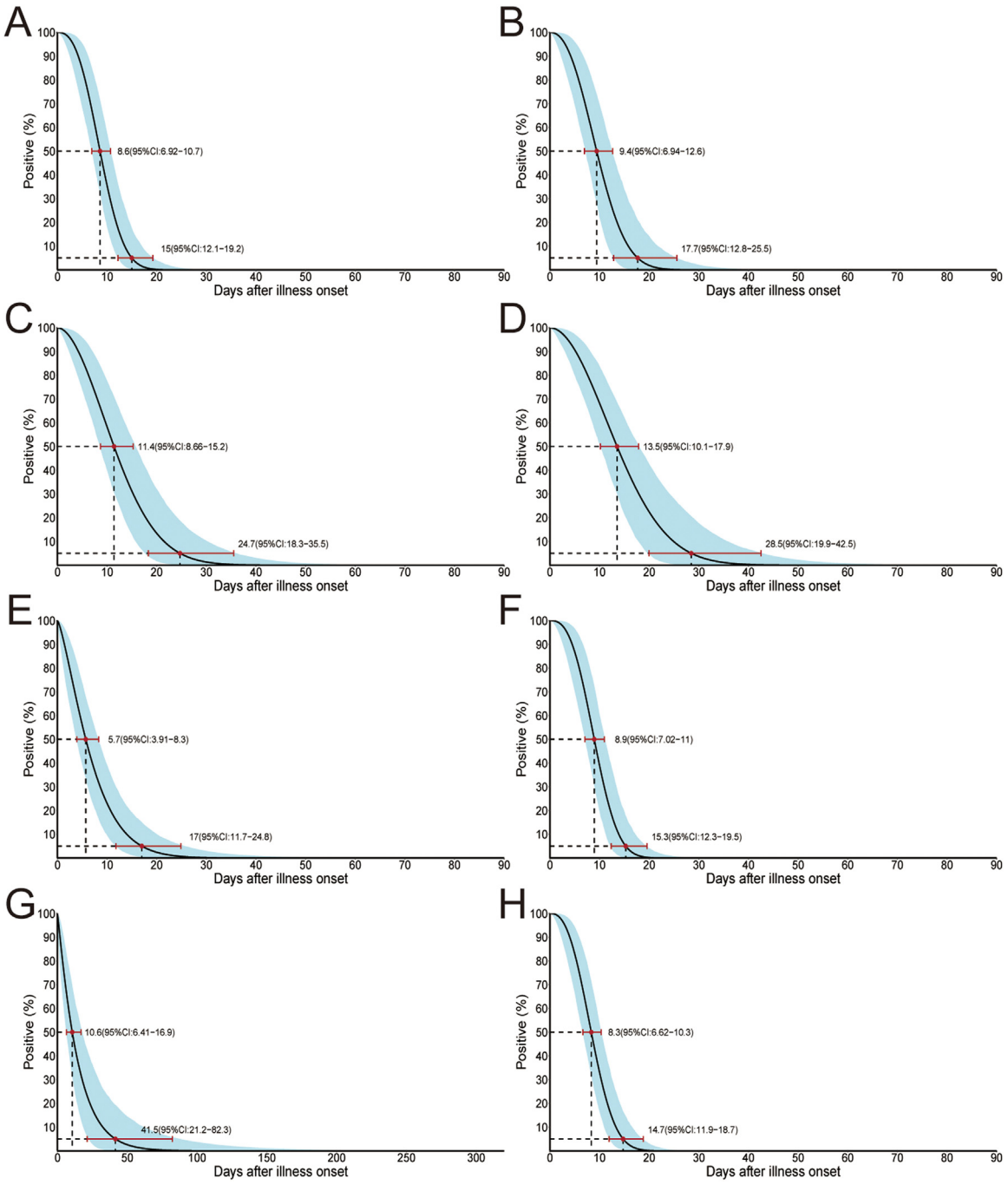

Fig. 1. Time until clearance of monkeypox DNA in nasopharyngeal swabs(A), feces(B), semen(C), urine(D), rash or skin lesions(E), saliva(F), blood(G),and rectal swabs(H) samples among MPX patients, as estimated with the use of Weibull regression. The medians and 95th percentiles of the time until the loss of detection are indicated; bars and shading indicate 95% CIs.

CI 8.58–14.9d) and the 95th percentile was 24.7d (95% CI 17.8–35.5d). Therefore, detection of MPXV DNA for cases in semen samples at the 54th day after illness onset should be rare, beyond the 95th percentile limit. Similarly, the detection of MPXV DNA in rash or skin lesions or blood samples from Nörz et al. were also close to the 95th percentile limit as we estimated (14.7d, 95% CI 12.0-18.2d; 41.5d, 95% CI 23.2-84.0d).

The fitted median time in urine (13.5d) was the longest, followed by semen (11.4d) and blood (10.6d) (Appendix Table 3). We found that there was no difference in the median time fitted by the three models (Appendix Table 3). In addition, the estimated time until the loss of DNA detection in various clinical samples was consistent with previous findings in case reports [5–7].

Our study hhave limitations. First, the infectivity of the specimens was not estimated. We focused on estimating the duration of MPXV DNA in various body fluids among MPX cases but did not imply the existence of infectious virus particles. Second, the date of first samplings may be deviated from the date of symptoms onset. We defined the time until loss of MPXV DNA detection in each specimen as the number of days between the day after illness onset and the day of the first negative PCR result, which means that the median and 95th percentile we estimated were shorter than expected because of the uncertainty of incubation time. Third, time estimated in this study may not be generalizable to all infections with MPXV, e.g. asymptomatic cases.

Our results provide a reference for the appropriate time for MPXV detection in clinic, which should be considered for clinical diagnostic recommendations, as well as control and prevention of MPXV onward transmission.

Authors' contributions

Study design: ZW Li, GX Zhu and JF Sun; Data analysis: ZW Li, XX Li, YL Chen and QQ Ruan; Administrative, technical, or material support: ZW Li, XX Li, YL Chen, QQ Ruan, XR Huang, HM Chen, XM Hu, GX Zhu and JF Sun; Critical revision of manuscript: ZW Li,QQ Ruan, GX Zhu and JF Sun. All authors reviewed and approved the final manuscript.

Funding

This work was supported by grants The National Key Research and Development Program of China (2020YFC1200100) and the Guangzhou Science and Technology Program (201904010012), as well as the National Natural Science Foundation of China (12171116).

Availability of data and materials

The code used for the model is available from the corresponding author.

Conflict of interest

All the authors declare that they have no conflicts of interest.

Supplementary materials

Supplementary material associated with this article can be found, in the online version, at doi:10.1016/j.jinf.2022.10.013.

References

1. Orviz E, Negredo A, Ayerdi O, Vázquez A, Muñoz-Gomez A, Monzón S, et al. Monkeypox outbreak in Madrid (Spain): clinical and virological aspects. *J Infect* 2022;**85**(4):412–17. doi:10.1016/j.jinf.2022.07.005.
2. Peiró-Mestres A, Fuertes I, Camprubí-Ferrer D, Marcos M, Vilella A, Navarro M, et al. Frequent detection of monkeypox virus DNA in saliva, semen, and other clinical samples from 12 patients, Barcelona, Spain, May to June 2022. *Eurosurveillance.* 2022;**27**(28):2200503. doi:10.2807/1560-7917.ES.2022.27.28.2200503.
3. Pettke A, Filén F, Widgren K, Jacks A, Glans H, Andreasson S, et al. Ten-week follow-up of monkeypox case-patient, Sweden, 2022. *Emerging Infectious Diseases* 2022;**28**(10):2074–7. doi:10.3201/eid2810.221107.
4. Nörz D, Brehm TT, Tang HT, Grewe I, Hermanussen L, Matthews H, et al. Clinical characteristics and comparison of longitudinal qPCR results from different specimen types in a cohort of ambulatory and hospitalized patients infected with monkeypox virus. *Journal of Clinical Virology* 2022;**155**:105254. doi:10.1016/j.jcv.2022.105254.
5. Nolasco S, Vitale F, Geremia A, Tramuto F, Maida C, Sciuto A, et al. First case of monkeypox virus, SARS-CoV-2 and HIV co-infection. *Journal of Infection* 2022 In press S0163-4453–0.. doi:10.1016/j.jinf.2022.08.014.
6. Mazzotta V, Mondi A, Carletti F, Carletti F, Baldini F, Meschi S, et al. Ocular involvement in monkeypox: description of an unusual presentation during the current outbreak. *Journal of Infection* 2022;**85**(5):573–607. doi:10.1016/j.jinf.2022.08.011.
7. Thornhill JP, Barkati S, Walmsley S, Rockstroh J, Antinori A, Harrison L. Monkeypox Virus Infection in Humans across 16 Countries - April-June 2022. *New England Journal of Medicine* 2022;**387**(8):679–91. doi:10.1056/NEJMoa2207323.

Zhaowan Li[1]
Guilin University of Electronic Technology, Guilin
Guangdong Provincial Center for Disease Control and Prevention, Guangzhou, China;Guangdong Workstation for Emerging Infectious Disease Control and Prevention, Chinese Academy of Medical Sciences, Beijing, China

Xin Xin Li[1]
Guangdong Provincial Center for Disease Control and Prevention, Guangzhou, China;Guangdong Workstation for Emerging Infectious Disease Control and Prevention, Chinese Academy of Medical Sciences, Beijing, China
Jinan University, Guangzhou, China

Yueling Chen[1]
Guangdong Provincial Center for Disease Control and Prevention, Guangzhou, China;Guangdong Workstation for Emerging Infectious Disease Control and Prevention, Chinese Academy of Medical Sciences, Beijing, China
Guangdong Pharmaceutical University, Guangzhou, China

Qianqian Ruan
Guangdong Provincial Center for Disease Control and Prevention, Guangzhou, China;Guangdong Workstation for Emerging Infectious Disease Control and Prevention, Chinese Academy of Medical Sciences, Beijing, China
Sun Yat-sen University, Guangzhou, China

Xiaorong Huang
Guangdong Provincial Center for Disease Control and Prevention, Guangzhou, China;Guangdong Workstation for Emerging Infectious Disease Control and Prevention, Chinese Academy of Medical Sciences, Beijing, China
Southern Medical University, Guangzhou, China

Guanghu Zhu
Guilin University of Electronic Technology, Guilin

Jiufeng Sun*
Guilin University of Electronic Technology, Guilin
Guangdong Provincial Center for Disease Control and Prevention, Guangzhou, China;Guangdong Workstation for Emerging Infectious Disease Control and Prevention, Chinese Academy of Medical Sciences, Beijing, China
Jinan University, Guangzhou, China
Guangdong Pharmaceutical University, Guangzhou, China
Sun Yat-sen University, Guangzhou, China
Southern Medical University, Guangzhou, China

*Corresponding author at: Guangdong Provincial Center for Disease Control and Prevention, Guangzhou, 511430, PR China.
E-mail address: sunjiuf@163.com (J. Sun)

[1] These authors contributed equally to this work (ZW Li, XX Li, YL Chen)

Accepted 11 October 2022
Available online 17 October 2022

https://doi.org/10.1016/j.jinf.2022.10.013

Efficacy and safety of fluvoxamine for the treatment of COVID-19 patients: A systematic review and meta-analysis

Dear Editor,

We read with great interest the recent article by Qian et al. that reported the efficacy of paxlovid for the treatment of COVID-19 patients.[1] However, the cost of currently approved oral antivirals, paxlovid and molnupiravir, restricts their access in developing countries.[2,3] Therefore, it is crucial to find affordable, widely ac-

Table 1
Characteristics of included studies.

Sr No	Author, year	Study Design	Country	Sample size	Age	Sex	Population	Intervention	Comparator
1	Lenze 2020	Phase 2, Double-Blind RCT	USA	152	46.0±13.0	Male: 43 (28.3) Female: 109 (71.7)	Adults with SARS-CoV-2 infection confirmed by polymerase chain reaction assay and who were symptomatic within 7 days of the first dose of study medication	Participants received a dose of 50 mg of fluvoxamine immediately after inclusion, then for 2 days at a dose of 100 mg twice daily as tolerated, and then increasing to a dose of 100 mg 3 times daily as tolerated through day 15 then stopped.	Participants received a dose of 50 mg of placebo immediately after inclusion, then for 2 days at a dose of 100 mg twice daily as tolerated, and then increasing to a dose of 100 mg 3 times daily as tolerated through day 15 then stopped.
2	STOP COVID 2, unpublished	Phase 3, triple-blind RCT	USA and Canada	547	47 (IQR 40-55) for Fluvoxamine group, 48 (IQR 41-56) for control	Male: 208 (38) Female: 339 (62)	Patients with age greater than 30 years who are unvaccinated and positive PCR result within 6 days of symptoms onset and a criterion of high risk	100 mg Fluvoxamine twice a day for 15 days	Placebo
3	Calusic 2021	Prospective cohort study	Croatia	102	NA	Male: 68 (66.7) Female: 34 (33.3)	Patients over age 18, with positive SARS-COV2 PCR test and acute COVID-19 infection requiring ICU admission	100 mg Fluvoxamine three times a day for 15 days, then taper off to 50 mg for the next 7 days	Standard care
4	Seftel 2021	Prospective cohort study	USA	113	42 (IQR 33-56)	Male: 85(75) Female: 28 (25)	Patients with positive COVID-19 antigen cards test coupled with PCR confirmation who consented to treatment with fluvoxamine	Fluvoxamine at a 50- to 100-mg loading dose, then 50 mg twice daily for 14 days	Standard care
5	Seo 2022	Phase 2 Single-blind RCT	Korea	52	53 (IQR 43.3-60)	Male: 31 (60) Female: 21 (40)	Patients over 18 with symptoms consistent with COVID-19 with onset less than 7 days after randomization and had positive RT-PCR results within 3 days of randomization	50 mg of fluvoxamine on day 1, then an increased dose of 100 mg twice daily, as tolerated, until discharge from the CTC (about 10 days).	50 mg of placebo (ursodeoxycholate) on day 1, then an increased dose of 100 mg twice daily, as tolerated, until discharge from the CTC (about 10 days).
6	Bramante 2022	Phase 3, Double-Blind RCT	USA	661	46 (IQR 38-53) for the intervention group, 43 (IQR 37-53) for the control group	Male: 273 (41.3) Female: 388 (58.7)	Patients from age 30 to 85 years; with a body-mass index (BMI) associated with overweight or obesity; proof of SARS-CoV-2 infection within the past 3 days; and the onset of symptoms within 7 days before randomization*	Fluvoxamine 50mg twice daily alone for 15 days or fluvoxamine 50 mg twice daily plus metformin up to 1500 mg for 15 days	Placebo or metformin up to 1500 mg for 15 days alone
7	Reis 2021	Phase 3, Double-Blind RCT	Brazil	1497	50 (IQR 18-102)	Male: 635 (42.4) Female: 862 (57.5)	Patients over 18 presenting to the OPD with symptoms consistent with COVID 19 or a positive SARS-COV2 antigen test at screening or 7 days within symptoms onset	Fluvoxamine# 100 mg twice a day	Placebo 100 mg twice a day
8	Pineda 2022	Prospective cohort study	Honduras	657	48.1 (mean)	Male: 330 (50.2) Female: 327 (49.8)	Patients fifteen years of age or older, with mild to moderate COVID-19 with a positive SARS-CoV-2 antigen or RT-PCR	Fluvoxamine 50 mg orally twice daily for three days and titrated up to 100 mg two or three times a day depending on patient tolerance and disease severity to complete a fourteen-day course	Standard care

* The six trial groups were assigned to receive the following drugs or combinations of drugs: group 1, metformin plus fluvoxamine; group 2, metformin plus ivermectin; group 3, metformin plus placebo; group 4, placebo plus fluvoxamine; group 5, placebo plus ivermectin; and group 6, placebo plus placebo.

741 patients received fluvoxamine, 756 were allocated to receive placebo while 1826 were allocated to other treatment groups like hydroxycholorquine, liponavir-ritonavir, previous placebo, metformin, ivermectin, doxazosin or interferon lambda.

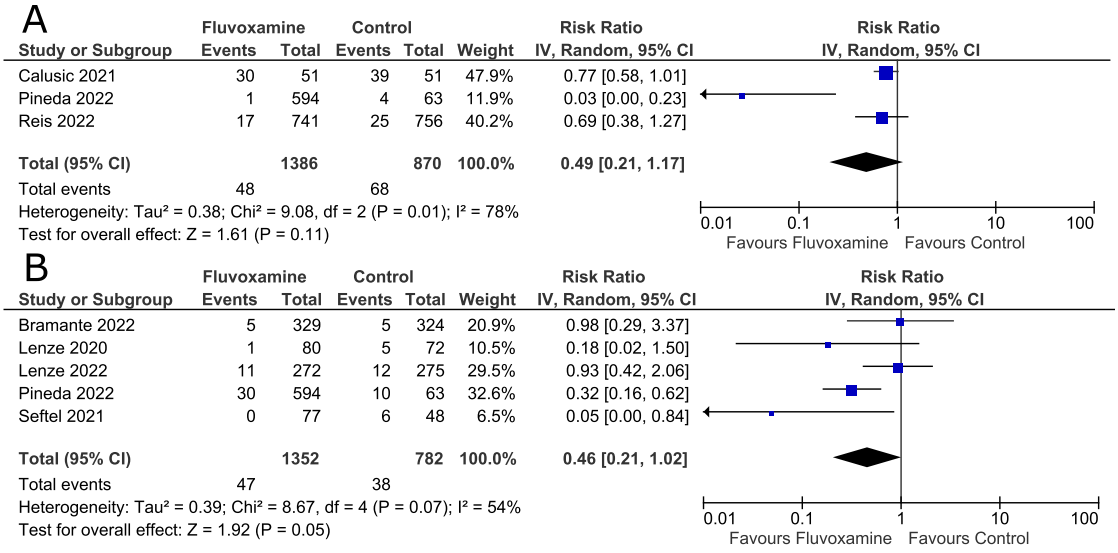

Fig. 1. Effect of fluvoxamine on: (A) all-cause mortality and (B) hospitalization in COVID-19 patients.

cessible, and potent treatments for COVID-19. Particularly appealing is the idea of repurposing currently available medications that are widely accessible and have known safety characteristics.[4]

Fluvoxamine, a widely available, inexpensive selective serotonin reuptake inhibitors (SSRIs), has shown potential for treating COVID-19 as an early outpatient treatment, despite many recommended repurposed medicines failing.[5] The underlying mechanism of the effect of fluvoxamine in COVID-19 patients is currently unclear, but it is thought to be multifactorial. In addition to functioning as an SSRI, fluvoxamine has a strong affinity for the σ-1 receptor (S1R), which is believed to be the mechanism by which it achieves its anti-inflammatory and immunomodulatory properties. S1R stimulation is thought to have an immunomodulatory effect by lowering stress in the endoplasmic reticulum brought on by viral replication, which in turn lowers the generation of inflammatory cytokines.[6] In order to combine the existing data and assess the efficiency and safety of fluvoxamine as a treatment for COVID-19, we undertook this updated meta-analysis.

Our pre-registered meta-analysis (PROSPERO CRD42022361850) was conducted in accordance with the Preferred Reporting Items for Systematic Reviews and Meta-Analyses (PRISMA) guidelines. PubMed, Embase, the Cochrane Library and ClinicalTrials.gov were searched from inception to September 2022 using a search strategy consisting of terms related to “fluvoxamine”, “SSRIs” and “COVID-19”. The reference lists of the relevant records were also checked. All randomized controlled trials (RCTs) and comparative observational studies evaluating fluvoxamine use for the treatment of COVID-19 patients were included in this review. After screening, five RCTs,[7–11] one quasi-randomized trial[12] and two prospective cohort studies[13,14] were found to be eligible for our meta-analysis. Table 1 provides a summary of the features of the included studies. For quality assessments of the RCTs, we used the revised Cochrane Risk of Bias tool (RoB2) (Supplementary Fig. 1) while for the non-randomized studies, we used the New-Castle-Ottawa scale (NOS) (Supplementary Table 1). Our primary outcome was all-cause mortality and the secondary outcomes were the risk of hospitalization and COVID-19 progression, and the incidence of adverse events. The meta-analysis was performed using RevMan 5.4 with risk ratio (RR), with corresponding 95% confidence interval (CI), as the effect measure.

Our findings demonstrated that fluvoxamine was associated with a nonsignificant reduction in the risk of mortality (RR 0.49; 95% CI: 0.21-1.17; I^2=78%; Fig. 1A) and hospitalization (RR 0.46; 95% CI: 0.21-1.02; I^2=54%; Fig. 1B) in COVID-19 patients. Fluvoxamine did not reduce the risk of COVID-19 progression (RR 0.74; 95% CI: 0.21-2.57; I^2=44%; Supplementary Fig. 2). The incidence of adverse events did not differ significantly between the fluvoxamine and the control groups (RR 0.94; 95% CI: 0.79-1.11; I^2=0%; Supplementary Fig. 3). In one study, one patient receiving fluvoxamine reported a serious adverse event as compared to six patients in the control group.[10] In sensitivity analyses by excluding Bramante et al. in which patients in the control group received metformin,[11] a drug known to be beneficial for COVID-19, the results for hospitalization (RR 0.37; 95% CI: 0.14-0.95; I^2=58%) became significant in favor of fluvoxamine but the outcome of COVID-19 progression (RR: 0.33; 95% CI: 0.03-4.35; I^2=57%) remained non-significant.

To the best of our knowledge, this is the largest meta-analysis to date to evaluate the potential effectiveness of fluvoxamine as a COVID-19 treatment. Our findings showed that fluvoxamine use was associated with a large but statistically non-significant reduction in mortality and hospitalization rates in patients with COVID-19 without increasing the incidence of adverse events. Our findings agree with a previous meta-analysis which showed that fluvoxamine did not decrease the risk of mortality or hospitalization.[15] However, this meta-analysis was based on only three studies and therefore, was relatively underpowered. After excluding a trial with an active comparator, we showed that fluvoxamine did reduce the risk of hospitalization in contrast with the previous meta-analyses which did not find any benefits of fluvoxamine use.[15,16] Moreover, the TOGETHER trial found that fluvoxamine decreased the risk of hospitalization in high-risk COVID-19 patients.[9] This suggests that fluvoxamine may not be effective for every patient on a routine basis and that outpatient populations with an elevated risk of comorbidities must be identified to maximize the benefits of fluvoxamine therapy.[9]

Fluvoxamine may be beneficial for treating COVID-19 because of its easy accessibility and affordable price. A 10-day regimen of fluvoxamine costs about $4; hence, in low-income countries, it is a cost-effective treatment for COVID-19 if compared with other approved oral antivirals, including paxlovid and molnupiravir.[2]

Due to the small number of available trials and the inclusion of observational studies, our study has several limitations, including low statistical power and a risk of confounding bias. Additionally, we could not assess long-term outcomes as they were not reported by the studies.

In conclusion, treatment with fluvoxamine did not decrease mortality and hospitalization rates in patients with COVID-19 but due to the imprecise CIs, a large possible benefit cannot be ruled out. The sensitivity analysis showing a statistically significant reduction in risk of hospitalization further reinforces this point and is highly encouraging. To strengthen these findings, further large-scale RCTs, especially for longer-term outcomes, are needed.

Financial support

No financial support was received for this study.

Availability of data

The data that support the findings of this study are available from the corresponding author, HAC, upon reasonable request.

Declaration of Competing Interest

The authors report no relationships that could be construed as a conflict of interest.

Acknowledgements

Not applicable.

Supplementary materials

Supplementary material associated with this article can be found, in the online version, at doi:10.1016/j.jinf.2022.10.012.

References

1. Qian Z., Pengfei M., Mingwei W., Yongran C., Mengyun Z., Lan Ye, et al. Efficacy and safety of Paxlovid for COVID-19:a meta-analysis. *J Infect* 2022. doi:10.1016/j.jinf.2022.09.027.
2. Junzheng W., Jacob L., Leah E., Andrew H.. Minimum manufacturing costs, national prices, and estimated global availability of new repurposed therapies for Coronavirus Disease 2019. *Open Forum Infect Dis* 2022;**9**(1). doi:10.1093/ofid/ofab581.
3. Maurish F., Saleha A., Junaid S., Abia S., Cheema H.A.. Efficacy and safety of molnupiravir for COVID-19 patients. *Eur J Intern Med* 2022;**102**:118–21. doi:10.1016/j.ejim.2022.05.024.
4. Rayner Craig R., Louis D., Park Jay J.H., Decloedt Eric H., Cotton Mark F., Vis N., et al. Accelerating clinical evaluation of repurposed combination therapies for COVID-19. *Am J Trop Med Hyg* 2020;**103**(4):1364–6. doi:10.4269/ajtmh.20-0995.
5. Sukhatme Vikas P., Reiersen Angela M., Vayttaden Sharat J., Sukhatme Vidula V.. Fluvoxamine: a review of its mechanism of action and its role in COVID-19. *Front Pharmacol* 2021;**12**:763. doi:10.3389/fphar.2021.652688.
6. Tamaki I., Yuko F., Kenji H.. Interaction of new antidepressants with sigma-1 receptor chaperones and their potentiation of neurite outgrowth in PC12 cells. *Eur J Pharmacol* 2014;**727**(1):167–73. doi:10.1016/j.ejphar.2014.01.064.
7. L. Eric, L. St. Fluvoxamine for early treatment of COVID-19: the STOP COVID 2 trial. ClinicalTrials.Gov. Available at https://clinicaltrials.gov/ct2/show/NCT04668950. Accessed October 4, 2022, 2022.
8. Hyeonji S., Haein K., Seongman B., Seonghee P., Hyemin C., Sup S.H., et al. Fluvoxamine treatment of patients with symptomatic COVID-19 in a community treatment center: a preliminary result of randomized controlled trial. *Infect Chemother* 2022;**54**(1):102. doi:10.3947/ic.2021.0142.
9. Gilmar R., Augusto S.M.S.E., Medeiros S.D.C., Lehana T., Cruz M.A., Santiago F.T., et al. Effect of early treatment with fluvoxamine on risk of emergency care and hospitalisation among patients with COVID-19: the TOGETHER randomised, platform clinical trial. *Lancet Glob Health* 2022;**10**(1):e42–51. doi:10.1016/S2214-109X(21)00448-4.
10. Lenze E.J., Caline M., Zorumski C.F., Angela S., Julie S., Nicol Ginger E., et al. Fluvoxamine vs placebo and clinical deterioration in outpatients with symptomatic COVID-19: a randomized clinical trial. *JAMA* 2020;**324**(22):2292–300. doi:10.1001/jama.2020.22760.
11. Bramante Carolyn T., Huling Jared D., Tignanelli Christopher J., Buse John B., Liebovitz David M., Nicklas Jacinda M., et al. Randomized trial of metformin, ivermectin, and fluvoxamine for Covid-19. *N Engl J Med* 2022;**387**(7):599–610. doi:10.1056/NEJMoa2201662.
12. David S., Boulware D.R.. Prospective cohort of fluvoxamine for early treatment of Coronavirus Disease 19. *Open Forum Infect Dis* 2021;**8**(2):ofab050. doi:10.1093/ofid/ofab050.
13. Estela P., Jarmanjeet S., Vargas P.M.F., Garay U.J.R., Fernando B., Luis B., et al. Impact of fluvoxamine on outpatient treatment of COVID-19 in Honduras. *MedRxiv* 2022. doi:10.1101/2022.09.27.22280428.
14. Martina C., Robert M., Lea L., Ivan J., Natasa K., Slobodan M., et al. Safety and efficacy of fluvoxamine in COVID-19 ICU patients: An open label, prospective cohort trial with matched controls. *Br J Clin Pharmacol* 2022;**88**(5):2065–73. doi:10.1111/bcp.15126.
15. Sapan B., Waleed K., Nithin K., Saffa I., Azizullah B., Mohammed M., et al. Fluvoxamine in nonhospitalized patients with acute COVID-19 infection and the lack of efficacy in reducing rates of hospitalization, mechanical ventilation, and mortality in placebo-controlled trials: a systematic review and meta-analysis. *Am J Ther* 2022;**29**(3):e298–304. doi:10.1097/MJT.0000000000001496.
16. Lz N.J., Mario S., Ingrid T., Agata M., Cornelius L., Ina M., et al. Fluvoxamine for the treatment of COVID-19. *Cochrane Database Syst Rev* 2022;**2022**(9):CD015391. doi:10.1002/14651858.CD015391.

Huzaifa Ahmad Cheema[1], Uzair Jafar[1]
Division of Infectious Diseases, Department of Medicine, King Edward Medical University, Nila Gumbad Chowk, Neela Gumbad, Lahore, Punjab 54000, Pakistan

Asmaa Ahmed Elrashedy
Faculty of Medicine, Kafr El-Shaikh University, Kafr El-Shaikh, Egypt

Abia Shahid
Division of Infectious Diseases, Department of Medicine, King Edward Medical University, Nila Gumbad Chowk, Neela Gumbad, Lahore, Punjab 54000, Pakistan

Rehmat Ullah Awan
Department of Medicine, Ochsner Rush Medical Center, Meridian, MS, United States

Muhammad Ehsan, Muhammad Ayyan
Division of Infectious Diseases, Department of Medicine, King Edward Medical University, Nila Gumbad Chowk, Neela Gumbad, Lahore, Punjab 54000, Pakistan

Syeda Sahra
Department of Infectious Diseases, University of Oklahoma Health Sciences Center, Oklahoma City, OK, United States

*Corresponding author.
E-mail address: huzaifacheema@kemu.edu.pk (H.A. Cheema)

[1] These authors contributed equally to this work.

Accepted 8 October 2022
Available online 13 October 2022

https://doi.org/10.1016/j.jinf.2022.10.012

Host-cell recognition of SARS-CoV-2 spike receptor binding domain from different variants

Dear Editor,

Previously in this journal, we predicted that the host cell surface chaperone glucose-regulated protein 78 (Cs-GRP78) could act for SARS-CoV-2 spike recognition.[1] Later on, this was supported by an experimental study by Carlos et al.[2] Further prediction studies reported its enhanced role in recognition of some new variants that emerged in the last two years.[3,4] For Cs-GRP78, the recognition of the spike receptor binding domain (RBD) is reflected in the predicted binding affinity of the GRP78 substrate binding domain β (SBD β) to the C480-C488 region of the spike.

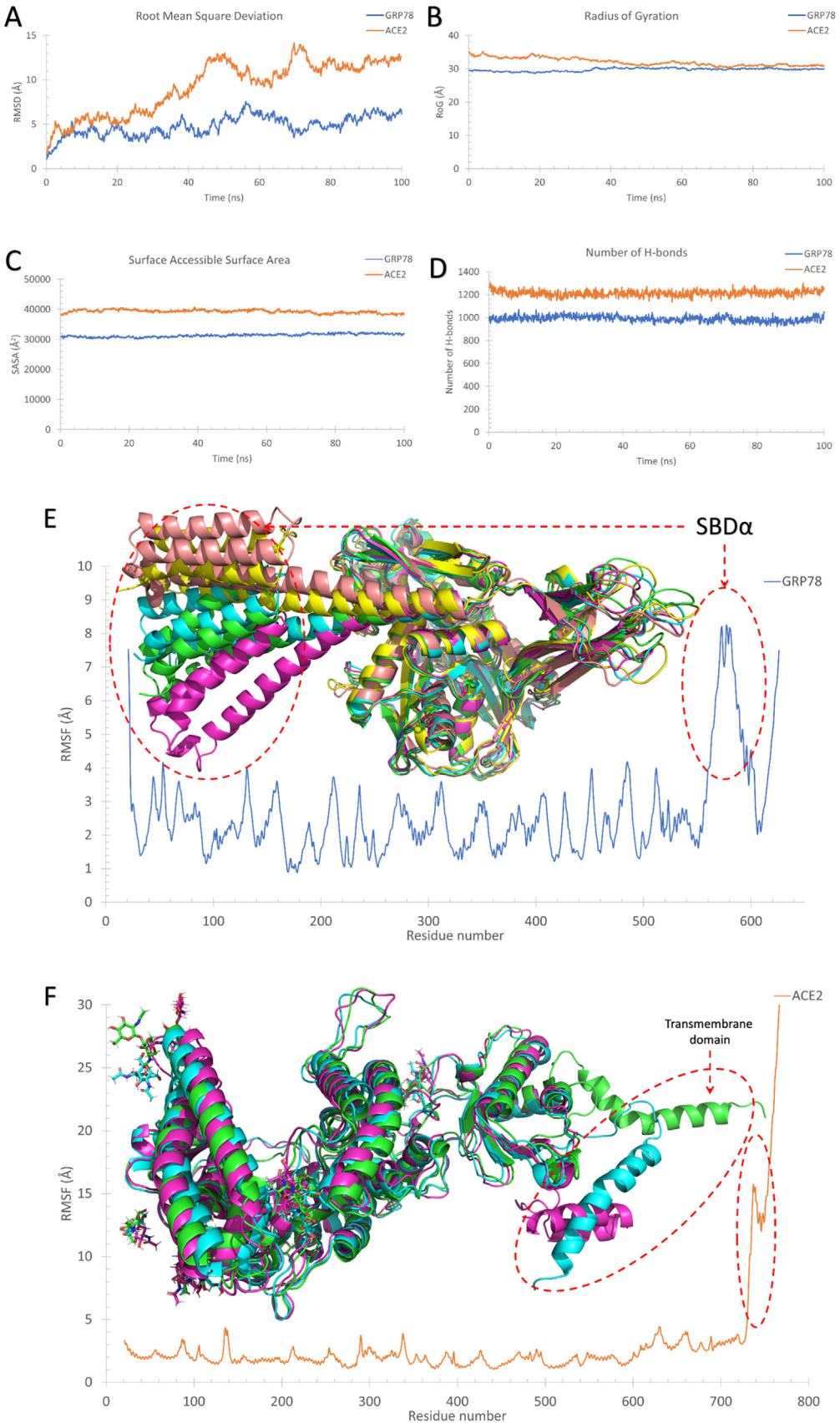

Fig. 1. The molecular dynamics simulation (MDS) analysis of the GRP78 and ACE2 systems. The root-mean-square deviation (RMSD) (A) in Å, the radius of gyration (RoG) in Å (B), surface accessible surface area (SASA) in Å^2 (C), and the number of H-bonds (D), versus time in ns are plotted for the GRP78 (blue) and ACE2 (orange) systems. The per-residue root-mean-square fluctuations (RMSF) of GRP78 (E) and ACE2 (F) systems are shown (bottom), with the representative cluster members superimposed and depicted in colored cartoons (top).

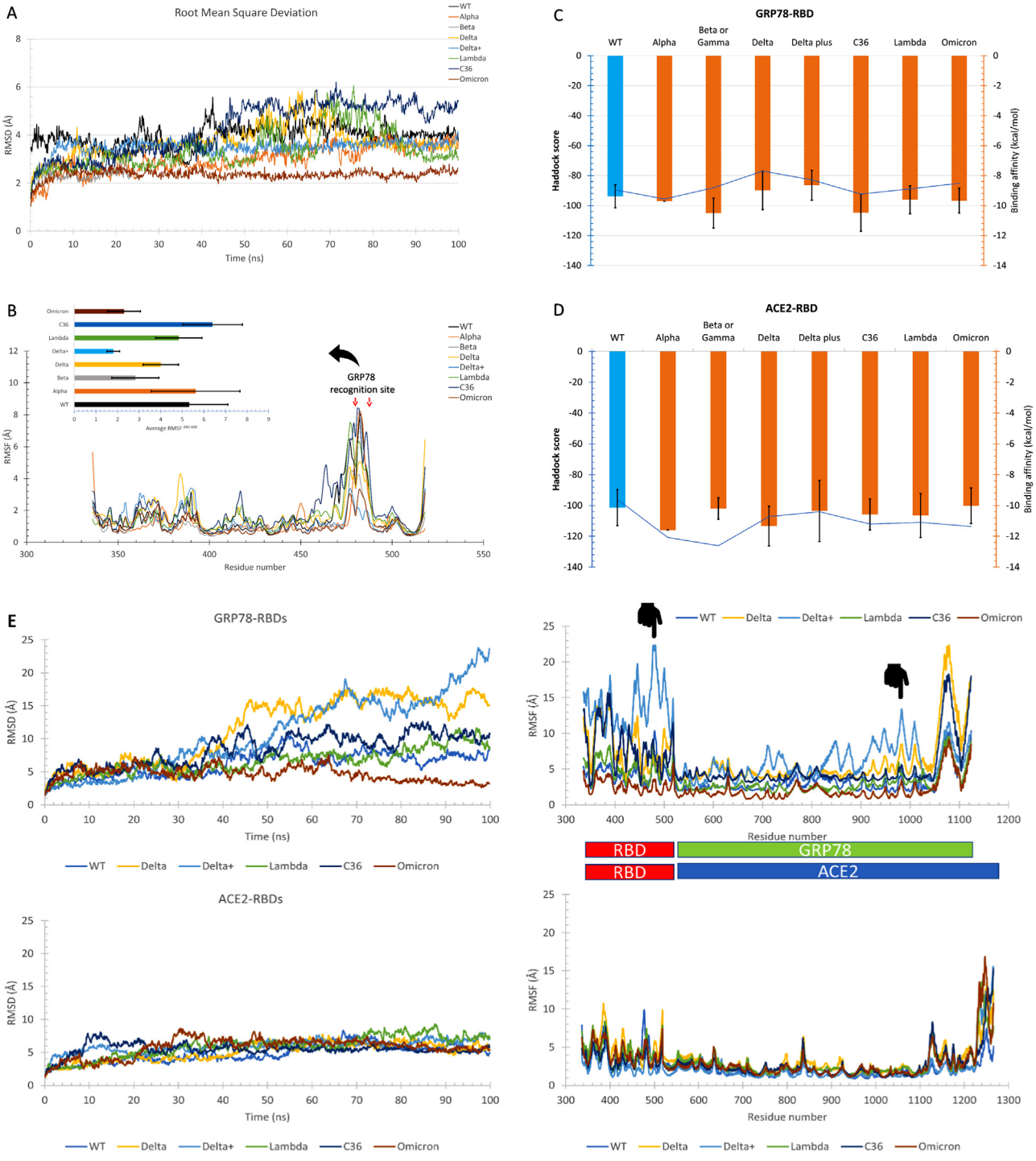

Fig. 2. (A) The root-mean-square deviation (RMSD) of the WT (black) and the mutated variants RBDs (alpha: orange, beta or gamma: gray, delta: yellow, delta+: cyan, lambda: green, C36: blue, and omicron: brown) versus the simulation time in ns. (B) the per-residue root-mean-square fluctuations (RMSF) of the WT and the mutated RBDs. The enlarged panel shows the average RMSF for the GRP78 binding region (C480-C488). The average binding affinity (kcal/mol) was predicted using PRODIGY for the docking of GRP78 (C) and ACE2 (D) against the WT (blue) and the different variants (orange) of SARS-CoV-2 spike RBDs. (E) shows the RMSD and RMSF of GRP78-RBDs (top) and ACE2-RBDs (bottom) complexes simulated for 100 ns. (F) The RMSF of the RBD C480-C488 region for the GRP78-RBDs (left) and ACE2-RBDs (right) systems. (G) The calculated average binding energies of the different systems of RBDs bound to GRP78 (green) and ACE2 (blue), with error bars, represent the standard deviation.

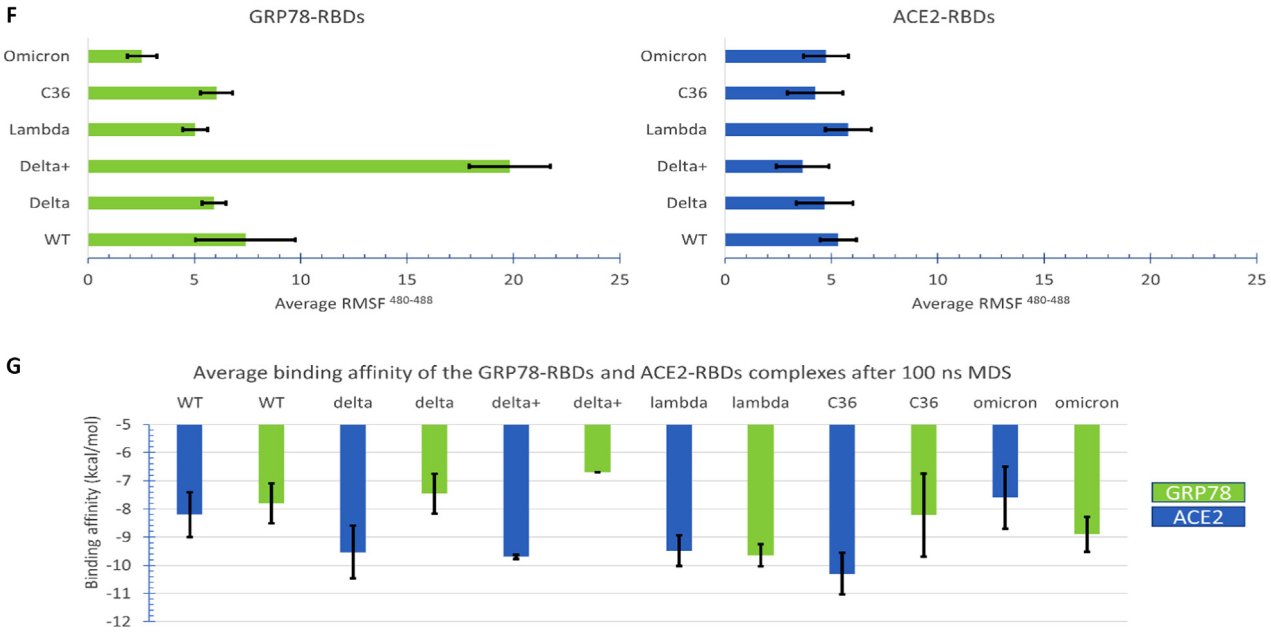

Fig. 2. Continued

In the current study, we equilibrate the GRP78 and ACE2 systems for 100 ns then we cluster the trajectories. Fig. 1 shows the molecular dynamics simulation (MDS) analysis performed using VMD 1.9.3 software. The two systems are equilibrated after 50 ns with RMSD values of 5 Å and 12 Å for GRP78 and ACE2, respectively (Fig. 1A). The two systems are found stable, as reflected by the RoG, SASA, and H-bonds. The radius of gyration for GRP78 and ACE2 started from 30 Å and 35 Å, respectively, but coincided at 31 Å at the end of the simulation (Fig. 1B). The SASA and the number of H-bonds are also stable during the simulation, with values around 30,000 $Å^2$ & 40,000 $Å^2$ and 1000 & 1200 for GRP78 & ACE2, respectively (Fig. 1C and D). The per-residue RMSF for the GRP78 and ACE2 systems are plotted in Fig. 1E and 1F. As reflected from the RMSF, both systems are stable with regions of high fluctuation (RMSF $<$ 5 Å) at the protein terminals, the region (565–590) in GRP78 and (730–760) in ACE2. These two regions are indicated in the structures at the upper part of the figure with dashed-red circles. The region (565–590) is part of the substrate binding domain α (SBDα) of GRP78 and was reported in previous studies to be highly flexible due to its vital role as a lid in covering the SBDβ during the inactivation of the protein (closed conformation). On the other hand, the highly flexible region from ACE2 is the transmembrane domain of the protein, and it is usually stabilized by binding to B(0)AT1 and the membrane.[5] The structures on the top of RMSF show the superposition of the representative conformations of the proteins that will be used to assess their binding affinity against RBDs.

Binding affinities of the GRP78 and ACE2 to different RBDs

Five representative structures for GRP78 and three for ACE2 are used to test their binding affinity to the WT and the mutated spike RBDs. The generated RBDs (WT, alpha, beta or gamma, delta, delta+, C36, lambda, and omicron) are equilibrated and then clustered (Fig. 2A and 2B). All of the RBDs are equilibrated with RMSD values between 2 and 6 Å. The RBDs are found stable during the simulation except for the GRP78 binding region (C480-C488). This region exhibits high fluctuations in the WT, alpha, delta, lambda, and C36 RBD variants, with RMSF $<$ 4 Å. The clusters representatives of each RBDs are docked using HADDOCK V2.4 against GRP78 and ACE2 representative clusters.[6] The active site for docking between the RBDs and ACE2 are F486, Q474, K417, Y453, Q498, N501, & T500 and Q24, M82, Q42, Y41, K353, R357, H34, & D30, respectively. On the other hand, the active site for docking between the RBDs and GRP78 are C480:C488 and T428, V429, V432, T434, F451, S452, V457 & I459, respectively.[7,8] In addition, we predicted the binding affinity using the PRODIGY web server for the docked complexes.[9] Fig. 2C and 2D show the average binding affinity (PRODIGY) and the corresponding HADDOCK scores for each RBD representative cluster conformation. Error bars represent the standard deviation. As reflected in Fig. 2C, the GRP78 has a moderate binding affinity (−8.64 up to −10.50 kcal/mol) against all RBDs, with some variants showing enhanced affinity compared to the WT RBD (beta or gamma and C36). On the other hand, the ACE2 (Fig. 2D) shows almost the same binding affinity against the WT and variant RBDs (−10.02 up to 11.60 kcal/mol), which are higher than that for GRP78. This coincides with the fact that ACE2 is the main recognition element and Cs-GRP78 is an auxiliary recognition site for SARS-CoV-2.[2,10]

Finally, for each of the docked results, the docked complex with a predicted binding affinity closest to the average binding affinity was used to perform another MDS run for 100 ns to study the stability of the established interactions. Fig. 2E shows the RMSD and RMSF of the GRP78-RBDs (left) and ACE2-RBDs (right) complexes. As reflected from the RMSD curves, the ACE2-RBDs in all the complexes are stable (RMSD 5–7 Å). On the other hand, the GRP78-RBDs complexes show RMSD values ranging from 3 up to 10 Å, except for delta (orange) and delta+ (cyan) variants that show higher values (up to 23 Å). This is also indicated in the RMSF curves (markers at the highly fluctuating RBD and SBDβ, for delta+ variant). The average RMSF at the C480-C488 is also plotted (Fig. 2F) for the different variants where the delta+ variant is not stable (RMSF $<$ 20 Å) at the GRP78-RBD complex compared to the WT and the other variants. While in ACE2-RBDs complexes, all the complexes show an average RMSF $^{480–488}$ around 4 Å.

After clustering the trajectories for the complexes, we calculated the binding energies using the PRODIGY web server (Fig. 2G). For GRP78-RBDs complexes (green), the omicron and lambda variants show enhanced binding affinity compared to WT, while C36 and delta variants show the same affinity as WT. This coincides with our previous results published earlier in this journal.[4] On the other hand, for the ACE2-RBDs complexes (blue), the delta, delta+,

lambda, and C36 variants show enhanced affinity compared to WT.

Conclusively, ACE2 and GRP78 can bind to, hence recognize, SARS-CoV-2 spike from different variants, including alpha, beta, delta, delta+, lambda, C36, and omicron. Accordingly, targeting these host-cell receptors would be successful in fighting the pandemic.

Declaration of Competing Interest

The authors declare that they have no known competing financial interests or personal relationships that could have appeared to influence the work reported in this paper.

Acknowledgement

Shaheen supercomputer of King Abdullah University of Science and Technology (KAUST) is used to perform the MDS study (under the project number k1482).

References

1. Ibrahim I.M., Abdelmalek D.H., Elshahat M.E., Elfiky A.A.. COVID-19 spike-host cell receptor GRP78 binding site prediction. *J Infect* 2020;**80**(5):554–62.
2. Carlos A.J., Ha D.P., Yeh D.W., Van Krieken R., Tseng C.C., Zhang P., et al. The chaperone GRP78 is a host auxiliary factor for SARS-CoV-2 and GRP78 depleting antibody blocks viral entry and infection. *J Biol Chem* 2021;**296**:100759.
3. Ibrahim I.M., Elfiky A.A., Elgohary A.M.. Recognition through GRP78 is enhanced in the UK, South African, and Brazilian variants of SARS-CoV-2; an *in silico* perspective. *Biochem Biophys Res Commun* 2021;**562**:89–93.
4. Elfiky A.A., Ibrahim I.M.. Host-cell recognition through Cs-GRP78 is enhanced in the new Omicron variant of SARS-CoV-2, *in silico* structural point of view. *J Infect* 2022;**84**(5):722–46.
5. Elfiky A.A., Ibrahim I.M., Ismail A.M., Elshemey W.M.. A possible role for GRP78 in cross vaccination against COVID-19. *J Infect* 2021;**82**(2):282–327.
6. van Zundert G.C.P., Rodrigues J., Trellet M., Schmitz C., Kastritis P.L., Karaca E., et al. The HADDOCK2.2 web server: user-friendly integrative modeling of biomolecular complexes. *J Mol Biol* 2016;**428**(4):720–5.
7. Yang J., Nune M., Zong Y., Zhou L., Liu Q.. Close and allosteric opening of the polypeptide-binding site in a human Hsp70 chaperone BiP. *Structure* 2015;**23**(12):2191–203.
8. Yan R., Zhang Y., Li Y., Xia L., Guo Y., Zhou Q.. Structural basis for the recognition of SARS-CoV-2 by full-length human ACE2. *Science* 2020;**367**(6485):1444–8.
9. Xue L.C., Rodrigues J.P., Kastritis P.L., Bonvin A.M., Vangone A.. PRODIGY: a web server for predicting the binding affinity of protein-protein complexes. *Bioinformatics* 2016;**32**(23):3676–8.
10. Elfiky A.A., Ibrahim I.M., Elgohary A.M.. SARS-CoV-2 Delta variant is recognized through GRP78 host-cell surface receptor, *in silico* perspective. *Int J Pept Res Ther* 2022;**28**(5):146.

Abdo A Elfiky, Ibrahim M Ibrahim
Biophysics Department, Faculty of Science, Cairo University, Giza, Egypt

Mohamed N Ibrahim
Clinical Laboratories Department, College of Applied Medical Sciences, Jouf University, Sakakah, Saudi Arabia

Wael M Elshemey
Biophysics Department, Faculty of Science, Cairo University, Giza, Egypt
Department of Physics, Faculty of Science, Islamic University of Madinah, Madinah 42351, Saudi Arabia

*Corresponding author.
E-mail addresses: dr_abdo@cu.edu.eg, abdo@sci.cu.edu.eg (A.A. Elfiky)

Accepted 5 October 2022
Available online

https://doi.org/10.1016/j.jinf.2022.10.009

The relationship between Post COVID symptoms in young people and their parents

Dear Editor,

We read with interest the recent study on risk factors for long COVID.[1] Similar risk factors, including female gender, older age and higher number of symptoms, have been reported in children and young people (CYP).[2] In England, the CLoCk study was established to investigate long COVID in a cohort of >30,000 CYP aged 11–17 years with PCR-confirmed SARS-CoV-2 infection and a contemporaneous PCR-negative group, matched by age, sex, geography and time.[3] Outcomes at 3 months follow-up have been published.[4] Anecdotal information suggested many CYP with ongoing symptoms had other household members with symptoms after COVID-19. We hypothesised that CYP reporting long COVID were more likely to have a parent with ongoing symptoms.

We examined this in a subset of CLoCk participants who completed their six-month questionnaire after a positive or negative SARS-CoV-2 PCR-test between October 2020 and March 2021 (n = 14,377). We excluded CYP with subsequent SARS-CoV-2 infections (48/6878 PCR-positive at baseline, 317/7499 PCR-negative at baseline), those who returned the questionnaire after 34 weeks (n = 1063) and those who did not answer the question of interest (n = 161). The final sample included 12,788 CYP (6334 PCR-positives, 6454 PCR-negatives).

The questionnaire included demographics, elements of the International Severe Acute Respiratory and Emerging Infection Consortium (ISARIC) questionnaire,[4] 21 symptoms as well as the Strengths and Difficulties questionnaire (SDQ)[6] embedded within it, the EQ-5D-Y scale,[5] Short Warwick Edinburgh Mental Health Wellbeing scale (SWEMBS),[6] Chalder Fatigue Scale,[7] and the following questions: "*Has COVID-19 affected family members (in your house): Does anyone have ongoing problems from Covid-19? If so, can you tell us who?*". We grouped responses as 'no', 'ongoing problems in parents', or 'other' if ongoing symptoms were reported in other family members or if the relationship was unclear (e.g., specific names given). The Delphi consensus research definition of long COVID adapted to CYP was used: experiencing ≥1 symptom AND problems with mobility, self-care, doing usual activities or having pain/discomfort or feeling very worried/sad, based on the EQ-5D-Y scale, at the time of questionnaire completion around 6 months after their PCR-test.[8] We assessed the association between ongoing symptoms in CYP and their parents having ongoing symptoms using a logistic regression model that adjusted for age, sex, deprivation (index of multiple deprivation [IMD] quintiles) and SARS-CoV-2 PCR-test status. All analyses were done in Stata v17.

Among test-positive CYP, 19.1% (1207/6334) reported having a parent with ongoing problems after COVID-19. In this group, the prevalence of long COVID six months post-test in CYP reporting a parent with ongoing problems was 33.3% (402/1207) compared to 22.6% (1156/5127) in CYP who did not report parents having ongoing problems after COVID-19 (Table 1).

The same pattern, albeit with lower prevalence, was observed among SARS-CoV-2 PCR-negative CYP, where 5.5% (354/6454) reported having parents with ongoing COVID-19 related symptoms. In this group, the prevalence of long COVID six months post-test in CYP reporting a parent with symptoms was 28.0% (99/354) compared to 17.3% (1052/6100) in CYP not reporting parents having ongoing symptoms (Table 1).

In the logistic regression model including age, sex, deprivation and SARS-CoV-2 status, CYP reporting parents with ongoing symptoms were 1.79-times (95% CI, 1.58–2.02) more likely to have long COVID at 6 months than CYP who did not report parents having ongoing symptoms, independently of age, sex, deprivation and SARS-CoV-2 PCR-status. Notably, Chalder Fatigue Scale, SWEMBS and SDQ scores (for total difficulties as well as subscales) were broadly similar, irrespective of the CYP's SARS-CoV-2 PCR-status or parental ongoing symptom status (Table 1).

Table 1
Number of CYP with LONG-COVID, number of symptoms and scores from the SDQ questionnaire, SWEMBS and Chalder fatigue scale six months post-test stratified by SARS-CoV-2 status and ongoing COVID-19 problems in parents (number and percentages).

	CYP SARS-CoV-2 positive at baseline only (n = 6334)		CYP SARS-CoV-2 negative since baseline (n = 6454)	
	Parents with ongoing COVID-19 problems		Parents with ongoing COVID-19 problems	
	Yes	No	Yes	No
	1207 (19.1%)	5127 (80.9%)	354 (5.5%)	6100 (94.5%)
LONG-COVID* in CYP				
Yes	402 (33.3%)	1156 (22.6%)	99 (28.0%)	1052 (17.3%)
No	805 (66.7%)	3,3971 (77.5%)	255 (72.0%)	5048 (82.8%)
No of symptoms (CYP)				
0	363 (30.1%)	2111 (41.2%)	163 (46.1%)	3505 (57.5%)
1	221 (18.3%)	1120 (21.9%)	56 (15.8%)	1151 (18.9%)
2	179 (14.8%)	594 (11.6%)	30 (8.5%)	523 (8.6%)
3	130 (10.8%)	437 (8.5%)	25 (7.1%)	290 (4.8%)
4	95 (7.9%)	291 (5.7%)	20 (5.7%)	195 (3.2%)
5+	219 (18.1%)	574 (11.2%)	60 (17.0%)	436 (7.2%)
SDQ				
SDQ Total Difficulties				
Median	11	10	12	11
(25th, 75th)	(7,16)	(6,15)	(2,18)	(6,16)
SDQ Emotional symptoms				
Median	4	3	4	3
(25th, 75th)	(2,6)	(1,5)	(2,6)	(1,5)
SDQ Conduct problems				
Median	1	1	2	1
(25th, 75th)	(0,2)	(0,2)	(1,3)	(0,2)
SDQ Hyperactivity/inattention				
Median (25th, 75th)	4	4	4	4
	(2,6)	(2,6)	(2,6)	(3,6)
SDQ peer relationship problem				
Median	2	2	2	2
(25th, 75th)	(1,3)	(1,3)	(1,3)	(1,3)
SWEMBS				
Median	21.5	21.5	20.0	20.7
(25th, 75th)	(18.5,24.1)	(18.5,24.1)	(18.0,23.2)	(18.6,24.1)
Chalder fatigue scale				
Median	13	12	13	11
(25th, 75th)	(11,15)	(11,18)	(11,17)	(11,15)

* *Using data from the questionnaire on symptoms and the EQ-5D-Y scale at the time of the questionnaire (*i.e.*, approximately 6 months after the PCR-test), LONG-COVID was operationalized as having at least 1 symptom and experiencing some/a lot of problems with respect to mobility, self-care, doing usual activities or having pain/discomfort or feeling very worried/sad.*

In summary, this association between having a parent with ongoing symptoms after COVID-19 and CYP experiencing long COVID 6 months after their SARS-CoV-2 test was present in test-positive and test-negatives CYP *albeit* at a lower prevalence among the latter. Possible explanations for the increased risk of long COVID in CYP with PCR-confirmed SARS-CoV-2 infection who reported parents with ongoing symptoms include exposure to an increased viral load when infected and shared genetic vulnerability to post-COVID syndrome, such as viral persistence. There could also be shared environmental and genetic factors related to pre-existing poor physical and mental health among both test positive and test negative participants, such as those arising from socioeconomic status, including higher living density which may increase exposure to viral shedding even in those testing negative.[9] Another explanation relevant to both groups might be an increased focus on symptoms among families with ongoing symptoms, potentially resulting in increased symptoms or reporting by their children. Additionally, this could result in proxy selection bias: parents with ongoing COVID-19 problems may have encouraged their children to participate in the study. The lack of substantial differences in mental health and wellbeing symptoms suggests that the increased risk of long COVID in CYP of parents with ongoing symptoms is not associated with the child's current mental wellbeing.

Strengths and limitations of the study methodology have been discussed previously.[4] Using a national dataset with PCR-confirmed test-positives and matched test-negatives is a strength of this analysis, highlighting the higher prevalence of symptoms in children of parents with ongoing problems independently of the children's own SARS-CoV-2 infection status. We excluded CYP who were (re)infected between their original PCR-test and questionnaire completion but acknowledge misclassification may still exist. Although CYP reported their own symptoms, there is a risk of selection bias as described above. Reporting bias might occur if children of parents with ongoing problems were hypervigilant regarding the same symptoms. Finally, we also have no information about the symptoms, duration or severity of ongoing problems in parents.

In conclusion, we have identified an association between having a parent with ongoing problems after COVID-19 and long COVID at six months post-test in CYP, irrespective of their SARS-CoV-2 positivity status. At present, services for post-COVID syndromes are separate for adults and children. The importance of working with the family in CYP clinics is highlighted. There may be some benefit for integrated joint services focussing on holistic strategies and interventions for the whole family unit, as is currently in place for other infections such as viral hepatitis and HIV.

Ethical approval

The study was approved by Yorkshire and the Humber–South Yorkshire Research Ethics Committee (REC reference: 21/YH/0060; IRAS project ID: 293495). UKHSA has legal permission, provided

by Regulation 3 of The Health Service (Control of Patient Information) Regulations 2002, to process patient confidential information for national surveillance of communicable diseases. Individual patient consent is not required for initial invitation to the study.

Data availability

Data are sensitive and not publicly available. All requests for data will be reviewed by the Children & young people with LONG-COVID (CLoCk) study team, to verify whether the request is subject to any intellectual property or confidentiality obligations. Requests for access to the participant-level data from this study can be submitted via email to clock@ukhsa.gov.uk with detailed proposals for approval. A signed data access agreement with the CLoCK team is required before accessing shared data. Code is not made available as we have not used custom code or algorithms central to our conclusions.

Declaration of Competing Interest

TS is Chair of the Health Research Authority and therefore recused himself from the research ethics application. All other authors declare no competing interests.

Acknowledgments

This work was supported by the Department of Health and Social Care, in their capacity as the National Institute for Health Research (NIHR), and by the UK Research and Innovation (UKRI) who have awarded funding grant number COVLT0022. All research at Great Ormond Street Hospital NHS Foundation Trust and UCL Great Ormond Street Institute of Child Health is made possible by the NIHR Great Ormond Street Hospital Biomedical Research centre. SMPP is supported by a UK Medical Research Council Career Development Award (ref: MR/P020372/1).

References

1. Righi E., Mirandola M., Mazzaferri F., Dossi G., Razzaboni E., Zaffagnini A., et al. Determinants of persistence of symptoms and impact on physical and mental wellbeing in Long COVID: a prospective cohort study. *J Infect* 2022;**84**(4):566–72.
2. Behnood S.A., Shafran R., Bennett S.D., Zhang A.X.D., O'Mahoney L.L., Stephenson T.J., et al. Persistent symptoms following SARS-CoV-2 infection amongst children and young people: a meta-analysis of controlled and uncontrolled studies. *J Infect* 2022;**84**(2):158–70.
3. Stephenson T., Shafran R., De Stavola B., Rojas N., Aiano F., Amin-Chowdhury Z., et al. Long COVID and the mental and physical health of children and young people: national matched cohort study protocol (the CLoCk study). *BMJ Open* 2021;**11**(8):e052838.
4. Stephenson T., Pinto Pereira S.M., Shafran R., de Stavola B.L., Rojas N., McOwat K., et al. Physical and mental health 3 months after SARS-CoV-2 infection (long COVID) among adolescents in England (CLoCk): a national matched cohort study. *Lancet Child Adolesc Health* 2022;**6**(4):230–9.
5. Ravens-Sieberer U., Wille N., Badia X., Bonsel G., Burström K., Cavrini G., et al. Feasibility, reliability, and validity of the EQ-5D-Y: results from a multinational study. *Qual Life Res* 2010;**19**(6):887–97.
6. Tennant R., Hiller L., Fishwick R., Platt S., Joseph S., Weich S., et al. The Warwick-Edinburgh mental well-being scale (WEMWBS): development and UK validation. *Health Qual Life Outcomes* 2007;**5**(1):63.
7. Chalder T., Berelowitz G., Pawlikowska T., Watts L., Wessely S., Wright D., et al. Development of a fatigue scale. *J Psychosom Res* 1993;**37**(2):147–53.
8. Stephenson T., Allin B., Nugawela M.D., Rojas N., Dalrymple E., Pinto Pereira S., et al. Long COVID (post-COVID-19 condition) in children: a modified Delphi process. *Arch Dis Child* 2022;**107**(7):674–80.
9. Cerami C., Popkin-Hall Z.R., Rapp T., Tompkins K., Zhang H., Muller M.S., et al. Household transmission of severe acute respiratory syndrome coronavirus 2 in the United States: living density, viral load, and disproportionate impact on communities of color. *Clin Infect Dis* 2021;**74**(10):1776–85.

Marta Bertran
Immunisations and Vaccine Preventable Diseases Division, UK Health Security Agency, 61 Colindale Avenue, London NW9 5EQ, United Kingdom

Snehal M Pinto Pereira
Division of Surgery & Interventional Science, Faculty of Medical Sciences, University College London, WC1E 6BT, United Kingdom

Manjula D Nugawela, Terence Stephenson, Roz Shafran
UCL Great Ormond Street Institute of Child Health, 30 Guilford Street, London, WC1N 1EH, United Kingdom

Tamsin Ford
Department of Psychiatry, University of Cambridge, Hershel Smith Building Cambridge Biomedical Campus, CB2 0SZ, United Kingdom

Marta Buszewicz
Research Department of Primary Care & Population Health, University College London Medical School London United Kingdom

Elizabeth Whittaker
Department of Paediatric Infectious Diseases, Imperial College Healthcare NHS Trust, London, United Kingdom

Isobel Heyman
UCL Great Ormond Street Institute of Child Health, 30 Guilford Street, London, WC1N 1EH, United Kingdom

Terry Y Segal
Paediatric and Adolescent Division, University College London Hospitals NHS Foundation Trust, London, United Kingdom

Emma Dalrymple
UCL Great Ormond Street Institute of Child Health, 30 Guilford Street, London, WC1N 1EH, United Kingdom

Shamez N Ladhani*
Immunisations and Vaccine Preventable Diseases Division, UK Health Security Agency, 61 Colindale Avenue, London NW9 5EQ, United Kingdom
Paediatric Infectious Diseases Research Group, St. George's University of London, Cranmer Terrace, London, SW17 0RE, United Kingdom

*Corresponding author at: Immunisations and Vaccine Preventable Diseases Division, UK Health Security Agency, 61 Colindale Avenue, London NW9 5EQ, United Kingdom.
E-mail address: shamez.ladhani@ukhsa.gov.uk (S.N. Ladhani)

Accepted 2 October 2022
Available online 8 October 2022

https://doi.org/10.1016/j.jinf.2022.10.005

Efficacy of Paxlovid in patients with acute kidney injury who developed COVID-19

Dear Editor,

The coronavirus disease 2019 (COVID-19) pandemic has affected public health on a global scale.[1] Recently, a letter in your journal analyzes the efficacy of Paxlovid on death and hospitalization for COVID-19 patients and shows that Paxlovid for COVID-19 is effective and safe.[2] Paxlovid, an oral protease inhibitor, is significantly effective in high-risk patients with SARS-Cov-2.[3] Older pa-

Table 1
Outcome of patients with stage I AKI and those with stage II and III AKI who had Paxlovid prescription and those who did not.

	Patients with stage I AKI				Patients with stage II and III AKI			
	All patients (n = 64)	Paxlovid		P value	All patients (n = 40)	Paxlovid		P value
		Patients who received Paxlovid (n = 40)	Patients who did not receive Paxlovid (n = 24)			Patients who received Paxlovid (n = 21)	Patients who did not receive Paxlovid (n = 19)	
RRT (n, %)	0	0	0		7 (17.5)	1 (4.8)	6 (31.6)	0.026
Male sex (n, %)	32 (50)	19 (47.5)	13 (54.2)	0.582	20 (50)	10 (47.6)	10 (52.6)	1.000
Lung infection (n, %)	42 (65.6)	22 (55)	20 (83.3)	0.030	31 (77.5)	16 (76.2)	15 (78.9)	1.000
CVD-related mortality (n, %)	3 (4.7)	1 (4.2)	2 (5.0)	0.551	9 (22.5)	3 (15.8)	6 (28.6)	0.265
All-cause mortality (n, %)	13 (20.3)	8 (20)	5 (20.8)	1.000	19 (47.5)	10 (47.6)	9 (47.4)	1.000
Non-invasive ventilation (n, %)	10 (15.9)	8 (20)	2 (8.7)	0.297	13 (32.5)	6 (28.6)	7 (36.8)	0.738
Invasive ventilation (n, %)	3 (4.7)	2 (5.0)	1 (4.2)	1.000	12 (30)	6 (28.6)	7 (36.8)	0.738
ICU (n, %)	30 (46.9)	19 (47.5)	11 (45.8)	1.000	31 (77.5)	15 (71.4)	16 (84.2)	0.457
ICU (d, x ± s)	5.94 ± 9.25	5.74 ± 7.87	6.32 ± 11.63	0.814	11.08 ± 9.84	11.57 ± 10.12	10.53 ± 9.75	0.742
Length of hospital stay	18.63 ± 8.75	16.93 ± 6.78	21.86 ± 11.10	0.031	22.28 ± 10.29	20.05 ± 6.53	24.74 ± 13.04	0.153
CCI (x ± s)	6.97 ± 2.86	6.74 ± 2.90	7.41 ± 2.79	0.376	7.53 ± 2.81	7.00 ± 2.57	8.11 ± 3.02	0.219
CT value upon diagnosis (ORF 1ab gene)	10.50 (7.00-16.00)	9.00 (6.75-11.25)	17.5 (11.00-21.00)	<0.001	11.00 (6.25-17.00)	7.00 (6.00-11.00)	17.00 (14.00-25.00)	<0.001
Time to viral elimination (days)	25.06 (20.82-32.53)	25.06 (21.28-31.29)	25.94 (19.38-38.99)	0.804	21.74 (18.49-24.02)	21.74 (18.91-24.98)	21.19 (18.28-24.03)	0.907

CCI=charlson comorbidity index; RRT=renal replacement treatment; CVD=cardiovascular disease; ICU=Intensive Care Unit.

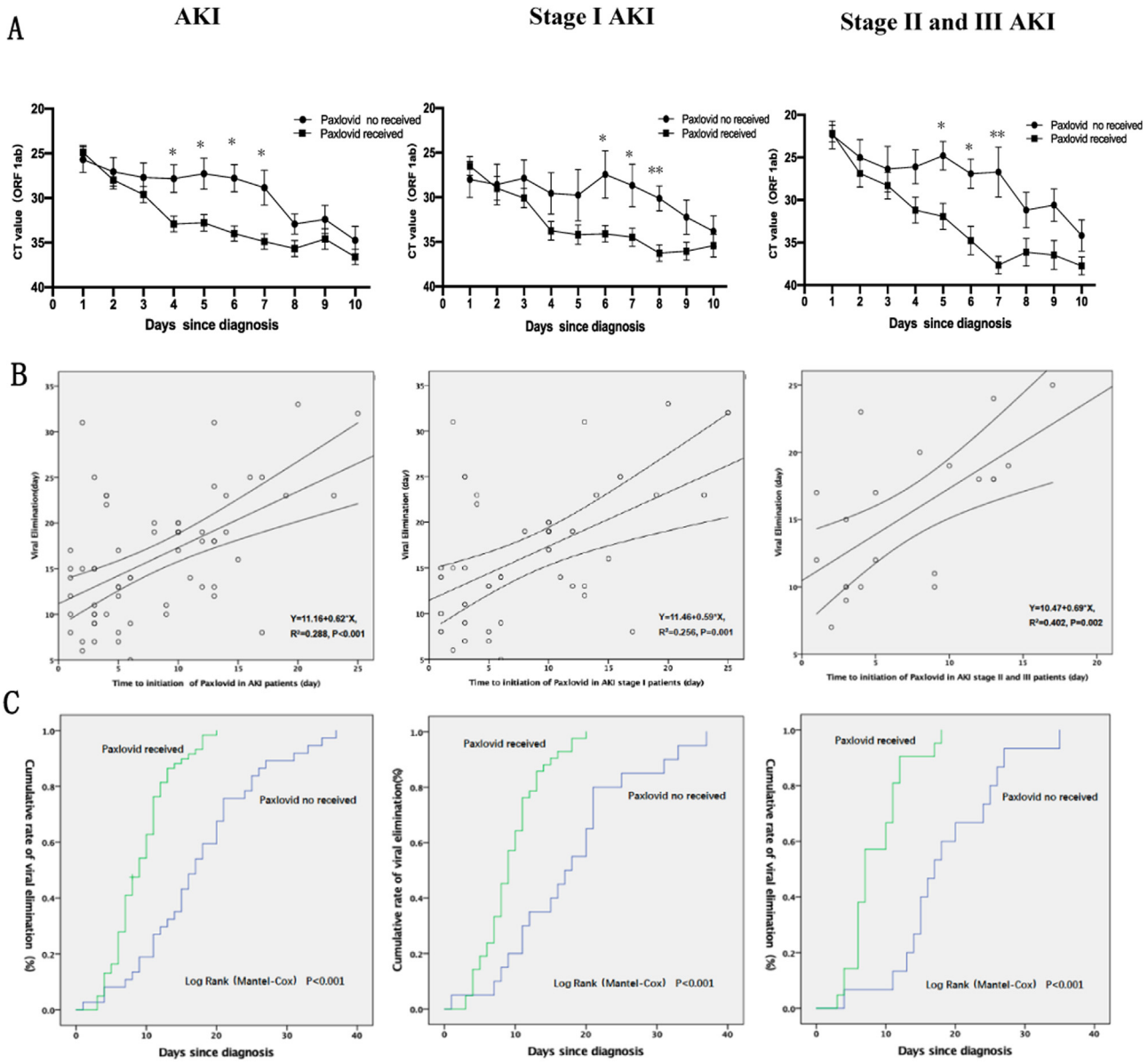

Fig. 1. Attenuation of viral load in patients with AKI who developed COVID-19 according to Paxlovid treatment. A) Changes in ORF1ab CT value in patients with AKI who received Paxlovid and those who did not. In total, 61 patients received Paxlovid, and an ORF1ab gene CT value of ≥35 based on real-time PCR was considered an indicator of virus elimination. The viral load of the Paxlovid group was significantly lower than that of the without Paxlovid group on the 4th day. The viral load of patients who received Paxlovid decreased significantly faster than that of patients who did not receive Paxlovid in the stage I, II and III subgroups, and the significant differences were observed between the two subgroups on the 6th and 5th days, respectively. B) Correlation between the timing of Paxlovid treatment and the duration of virus elimination in patients who received Paxlovid and those who did not. To validate the association between the time to Paxlovid initiation after viral positivity and the time of viral elimination, a correlation analysis was performed. The correlation between the time to Paxlovid initiation and viral elimination is liner in patients with AKI who developed COVID-19 ($R^2 = 0.288$, $P < 0.001$). There was still a liner correlation between viral elimination and the time to Paxlovid initiation in patients with stage I AKI and those with stage II and III AKI who developed COVID-19 ($R^2 = 0.256$, P=0.001; $R^2 = 0.402$, $P < 0.002$, respectively). C)
Cumulative rate of viral elimination in after Paxlovid treatment in patients with AKI who developed COVID-19. Patients with AKI who received Paxlovid had a short viral elimination time. Paxlovid had a better efficacy in patients with stage II and III AKI than in those who did not receive Paxlovid.

tients who received Paxlovid had lower hospitalization and mortality rates. Patients with acute kidney injury (AKI) who developed COVID-19 are at high risk of worse outcomes than those without AKI.[4] However, evidence on the efficacy of Paxlovid in high-risk patients such as those with AKI is limited. In part because of these findings, the current study aimed to evaluate the efficacy of Paxlovid in improving outcomes in patients with AKI.

We performed a retrospective, observational study on patients with AKI aged between 18 and 103 years who developed COVID-19 from April 7, 2022, to June 21,2022, in Shanghai. The study protocol was approved by the ethics committee of Renji Hospital, Shanghai JiaoTong university, school of medicine. All patients provided a written informed consent. The primary endpoints were viral elimination, which was defined as negativity for ORF1ab and N genes (a cycle threshold value of ≥35 based on real-time polymerase chain reaction) on 2 consecutive days, according to local guidelines, and CVD-related and all-cause mortality. The secondary endpoints were length of hospital and ICU stay, lung infection, and renal replacement treatment (RRT). Of 3311 patients,1083 were excluded due to do not have at least two serum creatinine, 881 due to age<18 years old, 3 due to mental illness. Total 1344 sample were enrolled and screen AKI patients. 69 due to hemodialysis and

peritoneal dialysis,1171 due to non-AKI patients. A total of 104 individuals were enrolled in the final analytic sample (Supplementary Fig. S1).

The mean age of 104 patients with AKI was 76.14 ± 13.47 years (Supplementary Tables S1-2). In total, 61 (58.65%) patients received Paxlovid. Compared with patients who did not receive Paxlovid, those who received Paxlovid had a lower incidence of lung infection (60.6% vs 81.4%, P=0.031), shorter length of hospital stay (18.15 ± 6.85 vs 22.70 ± 11.91 days, P=0.015) and viral elimination time (9.00 [6.00-11.00] vs 17.00 [11.00-22.50] days, $P < 0.001$), and less need for RRT(1 [1.6%] vs 6 [14.0%],P=0.019) (Supplementary Table S3). Compared with the no received Paxlovid group, the group of received Paxlovid were similar in terms of all-cause and CVD-related mortality rates, Charlson Comorbidity Index, and baseline estimated glomerular filtration rate. Univariate and binary logistic regression analyses were performed to identify the risk factors of lung infection. Results showed that Paxlovid treatment were independent predictors of lung infection (Supplementary Table S4). Multiple linear regression analysis showed that Paxlovid was correlated with the length of hospital stay in AKI patients with COVID-19(Supplementary Table S5). The patients who receive Paxlovid can effectively reduce the hospital stay and in cadence of lung infection.

In total, 64 patients presented with stage I AKI and 40 with stage II and III AKI. Patients with stage I AKI who received Paxlovid had a lower lung infection rate than those who did not receive Paxlovid (22 [55%] vs 20 [83.3%], P=0.030). However, there was no significant difference in terms of the incidence of lung infection in patients with stage II and III AKI. Patients with stage I AKI who received Paxlovid had a significantly shorter length of hospital stay (16.93 ± 6.78 vs 21.86 ± 11.10 days, P=0.031) than those who did not receive Paxlovid. Patients with stage II and III AKI who received Paxlovid had a lower length of hospital stay than those who did not receive Paxlovid. Nevertheless, the results did not significantly differ. Patients with stage II and III AKI received renal RRT. The Paxlovid group had a lower proportion of patients requiring RRT than the without Paxlovid group (1 [4.8%] vs 6 [31.6%], P=0.026). Regardless of AKI stage I or stage II and III, patients who received Paxlovid had a significantly shorter viral elimination time than those who did not receive Paxlovid (9.00 [6.75,11.25] vs 17.5 [11.00,21.00] days, $P < 0.001$; 7.00 [6.25,17.00] vs 17.00 [14.00,25.00] days, $P < 0.001$) (Table 1).

Within 10 days after the diagnosis of viral infection, the viral load, which was measured based on ORF1ab viral gene replication, decreased significantly in patients with AKI who received Paxlovid. In addition, the correlation between the time to Paxlovid initiation and viral elimination is linear ($R^2 = 0.288$, $P < 0.001$) (Fig. 1). The viral load of patients with stage I AKI and those with stage II and III AKI decreased significantly on day 6th and 5th, respectively, after treatment. There was still a linear correlation between viral elimination and time to Paxlovid initiation ($R^2 = 0.256$, P=0.001; $R^2 = 0.402$, $P < 0.002$, respectively) (Fig. 1).

In conclusion, Paxlovid can effectively shorten the length of hospital stay in patients with AKI who developed COVID-19. Further, it can reduce the incidence of lung infection and shorten the length of hospital stay in patients with early-stage AKI. In patients with late-stage AKI, Paxlovid can reduce the rate of RRT. Early treatment may accelerate viral elimination, shorten hospital stay, and improve outcome in patients with AKI.

Declaration of Competing Interest

None declared

Funding

This study is supported by National Natural Science Foundation of China (81970574, 82170685), Shanghai Municipal Health Commission (ZXYXZ-201904), Grant No. 18ZXY001 from Shanghai Jiaotong University School of Medicine. All the authors declare no competing interests. HC and JY contributed equally to this manuscript.

Acknowledgments

This work was supported by the Renal Division and Clinical Research Unit of Renji Hospital affiliated of Shanghai JiaoTong University. The authors thank all the doctors and nurse who fight for the COVID-19 in Renji Hospital, South campus, affiliated of Shanghai JiaoTong University.

Supplementary materials

Supplementary material associated with this article can be found, in the online version, at doi:10.1016/j.jinf.2022.10.002.

References

1. Heymann DL, Shindo N. WHO Scientific and Technical Advisory Group for Infectious Hazards. COVID-19: what is next for public health? *Lancet* 2020;**395**(10224):542–5 Epub 2020 Feb 13. PMID:32061313; PMCID: PMC7138015. doi:10.1016/S0140-6736(20)30374-3.
2. Zheng Qian, Ma Pengfei, Wang Mingwei, et al. Efficacy and safety of Paxlovid for COVID-19: a meta-analysis. *J Inf* 2022. doi:10.1016/j.jinf.2022.09.027.
3. Arbel R, Wolff Sagy Y, Hoshen M, et al. Nirmatrelvir use and severe Covid-19 outcomes during the omicron surge. *N Engl J Med* 2022 Epub ahead of print. PMID:36001529 . doi:10.1056/NEJMoa2204919.
4. Chan L, Chaudhary K, Saha A, et al. Mount Sinai COVID Informatics Center (MSCIC). AKI in Hospitalized patients with COVID-19. *J Am Soc Nephrol.* 2021;**32**(1):151–60 Epub 2020 Sep 3. PMID:32883700; PMCID: PMC7894657. doi:10.1681/ASN.2020050615.

Hong Cai[1], Jiayi Yan[1]
Department of Nephrology, Renji Hospital, School of Medicine, Shanghai Jiaotong University, Shanghai, China

Jieying Wang[1]
Clinical Research Unit, Renji Hospital, School of Medicine, Shanghai Jiaotong University, Shanghai, China

Xiajing Che*, Shan Mou*
Department of Nephrology, Renji Hospital, School of Medicine, Shanghai Jiaotong University, Shanghai, China

*Corresponding authors.
E-mail addresses: Chexj@126.com (X. Che), shan_mou@shsmu.edu.cn (S. Mou)

[1] Hong Cai and Jiayi Yan and Jieying Wang have contributed equally to this work.
Accepted 2 October 2022
Available online 8 October 2022

https://doi.org/10.1016/j.jinf.2022.10.002

Novel HIV-1 A6/B recombinant forms (CRF133_A6B and URF_A6/B) circulating in Krasnoyarsk region, Russia

Dear Editor,

This journal recently published the studies on characterization of novel HIV-1 circulation recombinant forms (CRF) identified in China.[1,2] In this report, we describe the identification of novel HIV-1 CRF detected in Krasnoyarsk region (KR), Russia. HIV-1 diversity is growing worldwide due to increased identification of distinct recombinant forms. Co-circulation of multiple HIV-1 subtypes/CRFs, among high-risk population such as PWID promotes the generation of new recombinant forms. By now, over 120 CRFs have been described.[3] CRFs play a substantial role in the complex and dynamic HIV-1 epidemic in Russia. Besides the predominant sub-subtype A6, subtypes B, C, CRF02_AG, CRF03_AB, CRF63_02A6 and other uncommon CRFs are constantly identified.[4,5] Earlier studies of our research team described the detection of numerous unique HIV-1 recombinant forms in Siberia.[6–8] Thus, during HIV-1 surveillance study in KR, an URF_A6/B was initially detected in 2017[8] and has been sporadically identified since then. The current report provides the detailed analysis of NFLG sequences of those novel HIV-1 A6 /B recombinants.

Starting in 2017 our research team performs HIV-1 drug resistance surveillance in KR. The samples were collected from ART-naive and ART-experienced HIV-1 infected individuals who attended local HIV/AIDS clinics. The study was approved by the Local Ethical Committee of the State Budgetary Healthcare Institution of Novosibirsk Region "City Infectious Clinical Hospital #1" (protocol # 2 of January 27, 2021). Written consent forms were provided by all the individuals.

As of June 2022, 542 *pol* gene sequences were obtained. Out of those sequences, 11 (2%) were preliminary identified as URF_A6/B or CRF03_A6B by phylogenetic analysis and automated HIV-1 subtyping tools. Subsequently, NFLG sequences for 10 (90.9%) of those sequences were obtained for more detailed analysis (**OP056069-OP056079**). The detailed patient characteristics and information on drug resistance mutations and coreceptor tropism of those viruses are presented in Table S1.

Phylogenetic analysis of NFLG sequences has shown that the study sequences are most closely related to sub-subtype A6 sequences (Fig. 1A). An additional sequence with similar genomic structure to the study A6/B recombinant sequences was identified; this sequence (**MT369971**)[9] was also included in the analysis. All the A6/B recombinants form a distinct monophyletic clade indicating origination from a single ancestor. The analysis of NFLG sequences revealed that the patient with the earliest date of HIV-1 diagnosis (#64) had dual (sub-subtype A6 and URF_A6B) HIV-1 infection. Preliminary recombination analysis using local jpHMM revealed at least two recombination breakpoints in all ten study sequences (Fig. 1B); recombination breakpoints were confirmed by Simplot (Fig. 2C). The recombination analysis revealed complex recombination profiles of those sequences. Thus, eight sequences (#12, #21, #100, #128, #132, #189, #263, #349) had nearly identical recombination profiles with six breakpoints dividing genome into seven (I-VII) genomic subregions, one sequence (#131) had four breakpoints, which divide the genome into five subregions (I-IV, V+VII+VII), and the other sequence (#64) was divided into three subregions (I+II+III, IV, V+VI+VII) by two breakpoints.

The further phylogenetic analysis was performed for each potential sub-region to verify recombination events and to identify phylogenetic relatedness of study sequences (Fig. 1D). Phylogenetic analyses of subregions I, III, V, and VII confirmed the relatedness to sub-subtype A6 circulating in FSU countries. Phylogenetic analysis of fragments II, IV, and VI revealed that those subregions belong to subtype B. Subregion II of study sequences was most closely related to subtype B sequences from Canada, USA, and Spain; subregion IV of study sequences was most closely related to subtype B sequences from FSU countries; subregion VI of study sequences showed more relatedness to subtype B sequences from Russia and Georgia, and CRF03_AB sequence from Russia.

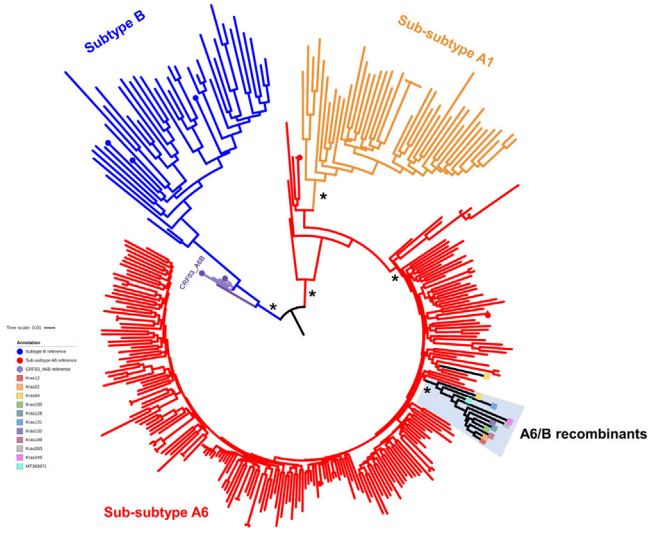

Fig. 1. Maximum-likelihood phylogenetic tree (IQ-Tree) of near full-length genome sequences of 12 novel HIV-1 A6/B recombinants from Krasnoyarsk region. Besides the study sequences, phylogenetic tree also includes the following sequences from LANL HIV sequence database: subtype reference sequences for sub-subtype A6, subtype B, and CRF03_A6B, and full-length or near full-length genome sequences collected in the former Soviet Union (FSU) countries. Sub-subtype A6 sequences are colored by red, sub-subtype A1 – yellow, subtype B – blue, and CRF03_A6B – green. Sequences are color-codded according to the legend on the left. Branch support >95 indicates by asterisk.

According to the LANL HIV Sequence Database standardized nomenclature the eight (#12, #21, #100, #128, #132, #189, #263, #349) of the study sequences were designated as CRF133_A6B. The other two study sequences (#64 and #131) were classified as URF_A6/B.

Dated phylogenetic analysis of concatenated sub-subtype A6 and subtype B subregions A6/B recombinant sequences revealed that the time to the most recent common ancestor (tMRCA) of sub-subtype A6 of was estimated as 1995 (Fig. 2). The origin date of CRF133_A6B sub-subtype A6 subregion was identified as 2000. The tMRCA of subtype B subregion was identified as 2009 (Fig. 2B). CRF133_A6B subtype B sequences originated from subtype B sequence (98GEMZ003; **DQ207943**) from Georgia that was previously identified as a parental subtype B strain for CRF03_A6B.[10]

Eight of 12 study individuals with the novel HIV-1 A6/B infection were PWID, most of them reported sharing injectable equipment with other HIV-infected PWID. The remaining four patients were women who acquired HIV-infection through the sexual contacts, two of them reported sexual contact with HIV-infected PWID. Results of molecular-epidemiological analysis of novel A6/B recombinants combining with clinical and behavioral information of study patients established that the CRF133_A6B and novel URF_A6/B in KR predominantly circulate among PWID and their sexual partners but could transmit to the heterosexual population.

Dated phylogenetic analysis identified that sub-subtype A6 subregion of URF_A6B originated in 1995, and the sub-subtype A6 subregion of CRF133_A6B originated in 2000. The tMRCA of subtype B subregion of CRF133_A6B was estimated almost a decade later. This indicates that the CRF133_A6B circulates in KR for over a decade. Potentially, CRF133_A6B circulates in the region at a relatively low prevalence and may have a lower fitness compared to

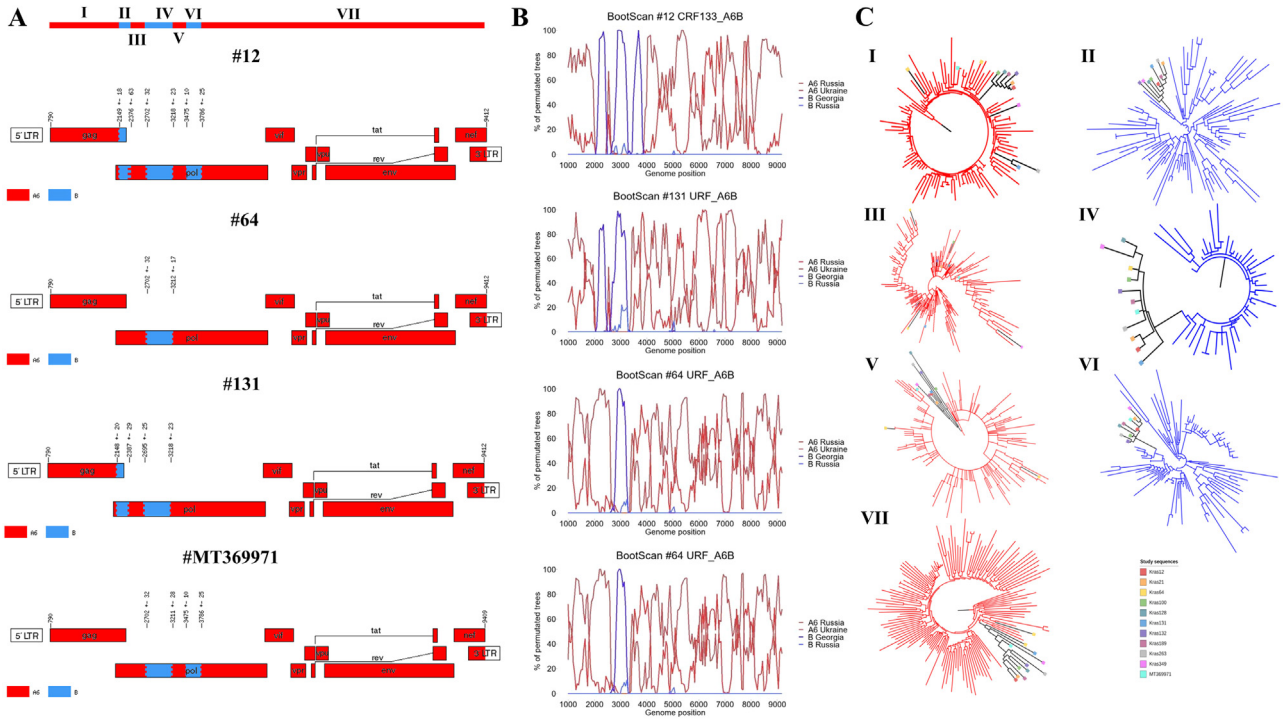

Fig. 2. Recombination analysis of novel HIV-1 A6/B. Genomic structure (A) and Bootscan analysis (B) of CRF133_A6B (top) and other URF_A6/B. Genomic structure and Bootscan plot of CRF133_A6B is shown for a single virus strain (#12); genomic structure for other seven CRF133_A6B are nearly identical. (A) Recombination analysis was performed using a local instance of jpHMM. (B) Bootscan analysis using 400 bp window and 50 bp step using list of selected HIV-1 sub-subtype A6 and subtype B sequences as references. (C) Maximum-likelihood (IQ-Tree) phylogenetic analysis of sub-subtype A6 and subtype B subregions of novel HIV-1 A6/B recombinants. Tree branches are colored according to the HIV-1 subtypes (sub-subtype A6 sequences colored by red, subtype B – blue); study sequences are indicated by black branches and also color-coded according to the right bottom legend.

the prevalent sub-subtype A6. In addition to the described HIV-1 CRFs, there may be other recombinant forms circulating at the lower prevalence.

The identification of novel HIV-1 CRF133_A6B and other URF_A6B emphasizes the growing HIV-1 diversity in Russia as well as a key role of high-risk groups such as PWID and their sexual partners in the process. The further surveillance study with larger study cohorts is needed to determine the size of the CRF133_A6B-infected population and to estimate the potential public health impact of this newly identified virus in the region. The current report supplements other studies of identification of novel HIV-1 recombinant forms. Comprehensive surveillance and improved prevention interventions are crucial to limit the spread of existing and to prevent emergence of novel HIV-1 recombinant forms.

Declaration of Competing Interest

The authors declare no competing financial interests.

Funding

This work was supported by the State Research and Development Program #5–21 State Research Center of Virology and Biotechnology “Vector”.

Acknowledgments

We thank the members of the clinical laboratory in Krasnoyarsk Regional Center for Prevention and Control of AIDS for collection of samples and epidemiological data.

Supplementary materials

Supplementary material associated with this article can be found, in the online version, at doi:10.1016/j.jinf.2022.10.001.

References

1. Xiao M., Feng Y., Gao L., Yang C., Liu J., He M., et al. Characterization of a newly emerging HIV-1 second-generation recombinant form (CRF125_0107) Among heterosexuals in Yunnan, China. *J Infect* 2022;**84**(6):112–15.
2. Xing Y., Wang L., Li Y., Wang Y., Han L., Huang G., et al. Identification of a new HIV-1 intersubtype circulating recombinant form (CRF123_0107) in Hebei province, China. *J Infect* 2022;**84**(3):36–9.
3. https://www.hiv.lanl.gov/content/sequence/HIV/CRFs/crfs.comp, 2022
4. Lebedev A., Lebedeva N., Moskaleychik F., Pronin A., Kazennova E., Bobkova M.. Human immunodeficiency virus-1 diversity in the Moscow region, Russia: phylodynamics of the most common subtypes. *Front Microbiol* 2019;**10**(320). doi:10.3389/fmicb.2019.00320.
5. Ozhmegova E.N., Antonova A.A., Lebedev A.V., Melnikova T.N., Krylova T.V., Kazachek A.V., et al. Genetic profile of HIV-1 in the Vologda region: domination of CRF03_AB and rapid distribution of URFs. *HIV Infect Immunosuppr* 2020;**12**(2):79–88.
6. Sivay M.V., Maksimenko L.V., Osipova I.P., Nefedova A.A., Gashnikova M.P., Zyryanova D.P., et al. (2022) Spatiotemporal dynamics of HIV-1 CRF63_02A6 sub-epidemic. *Front Microbiol* 2020;**13**(946787). doi:10.3389/fmicb.2022.946787.
7. Gashnikova N.M., Bogachev V.V., Baryshev P.B., Totmenin A.V., Gashnikova M.P., Kazachinskaya A.G., et al. A rapid expansion of HIV-1 CRF63_02A1 among newly diagnosed HIV-infected individuals in the Tomsk Region, Russia. *AIDS Res Hum Retrovir* 2015;**31**(4):456–60. doi:10.1089/AID.2014.0375.
8. Maksimenko L.V., Totmenin A.V., Gashnikova M.P., Astakhova E.M., Skudarnov S.E., Ostapova T.S., et al. Genetic diversity of HIV-1 in Krasnoyarsk Krai: area with high levels of HIV-1 recombination in Russia. *Biomed Res Int* 2020;**10**. doi:10.1155/2020/9057541.
9. Lapovok I.A., Baryshev P.B., Saleeva D.V., Kirichenko A.A., Shlykova A.V., Kireev D.E.. Application of next generation sequencing in dual HIV infection studies. *J Microbiol Epidemiol Immunobiol* 2022;**98**(6):627–38.

10. Zarandia M., Tsertsvadze T., Carr J.K., Nadai Y., Sanchez J.L., Nelson K. HIV-1 genetic diversity and genotypic drug susceptibility in the Republic of Georgia. *AIDS Res Hum Retrovir* 2006;**22**(5):470–6. doi:10.1089/aid.2006.22.470.

Lada V Maksimenko[1], Mariya V Sivay[1], Alexei V Totmenin
Department of Retroviruses, State Research Center of Virology and Biotechnology "Vector", ABK 12A, Koltsovo., Novosibirsk 630559, Russia

Alexander N Shvalov
Department of Molecular Virology, State Research Center of Virology and Biotechnology "Vector", ABK 12A, Koltsovo, Novosibirsk 630559, Russia

Sergey E Skudarnov, Tatyana S Ostapova, Svetlana V Yaschenko
Krasnoyarsk Regional Center for Prevention and Control of AIDS, Karl Marks Street, 45, Bld 1, Krasnoyarsk 660049, Russia

Rinat A Maksutov
Department of Molecular Virology, State Research Center of Virology and Biotechnology "Vector", ABK 12A, Koltsovo, Novosibirsk 630559, Russia

Natalya M Gashnikova
Department of Retroviruses, State Research Center of Virology and Biotechnology "Vector", ABK 12A, Koltsovo., Novosibirsk 630559, Russia

*Corresponding author.
E-mail address: sivay_mv@vector.nsc.ru (M.V. Sivay)

[1] These authors contributed equally in this work.

Accepted 2 October 2022
Available online 8 October 2022

https://doi.org/10.1016/j.jinf.2022.10.001

CXCL16 associates with adverse outcome and cardiac involvement in hospitalized patients with Covid-19

Dear Editor,

We read with great interest the paper by Kim et al. suggesting KL-6 and IL-6 as predictive markers in severely ill Covid-19 patients.[1] The gene for CXCR6, the receptor for the chemokine CXCL16, has been showed to be negatively correlated with disease severity in Covid-19 disease.[2] Several studies has demonstrated that soluble CXCL16 gives prognostic information in cardiovascular and inflammatory disorders[3–6] and CXCL16 expression is reported to be increased in lung macrophages in moderate compared to severe Covid-19.[7] But most studies have focused on the expression of its receptor CXCR6, and the prognostic value of CXCL16 in Covid-19 is not known.

In the present study we examined the prognostic value of circulating CXCL16 levels (examined by enzyme immunoassay) in two separate cohorts of hospitalized Covid-19 patients in Norway compromising the first three waves of the Covid-19 pandemic (March 2020-September 2021). For more details on materials and methods, see Supplemental file.

In our combined cohort, 110 of 414 patients (27%) were admitted to intensive care unit (ICU), and 125 (31%) patients developed respiratory failure (RF; i.e., P/F-ratio < 26.6 kPa) the first 10 days after admission (Table 1). CXCL16 levels were significantly higher in ICU patients as compared to patients not admitted to ICU, as evaluated by a linear mixed model adjusting for age, sex, specific Covid-19 treatment (randomized controlled trial [RCT] in cohort 1, dexamethasone use in cohort 2), eGFR and CRP (Fig. 1A). CXCL16 levels increased in both groups during hospitalization, but the increase was more pronounced in the ICU group. The same pattern was seen for patients with RF (Fig. S1). In the combined cohort, 37 of 414 patients died within 60 days of hospital admission (Table 1). Kaplan-Meier analysis of admission levels showed that patients in the upper tertile of CXCL16 were at increased risk of death within 60 days (Fig. 1B). Evaluated as a continuous variable, a one SD increase in CXCL16 was associated with a 2.11 (95% CI 1.60–2.78, $p < 0.001$) times higher risk of death. The increased risk of death was present in patients treated with dexamethasone (HR 1.83, $p = 0.001$), but especially in those not treated with dexamethasone (HR 2.51, $p < 0.001$). The association of CXCL16 with 60-day total mortality was still significant (HR 1.50 [1.08–2.10] $p = 0.017$) after adjustments for other predictors of unfavorable outcomes such as age, sex, randomized treatment (cohort 1), dexamethasone use (cohort 2), eGFR and CRP (Fig. S2). Evaluation of the temporal profile during the first 10 days after inclusion revealed that patients who died had consistently higher levels of CXCL16 than survivors, with the largest differences at the end of the observation period (Fig. 1C).

Due to its known role in cardiovascular pathologies, we explored the association between CXCL16 and markers of cardiac function. Mixed models regression with NT-proBNP as dependent and CXCL16 and time as covariates, revealed a positive correlation (Estimate 0.05, $t = 4.9$, $p < 0.001$). We found a similar correlation with TnT as dependent variable (Estimate 0.03, $t = 5.6$, $p < 0.001$). Both markers showed a consistent correlation across all time-points (Fig. 1D, E). Partial correlation analysis, controlling for the P/F ratio, revealed little influence of respiratory function on the association between CXCL16 and NT-proBNP (admission $r = 0.36$, $p < 0.001$; 3–5 days $r = 0.18$, $p = 0.013$; 7–10 days $r = 0.26$, $p = 0.003$) or TnT (admission $r = 0.27$, $p < 0.001$; 3–5 days $r = 0.21$, $p = 0.002$; 7–10 days $r = 0.26$, $p = 0.003$).

To obtain further insight into the regulation of CXCL16 and its receptor CXCR6 in relation to cardiac involvement during Covid-19 disease, we evaluated the expression of CXCL16/CXCR6 in cardiac related cells exposed to SARS-CoV-2 infection in vitro and in cardiac tissue samples from Covid-19 patients in RNA sequencing datasets deposited in public repositories (Supplemental Table S1). Despite some discrepancies, it seems that CXCL16 may be expressed within the myocardium of Covid-19 patients. In particular, when extracting CXCL16/CXCR6 RNA expression from a Covid-19 tissue atlas,[8] using a single cell approach in autopsy cardiac tissue samples from 15 Covid patients and 28 healthy controls, we found increased expression of CXCL16, but not of CXCR6, in cardiac fibroblasts and to some degree also in cardiac macrophages, as compared with controls (Fig. S3).

Recently, Smieszek et al. reported elevated CXCL16 levels in hospitalized Covid-19 patients as compared to healthy controls, with the highest levels in those with the most severe disease, according to the current WHO classification.[9] In the present study we extend these findings by including a larger number of patients (414 versus 141 patients), from two separate cohorts, recruited during the first three waves of Covid-19 that also included dexamethasone treatment that was used as SoC since autumn 2020. Our findings suggest that CXCL16 could be a novel and robust marker of Covid-19 severity including total mortality, and potentially also cardiac involvement during hospitalization. Interestingly, whereas patients with and without dexamethasone treatment showed similar

Table 1
Demographic, clinical, and biochemical characteristics in 414 patients hospitalized for Covid-19, stratified by two large multi-center cohorts in Norway.

Parameter	Cohort 1 $n = 162$	Cohort 2 $n = 252$	Combined $n = 414$
Age, years	59.7 ± 15.4	57.0 ± 15.3	58.0 ± 15.4
Male gender, n (%)	103 (64)	159 (63)	262 (63)
Body Mass Index, kg/m^2	28.2 ± 4.6	28.8 ± 5.2	28.5 ± 4.9
Treatment group			
Standard of Care (SoC), n (%)	81 (50)	254 (100)	333 (80)
SoC + Hydroxychloroquine, n (%)	43 (27)	0 (0)	43 (10)
SoC + Remdesivir, n (%)	38 (24)	0 (0)	38 (9)
Dexametasone	2 (1)	134 (53)*	136 (33)
Oxygen therapy	91 (56)	194 (77)*	285 (69)
Comorbidities			
Chronic cardiac disease, n (%)	24 (15)	47 (19)	71 (17)
Hypertension, n (%)	51 (32)	84 (35)	135 (34)
Chronic pulmonary disease, n (%)	31 (20)	67 (27)	98 (24)
Obesity, n (%)	43 (29)	70 (28)	113 (28)
Diabetes, n (%)	27 (17)	58 (25)	85 (22)
Current smoker, n (%)	5 (4)	16 (7)	21 (6)
Outcomes			
ICU admission, n (%)	31 (19)	79 (31)*	110 (27)
Respiratory failure, n (%)	50 (31)	75 (30)	125 (31)
60-day death, n (%)	8 (5)	29 (12)	37 (9)
P/F-ratio at admission, kPa	42.4 (32.4,49.6)	40.0 (28.1,48.3)	41.3 (30.0,49.3)
Hemoglobin, g/dL	13.2 ± 1.5	12.9 ± 1.8	13.0 ± 1.7
C-reactive protein, mg/L	70 (35,136)	53 (24,117)	62 (29,125)
Ferritin, µg/L	612 (358,1111)	617 (297,1146)	615 (322,1127)
White blood cell count, x 10^9/L	6.5 ± 2.8	6.9 ± 3.2	6.7 ± 3.1
Neutrophils, x 10^9/L	4.8 ± 2.7	5.3 ± 3.1	5.1 ± 3.0
Lymphocytes, x 10^9/L	1.2 ± 0.53	1.1 ± 0.5	1.1 ± 0.5
eGFR	87 ± 25	90 ± 29	89 ± 27

Continuous data are given as mean ± SD or median (25th, 75th) percentile.
Abbrevations: SoC; standard of care, ICU; intensive care unit, P/F-ratio; PaO2/FiO2-ratio; eGFR; estimated glomerular filtration rate.
*$P < 0.05$ between cohorts 1 and 2.

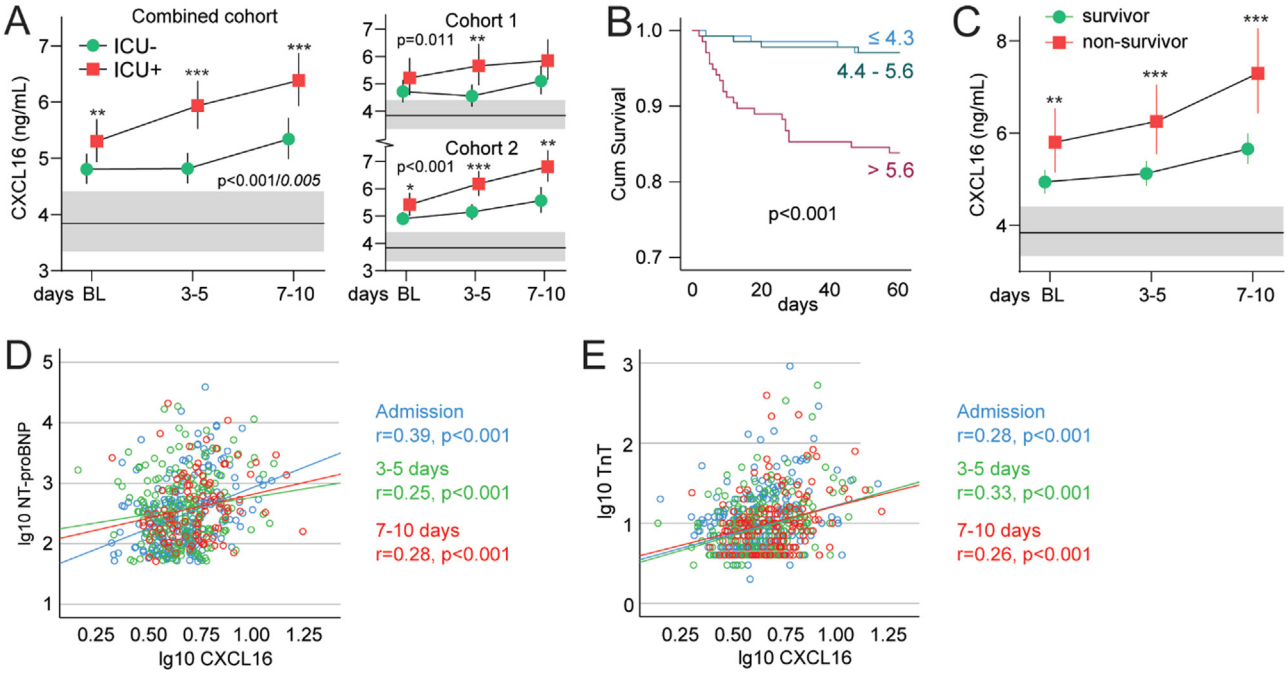

Fig. 1. Intra-hospital temporal profile of CXCL16 according to (A) ICU admission during the first 10 days after inclusion in the combined cohort and within cohorts. (B) CXCL16 and 60-day mortality in severe Covid-19. (C) Temporal profile of CXCL16 during the first 10 days after inclusion according to 60-day mortality. (D) Correlation plot between CXCL16 and NT-proBNP and (E) TnT during the first 10 days after inclusion. Blue circles are at admission, green circles at 3–5 days and red circles at 7–10 days. The correlation coefficients are Pearson. The p-values reflect the group (outcome) effect from the linear mixed models and the interaction p-value (group*time) is shown in italic if significant. gray areas reflect reference value range from age- and sex-matched healthy controls. *$p < 0.05$, **$p < 0.01$, ***$p < 0.001$ between groups. BL; baseline, RF; acute respiratory failure, ICU; intensive care unit; NT-proBNP; N-terminal-pro-B-type natriuretic peptide, Tnt; Troponin.

CXCL16 levels at inclusion, patients that received dexamethasone showed increased CXCL16 levels during follow-up, possibly reflecting more severe disease in dexamethasone user, and/or indicating the need for additional treatment modalities in these patients.

The present study has some limitations such as lack of data on CXCL16 expression in immune cells and pulmonary tissue. We also lack cardiac imaging data from the hospitalized Covid-19 patients and the data on association with cardiac involvement should be interpreted cautiously. Moreover, correlations do not necessarily mean any causal relationship. Although our study included data from the three first waves of SARS-CoV-2, we lack data from Covid-19 disease driven by the omicron variant.

In sum, we show that a significant elevated CXCL16 at admission and during hospitalization were associated with adverse outcome such as RF, the need for treatment at ICU and 60-day total mortality also after adjusting for several variables including CRP. High levels of CXCL16 were also associated with cardiac involvement during hospitalization as assessed by high levels of TnT and NT-proBNP. Our findings suggest that CXCL16 could be a novel and reliable marker for adverse outcome in hospitalized Covid-19 patients, potentially also involved in the pathogenesis of severe Covid-19 disease including myocardial injury.

Declaration of Competing Interest

JCH and AMDR has received funding from Vivaldi Invest A/S owned by Jon Stephenson von Tetzchner; LH has stock ownership in Algipharma AS; ARH has received honoraria from Pfizer for lectures: TE is former (immediate past) President European Association of Cardiovascular Imaging. The other authors report no conflict of interest.

Funding

This study received the following funding: Oslo University Hospital, Research Council of Norway (Grant No. 312780), South-Eastern Norway Regional Health Authority (Grant No. 2021—071) and a philantropic donation from Vivaldi Invest A/S owned by Jon Stephenson von Tetzchner. The funders had no role in study design, data collection, or decision to publish this article.

Study group members

The Norwegian SARS-CoV-2 study group investigators are:

Cathrine Austad, Mette Bogen, Anne Hermann, Karl Erik Müller, Hanne Opsand, Trude Steinsvik, Bjørn Martin Woll (Vestre Viken Hospital Trust); Erik Egeland Christensen, Susanne Dudman, Kristin Eftestøl, Børre Fevang, Beathe Kiland Granerud, Liv Hesstvedt, Synne Jenum, Marthe Jøntvedt Jørgensen, Elisabeth Toverud Landaas, Andreas Lind, Sarah Nur, Vidar Ormaasen, Frank Olav Pettersen, Else Quist-Paulsen, Dag Henrik Reikvam, Kjerstin Røstad, Linda Skeie, Anne Katrine Steffensen, Birgitte Stiksrud, Kristian Tonby (Oslo University Hospital); Berit Gravrok, Vegard Skogen, Garth Daryl Tylden (University Hospital of North Norway); Simen Bøe (Hammerfest County Hospital).

The NOR-SOLIDARITY consortium members are:

Jan Terje Andersen, Anette Kolderup, Trine Kåsine, Fridtjof Lund-Johansen, Inge Christoffer Olsen, Karoline Hansen Skåra, Trung Tran, Cathrine Fladeby, Liv Hesstvedt, Mona Holberg-Petersen, Synne Jenum, Simreen Kaur Johal, Dag Henrik Reikvam, Kjerstin Røstad, Anne Katrine Steffensen, Birgitte Stiksrud, Eline Brenno Vaage, Erik Egeland Christensen, Marthe Jøntvedt Jørgensen, Fridtjof Lund-Johansen, Sarah Nur, Vidar Ormaasen, Frank Olav Pettersen (Oslo University Hospital); Saad Aballi, Jorunn Brynhildsen, Waleed Ghanima, Anne Marie Halstensen (Østfold Hospital Trust); Åse Berg (Stavanger University Hospital); Bjørn Blomberg, Reidar Kvåle, Nina Langeland, Kristin Greve Isdahl Mohn (Haukeland University Hospital); Olav Dalgard (Akershus University Hospital); Ragnhild Eiken, Richard Alexander Molvik, Carl Magnus Ystrøm (Innlandet Hospital Trust); Gernot Ernst, Lars Thoresen (Vestre Viken Hospital Trust); Lise Tuset Gustad, Lars Mølgaard Saxhaug, Nina Vibeche Skei (Nord-Trøndelag Hospital Trust); Raisa Hannula (Trondheim University Hospital); Mette Haugli, Roy Bjørkholt Olsen (Sørlandet Hospital Trust); Dag Arne Lihaug Hoff (Ålesund Hospital); Asgeir Johannessen, Bjørn Åsheim-Hansen (Vestfold Hospital Trust); Bård Reikvam Kittang (Haraldsplass Deaconess Hospital); Lan Ai Kieu Le (Haugesund Hospital); Ravinea Manotheepan, Hans Schmidt Rasmussen, Grethe-Elisabeth Stenvik, Ruth Foseide Thorkildsen, Leif Erik Vinge (Diakonhjemmet Hospital); Pawel Mielnik (Førde Hospital); Vegard Skogen (University Hospital of North Norway); Hilde Skudal (Telemark Hospital Trust); Birgitte Tholin (Molde Hospital).

Supplementary materials

Supplementary material associated with this article can be found, in the online version, at doi:10.1016/j.jinf.2022.09.029.

References

1. Kim S.H., et al. Diagnostic value of serum KL-6 and IL-6 levels in critically ill patients with Covid-19-associated pneumonia. *J Infect* 2022.
2. Ellinghaus D., et al. Genomewide association study of severe Covid-19 with respiratory failure. *N Engl J Med* 2020;**383**(16):1522–34.
3. Jansson A.M., et al. Soluble CXCL16 predicts long-term mortality in acute coronary syndromes. *Circulation* 2009;**119**(25):3181–8.
4. Schranz D., et al. Fatty acid-binding protein 3 and CXC-chemokine ligand 16 are associated with unfavorable outcome in aneurysmal subarachnoid hemorrhage. *J Stroke Cerebrovasc Dis* 2021;**30**(11):106068.
5. Villar J., et al. Clinical and biological markers for predicting ARDS and outcome in septic patients. *Sci Rep* 2021;**11**(1):22702.
6. Turgunova L., et al. Association of biomarker level with cardiovascular events: results of a 4-year follow-up study. *Cardiol Res Pract* 2020;**2020**:8020674.
7. Liao M., et al. Single-cell landscape of bronchoalveolar immune cells in patients with Covid-19. *Nat Med* 2020;**26**(6):842–4.
8. Delorey T.M., et al. Covid-19 tissue atlases reveal SARS-CoV-2 pathology and cellular targets. *Nature* 2021;**595**(7865):107–13.
9. Smieszek S.P., et al. Elevated plasma levels of CXCL16 in severe Covid-19 patients. *Cytokine* 2022;**152**:155810.

Ida Gregersen*
for the *Research Institute for Internal Medicine, Oslo University Hospital Rikshospitalet, Oslo 0027, Norway*

Thor Ueland
Research Institute for Internal Medicine, Oslo University Hospital Rikshospitalet, Oslo 0027, Norway
Faculty of Medicine, Institute of Clinical Medicine, University of Oslo, Oslo 0318, Norway
Thrombosis Research and Expertise Center, University of Tromsø, Tromsø, Norway

Jan Cato Holter
Faculty of Medicine, Institute of Clinical Medicine, University of Oslo, Oslo 0318, Norway
Department of Microbiology, Oslo University Hospital, Oslo 0424, Norway

Maria Belland Olsen
Research Institute for Internal Medicine, Oslo University Hospital Rikshospitalet, Oslo 0027, Norway

Annika E Michelsen, Sarah L Murphy
Research Institute for Internal Medicine, Oslo University Hospital Rikshospitalet, Oslo 0027, Norway
Faculty of Medicine, Institute of Clinical Medicine, University of Oslo, Oslo 0318, Norway

Anders Aune Tveita
Department of Internal Medicine, Bærum Hospital, Vestre Viken Hospital Trust, Gjettum 1346, Norway
Division of Laboratory Medicine, Department of Immunology, Oslo University Hospital, Oslo 0424, Norway

Katerina Nezvalova Henriksen
Department of Hematology, Oslo University Hospital, Oslo, Norway
Hospital Pharmacies, South-Eastern Norway Enterprise, Oslo, Norway

Hedda Hoel
Research Institute for Internal Medicine, Oslo University Hospital Rikshospitalet, Oslo 0027, Norway
Faculty of Medicine, Institute of Clinical Medicine, University of Oslo, Oslo 0318, Norway
Medical Department, Lovisenberg Diaconal Hospital, Oslo, Norway

Lena Bugge Nordberg
Medical Department, Diakonhjemmet Hospital, Oslo, Norway

Aleksander Rygh Holten
Faculty of Medicine, Institute of Clinical Medicine, University of Oslo, Oslo 0318, Norway
Department of Acute Medicine, Oslo University Hospital, Oslo, Norway

Thor Edvardsen
Department of Cardiology, Oslo University Hospital, Rikshospitalet, University of Oslo, Oslo, Norway

Kuan Yang
Research Institute for Internal Medicine, Oslo University Hospital Rikshospitalet, Oslo 0027, Norway

Lars Heggelund
Department of Internal Medicine, Drammen Hospital, Vestre Viken Hospital Trust, Drammen 3004, Norway
Department of Clinical Science, Faculty of Medicine, University of Bergen, Bergen 5009, Norway

Marius Trøseid
Research Institute for Internal Medicine, Oslo University Hospital Rikshospitalet, Oslo 0027, Norway
Faculty of Medicine, Institute of Clinical Medicine, University of Oslo, Oslo 0318, Norway
Section of Clinical Immunology and Infectious Diseases, Oslo University Hospital, Oslo, Norway

Fredrik Müller
Faculty of Medicine, Institute of Clinical Medicine, University of Oslo, Oslo 0318, Norway
Department of Microbiology, Oslo University Hospital, Oslo 0424, Norway

Anders Benjamin Kildal
Department of Anesthesiology and Intensive Care, University Hospital of North Norway, Tromsø, Norway

Anne Ma Dyrhol-Riise
Faculty of Medicine, Institute of Clinical Medicine, University of Oslo, Oslo 0318, Norway
Department of Infectious Diseases, Oslo University Hospital, Ullevål, Oslo, Norway

Andreas Barratt-Due
Division of Laboratory Medicine, Department of Immunology, Oslo University Hospital, Oslo 0424, Norway
Department of Anaesthesia and Intensive Care Medicine, Oslo University Hospital, Oslo, Norway

Tuva B Dahl
Research Institute for Internal Medicine, Oslo University Hospital Rikshospitalet, Oslo 0027, Norway
Department of Acute Medicine, Oslo University Hospital, Oslo, Norway

Pål Aukrust
Research Institute for Internal Medicine, Oslo University Hospital Rikshospitalet, Oslo 0027, Norway
Faculty of Medicine, Institute of Clinical Medicine, University of Oslo, Oslo 0318, Norway
Section of Clinical Immunology and Infectious Diseases, Oslo University Hospital, Oslo, Norway

Bente Halvorsen
Research Institute for Internal Medicine, Oslo University Hospital Rikshospitalet, Oslo 0027, Norway
Faculty of Medicine, Institute of Clinical Medicine, University of Oslo, Oslo 0318, Norway

*Corresponding author.
E-mail address: ida.gregersen@medisin.uio.no (I. Gregersen)

Accepted 30 September 2022
Available online 8 October 2022

https://doi.org/10.1016/j.jinf.2022.09.029

Aneuploidy underlies paradoxical growth of rezafungin and enables cross-tolerance to echinocandins in *Candida albicans*

Dear Editor,

Echinocandins, including caspofungin (CSP), micafungin (MCF), and anidulafungin (ANF), are first-line antifungal agents for the treatment of invasive candidiasis. Rezafungin (RZF) is a next-generation echinocandins drug currently in phase 3 development. It has a long half-life and a good safety profile.[1] While susceptible yeast cells are fully killed at intermediate-to-low concentrations of echinocandins, they can grow in the presence of high antifungal doses. This phenomenon, known as paradoxical growth (PG), is often observed *in vitro*. PG seen in *Candida* and *Aspergillus* species has four phases: phase 1, growth at sub-MIC concentrations; phase 2, inhibition of growth at supra-MIC concentrations; phase 3, growth at higher concentrations; and phase 4, inhibition of growth at the highest drug concentrations (reviewed in[2]). Echinocandin-resistant clinical isolates usually carry point mutations of *FKS* genes, which encode the target protein of echinocandins, yet PG is not associated with *FKS* mutations. Although the molecular mechanism of PG is largely unknown, one hypothesis is that PG is a compensatory physiological response to the drug. [3]

Here we investigated the PG effect of RZF in *C. albicans*, the most prevalent opportunistic human fungal pathogen. We found growth of lab strain SC5314 (RZF MIC was 25 ng/ml) on YPD in the presence RZF also exhibited four phases: at 6.25 ng/ml and 12.5 ng/ml of RZF, growth was comparable to the no drug control; at 25 ng/ml and 50 ng/ml of RZF, growth was obviously inhibited; in a broad range of RZF from 100 ng/ml to 6400 ng/ml, growth was reduced, but not inhibited, with smaller colonies indicative of slow growth; and at 12,800 ng/ml, the highest RZF concentration tested, growth was inhibited. Therefore, RZF displayed a PG response in

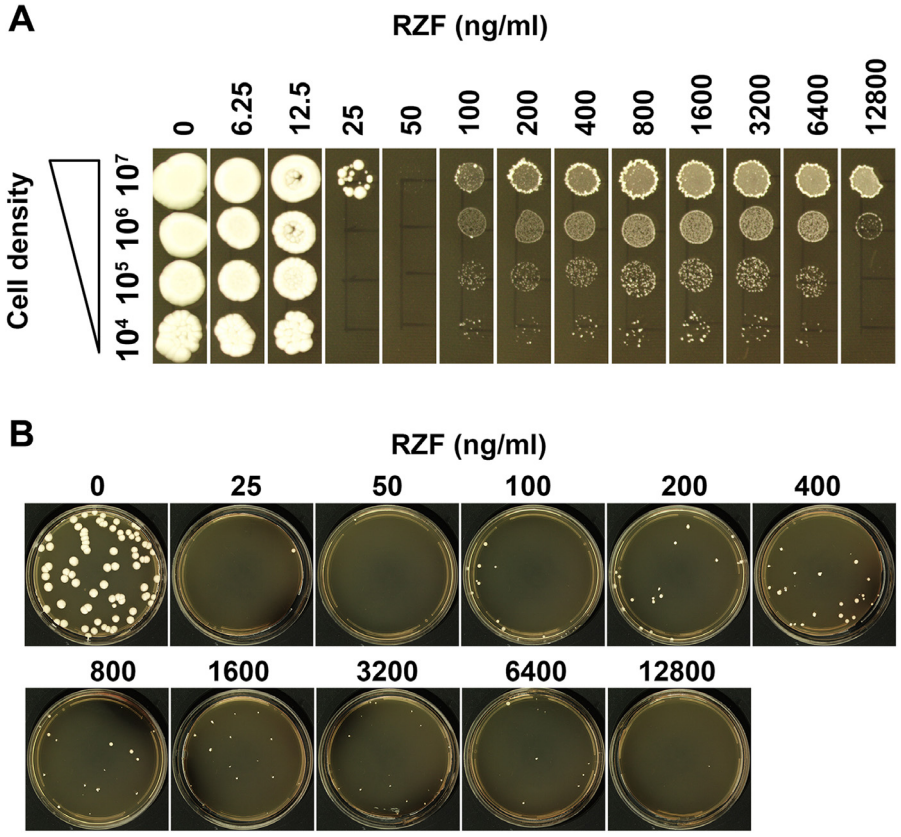

Fig. 1. Paradoxical growth effect of rezafungin in *Candida albicans*.
(A), 3 µl of 10-fold serial dilutions of strain SC5314 was spotted on YPD plates containing rezafungin (RZF) at concentrations indicated. The plates were incubated at 37°C and photographed after 48h (B), plating of approximately 100 cells of SC5314 on YPD plates containing RZF, incubated at 37°C and photographed after 5 days.

SC5314 (Fig. 1A). To investigate mechanisms by which *C. albicans* colonies grew at high concentrations of RZF, we spread approximately 100 SC5314 cells onto YPD plates supplemented with 25 to 12,800 ng/ml of RZF in two-fold increase (Fig. 1B), each drug concentration having three technical repeats. After 5 days of incubation at 37°C, we collected all colonies (adaptors) from all the drug plates, yielding 264 adaptors, which were archived at -80°C. We then re-streaked each colony on YPD and performed spot assays, which indicated that most of the adaptors (243 out of 264) grew similarly to the parent strain in the presence of RZF, consistent with the hypothesis that PG might be a non-heritable physiological response. However, 21 adaptors (8%) displayed better growth than the parent strain (Fig. S1). One adaptor, adaptor #33 derived from 1600 ng/ml of RZF (Fig. S1), appeared to grow very slowly and to be highly unstable (yielding large, more stable colonies in addition to the majority of small ones) and thus was not analyzed further. Whole genome sequencing of the 20 tolerant adaptors revealed that they all carried aneuploid chromosomes (Figs. S2 and 2A). Of note, none of the sequenced adaptors had mutations in *FKS* genes (*GSC1, GSL1, GSL2*). The karyotypes of the adaptors could be classified into 5 types based on the types of chromosomal aneuploidies. Type 1 adaptors (15 independent isolates) all were monosomic for a segment of chromosome R (SegChrRx1) from 1.9Mb to the right telomere of ChrR (Fig. S2) and had been isolated from plates containing RZF at 200 ng/ml (1 isolate), 400 ng/ml (5 isolates), 800 ng/ml (2 isolates), 1600 ng/ml (5 isolates), and 3200 ng/ml (2 isolates). Type 2 adaptors (2 isolates) carried a duplication of the B homolog of Chr2 (Chr2 × 3, ABB) and were derived from plates containing RZF at 200 ng/ml (1 isolate) and 800 ng/ml (1 isolate). The only Type 3 adaptors carried a duplication of the A homolog of Chr2 (Chr2 × 3, AAB). It was isolated from an RZF plate containing 3200 ng/ml of RZF. The only Type 4 adaptor was isolated from a 1600 ng/ml RZF plate and had a segmental duplication of the left arm of ChrR (SegChrRx3). Type 5 adaptor appear to be a mixed population composed of some cells carrying different aneuploid chromosomes, including the segmental monosomy seen in Type 1 adaptors, as well as duplication of the rest ChrR. In addition, some cells in the population had whole chromosome duplication of Chr5. The type 5 adaptor was derived from YPD plate supplemented with 12,800 ng/ml of RZF.

In *C. glabrata*, CSP-tolerant adaptors usually become hypersensitive to MCF. The so-called CRS-MIS (CSP Reduced Susceptibility and MCF Increased Susceptibility) is due to altered membrane sphingolipids.[4] Furthermore, we previously found that aneuploidy enabled cross-tolerance to unrelated drugs in *C. albicans*[5] and *C. parapsilosis*.[6] Therefore, we asked if the RZF adaptors also had CRI-MIS or, alternatively, if they obtained cross-tolerance to echinocandins. Indeed, all five types of karyotypes enabled cross-tolerance to all 4 echinocandin drugs (CSP, MCF, ANF and RZF) (Fig. 2B). Therefore, unlike the CRS-MIS observed in *C. glabrata*, in *C. albicans,* tolerance to RZF caused by aneuploidy was accompanied with cross-tolerance to other echinocandins drugs.

Most *C. albicans* strains are diploid with eight pairs of chromosomes. We previously demonstrated that *C. albicans* was highly tolerant to aneuploidy, and each chromosome could be trisomic. Although aneuploidy generally caused some fitness loss in the absence of stress, under stress conditions, aneuploidy conferred better fitness to particular stresses and cross-tolerance to other unrelated stresses[7] and this is often due to different genes on the same chromosome. For example, in *C. albicans* adapted to low but inhibitory concentrations of CSP via Chr5 × 1[8]) or Chr2 × 3[9] and Chr2 × 3 also confers cross tolerance to hydroxyurea and to tu-

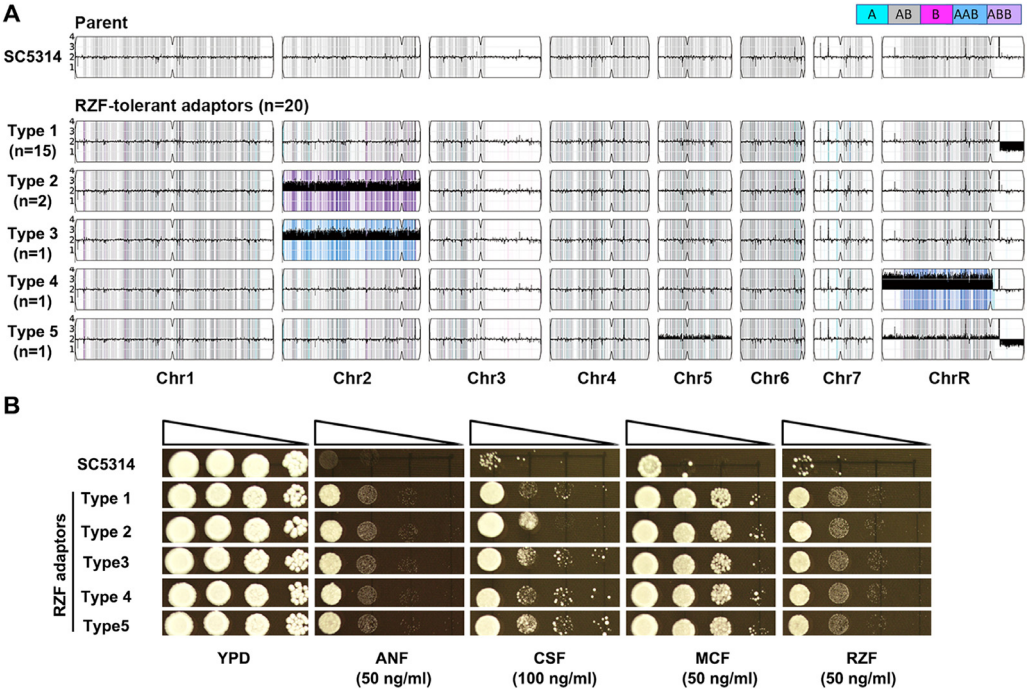

Fig. 2. Paradoxical growth facilitates cross-tolerance to echinocandins via aneuploidy**.**
RZF-tolerant adaptors were sequenced and unique karyotypes, as well as the number of adaptors bearing the karyotypes, were shown in (A). The sequencing data was visualized using Ymap.[10] Read depth (normalized to that of the diploid parent) is shown on the y-axis on a log2 scale converted to absolute copy number (1–4). Allelic ratios (A:B) are color-coded: gray, 1:1 (A/B); cyan, 1:0 (A or A/A); magenta, 0:1 (B or B/B); purple, 1:2 (A/B/B); blue, 2:1 (A/A/B); The sequencing data have been deposited in the ArrayExpress database at EMBL-EBI (www.ebi.ac.uk/arrayexpress) under accession number E-MTAB-12,116. In (B), strains bearing the different karyotypes were tested for tolerance to all echinocandin drugs, including anidulafungin (ANF), caspofungin (CSP), micafungin (MCF), and rezafungin (RZF). The plates were incubated at 37°C for 48 h then photographed.

nicamycin.[5] However, to the best of our knowledge, this current study is the first to identify a genomic change associated with PG in yeasts.

Although only a small percentage of adaptors derived from exposure to high concentrations of RZF gained tolerance to RZF, all the tolerant adaptors were aneuploid and all were cross-tolerant to all echinocandins drugs. The karyotypes were diverse, indicating multiple aneuploidies enabled survival from the fungicidal drugs and conferred drug tolerance. SegChrRx1 was the most prevalent change and was recurrently isolated from plates containing different concentrations of RZF, indicating that the occurrence of SegChrRx1 was RZF dose-independent, and it conferred tolerance to wide range of RZF doses. Future work is warranted to test if this mechanism, or an alternative mechanism, is implicated in clinical treatment failure of candidiasis with echinocandins and in the development of drug tolerance *in vivo*.

Fig. S1. **Spot assay screening of all the adaptors**.

Colonies that appeared on all of the plates supplemented with RZF were tested with spot assay for tolerance to RZF.

Acknowledgements

This work was supported by National Natural Science Foundation of China (NO. 82020108032), and the Innovation Program of Shanghai Municipal Education Commission (NO. 202101070007E00094) to Yuan-ying Jiang). National Natural Science Foundation of China (NO. 81872910), and Shanghai Key Basic Research Project (NO. 19JC1414900) to Yong-bing Cao.

Supplementary materials

Supplementary material associated with this article can be found, in the online version, at doi:10.1016/j.jinf.2022.09.028.

References

1. Zhao Y., Perlin DS.. Review of the novel echinocandin antifungal rezafungin: animal studies and clinical data. *J Fungi* 2020;**6** (Basel).
2. Vanstraelen K., Lagrou K., Maertens J., Wauters J., Willems L., Spriet I.. The Eagle-like effect of echinocandins: what's in a name? *Expert Rev Anti Infect Ther* 2013;**11**:1179–91.
3. Walker L.A., Munro C.A., de Bruijn I., Lenardon M.D., McKinnon A., Gow NA.. Stimulation of chitin synthesis rescues *Candida albicans* from echinocandins. *PLoS Pathog* 2008;**4**:e1000040.
4. Healey K.R., Katiyar S.K., Raj S., Edlind T.D.. CRS-MIS in Candida glabrata: sphingolipids modulate echinocandin-Fks interaction. *Mol Microbiol* 2012;**86**:303–13.
5. Yang F., Gritsenko V., Slor Futterman Y., Gao L., Zhen C., Lu H., et al. Tunicamycin potentiates antifungal drug tolerance via aneuploidy in *Candida albicans*. *mBio* 2021;**12**:e0227221.
6. Yang F., Lu H., Wu H., Fang T., Berman J., Jiang YY.. Aneuploidy underlies tolerance and cross-tolerance to drugs in candida parapsilosis. *Microbiol Spectr* 2021;**9**:e0050821.
7. Yang F., Todd R.T., Selmecki A., Jiang Y.Y., Cao Y.B., Berman J.. The fitness costs and benefits of trisomy of each *Candida albicans* chromosome. *Genetics* 2021;**218**.
8. Yang F., Zhang L., Wakabayashi H., Myers J., Jiang Y., Cao Y., et al. Tolerance to caspofungin in *candida albicans* is associated with at least three distinctive mechanisms that govern expression of FKS genes and cell wall remodeling. *Antimicrob Agents Chemother* 2017;**61**.
9. Yang F., Teoh F., Tan A.S.M., Cao Y., Pavelka N., Berman J.. Aneuploidy enables cross-adaptation to unrelated drugs. *Mol Biol Evol* 2019;**36**:1768–82.
10. Abbey D.A., Funt J., Lurie-Weinberger M.N., Thompson D.A., Regev A., Myers C.L., et al. YMAP: a pipeline for visualization of copy number variation and loss of heterozygosity in eukaryotic pathogens. *Genome Med.* 2014;**6**:100.

Hao Li
Department of Pharmacy, Shanghai Tenth People's Hospital, Tongji University School of Medicine, Shanghai, China
Department of Physiology and Pharmacology, School of Basic Medicine and Clinical Pharmacy, China Pharmaceutical University, Nanjing, China

Yong-bing Cao
Institute of Vascular Disease, Shanghai TCM-Integrated Hospital, Shanghai University of Traditional Chinese Medicine, Shanghai, China

Tian-hua Yan
Department of Physiology and Pharmacology, School of Basic Medicine and Clinical Pharmacy, China Pharmaceutical University, Nanjing, China

Yuan-ying Jiang*, Feng Yang*
Department of Pharmacy, Shanghai Tenth People's Hospital, Tongji University School of Medicine, Shanghai, China

*Corresponding authors.
E-mail addresses: jiangyy@tongji.edu.cn (Y.-y. Jiang), feng.yang0405@gmail.com (F. Yang)

Accepted 1 September 2022
Available online 1 October 2022

https://doi.org/10.1016/j.jinf.2022.09.028

Increase of multidrug-resistant bacteria after the COVID-19 pandemic in South Korea: Time-series analyses of a long-term multicenter cohort

Dear Editor,

Concerns are being raised about whether the long-standing coronavirus disease 2019 (COVID-19) pandemic will increase the burden of multidrug-resistant organisms (MDROs).[1] The healthcare practices may have been disrupted and overloaded owing to the lack and exhaustion of frontline healthcare workers (HCWs), particularly during the COVID-19 crisis.[2] This situation could cause the overuse of antibiotics and inappropriate environmental management, given the move away from priorities of antimicrobial stewardship programs (ASP) and contact precautions.[3] On the contrary, unprecedentedly strict implementation of non-pharmacological interventions (NPIs) may help reduce the intra-hospital spread of MDROs through excellent hand hygiene and the use of personal protection equipment. The inconsistent results from previous studies, which were conducted in the early stages of the COVID-19 pandemic and included relatively short observation periods,[3–7] warrant close monitoring of the epidemiology trends of MDROs in various. We aimed to investigate the changing trends in new case and bacteremia with MDROs before and after the COVID-19 pandemic in South Korea, where the frequency of MDROs is high.[8]

This multicenter retrospective cohort study included six medical university-affiliated hospitals that were located in three different provinces of South Korea. We collected the monthly numbers of new case (first identification in clinical specimens or stool) and first bacteremia of extensively drug-resistant *Acinetobacter baumanii* (XDR-ABA), difficult-to-treat *Pseudomonas aeruginosa* (DTR-PAE), vancomycin-resistant *Enterococci* (VRE), and carbapenem-resistant *Enterobacterales* (CRE) as well as numbers of stool examinations for VRE and CRE between January 2012 and December 2021. The VRE or CRE stool tests were categorized into two kinds of data: (1) total negative results, best reflecting the efforts to detect VRE and CRE, and (2) first examination after hospitalization, including positive and negative results (except for the stool tests performed after VRE or CRE was detected in a clinical sample), which would represent the active surveillance performance appropriately. We divided the case of MDROs into pre- and post-COVID-19 periods, using the cutoff date of January 2020. The study was approved by the local Institutional Review Board from each hospital with the waiver of the informed consent (YUHS:3–2022–0176, KUAM:2022AN0027, KNUH:2022–01–002, and HUCH:2022–01–016).

Isolates were categorized as XDR when they showed non-susceptibility to ≥1 antimicrobial agent in all but ≤2 antimicrobial categories. Isolate were categorized as DTR when there was no susceptibility to the antimicrobial categories of carbapenems, antipseudomonal β-lactams, and fluoroquinolones. We included CRE isolates that were not susceptible to any carbapenem, regardless of carbapenemase-producing strains (CPE).[9]

We applied the Bayesian structural time series (BSTS) model, which is the state-space analysis proposed by Google, Inc.,[10] using the R-language (version 4.1.3). The BSTS model can determine the causalities and regression of an intervention using its counterfactual prediction function by artificial control of what would have taken place had the intervention not occurred and the observed data.[10] We expressed the relative ([observed–predicted]/predicted × 100) causal effects as percentages and 95% credible prediction intervals (CIs). The autoregressive integrated moving average (ARIMA) model was adjusted for the stool examinations in VRE or CRE using SAS (version 9.4) to minimize the impact of test numbers on the new case. A two-tailed p-value < 0·05 was considered statistically significant.

The BSTS models revealed that both new case and first bacteremia of XDR-ABA (relative effects; 47% [95% CI:19–79%], $p = 0.003$ and 150% [93–211%], $p = 0.001$, respectively) and DTR-PAE (41% [17–67%], $p = 0.002$ and 103% [65–145%], $p = 0.001$, respectively) had significantly increased in the post-COVID period. In addition, the observed values of VRE were significantly higher than the predicted values after the COVID-19 pandemic for both new case (10% [3–17%], $p = 0.007$) and first bacteremia (65% [48–83%], $p = 0.001$). The first CRE bacteremia numbers also showed a significant increase in the post-COVID-19 era (106% [78–135%], $p = 0.001$). However, the observed data for new case of total CRE ($p = 0.056$) did not differ from the predicted values (Table 1 and Fig. 1). After adjustment for stool test numbers, which were decreased in the post-COVID-19 period, the new case (32% in model 3 adjusted for total negative and first examination) and first bacteremia (12%) of VRE showed a significant increase compared to the predicted values (all $p < 0.001$). The reduction in stool examinations did not affect the number of first bacteremia of CRE (4%, $p = 0.025$) (Table 2).

Two recent studies presented the protective effect of the COVID-19 pandemic against extended-spectrum β-lactamase-producing *E. coli* isolates and CPE using data until December 2020 in France.[4,6] The authors attributed these results to the decrease in antibiotic usage or testing of urine samples and hospital visits due to the overall lockdown as well as increased implementation of NPIs.[4,6] It seems unclear whether these beneficial effects would extend beyond developed countries or after a period of well-executed strong national policies mitigating COVID-19 and

[1] The vertical dotted lines in all graphs represent January 2020, the beginning of the COVID-19 pandemic. The straight and dotted lines in the original panels indicate the observed and predicted values using the BSTS model, respectively. The dotted lines in the pointwise impact panels indicate the differences between the observed and predicted values, which are called residuals. The dotted lines in the cumulative impact panels represent the accumulated residuals.

Table 1
Changes in new case and first bacteremia with MDROs during the pre- and post-COVID pandemic using the Bayesian structural time series model.

MDROs	Variables	COVID-19 pandemic					
		Before (2012~2019)	After (2020~2021)				
		Observed (N)	Observed (N)	Predicted (N)	Absolute effect (N)	Relative effect (%)	*p*-value
VRE	**New case**						
	Total	54.9	86.0	78.2 (72.3–84·1)	7.7 (2.4–13.6)	10 (3–17)	0.007
	VR-*E. faecium*	24.5	54.0	33.7 (28.9–38·3)	20.3 (16.2–24.8)	60 (48–73)	0.001
	New bacteremia						
	Total	12.2	23.5	14.3 (12.2–16·9)	9.2 (6.8–11.8)	65 (48–83)	0.001
	VR-*E. faecium*	9.5	18.8	11.4 (9.2–13·0)	7.4 (5.3–9.6)	64 (46–84)	0.001
CRE	**New case**						
	Total	57.9	74.3	67.2 (58.1–75·9)	7.2 (−1.5–16.6)	11 (−2–25)	0.056
	CR-*Klebsiella* spp.	36.4	51.6	49.7 (42.7–56·2)	1.9 (−4.6–9.1)	4 (−9–18)	0.301
	CR-*E. coli*	14.5	16.0	14.0 (11.1–17·3)	2.0 (−0.7–4.8)	14 (−5–35)	0.073
	New bacteremia						
	Total	10.2	15.4	7.5 (5.3–9·5)	7.9 (5.8–10.1)	106 (78–135)	0.001
	CR-*Klebsiella* spp.	5.2	10.0	4.7 (3.2–6·1)	5.2 (3.8–6.8)	111 (81–143)	0.001
	CR-*E. coli*	3.9	3.8	2.4 (1.4–3·4)	1.4 (0.5–2.5)	59 (19–102)	0.005
XDR-ABA	**New case**	64.7	52.8	35.8 (24.8–46·4)	17.0 (6.7–28.2)	47 (19–79)	0.003
	New bacteremia	9.1	8.5	3.4 (1.3–5·3)	5.1 (3.2–7.1)	150 (93–211)	0.001
DTR-PAE	**New case**	46.3	45.9	32.7 (23·8–41.2)	13.3 (5.4–21.8)	41 (17–67)	0.002
	New bacteremia	4.0	5.5	2.7 (1.6–3.7)	2.8 (1.8–3.9)	103 (65–145)	0.001

Data are expressed as numbers or numbers (95% credible prediction intervals).

beyond β-lactamase-producing MDROs because other studies have reported conflicting results.[3,7]

Our study showed that the occurrence of the most problematic MDROs had increased after the COVID-19 pandemic, especially in case of bacteremia. Surprisingly, the MDR-ABA and DTR-PAE, which had been steadily decreasing before the pandemic, showed an increasing trend in both new case and first bacteremia after COVID-19 (Figs. S1 and S2). Our results are similar to the trends of national data from the Korea Centers for Disease Control and Prevention. The total number of CRE infections and colonization,

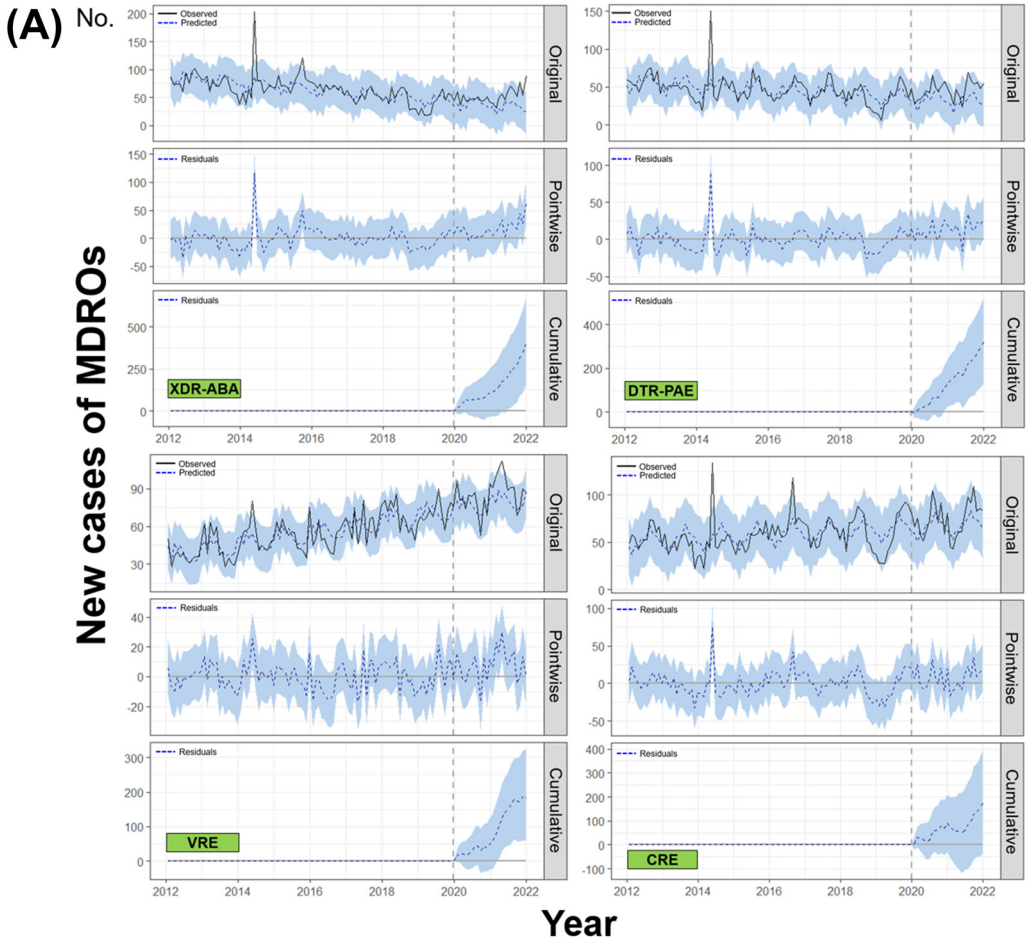

Fig. 1. Changes in numbers of new case and first bacteremia patients of several MDROs before and after the COVID-19 pandemic evaluated by the Bayesian structural time series model (A) New case (B) First bacteremia.[1]

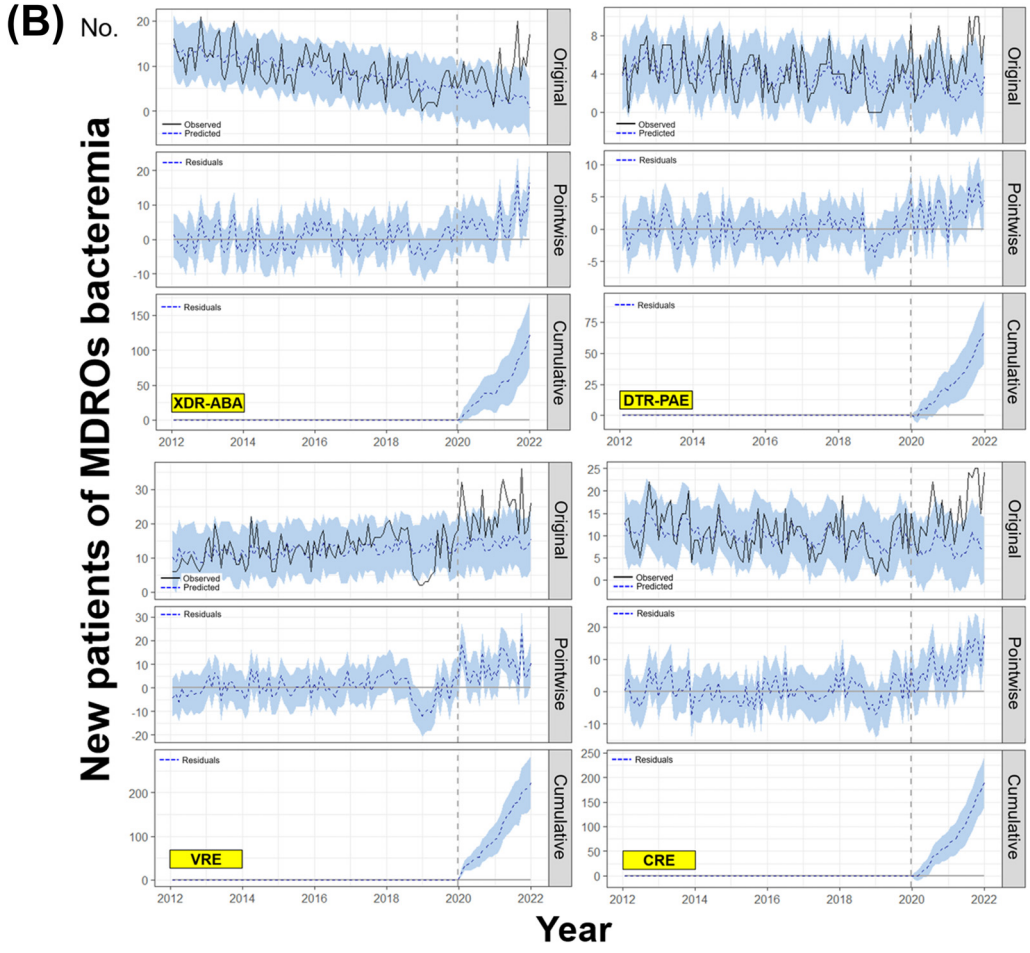

Fig. 1. Continued

Table 2
Multivariable analyses adjusted by numbers of VRE or CRE stool tests in the autoregressive integrated moving average (ARIMA) model.

MDROs	Variables	Model 1		Model 2		Model 3	
		Estimate (SE)	*p*-value	Estimate (SE)	*p*-value	Estimate (SE)	*p*-value
VRE	**New case**						
	Total	29.85 (7.24)	<0.001	32.36 (5.50)	<0.001	31.76 (5.45)	<0.001
	VR-*E. faecium*	25.43 (4.72)	<0.001	24.45 (4.76)	<0.001	25.06 (4.89)	<0.001
	New bacteremia						
	Total	11.98 (2.07)	<0.001	11.88 (2.01)	<0.001	11.97 (2.06)	<0.001
	VR-*E. faecium*	9.83 (1.75)	<0.001	9.84 (1.69)	<0.001	9.81 (1.71)	<0.001
CRE	**New case**						
	Total	12.39 (7.44)	0.099	12.40 (7.53)	0.103	12.53 (7.67)	0.106
	CR-*Klebsiella spp.*	18.73 (10.34)	0.074	18.93 (5.50)	<0.001	15.77 (7.02)	0.027
	CR-*E. coli*	0.92 (1.66)	0.582	0.96 (1.63)	0.558	0.98 (1.63)	0.549
	New bacteremia						
	Total	4.51 (1.93)	0.022	4.51 (1.93)	0.022	4.45 (1.96)	0.025
	CR-*Klebsiella spp.*	4.51 (1.45)	0.002	4.52 (1.44)	0.002	4.52 (1.45)	0.003
	CR-*E. coli*	0.15 (0.61)	0.803	0.15 (0.62)	0.813	0.15 (0.62)	0.809

The estimate (standard error) is expressed as a percentage. Model 1: adjusted for total negative results of stool VRE or CRE tests (category 1); model 2: adjusted for total stool VRE or CRE tests performed as the first examination after admission (category 2); model 3: adjusted for categories 1 and 2.

designated as a legal infectious disease in June 2017 and converted to a surveillance system with mandatory reporting within 24 h in South Korea, significantly increased since the COVID-19 pandemic (Fig. S3).

As a limitation, we did not quantify the performance rate of various elements of NPIs and ASP as well as an overload of HCWs at several hospitals. As the duration of the pandemic increases, the rate of implementation of initially strong policies would decrease. Taken together, our findings are concerning because the effects of MDROs on global health are critical, and it is difficult and time-consuming to reduce the resistance to the same levels as before. Hence, we need to actively and continuously monitor the increase

in infections with MDROs as well as occurrence of new resistance in various regions.

Supplementary materials

Supplementary material associated with this article can be found, in the online version, at doi:10.1016/j.jinf.2022.09.026.

References

1. Pelfrene E., Botgros R., Cavaleri M.. Antimicrobial multidrug resistance in the era of COVID-19: a forgotten plight? *Antimicrob Resist Infect Control* 2021;**10**:21.
2. Karan A., Wadhera R.K.. Healthcare system stress due to COVID-19: evading an evolving crisis. *J Hosp Med* 2021;**16**:127.
3. Bork J.T., Leekha S., Claeys K., Seung H., Tripoli M., Amoroso A., et al. Change in hospital antibiotic use and acquisition of multidrug-resistant gram-negative organisms after the onset of coronavirus disease 2019. *Infect Control Hosp Epidemiol* 2021;**42**:1115–17.
4. Lemenand O., Coeffic T., Thibaut S., Colomb Cotinat M., Caillon J., Birgand G. Decreasing proportion of extended-spectrum beta-lactamase among E. coli infections during the COVID-19 pandemic in France. *J Infect* 2021;**83**:664–70.
5. Taylor L.. COVID-19: antimicrobial misuse in Americas sees drug resistant infections surge, says WHO. *BMJ* 2021;**375**:n2845.
6. Duverger C., Monteil C., Souyri V., Fournier S.. Decrease of carbapenemase-producing enterobacteriaceae incidence during the first year of the COVID-19 pandemic. *J Infect* 2022;**85**:90–122.
7. Segala F.V., Bavaro D.F., Di Gennaro F., Salvati F., Marotta C., Saracino A., et al. Impact of SARS-CoV-2 epidemic on antimicrobial resistance: a literature review. *Viruses* 2021;**13**.
8. Lee H., Yoon E.J., Kim D., Jeong S.H., Won E.J., Shin J.H., et al. Antimicrobial resistance of major clinical pathogens in South Korea, May 2016 to April 2017: first one-year report from Kor-GLASS. *Euro Surveill* 2018;**23**.
9. Magiorakos A.P., Srinivasan A., Carey R.B., Carmeli Y., Falagas M.E., Giske C.G., et al. Multidrug-resistant, extensively drug-resistant and pandrug-resistant bacteria: an international expert proposal for interim standard definitions for acquired resistance. *Clin Microbiol Infect* 2012;**18**:268–81.
10. Brodersen K.H., Gallusser F., Koehler J., Remy N., Scott S.L.. Inferring causal impactusing Bayesian structural time-series models. *Ann Appl Stat* 2015;**9**:247–74.

Yeonju La[1]
Division of Infectious Disease, Department of Internal Medicine, Kangwon National University Hospital, Chuncheon, Gangwon-do, Republic of Korea

Ji Young Hong[1]
Division of Pulmonary, Allergy and Critical Care Medicine, Department of Internal Medicine, Chuncheon Sacred Heart Hospital, Hallym University Medical Center, Republic of Korea

Hye Sun Lee
Biostatistics Collaboration Unit, Yonsei University College of Medicine, Seoul, Republic of Korea

Eun Hwa Lee, Kyoung Hwa Lee, Young Goo Song
Division of Infectious Disease, Department of Internal Medicine, Yonsei University College of Medicine, 211 Eonju-ro, Gangnam-gu, Seoul 06273, Republic of Korea

Sun Bean Kim*
Division of Infectious Diseases, Department of Internal Medicine, Korea University College of Medicine, 73 Goryeodae-ro, Seongbuk-gu, Seoul 02841, Republic of Korea

Sang Hoon Han*
Division of Infectious Disease, Department of Internal Medicine, Yonsei University College of Medicine, 211 Eonju-ro, Gangnam-gu, Seoul 06273, Republic of Korea

*Corresponding authors.
E-mail addresses: puppybin@gmail.com (S.B. Kim), shhan74@yuhs.ac (S.H. Han)

[1] These authors contributed equally to this work (Co-first authorship).

Accepted 24 September 2022
Available online 30 September 2022

https://doi.org/10.1016/j.jinf.2022.09.026

Coronavirus disease 2019 vaccination and live birth outcome after fresh embryo transfer

Dear Editor,

Coronavirus disease 2019 (COVID-19) has become a global pandemic and vaccination is a key strategy to reduce morbidity and mortality from the disease. This is especially important for reproductive-aged women planning to conceive, since COVID-19 could result in unfavorable obstetric and neonatal outcomes during pregnancy as addressed by a living systematic review with meta-analysis[1] and two recent articles published in the *Journal of Infection*.[2,3] However, vaccination coverage remains slow-moving despite of increased access, with fertility concern identified as a major source of hesitancy.[4] Among *in vitro* fertilization (IVF) cycles, accumulating studies have demonstrated no significant association of COVID-19 vaccines with ovarian response, oocyte quality, and embryo implantation.[5–8] Nonetheless, data on live birth, the key outcome of IVF treatment, is still lacking due to the short follow-up period. The purpose of our study was to evaluate the effect of inactivated COVID-19 vaccination on live birth outcome after fresh embryo transfer (ET).

This was a retrospective cohort study of all infertile women undergoing fresh ET cycles from June 1st to October 18th 2021 at our reproductive center with ISO 9001:2015 quality control. Study approval was obtained from the Ethics Committee of Jiangxi Maternal and Child Health Hospital (No. 2021–02), and all patients provided written informed consents. The study group consisted of patients who completed two full doses of inactivated COVID-19 vaccines (Sinopharm or Sinovac) before ET, while those unvaccinated were categorized into the control group. We excluded patients with partial vaccination, other vaccine types, self-reported COVID-19 history, donor sperm or oocyte, repeated cycles, loss to follow-up, and missing IVF data. The primary outcome was the rate of live birth, defined as the delivery of a viable infant at $\geq$24 weeks of gestation. Details on vaccination status ascertainment, routine IVF protocol, and other outcome measures have been described in our previous study of the same cohort.[8]

For between-group comparison, we used Student's *t*-test, Mann-Whitney U-test, Pearson's Chi-square test, or Fisher's exact test as appropriate. Multiple logistic regression analysis was applied to control for potential confounders. Based on an overall live birth rate (LBR) of 55% in our center, a sample size of 117 patients *per* group was estimated to detect a 18% post-vaccination decrease with 80% power and alpha of 0.05. Data analysis was conducted in SAS version 9.4 (SAS Institute, USA), and a two-sided $P < 0.05$ was considered as statistically significant.

Of the 1385 patients included, 124 were vaccinated and 1261 were unvaccinated. The two groups differed significantly in female age, uterine factor infertility, previous transfer times, ovarian stimulation protocol, fertilization method, and male vaccination status. No significant differences were observed in other baseline de-

Table 1
Baseline demographics, cycle characteristics, and laboratory outcomes of included patients.

	Vaccinated (n = 124)	Unvaccinated (n = 1261)	P-value
Age (years)	31.8 ± 4.3	31.0 ± 4.4	0.017
Body mass index (kg/m^2)	21.9 ± 3.2	22.2 ± 3.1	0.101
Antral follicle count	13.5 ± 6.1	13.9 ± 5.8	0.238
Infertility duration (years)	4.4 ± 2.9	4.2 ± 3.0	0.338
Type of infertility, n (%)			0.959
Primary	47 (37.9)	475 (37.7)	
Secondary	77 (62.1)	786 (62.3)	
Infertility diseases			
Tubal factor, n (%)	88 (71.0)	917 (72.7)	0.677
Male factor, n (%)	30 (24.2)	301 (23.9)	0.936
Ovulatory dysfunction, n (%)	14 (11.3)	175 (13.9)	0.423
Diminished ovarian reserve, n (%)	10 (8.1)	105 (8.3)	0.920
Endometriosis, n (%)	13 (10.5)	85 (6.7)	0.121
Uterine factor, n (%)	25 (20.2)	145 (11.5)	0.005
Male vaccination status, n (%)			<0.001
Unvaccinated	42 (33.9)	1115 (88.4)	
Partially vaccinated	10 (8.1)	77 (6.1)	
Fully vaccinated	72 (58.1)	69 (5.5)	
Previous retrievals	1.2 ± 0.5	1.2 ± 0.6	0.209
Previous transfers	0.3 ± 0.8	0.2 ± 0.6	0.043
Ovarian stimulation protocol, n (%)			0.001
Agonist	120 (96.8)	1255 (99.5)	
Antagonist	4 (3.2)	6 (0.5)	
Fertilization method, n (%)			0.015
IVF	96 (77.4)	946 (75)	
ICSI	27 (21.8)	222 (17.6)	
IVF+ICSI	1 (0.8)	93 (7.4)	
Stimulation duration (days)	10.9 ± 1.9	11 ± 2.0	0.746
Total gonadotropin dose (IU)	2175.8 ± 731.2	2136.2 ± 809.4	0.389
Trigger day estradiol level (pg/mL)	1658.6 ± 901.1	1780.7 ± 845.7	0.081
Trigger day progesterone level (ng/mL)	0.4 ± 0.3	0.4 ± 0.3	0.497
Trigger day endometrial thickness (mm)	10.8 ± 2.8	11.0 ± 2.5	0.160
Number of oocytes retrieved	10.8 ± 4.9	11.4 ± 4.6	0.174
ICSI mature oocyte rate (%)	75.0 ± 12.8	77.9 ± 19.8	0.192
Normal fertilization rate (%)	68.6 ± 20.5	67.3 ± 19.8	0.376
Cleavage rate (%)	96.1 ± 7.8	96.7 ± 8.0	0.180
Day 3 good-quality embryo rate (%)	29.5 ± 25.1	28.1 ± 23.5	0.699
Blastocyst formation rate (%)	74.3 ± 29.4	72.7 ± 30.3	0.683
Number of viable embryos	3.9 ± 2.2	3.7 ± 2.0	0.333
Number of embryos transferred, n (%)			0.497
Single	40 (32.3)	370 (29.3)	
Double	84 (67.7)	891 (70.7)	
Embryo developmental stage, n (%)			0.688
Cleavage	92 (74.2)	956 (75.8)	
Blastocyst	32 (25.8)	305 (24.2)	
Transfer of at least 1 good-quality embryo, n (%)	80 (64.5)	883 (70.0)	0.204

Note: Data are presented as mean ± standard deviation or number (percentage). IVF = *in vitro* fertilization; ICSI = intracytoplasmic sperm injection.

mographics, cycle characteristics, as well as laboratory outcomes (Table 1).

LBR was 49.2% and 54.4% in vaccinated and unvaccinated patients respectively (P = 0.267), resulting in a crude odds ratio (OR) of 0.81 (95% confidence interval [CI] 0.56–1.77) and an adjusted OR of 0.97 (95% CI 0.62–1.51). Similarly, there were no significant differences in biochemical pregnancy, clinical pregnancy, and miscarriage rates, which remained consistent on crude and adjusted analyses (Table 2). Obstetric and neonatal outcomes were also followed-up during pregnancy, and no evidently increased complications were observed in the vaccinated group (Supplementary Table S1).

For vaccinated patients, the mean time interval between complete vaccination and ET was 126.5 ± 64.0 (range 13–246) days. As demonstrated in Supplementary Table S2, both laboratory and pregnancy outcomes remained comparable when these patients were subdivided into ≤2-month and >2-month groups.

For the first time, our study showed that COVID-19 vaccination had no measurable effect on LBR in IVF cycles, which adds to the growing evidence on its reproductive safety and provides reassurance for fertility-seeking women. Consistent with guidelines from the American Society for Reproductive Medicine and European Society of Human Reproduction and Embryology,[9,10] our preliminary data also demonstrated no significant impact of vaccination interval on IVF outcome, as long as the immune response was stabilized after several days.

This study is limited by its small sample size in a single center and retrospective design with potential residual confounding and selection bias. Moreover, the generalization of our finding could be restricted by the inclusion of only inactivated vaccines and the majority of double cleavage-stage embryo transfer. Further larger prospective cohort studies are needed to confirm our conclusion.

Table 2
Pregnancy outcomes of vaccinated *versus* unvaccinated patients after fresh embryo transfer.

	Vaccinated (n = 124)	Unvaccinated (n = 1261)	P-value	cOR (95% CI)	aOR (95% CI) [a]
Biochemical pregnancy, n (%)	89 (71.8)	928 (73.6)	0.662	0.91 (0.61–1.38)	1.39 (0.84–2.31)
Clinical pregnancy, n (%)	76 (61.3)	799 (63.4)	0.648	0.92 (0.63–1.34)	1.26 (0.80–2.00)
Embryo implantation, n/N (%)	98/208 (47.1)	1027/2152 (47.7)	0.867	–	–
Miscarriage, n/N (%)	14/76 (18.4)	104/799 (13.0)	0.187	1.51 (0.82–2.79)	1.40 (0.71–2.76)
Live birth, n (%)	61 (49.2)	686 (54.4)	0.267	0.81 (0.56–1.17)	0.97 (0.62–1.51)

Note: cOR = crude odds ratio; CI = confidence interval; aOR = adjusted odds ratio.
[a] Adjusted for age, body mass index, infertility type, duration of infertility, infertility diseases, male vaccination status, previous retrievals and transfers, ovarian stimulation protocol, fertilization method, trigger day estradiol and progesterone level, number of oocytes retrieved, endometrial thickness, number of embryos transferred, embryo developmental stage, and embryo quality.

Funding

This study was funded by the National Natural Science Foundation of China (82,260,315).

Disclosure statement

None declared.

Declaration of Competing Interest

The authors declare that they have no conflict of interest.

Supplementary materials

Supplementary material associated with this article can be found, in the online version, at doi:10.1016/j.jinf.2022.09.023.

References

1. Allotey J., Stallings E., Bonet M., Yap M., Chatterjee S., Kew T., et al. Clinical manifestations, risk factors, and maternal and perinatal outcomes of coronavirus disease 2019 in pregnancy: living systematic review and meta-analysis. *BMJ* 2020;**370**:m3320.
2. Huang W., Zhao Z., He Z., Liu S., Wu Q., Zhang X., et al. Unfavorable outcomes in pregnant patients with COVID-19. *J Infect* 2020;**81**:e99–e101.
3. Liu Y., Chen H., Tan W., Kuang Y., Tang K., Luo Y., et al. Clinical characteristics and outcome of SARS-CoV-2 infection during pregnancy. *J Infect* 2021;**82**:e9–e10.
4. Diaz P., Zizzo J., Balaji N.C., Reddy R., Khodamoradi K., Ory J., et al. Fear about adverse effect on fertility is a major cause of COVID-19 vaccine hesitancy in the United States. *Andrologia* 2022;**54**:e14361.
5. Orvieto R., Noach-Hirsh M., Segev-Zahav A., Haas J., Nahum R., Aizer A.. Does mRNA SARS-CoV-2 vaccine influence patients' performance during IVF-ET cycle? *Reprod Biol Endocrinol* 2021;**19**:69.
6. Aizer A., Noach-Hirsh M., Dratviman-Storobinsky O., Nahum R., Machtinger R., Yung Y., et al. The effect of coronavirus disease 2019 immunity on frozen-thawed embryo transfer cycles outcome. *Fertil Steril* 2022;**117**:974–9.
7. Avraham S., Kedem A., Zur H., Youngster M., Yaakov O., Yerushalmi G.M., et al. Coronavirus disease 2019 vaccination and infertility treatment outcomes. *Fertil Steril* 2022;**117**:1291–9.
8. Huang J., Xia L., Lin J., Liu B., Zhao Y., Xin C., et al. No Effect of inactivated SARS-CoV-2 vaccination on *in vitro* fertilization outcomes: a propensity score–matched study. *J Inflamm Res* 2022;**15**:839–49.
9. Coronavirus/COVID-19 Task Force of the American Society for Reproductive Medicine. ASRM patient management and clinical recommendations during the coronavirus (COVID-19) pandemic: upate no. 13—Variants, vaccines, and vaccination February 22, 2021. https://www.asrm.org/globalassets/asrm/asrm-content/news-and-publications/covid-19/covidtaskforceupdate13.pdf (accessed August 31, 2022).
10. ESHRE COVID-19 Working Group. Eshre statement on COVID-19 vaccination and medically assisted reproduction. https://www.eshre.eu/Europe/Position-statements/COVID19/vaccination (accessed August 31, 2022).

Jialyu Huang[1]
Leizhen Xia[1]
Yan Zhao
Xingwu Wu
Jia Chen
Mengxi Li
Lifeng Tian
Qiongfang Wu*
Center for Reproductive Medicine, Jiangxi Maternal and Child Health Hospital, Nanchang Medical College, Nanchang, China
*Corresponding author.
E-mail address: wuqfivf@126.com (Q. Wu)

[1] J.H. and L.X. should be considered as co-first authors.

Accepted 17 September 2022
Available online 26 September 2022

https://doi.org/10.1016/j.jinf.2022.09.023

Genomic characteristics of a notable emerging serotype O10:K4 of *Vibrio parahaemolyticus* from food-borne cluster events in Guangzhou, China

Dear Editor,

Pandemic *V. parahaemolyticus* was recognized as one of the important causes of acute gastroenteritis globally. Recently, increasing numbers of new *Vibrio parahaemolyticus* serotype O10:K4 were discovered during food-borne incidents in Guangzhou, the third biggest city in China. The same increasing occurrences were also reported in other cities until very recently, suggesting its ability of rapid dissemination.[1] However, these reports just described the serotype and common virulence gene, and their genetic characteristics were little discovered. In this context, the chromosomal sequences of this new serotype were obtained, and genetic features were detailed. In addition, the phylogenic relationship and genes related with seroconversion were also revealed. These should help us understand the evolution of *V. parahaemolyticus*, alarmed on this new serovariant isolates with pandemic potential.

Six of twelve districts in Guangzhou city have discovered the new serotype O10:K4 during 14 cluster events, affecting more than 130 persons from 2020 to May 2022. The first cluster event was reported in June 2020, more than 40 persons registered with abdominal pain, vomiting, and fever. Seventeen O3:K6 and ten O10:K4 serotypes were isolated. In 2020, four cases were correlated with O10:K4 in twelve food poisoning outbreaks caused by *V. parahaemolyticus* (33.33%), and the percentage arrived at 90.00% (9/10)

Abbreviations: Vibrio parahaemolyticus, serotype O10:K4; food-borne cluster events, Genomic characteristics.

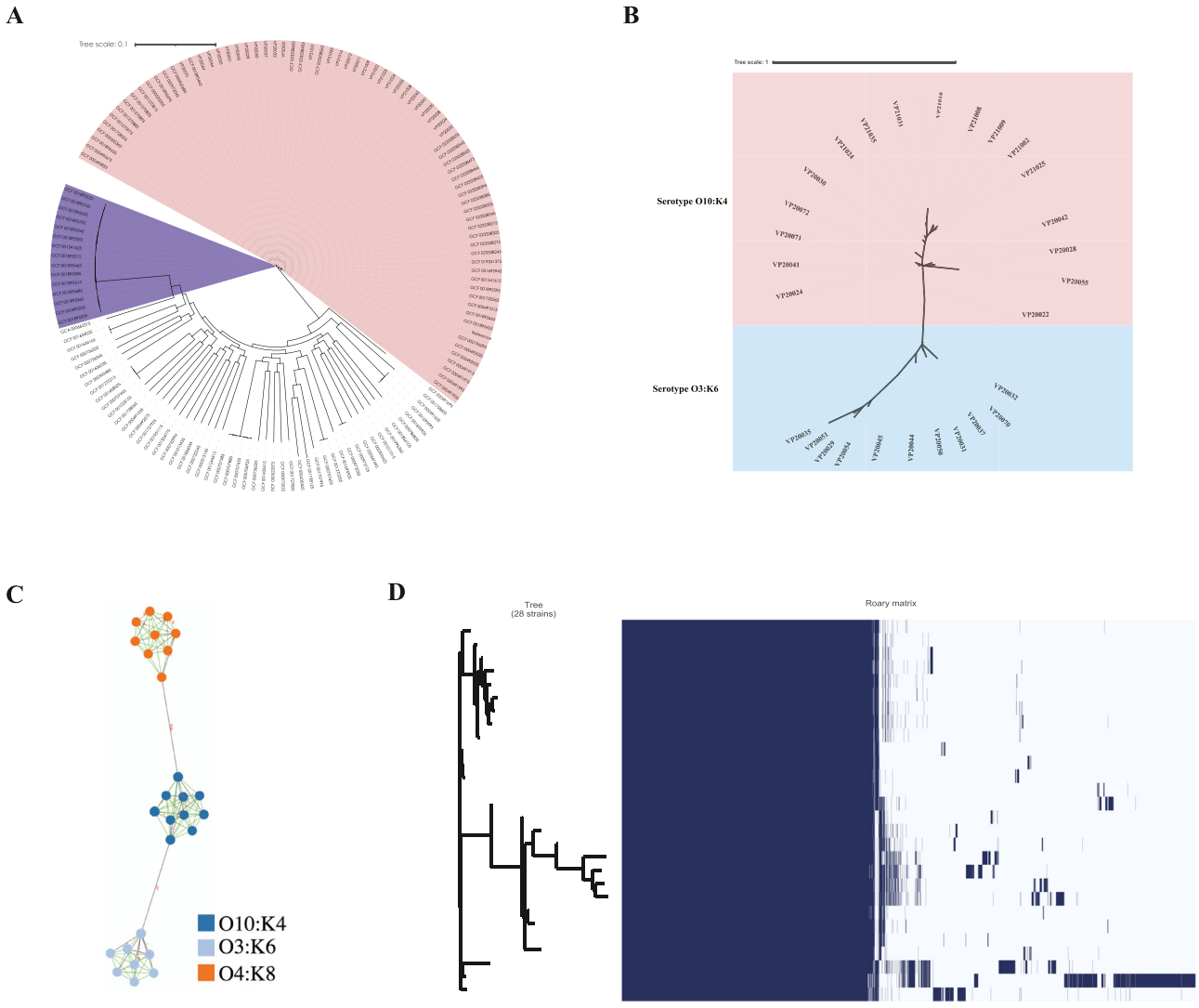

Fig. 1. A) SNP analysis of *V. parahaemolyticus*. 142 of *V. parahaemolyticus* were adopted to construct the phylogenetic tree. Thirty-three were O10:K4, and the rest were other serotypes obtained from GenBank (Suppl.Table 1). The SNP detection was performed by the snippy pipeline with the RIMD 2,210,633 as reference. The pink color was the O3:K6 and O10:K4 serotype, and the purple color represented the O4:K8 group; B) Pan-genome analysis between serotype O10:K4 and O3:K6. The analysis was conducted by roary pipeline. The phylogenetic tree is based on the binary presence and absence of accessory genes. The pink color represented the strains of O10:K4 and the light blue meat the isolates of O3:K6; C) The cg-MLST analysis. The cg-MLST was conducted with the ChewBBACA pipeline. The serotype O10:K4 strains were clustered, different from that of O3:K6 and O4:K8, and O10:K4 were close to the O3:K6 serotype. The numbers on the line were the distance between strains in the same cluster. The red, dark blue, and light blue clusters were serotypes of O4:K8, O10:K4, and O3:K6, respectively; D: the cluster analysis based on core and accessory gens.

in the year 2021. Until August 2022, three food-borne incidents were reported, and all was identified as O10:K4. The same growing trend was also reported in other coastal cities in China[2] and even inland cities,[1] suggesting the new pathogen's ability of rapid dissemination (Suppl. Fig. 1). The high pathogenicity and rapid spreading of this new serotype promoted us to reveal its genetic characteristics.

The high-throughput sequencing was adopted to reveal the characteristics of pathogenic microorganisms. The 28 strains (eighteen O10:K4 and ten O3:K6 strains) isolated in food-borne diarrheal cases during 2020 and 2021 were sequenced (Suppl. Figs. 2 and 3). The results indicated they all belonged to the ST3. All of the GIs, including pandemic genes (tdh^+/ORF-8^+/$toxRS^+$) discovered in the original serotype O3:K6 strain, were also identified in the new serotype O10:K4. These genetic characteristics and virulence factors suggested the new serotype should be regarded as the pandemic clone, with a remarkable ability to cause outbreaks. In fact, its occurrence was increasing in food-borne diarrheal cases.

The phylogenetic tree based on cgSNP was conducted to determine its closest species. It indicated the O10:K4 and O3:K6 clustered in a group, which differed from O4:K8 (Fig. 1A). The O3:K6 and O4:K8 were the common serotypes discovered in food-borne cluster events in Guangzhou.[3] Now the new serotype O10:K4 has been dominant. Interestingly, although SNP-based analyses have been successfully applied in resolving large national and international outbreaks, they could not accurately distinguish these two different serotypes of *V. parahaemolyticus* (Fig. 1A). These may attribute to their genetic similarity, as indicated by PFGE profiles of these two serotypes.[2] The different serovariants may generate by the incorporation of genes of related species (Horizontal gene transfer, HGT).[4] Therefore, building phylogenetic trees incorporating the exclusive DNA of each isolate may help distinguish different serotypes. The cgMLST profiles based on core genotype (Fig. 1C) and the pan-genome analysis based on gene presence/absence (Fig. 1B and D) provided good resolution of the serotype classification.

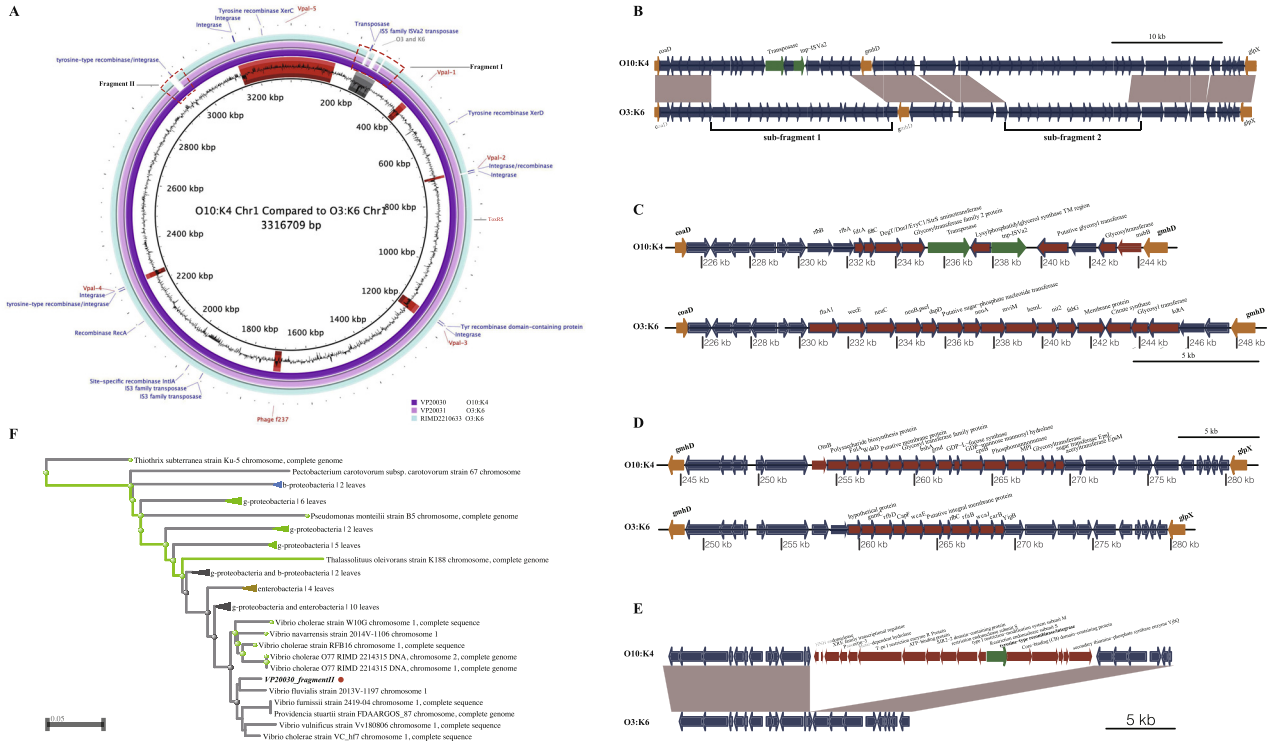

Fig. 2. A) BLAST Ring Image Generator (BRIG) analysis of different serotypes of *V. parahaemolyticus*. The chromosome I of the new serotype O10:K4 was adopted as a reference. The co-occurrence of O3:K6 in the same food poison case and the classical serotype O3:K6 RIMD 2,210,633 were blasted against the reference strain. The innermost rings show GC content; the next arc indicated the VpaI1–5 and phage f237 (marked with red font); the gray arc suggested the genes correlated with O- and K- antigens. The following colored ring was strains of serotype O10:K4, O3:K6, and RIMD 2,210,633, as legend suggested. Genes played a role in horizontal gene transfer was also indicated in the figure (blue font); B-E) The comparative analysis between serotype O10:K4 and O3:K6. The fragment I noted in A is shown in B. The sub-fragment I (C) and sub-fragment II (D) in B were correlated with O- and K- antigens, respectively. The details of sub-fragment I and sub-fragment II was further depicted in C and D. The detailed genes on sub-fragment III indicated in B were shown in E. The orange arrows indicated the conserved genes correlated with serotype. The blue arrows meant the same genes between O10:K4 and O3:K6. The red arrows represented the different genes between O10:K4 and O3:K6, and the green arrows represented the genes correlated with gene insertion and recombination. The genes and their position relationship were visualized with the genoPlotR (v 0.8.11) package in R (v 3.6.2); F) The phylogenic analysis between fragment II and the most related species in the NCBI database. Fragment II was blasted against the NCBI database to find the closest sequences. The most correlated species were used to build the phylogenetic tree. As suggested, the *Vibrio fluvialis* strain was closed to the fragment inserted in O10:K4.

The BRIG analysis of different serotypes of *V. parahaemolyticus* further indicated two long fragment insertions or transversions on the O10:K4 chromosome (Fig. 2A). The core oligosaccharide was correlated with O serotypes of *V. parahaemolyticus*, located in regions between border marker gene coaD and gmhD.[5] Our research suggested that this part was located on the insertion sub-fragment I (Fig. 2B), and ten genes between these two markers have changed (Fig. 2C). Most of which encoded glycosyl transferase and enzymes correlated with external polysaccharide biosynthesis (Suppl.Table 2). Notably, the gene linked with the lysylphosphatidylglycerol (LPG) synthase TM region was identified, which may be transferred with the help of its bilateral transposon (Fig. 2C). It could modify membrane lipids correlated with seroconversion by adding lysyl groups. More importantly, as human defense systems usually leverage cationic properties to fight against bacteria by its affinity to bacterial profound negative net charged membranes.[6] The added positively-charged L-lysine may confer O10:K4 the ability to resistance to host defense systems.

The K-serogroups related genes are located between *gmhD* and *rig*.[7] Twenty-seven and twenty-two genes were involved in O10:K4 and O3:K6 serotypes, respectively (Fig. 2D). The function of sixteen genes in O10:K4 was different from that of eleven genes in O3:K6, and most of them were involved in the pathways for high molecular weight polysaccharide biosynthesis (Suppl.Table 2). These various genes may result in the K serotype conversion. Besides, *EpsL* and *EpsM* were exclusively identified on this inserted fragment. These two genes were reported to be included in the type II secretion system (T2SS) and regarded as the critical components of the secretion machinery in *Vibrio cholerae*.[8] Notably, *epsM* was a target gene for detecting *V. cholerae*.[9] Therefore, it would generate false positive results when this new serotype *V. parahaemolyticus* was involved in the tested samples.

Most genes on fragment II were correlated with the DNA molecules recombination or integration, such as tyrosine-type recombinase/integrase, HNH endonuclease, type I restriction enzyme R Protein, restriction endonuclease subunit S, SIR2–2 domain-containing protein, and type I restriction-modification system subunit M (Fig. 2E). These may favor the insertion or recombination of fragments I and II discovered in the new serotype O10:K4. The phylogenic analysis suggested this fragment may come from *Vibrio fluvialis* (Fig. 2F). Significantly, the gene encoding the XRE family transcriptional regulator was inserted into the fragment. This gene was reported to be involved in oxidative and high-temperature stress tolerance.[10] The inserted genes may improve the adaptability of the new serotype to the environment, increasing its spreading.

In conclusion, the new serotypes O10:K4 carried entire *vibrio pathogenicity* islands and pandemic genes (tdh^+/ORF-8^+/$toxRS^+$). It was close to the O3:K6 serotype and showed highly similar genetic backbones. There were two insertion fragments in O10:K4 on chromosome I compared with O3:K6. One of these fragments was correlated with the seroconversion of O- and K-antigen. The other fragment may come from *Vibrio fluvialis*, which contained many genes related to insertion or recombination. The new serovariant strain may likely arise from O3:K6 by horizontal transfer and replacement of both O- and K-antigen genetic elements on fragment I. The present work should help advance understand-

ing of the serovariation in *V. parahaemolyticus* and provide valuable information for developing diagnostically relevant serotyping methods.

Funding

This work was supported by grants from the National Nature Science Foundation of China (grant number 82103800); The Key Project of Medicine Discipline of Guangzhou (grant numbers 2021-2023-11, 2021-2023-12); Basic Research Project of Key Laboratory of Guangzhou (grant number 202102100001).

Supplementary materials

Supplementary material associated with this article can be found, in the online version, at doi:10.1016/j.jinf.2022.09.012.

References

1. Huang Y., Du Y., Wang H., Tan D., Su A., Li X., et al. New Variant of Vibrio parahaemolyticus, Sequence Type 3, Serotype O10:K4, China, 2020. *Emerg Infect Dis.* 2022;**28**(6):1261–4.
2. Zhang P., Wu X., Yuan R., Yan W., Xu D., Ji L., et al. Emergence and predominance of a new serotype of Vibrio parahaemolyticus in Huzhou, China. *Int J Infect Dis* 2022;**122**:93–8.
3. Li B., Yang X., Tan H., Ke B., He D., Ke C., et al. Vibrio parahaemolyticus O4:K8 forms a potential predominant clone in southern China as detected by whole-genome sequence analysis. *Int J Food Microbiol* 2017;**244**:90–5.
4. Frazao N., Sousa A., Lassig M., Gordo I.. Horizontal gene transfer overrides mutation in Escherichia coli colonizing the mammalian gut. *Proc Natl Acad Sci USA* 2019;**116**(36):17906–15.
5. Okura M., Osawa R., Tokunaga A., Morita M., Arakawa E., Watanabe H.. Genetic analyses of the putative O and K antigen gene clusters of pandemic Vibrio parahaemolyticus. *Microbiol Immunol* 2008;**52**(5):251–64.
6. Staubitz P., Neumann H., Schneider T., Wiedemann I., Peschel A.. MprF-mediated biosynthesis of lysylphosphatidylglycerol, an important determinant in staphylococcal defensin resistance. *FEMS Microbiol Lett* 2004;**231**(1):67–71.
7. Chen Y., Dai J., Morris J.G. Jr., Johnson J.A. Genetic analysis of the capsule polysaccharide (K antigen) and exopolysaccharide genes in pandemic Vibrio parahaemolyticus O3:K6. *BMC Microbiol* 2010;**10**:274.
8. Michel-Souzy S., Douzi B., Cadoret F., Raynaud C., Quinton L., Ball G., et al. Direct interactions between the secreted effector and the T2SS components GspL and GspM reveal a new effector-sensing step during type 2 secretion. *J Biol Chem* 2018;**293**(50):19441–50.
9. Bonny S.Q., Hossain M.A.M., Uddin S.M.K., Pulingam T., Sagadevan S., Johan M.R.. Current trends in polymerase chain reaction based detection of three major human pathogenic vibrios. *Crit Rev Food Sci Nutr* 2020:1–19.
10. Hu Y., Hu Q., Wei R., Li R., Zhao D., Ge M., et al. The XRE family transcriptional regulator SrtR in streptococcus suis is involved in oxidant tolerance and virulence. *Front Cell Infect Microbiol* 2019;**8**(452) 2019-January-10.

Peng He[1], Jing Zhang[1], Yong Zhou, Shuiping Hou, Xia Tao, Anna Wang, Zhicong Yang*, Zhijun Bai*, Xinwei Wu*

Guangzhou Center for Disease Control and Prevention, Guangzhou 510440, Guangdong province, China

Institute of Public Health, Guangzhou Medical University & Guangzhou Center for Disease Control and Prevention, Guangzhou 510440, Guangdong province, China

*Corresponding authors at: Department of Microbiology, Guangzhou Center for Disease Control and Prevention, Jiahe qide Road, Baiyun district, Guangzhou 510440, Guangdong, China.
E-mail address: tomwu@126.com (X. Wu)

[1] Peng He and Jing Zhang contributed equally to this work.

Accepted 12 September 2022
Available online 21 September 2022

https://doi.org/10.1016/j.jinf.2022.09.012

Monkeypox outbreak in a correctional center in North Eastern Nigeria

Dear Editor,

Orviz et al.[1] report that Monkeypox in Spain is associated with person-to-person transmission and that infected individuals are more likely to have concomitant sexually transmitted infections, pointing to a potential sexual transmission. Monkeypox, is the most prevalent orthopoxvirus[2] since the eradication of smallpox and has long been reported from Africa, with outbreaks in Central and West Africa, corresponding to the Congo Basin and the West African clades (renamed clades 1 and 2, respectively).[3] Although infection in Africa is zoonotic, human-to-human transmission is the predominant route of transmission for outbreaks outside Africa,[4] with most infections occurring after meeting in conglomerate settings and close contact. Until recently, clusters outside Africa were associated with travel, notably in Europe and the Americas.[5] However, in the last decade numerous outbreaks outside the African continent do not have clear travel linkages and there is considerable debate on whether sexual behavior is a route of transmission or merely a marker of behavioral patterns. There has also been an increase of cases reported from Africa,[2] and Monkeypox reemerged in Nigeria in 2017.[6] The first case of Monkeypox in Adamawa State, in the Northeast, was only reported in January 2022 and human-to-human transmission is considered to be rare. Up to now, most cases are less than 40 years old, born after the cessation of the smallpox vaccination.[3] Here, we report the first outbreak of Monkeypox occurring in a prison in Nigeria, in which the predominant route of transmission seems to be person-to-person contact. To our knowledge, Monkeypox outbreaks have not been reported from prisons anywhere in the world (Fig. 1).

The outbreak

On the 2nd of March 2022, Adamawa State Ministry of Health was notified of inmates with rashes occurring in Yola prison and a joint rapid response team (RRT) from the State Field Office and the World Health Organization (WHO) initiated outbreak investigations. An initial head count identified 21 affected individuals under 40 years old. Some inmates had almost recovered at the time of examination, while others had just started to have symptoms, indicating the outbreak had lingered for several weeks before the investigation. The index case had a rash three months before the visit and cases had occurred over 18 weeks. Inmates were undernourished and untidy, had fever, rashes, body weaknesses and sometimes had collapsed. Rashes involved the face, head, neck, trunk, buttocks, the extremities (Fig. 2), and genitalia. All participants had enlarged inguinal and some cervical lymph nodes, which were firm, non-fluctuant and tender. Individuals with overt infections were isolated and inmates were monitored for signs and symptoms of infection. A visit 72 h later identified further seven cases and one further case was reported from the specialist hospital. Two of the five samples tested at the National Reference Laboratory were PCR-positive for monkeypox. Suspected cases were reported to Local and State Government authorities, NCDC and WHO.

Although Monekypox transmission in West Africa if considered a zoonotic infection occurring sporadically or in clusters, transmission in conglomerates is rarely documented and we have not found previous reports of outbreaks occurring in prison centers. It is surprising that outbreaks in prisons have not been reported, as the likelihood of transmission is high due to their crowded conditions, frequency of skin-to-skin contact and infestations with rodents.[7] A single case of human-to-human transmission was reported in Nigeria during the reemergence of Monkeypox in 2017.[6] However, this case did not lead to further cases. As a

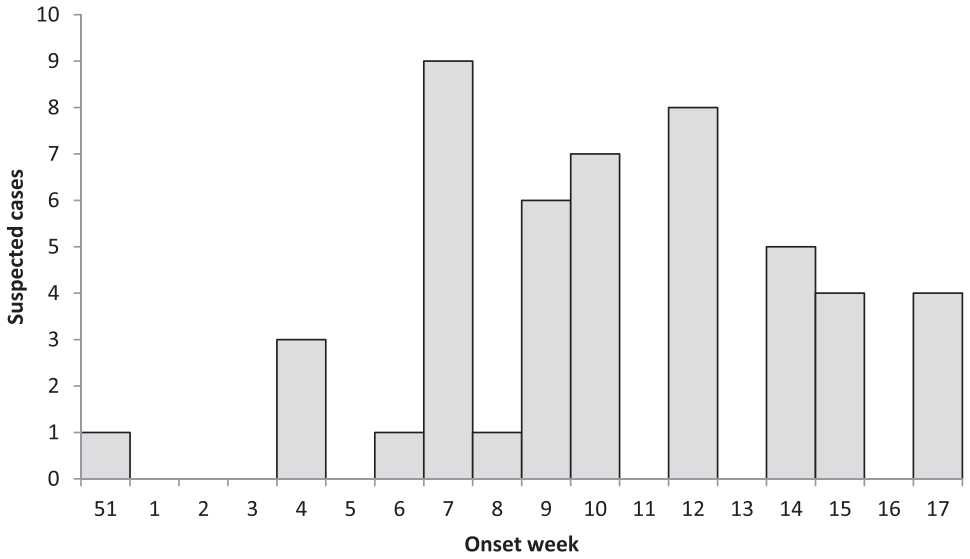

Fig. 1. Number of Monkey pox cases by symptom onset by epidemiologcal weeks (51 2021 to 17 2022).

Fig. 2. Monkeypox lesions among inmates.

reemerging infection in Nigeria, staff and inmates had low awareness of Monkeypox and were even unaware of its namesake, its mode of transmission and potential for human-to-human infection. Although prompt investigation, engagement of stakeholders and quality response can halt the spread of monkeypox in a closed system, the outbreak continued to spread due to sub-optimal adherence of the control measures proposed, administration bottlenecks and limited funding. Local partners were advised to suspend presential court sessions and delay transfers between prisons; the provision of individually named uniforms and bed linen, washing uniforms and bedding with disinfectants and the elimination of rodents. Ideally, at-risk prison health care workers should

have been vaccinated and provided with personal protective equipment.

Similar to Orviz et al.[1] report, most inmates in Yola lived under conditions that could facilitate human-to-human transmission, and potentially sexual transmission. However, the living conditions could also maintain zoonotic transmission and the actual route of infection remains conjectural, but difficult to identify while investigating the outbreak in a confined population with high contact intensity. It is now well established that the epidemiology of Monkeypox has changed in recent months, with more than 30,000 cases reported in the four months from May 2022, with cases reported in 82 countries, including countries which historically have not reported cases of the virus and more cases reported in countries that were not traditionally endemic. Although the outbreak reported here occurred in a West African endemic country, cases in Nigeria have also increased in since its re-emergence in 2017, and further studies are needed to document changes in its epidemiology in endemic countries.

About the authors

Emmanuel Pembi, Public Health expert, Adamawa State Ministry of Health and Human Services, Nigeria; Semeeh Omoleke participates in the Doctoral Programme in International Public Health, Euclid University, Central African Republic and is a member of the Field Presence, WHO, Nigeria; Hyelhara Paul works at the Public Health Laboratory, Specialist Hospital Yola, Adamawa state Ministry of Health in Nigeria. Theophilus Augustine works at the Yola North Correctional Centre and Luis E. Cuevas is Professor of International Health and Epidemiology at the Liverpool School of Tropical Medicine, UK.

Sources of funding

LEC is funded by the UK Medical Research Council Public Health Intervention Development (PHIND) (MR/W004313/1).

Authors' contributions

The study was conceived by EP and SO. The study design was developed by EP, SO, and LC. Data extraction was conducted by PE, TA and HP. Data analysis and interpretation were conducted by PE, SO and LC. The initial manuscript was prepared by PE, and SO. All authors, EP, SO, HP, TA and LC edited and approved the final manuscript.

Declaration of Competing Interest

The authors have no conflicts of interest to declare. The opinions expressed in this manuscript do not represent the views of the authors' affiliated institutions.

References

1. Orviz E., Negredo A., Ayerdi O., et al. Monkeypox outbreak in Madrid (Spain): clinical and virological aspects. *J Infect* 2022;**85**(4):412–17. doi:10.1016/j.jinf.2022.07.005.
2. Kabuga A.I., El Zowalaty M.E.. A review of the monkeypox virus and a recent outbreak of skin rash disease in Nigeria. *J Med Virol* 2019;**91**(4):533–40.
3. Ogoina D., Izibewule J.H., Ogunleye A., et al. The 2017 human monkeypox outbreak in Nigeria-report of outbreak experience and response in the Niger Delta University Teaching Hospital, Bayelsa State, Nigeria. *PLoS One* 2019;**14**(4):e0214229.
4. WHO. *Monkeypox. whoint/news-room/fact-sheets/detail/monkeypox 2022.*
5. Cohen J.. Global outbreak puts spotlight on neglected virus. *Science* 2022;**376**(6597):1032–3.
6. Yinka-Ogunleye A., Aruna O., Dalhat M., et al. Outbreak of human monkeypox in Nigeria in 2017-18: a clinical and epidemiological report. *Lancet Infect Dis* 2019;**19**(8):872–9.
7. CDC, Clinical Recognition, 2022, CDC https://www.cdcgov/poxvirus/monkeypox/clinicians/clinical-recognition.

Emmanuel Pembi
Department of Public Health, State Ministry of Health and Human Services, Yola, Adamawa, Nigeria

Semeeh Omoleke
Doctoral Programme in International Public Health, Euclid University, Central African Republic
Field Presence, World Health Organization, Nigeria

Hyelhara Paul
Public Health Laboratory, Specialist Hospital Yola, Adamawa state Ministry of Health, Adamawa, Nigeria

Theophilus Augustine
Yola North Correctional Centre, Adamawa, Nigeria

Luis E. Cuevas*
Department of Clinical Sciences, Liverpool School of Tropical Medicine, Pembroke Place, L3 5QA, UK

*Corresponding author.
E-mail address: Luis.Cuevas@lstmed.ac.uk (L.E. Cuevas)

Accepted 9 September 2022
Available online 15 September 2022

https://doi.org/10.1016/j.jinf.2022.09.010

Reduced T-cell response following a third dose of SARS-CoV-2 vaccine in infection-naïve people living with HIV

Dear Editor,

Hagiya and colleagues recently reported a poor humoral immune response towards third dose of SARS-CoV-2 mRNA vaccine in the older Japanese population.[1] This observation highlights that generalisation of results obtained from vaccine trials to specific subpopulations may be hazardous. People living with HIV (PLWH) represent another population poorly represented in large-scale vaccine trials. Despite the fact that PLWH are at higher risk of severe coronavirus disease 2019,[2] immunological data following vaccination in this population remain sparse.[3–6]

We prospectively evaluated humoral and T-cell immune responses before (T0) and after (T1) administration of a third dose of SARS-CoV-2 vaccine, either BNT162b2 or mRNA-1273, in PLWH followed-up at the University Hospital of Liège (Belgium) and in HIV-negative healthcare workers (HCWs). Biological analyses included quantification of anti-trimeric spike protein specific IgG (anti-S IgG), 50% neutralising antibody titres (NT_{50}) against wild-type (WT) and Omicron (BA.1/B.1.1.529) strains, and SARS-CoV-2-specific interferon-gamma (IFN-γ) release using the QuantiFERON SARS-CoV-2 assay which contains two different pools (Ag1 and Ag2) of spike-embedded peptides (Appendix p1-2). We compared immune parameters at both timepoints between PLWH and HCWs using linear regression models on $\log_{10}$-transformed variables. Evolution of the immune parameters was analysed using signed-rank test for paired observations. Results were contrasted according to participants' prior SARS-CoV-2 infection. All models were adjusted

Table 1
Background characteristics of PLWH and HCWs individuals at T0 and T1.

Variable	PLWH at T0 (n=119)	HCWs at T0 (n=79)	p-value	PLWH at T1 (n=80)	HCWs at T1 (n=51)	p-value
Male sex	59 (49.6)	13 (16.5)	<0.0001	43 (53.8)	11 (21.6)	0.0003
Age (Years)	45.2 ± 10.6	43.7 ± 11.5	0.36	45.6 ± 10.7	43.0 ± 10.0	0.18
18-29	6 (5.0)	7 (8.9)		4 (5.0)	2 (3.9)	
30-39	36 (30.2)	27 (34.2)		24 (30.0)	22 (43.1)	
40-49	36 (30.2)	19 (24.0)		21 (26.2)	13 (25.5)	
50-59	29 (24.4)	17 (21.5)		22 (27.5)	10 (19.6)	
≥60	12 (10.1)	9 (11.4)		9 (11.3)	4 (7.8)	
BMI (kg/m²)	28.0 ± 5.1	25.1 ± 6.2, n=76	0.0006	27.5 ± 5.6	25.9 ± 6.9, n=50	0.13
Underweight (<18.5)	0 (0.0)	2 (2.6)		0 (0.0)	2 (4.0)	
Normal range (18.5-24.9)	34 (28.6)	38 (50.0)		29 (36.2)	22 (44.0)	
Overweight (25-29.9)	50 (42.0)	24 (31.6)		34 (42.5)	17 (34.0)	
Obese (≥30)	35 (29.4)	12 (15.8)		17 (21.3)	9 (18.0)	
Ethnicity			-			-
Caucasian	45 (37.8)	-		34 (42.5)	-	
African	69 (58.0)	-		41 (51.3)	-	
Other	5 (4.2)	-		5 (6.2)	-	
Medical history						
Diabetes mellitus	8 (6.7)	3 (3.8)	0.53	5 (6.2)	1 (2.0)	0.40
Hypertension	32 (26.9)	14 (17.7)	0.13	18 (22.5)	7 (13.7)	0.21
Heart failure coronary artery disease	2 (1.7)	1 (1.3)	-	2 (2.5)	0 (0.0)	-
Stroke	2 (1.7)	0 (0.0)	-	1 (1.2)	0 (0.0)	-
Liver disease	1 (0.8)	0 (0.0)	-	1 (1.2)	0 (0.0)	-
Kidney disease	0 (0.0)	0 (0.0)	-	0 (0.0)	0 (0.0)	-
Chronic lung disease	1 (0.8)	0 (0.0)	-	1 (1.2)	0 (0.0)	-
Asthma	0 (0.0)	6 (7.6)	0.0036	0 (0.0)	3 (5.9)	0.0028
Autoimmune disease	1 (0.8)	4 (5.1)	0.083	0 (0.0)	2 (3.9)	-
Hematological cancer	0 (0.0)	4 (5.1)	-	0 (0.0)	1 (2.0)	-
Non hematological cancer	9 (7.6)	4 (5.1)	0.74	7 (8.8)	4 (7.8)	1.0
Solid-organ/cell transplantation	0 (0.0)	0 (0.0)	-	0 (0.0)	0 (0.0)	-
Immunosuppressive drugs			-			-
Corticosteroids	0 (0.0)	0 (0.0)		0 (0.0)	0 (0.0)	
Other	1 (0.8)	1 (1.3)		0 (0.0)	0 (0.0)	
Previous SARS-CoV-2 infection (before T0)						
Questionnaire	26 (21.9)	19 (24.0)	0.72	14 (17.5)	15 (29.4)	0.11
Positive anti-N antibody	50 (42.0)	13 (16.9), n=77	0.0002	30 (37.5)	10 (20.0), n=50	0.035
SARS-CoV-2 experienced*	55 (46.2)	21 (26.6)	0.0054	32 (40.0)	16 (31.4)	0.32
Previous SARS-CoV-2 infection (before T1)	-	-	-			
Questionnaire	-	-	-	15 (18.8)	18 (35.3)	0.033
Positive anti-N antibody	-	-	-	40 (50.0)	17 (34.0), n=50	0.074
SARS-CoV-2 experienced*	-	-	-	41 (51.2)	22 (43.1)	0.37
Experienced (between T0 and T1)	-	-	-	9 (11.2)	6 (11.7)	-
First vaccine dose			-			-
BNT162b2 mRNA (Pfizer)	101 (84.9)	79 (100.0)		69 (86.2)	51 (100.0)	
mRNA-1273 (Moderna)	8 (6.7)	0 (0.0)		4 (5.0)	0 (0.0)	
ChAdOx1-S (Astra Zeneca)	10 (8.4)	0 (0.0)		7 (8.8)	0 (0.0)	
Second vaccine dose			-			-
BNT162b2 mRNA (Pfizer)	100 (84.0)	79 (100.0)		69 (86.2)	51 (100.0)	
mRNA-1273 (Moderna)	9 (7.6)	0 (0.0)		4 (5.0)	0 (0.0)	
ChAdOx1-S (Astra Zeneca)	10 (8.4)	0 (0.0)		7 (8.8)	0 (0.0)	
Third vaccine dose			-			-
BNT162b2 mRNA (Pfizer)	-	-		42 (52.5)	51 (100.0)	
mRNA-1273 (Moderna)	-	-		38 (47.5)	0 (0.0)	
Time between first and second vaccine dose (weeks)	5.0 (4.0-5.0)	3.0 (3.0-3.1)	<0.0001	5.0 (4.4-5.0)	3.0 (3.0-3.1)	<0.0001
Time between second vaccine dose and sample at T0 (weeks)	25 (23-28)	24 (24-24)	0.025	25 (23-27)	24 (24-24)	0.014
Time between second and third vaccine dose (weeks)	-	-	-	27 (25-31)	38 (35-39)	<0.0001
Time between third vaccine dose and sample at T1 (weeks)	-	-	-	2.4 (3.1-3.9)	4.7 (4.0-8.0)	<0.0001
Time between T0 and T1 (weeks)	-	-	-	5 (4-6)	19 (18-19)	<0.0001
HIV infection			-			-
HIV-1	118 (99.2)	-		79 (98.8)	-	
HIV-2	1 (0.8)	-		1 (1.2)	-	
Prior AIDS diagnosis	45 (37.8)	-		27 (33.8)	-	
Time at T0 since HIV diagnosis (years)	11 (6-18)	-	-	11 (6.5-18)	-	-
<1	1 (0.8)	-		1 (1.2)	-	
1-5	27 (22.7)	-		17 (21.3)	-	
6-10	26 (21.9)	-		17 (21.3)	-	
>10	65 (54.6)	-		45 (56.2)	-	
Nadir CD4+T cell count per μL	259 (163-462)	-	-	292 (166-502)	-	-
<200	39 (32.8)	-		25 (31.2)	-	
≥200	80 (67.2)	-		55 (68.8)	-	
Last CD4+T cell count per μL (2021 or 2022)	680 (546-898)	-	-	743 (592-940)	-	-
<350	8 (6.7)	-		3 (3.7)	-	
350-499	17 (14.3)	-		11 (13.8)	-	
≥500	94 (79.0)	-		66 (82.5)	-	
CD4/CD8 ratio, n=117	1.03 ± 0.57	-	-	1.1 ± 0.57	-	-
<0.6	25 (21.4)	-		16 (20.0)	-	
0.6-1	40 (34.2)	-		26 (32.5)	-	
>1	52 (44.4)	-		38 (47.5)	-	
Last plasma viral load copies/mL	<20 (<20-<20)	-	-	<20 (<20-<20)	-	-
<50	112 (94.1)	-		75 (93.8)	-	
Time on ART (years)	10.7 ± 6.6	-		10.7 ± 6.9	-	

Results are expressed as n (%), mean ± SD, or Median (Q1-Q3) as appropriate and p-values of Chi-square or Fisher exact test, ANOVA, or Kruskal-Wallis test respectively.
* : Previous SARS-CoV-2 infection if 'Yes' at questionnaire or positive anti-nucleocapsid antibodies.

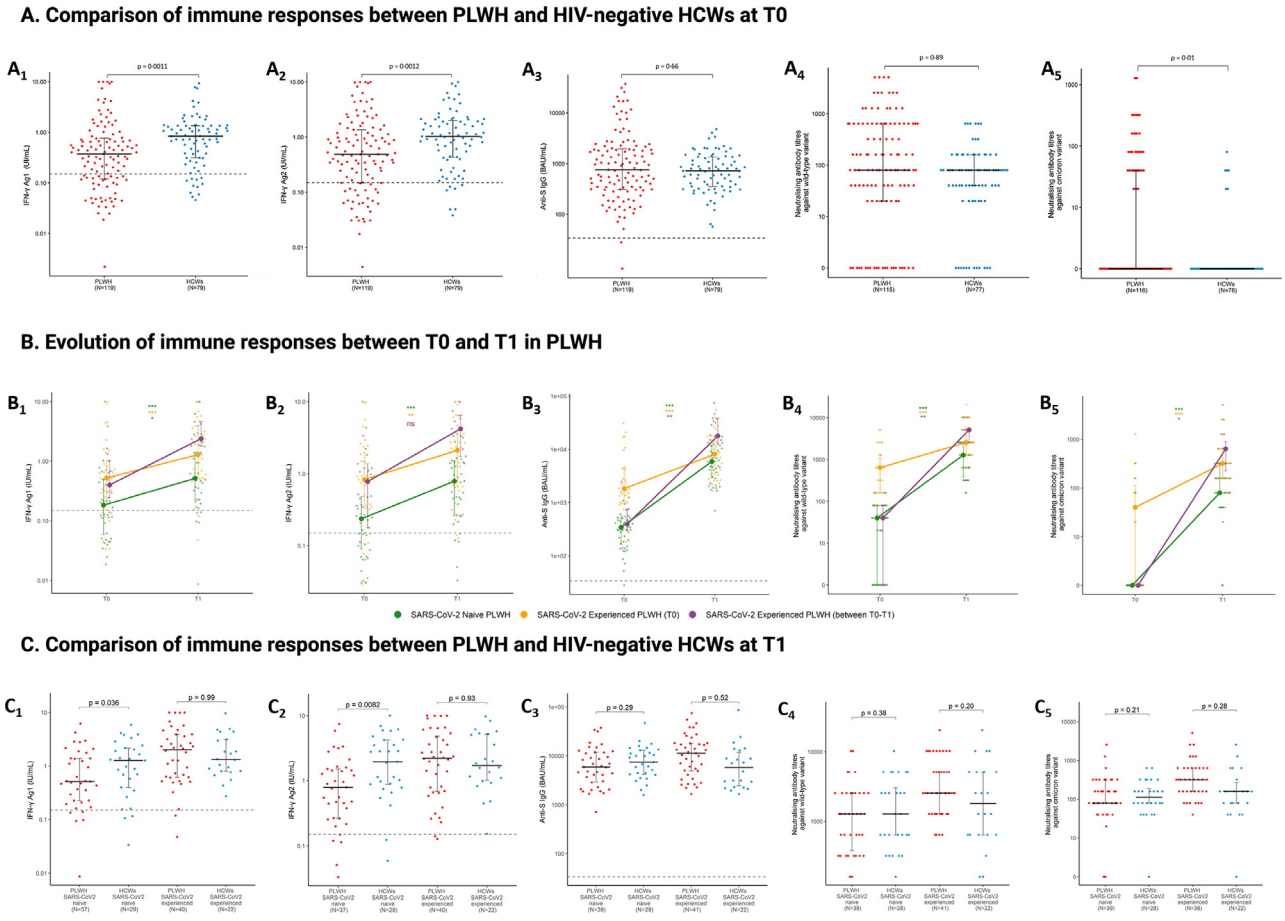

Fig. 1A. Comparison of cellular and humoral immune responses between people living with HIV and HIV-negative healthcare workers before administration of the third dose of SARS-CoV-2 mRNA vaccine (T0).
SARS-CoV-2-specific IFN-γ release for Ag1 (A_1), SARS-CoV-2-specific IFN-γ release for Ag2 (A_2), Anti-S IgG (A_3), neutralising antibody titres against Wild-type variant (A_4), and neutralising antibody titres against Omicron variant (A_5) were measured and compared between PLWH (n=119) and HCWs (n=79) who had received two doses of the SARS-CoV-2 vaccine. Dots represent subjects, whiskers represent median and IQR, and horizontal dashed line corresponds to the positivity cutoff (IFN-γ > 0.15 IU/mL and anti-S IgG $\geq$ 33.8 BAU/mL were considered positive). Statistics were calculated using adjusted linear regression models on log10-transformed variables. Exact number of participants in each group is indicated in Table S1.
Fig 1B. Evolution of cellular and humoral immune responses following the third dose of SARS-CoV-2 mRNA vaccine in SARS-CoV-2 naïve and experienced PLWH.
SARS-CoV-2-specific IFN-γ release for Ag1 (B_1), SARS-CoV-2-specific IFN-γ release for Ag2 (B_2), Anti-S IgG (B_3), neutralising antibody titres against Wild-type variant (B_4), and neutralising antibody titres against Omicron variant (B_5) were measured and compared before (T0) and after a third dose (T1) of the SARS-CoV-2 mRNA vaccine among PLWH (n=80), divided into 3 subgroups according to history of SARS-CoV-2 infection (naïve, experienced before T0, and experienced between T0 and T1). Dots represent subjects, whiskers represent median and IQR, and horizontal dashed line corresponds to the positivity cutoff (IFN-γ > 0.15 IU/mL and anti-S IgG $\geq$ 33.8 BAU/mL were considered positive). Statistics were calculated using linear regression models on log10-transformed variables. Exact number of participants for each group is indicated in Table S5.
Fig 1C. Comparison of cellular and humoral immune responses between people living with HIV and healthcare workers after administration of the third dose of SARS-CoV-2 mRNA vaccine (T1).
SARS-CoV-2-specific IFN-γ release for Ag1 (C_1), SARS-CoV-2-specific IFN-γ release for Ag2 (C_2), Anti-S IgG (C_3), neutralising antibody titres against Wild-type variant (C_4), and neutralising antibody titres against Omicron variant (C_5) were measured and compared between SARS-CoV-2 experienced and naïve PLWH (n=80) and HCWs (n=51) two to eight weeks after administration of a third dose of the SARS-CoV-2 mRNA vaccine. Dots represent subjects, whiskers represent median and IQR, and horizontal dashed line corresponds to the positivity cutoff (IFN-γ > 0.15 IU/mL and anti-S IgG $\geq$ 33.8 BAU/mL were considered positive). Statistics were calculated using adjusted linear regression models on log10-transformed variables. Exact number of participants for each group is indicated in Table S6.

for participants and process-related characteristics that had a significant univariate impact on at least one variable of interest (Appendix p2).

119 PLWH and 79 HCWs were enrolled in the study and constituted the study cohort for analysis at T0. Among them, 80 PLWH and 51 HCWs completed the whole study and constituted the study cohort for T1 (Fig. S1). Participants' characteristics are displayed in Table 1. 84% PLWH and all HCWs received BNT162b2 as first two doses of vaccine. For the third dose, all HCWs and 52.5% PLWH received BNT162b2 and the remaining 47.5% received mRNA-1273. All PLWH except one were infected with HIV-1, with a median time since diagnosis of 11 years. All were on antiretroviral therapy. Among PLWH initially included at T0, median $CD4^+$ T cell count was 680/μL (IQR 546-898) and 7 patients had a viral load over 50 copies/mL.

Overall, before the third vaccine dose (T0), SARS-Cov-2 specific IFN-ɣ production was significantly lower in PLWH than in HCWs ($p < 0.01$) (Fig. 1A, Table S1). In contrast, neutralising antibody titres (nAbTs) against Omicron were higher in PLWH ($p = 0.01$). Anti-S IgG levels and nAbTs against WT were similar between the two groups. Considering participants' history of SARS-CoV-2 infection, IFN-ɣ production was lower only among SARS-CoV-2 naïve PLWH ($p < 0.01$) (Table S1). Also, nAbTs against Omicron were increased only among SARS-CoV-2 experienced PLWH ($p < 0.01$). It is worth noting that sampling at T0 had been performed earlier for HCWs, before the emergence of Omicron, preventing our HIV-

negative population from being infected by this specific variant. Administration of a third dose of the SARS-CoV-2 vaccine elicited a significant increase in every parameter reflecting immune response among both HCWs and PLWH ($p < 0.001$) (Fig. 1B, Table S2). Evolution between T0 and T1 of any of the parameters was not significantly different between PLWH and HCWs. The proportion of PLWH with detectable Omicron nAbTs rose from 27.3% to 87.4% but median nAbT against Omicron remained 8-fold lower than median nAbT against WT ($p < 0.001$). Furthermore, nAbTs against Omicron and WT were both significantly lower among SARS-CoV-2 naïve PLWH compared to those previously infected ($p < 0.001$). After three doses of vaccine, we did not find a significant difference between PLWH and HCWs in any of the immune parameters investigated (Table S3). However, considering participants' history of SARS-CoV-2 infection, IFN-ɣ production was still lower among SARS-CoV-2 naïve PLWH compared to naïve HCWs ($p < 0.05$ and $p < 0.01$ for Ag1 and Ag2, respectively), whereas it was similar between SARS-CoV-2 experienced PLWH and HCWs (Fig. 1C, Table S3). Subgroups analyses found no significant difference between immune responses of HIV-infected individuals according to their $CD4^+$ T cell count or $CD4^+/CD8^+$ T cell ratio (Table S4, S5).

Factors impacting the magnitude of immune responses in PLWH are displayed in Appendix (Table S6to S10). Of interest, SARS-CoV-2 infection either before T0 ($p < 0.001$) or between T0 and T1 ($p < 0.05$) was associated with higher anti-S IgG titres and nAbTs against both variants after three doses. Among PLWH specifically, the magnitude of T-cell-mediated response elicited by the mRNA-1273 vaccine was more important than that elicited by BNT162b2 vaccine ($p < 0.01$).

Administration of a third dose of SARS-CoV-2 vaccine induced robust humoral and T-cell immune responses against SARS-CoV-2 in almost all participants. Humoral immune responses were similar between PLWH and HCWs, both before and after the third dose, which is in line with recently published data.[4,7] Although SARS-CoV-2 specific IFN-ɣ production increased after the third dose, it remained significantly lower among SARS-CoV-2 naïve PLWH compared to HCWs. Our data suggest that dysfunction of virus-specific T cell immunity, which is even found among HIV-positive patients with undetectable viral load, might lead to a suboptimal cell-mediated immune response following vaccination, especially in patients with no history of SARS-CoV-2 infection. In contrast, hybrid immunity conferred a similar T-cell immune response between PLWH and HIV-negative individuals. This observation could be attributed to the development of a distinct population of IFN-ɣ and IL-10-expressing memory SARS-CoV-2 spike-specific $CD4^+$ T cells following vaccination of previously infected individuals.[8]

Our results suggest that vaccine boosting enables broad neutralising immunity.[9] Indeed, the third dose elicited the production of anti-Omicron nAbTs in almost all participants. However, anti-Omicron nAbTs remained eight-fold lower compared to those against WT, which is in line with earlier reports and may reflect a less effective protection against this variant.[4,10]

In conclusion, a third dose of SARS-CoV-2 vaccine considerably enhanced SARS-CoV-2 specific humoral and cellular immunity in PLWH. Humoral immune responses were similar between PLWH and HIV-negative individuals. However, our data raise concerns about the vaccine's ability to induce protective T-cell immune response among PLWH with no history of SARS-CoV-2 infection. Further studies are needed to understand the clinical consequences of such observations and characterise the potential protective advantage of hybrid immunity in PLWH.

Fig. 1 was created using BioRender.com.

Funding

This work was supported by the Léon Fredericq Foundation (To GD and MM) and the FNRS (Fonds National de la Recherche Scientifique) (To SR, grant number PER/PGY H.P 030.20). M.E. and N.L. are FNRS doctoral clinical specialist candidates, AT is aspirant FNRS (PhD fellow), GD is an FNRS postdoctoral clinical master specialist and SR is an FNRS Senior Research Associate.

Role of the funder/sponsor

The funders had no role in study design, data collection and analysis, decision to publish, or preparation of the manuscript.

Ethic committee

Written informed consent was obtained from each participant and the study was approved by the Research Ethic Committee of the University Hospital of Liège (approval reference number: 2021-54).

Declaration of Competing Interest

All other authors declare no competing interests.

Acknowledgments

We thank the study participants for their voluntary contribution.

Supplementary materials

Supplementary material associated with this article can be found, in the online version, at doi:10.1016/j.jinf.2022.09.006.

References

1. Hagiya H., Hikita T., Habu T., Asada M., Yorifuji T., Toyooka S., et al. Poor vaccine responsiveness towards third-dose mRNA vaccine of COVID-19 in Japanese older people. *J Infect* 2022;**S0163-4453**(22):00413 -3. doi:10.1016/j.jinf.2022.07.007.
2. Boffito M., Waters L.. More evidence for worse COVID-19 outcomes in people with HIV. *Lancet HIV* 2021;**8**(11):e661–2. doi:10.1016/S2352-3018(21)00272-1.
3. Hassold N., Brichler S., Ouedraogo E., Leclerc D., Carroue S., Gater Y., et al. Impaired antibody response to COVID-19 vaccination in advanced HIV infection. *AIDS* 2022;**36**(4):F1–5. doi:10.1097/QAD.0000000000003166.
4. Lapointe H.R., Mwimanzi F., Cheung P.K., Sang Y., Yaseen F., Umviligihozo G., et al. People with HIV receiving suppressive antiretroviral therapy show typical antibody durability after dual COVID-19 vaccination, and strong third dose responses. *J Infect Dis* 2022:jiac229. doi:10.1093/infdis/jiac229.
5. Tau L., Turner D., Adler A., Marom R., Ahsanov S., Matus N., et al. SARS-CoV-2 humoral and cellular immune responses of patients with HIV after vaccination with BNT162b2 mRNA COVID-19 vaccine in the Tel-Aviv medical center. *Open Forum Infect Dis* 2022;**9**(4):ofac089 Published 2022 Feb 23. doi:10.1093/ofid/ofac0896.
6. Antinori A., Cicalini S., Meschi S., Bordoni V., Lorenzini P., Vergori A., et al. Humoral and cellular immune response elicited by mRNA vaccination against SARS-CoV-2 in people living with HIV (PLWH) receiving antiretroviral therapy (ART) according with current CD4 T-lymphocyte count [published online ahead of print, 2022 Apr 2]. *Clin Infect Dis* 2022:ciac238. doi:10.1093/cid/ciac238.
7. Brumme Z.L., Mwimanzi F., Lapointe H.R., Cheung P.K., Sang Y., Duncan M.C., et al. Humoral immune responses to COVID-19 vaccination in people living with HIV receiving suppressive antiretroviral therapy. *NPJ Vaccines* 2022;**7**:28. doi:10.1038/s41541-022-00452-6.
8. Rodda L.B., Morawski P.A., Pruner K.B., Fahning M.L., Howard C.A., Franko N., et al. Imprinted SARS-CoV-2-specific memory lymphocytes define hybrid immunity. *Cell* 2022;**185**(9):1588–601 e14.. doi:10.1016/j.cell.2022.03.018.
9. Evans J.P., Zeng C., Carlin C., Lozanski G., Saif L.J., Oltz E.M., et al. Neutralizing antibody responses elicited by SARS-CoV-2 mRNA vaccination wane over time and are boosted by breakthrough infection. *Sci Transl Med* 2022;**14**(637):eabn8057. doi:10.1126/scitranslmed.abn805710.
10. Ogbe A., Pace M., Bittaye M., Tipoe T., Adele S., Alagaratnam J., et al. Durability of ChAdOx1 nCoV-19 vaccination in people living with HIV. *JCI Insight* 2022;**7**(7):e157031. doi:10.1172/jci.insight.157031.

Majdouline El Moussaoui*[1]
Department of Infectious Diseases and General Internal Medicine, University Hospital of Liège, Avenue de l'Hôpital, 1, 4000 Liège, Belgium

Salomé Desmecht[1], Aleksandr Tashkeev
Laboratory of Animal Genomics, GIGA-Medical Genomics. GIGA-Institute, University of Liege, Belgium

Nicolas Lambert
Department of Neurology, University Hospital of Liège, Belgium

Nathalie Maes
Department of Biostatistics and Medico-Economic Information, University Hospital of Liège, Belgium

Joachim Braghini, Nicole Marechal, Céline Quintana, Karine Briquet
Department of Infectious Diseases and General Internal Medicine, University Hospital of Liège, Avenue de l'Hôpital, 1, 4000 Liège, Belgium

Stéphanie Gofflot
Department of Biothèque Hospitalo-Universitaire de Liège (BHUL), University Hospital of Liège, Belgium

Françoise Toussaint, Marie-Pierre Hayette
Department of Clinical Microbiology, University Hospital of Liège, Belgium

Pieter Vermeersch
Department of Laboratory Medicine, University Hospital of Leuven, Leuven, Belgium

Laurence Lutteri
Department of Clinical Chemistry, University Hospital of Liège, Belgium

Céline Grégoire
Department of Haematology, University Hospital of Liège, University of Liège, Belgium

Yves Beguin
Department of Biothèque Hospitalo-Universitaire de Liège (BHUL), University Hospital of Liège, Belgium
Department of Haematology, University Hospital of Liège, University of Liège, Belgium

Souad Rahmouni
Laboratory of Animal Genomics, GIGA-Medical Genomics. GIGA-Institute, University of Liege, Belgium

Michel Moutschen
Department of Infectious Diseases and General Internal Medicine, University Hospital of Liège, Avenue de l'Hôpital, 1, 4000 Liège, Belgium

Daniel Desmecht[1]
Department of Animal Pathology, Fundamental and Applied Research for Animals and Health, University of Liège, Liège 4000, Belgium

Gilles Darcis[1]
Department of Infectious Diseases and General Internal Medicine, University Hospital of Liège, Avenue de l'Hôpital, 1, 4000 Liège, Belgium

*Corresponding author.
E-mail address: melmoussaoui@chuliege.be (M.E. Moussaoui)

[1] These authors contributed equally to this work.

Accepted 5 September 2022
Available online 9 September 2022

https://doi.org/10.1016/j.jinf.2022.09.006

Repurposing antiviral drugs against the human monkeypox virus DNA-dependent RNA polymerase; *in silico* perspective

Dear Editor,

We read with great interest the paper that was recently published in this journal by Orvis et al.[1] regarding the emerging outbreak of human monkeypox in Madrid, Spain. According to the Centers for Disease Control and Prevention surveillance, the virus is reported in 99 countries and territories, with 47,652 confirmed cases (until August 26, 2022). The DNA-dependent RNA polymerase (DdRp) of poxvirus is a promising drug target for developing new chemotherapeutic antiviral drugs against DNA viruses. In this study, the DdRp of the HMV is modeled using its vaccinia virus as a homolog. After that, we repurposed 29 antiviral drugs on the equilibrated model (after a 100 ns molecular dynamics simulation run). The results revealed The effectiveness of the two antiviral drugs (Norov-29 and bemnifosbuvir) in binding the HMV DdRp active site with a comparable binding affinity (-24.26 ±4.43 and -21.32 ±6.43 kcal/mol) with the positive control, guanosine triphosphate (GTP) (-21.03 ±7.55 kcal/mol). These results need further experimental validation but promising as it was previously tested clinically in other viruses and had good pharmacological profiles. This may also pave the way for finding new circulating HMV inhibitors.

Modeling and simulation dynamics of DdRp

The model of HMV was built via SWISS-MODEL server[2] based on the solved structure of the Vaccinia virus elongation complex (PDB ID: 6RID). The predicted model has good quality as judged by MolProbity analysis.[3] Only 0.4% of residues (five) have phi or psi angles in the generously allowed region and no outliers in the Ramachandran plot. In HMV, the active site (D415, D417, and D419) was predicted in the Rpo147 chain at a β-turn between two helices.

The structure of the Apo DdRp was subjected to 100 ns molecular dynamics (MD) simulation[4] run aiming to equilibrate the system and visit the available conformations of the protein during this time domain.

Molecular docking

The molecular docking of analogs was performed by AutoDock Vina.[2] All active site residues (Asp415, Asp417, and Asp419) were treated as flexible. The search box was centered at the metal ion of the active site, and the box dimensions were set to 30 × 30 × 30 Å. In addition, the exhaustiveness was increased to 256 to account for the high torsions of the ligands.[5] The other parameters were accepted in their default values.

The average binding affinities of the nucleoside analogs against the active site of HMV DdRp ranged from −5.92 to −6.59 kcal/mol. The average scores of the top ten compounds (including the positive controls; ATP, CTP, GTP, and UTP) are depicted graphically in Fig. 1. As shown in Fig. 1; Valopicitabine, HCV-1, and Bemnifosbuvir are the best compounds with average binding affinity values of -6.58 ±0.01 kcal/mol. These three compounds show lower binding energies than the four positive controls. At the same time, HCV-2 and Norov-29 compounds show lower binding energies than ATP, GTP, and UTP (-6.51 ±0.01 kcal/mol). Finally, BMS-986094 shows lower binding energies than ATP and GTP (-6.48 ±0.08 kcal/mol).

The detailed interactions established upon docking are listed in Table 1. The primary interaction type between the compounds and the DdRp is the formation of hydrogen bonds (at least six H-bonds). Additionally, all these drugs establish at least one salt

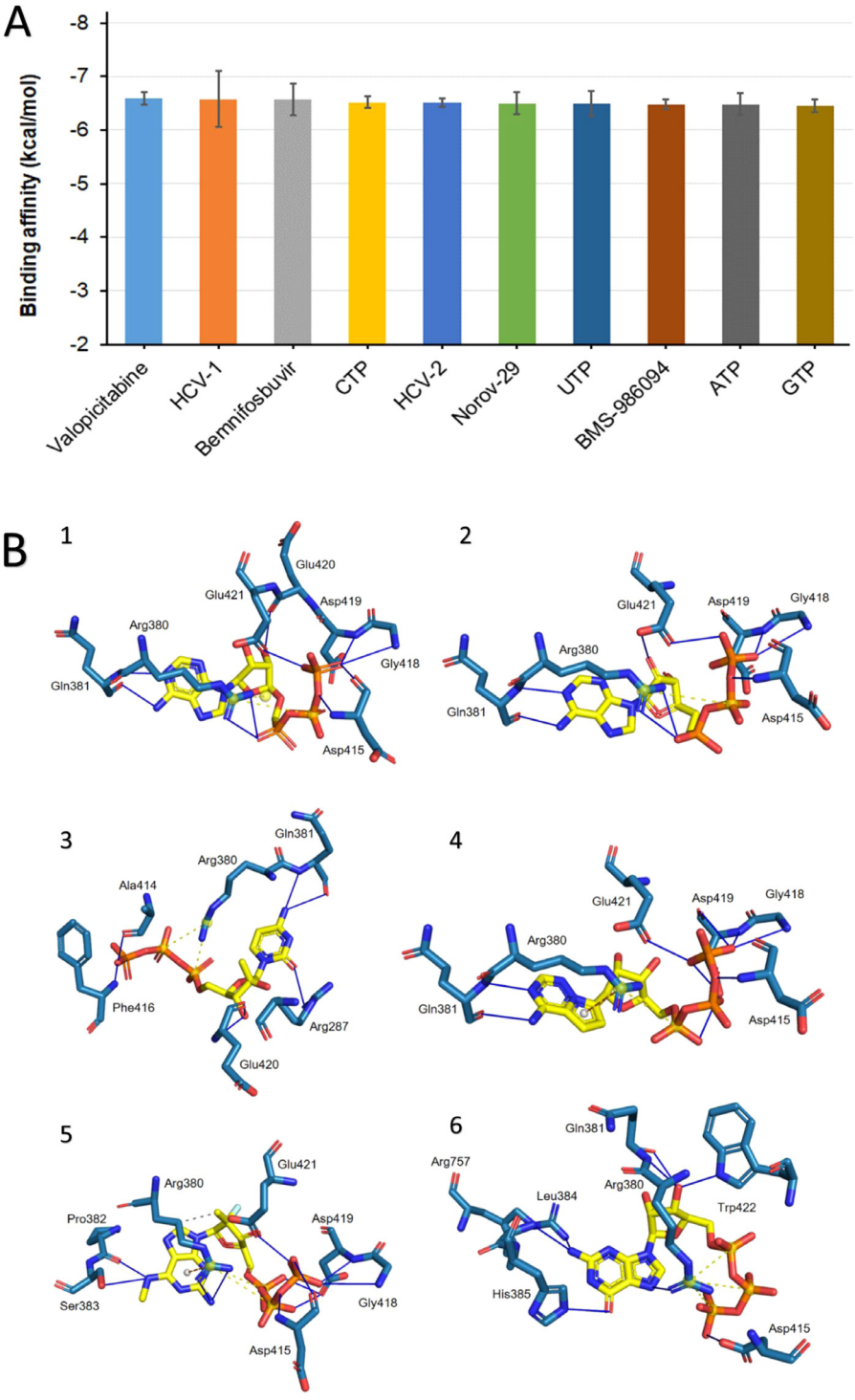

Fig. 1. (A) Average calculated binding energies of the top six drugs along with the physiological substrates (ribonucleotides; ATP, CTP, GTP, and UTP). Error bars represent the standard deviation of binding affinity (kcal/mol) of three clusters of representative protein conformations after MD simulation. (B) Established interactions after docking the top compounds against DdRp of HMV. (1) HCV-1, (2) HCV-2, (3) Valopicitabine, (4) Norov-29, (5) Bemnifosbuvir, and (6) GTP.

bridge interaction with R380. The active site residues (D415, D417, and D419) are bolded in Table 1 and are involved in H-bond formation in all the formed complexes except for the Valopicitabine-DdRp complex. The interactions are graphically rendered in Fig. 1B, where the formed interactions are depicted by blue lines (H-bonds) and dashed yellow lines (salt bridges). Cyan sticks show the interacting residues of the DdRp, whereas the other sticks are the ligands.

MD simulation of top analogs and binding free energy calculations

We performed another round of MD simulation for the best five hits (Valopicitabine, HCV-1, Bemnifosbuvir, HCV-2, and Norov-29) and the positive control GTP to study the protein dynamics upon ligand binding. We neglected the compounds BMS-986094 and Lumicitabine as their clinical trials were terminated for safety issues.[6,7]

Table 1
The established interactions upon docking the top six drugs and the physiological ribonucleotides (ATP, CTP, GTP, and UTP) against HMV DdRp after dynamics.

Compound (PubChem ID)	Hydrogen bonds		Hydrophobic interactions		Others	
	number	Residues	number	Residues	number	Residues
Valopicitabine (15940324)	7	R287, Q381, A414, F416, and E420	-	-	2	R380 [a]
HCV-1 (5276734)	11	R380, Q381, **D415**, G418, **D419**, E420, and E421	-	-	2	R380 [a]
Bemnifosbuvir (122527275)	13	R380, P382, S383, **D415**, G418, **D419**, and E421	1	R380	3	R380 [a,b]
CTP	7	R287, Q381, **D415**, E420, and W422	-	-	3	R287 [a] and R380 [a]
HCV-2 (11290467)	10	R380, Q381, **D415**, G418, **D419**, and E421	-	-	1	R380 [a]
Norov_29 (88571722)	9	Q381, **D415**, G418, **D419**, and E421	-	-	2	R380 [a,b]
UTP	6	R380, Q381, P382, **D415, D419**, and W422	-	-	3	R380 [a]
BMS-986094 (49862756)	7	P382, H385, **D419**, E420, W422, and R757	-	-	3	R287 [a], R380 [a]
ATP	9	R380, P382, S383, **D415, D417, D419**, E420, and E421	-	-	3	R380 [a,b]
GTP	8	R380, Q381, L384, H385, **D415**, W422, and R757	-	-	3	R380 [a]

[a] salt bridge and
[b] π-cations. Active site residues are in bold.

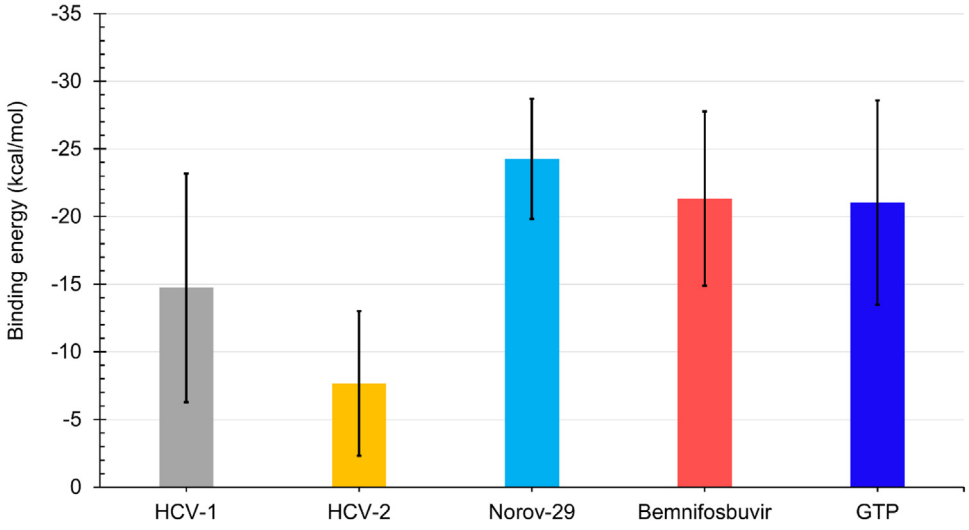

Fig. 2. The calculated MM/GBSA for the positive control (GTP) and the best four ligands (HCV-1, HCV-2, Norov-29, and bemnifosbuvir)-HMV DdRp.

Fig. 2 shows the calculated MM/GBSA of the top four complexes (HCV-1-DdRp, HCV-2-DdRp, Norov-29-DdRp, and bemnifosbuvir-DdRp) in addition to the GTP-DdRp complex. Norov-29 (sky blue) and bemnifosbuvir (red) are the best two compounds based on the MM/GBSA calculations in binding DdRp of HMV with values (-24.26 ±4.43 and -21.32 ±6.43 kcal/mol) near the positive control (GTP) (blue) (-21.03 ±7.55 kcal/mol). These two drugs may be potential anti-DdRp and are suggested further analyzed by *in vitro* and *in vivo* assays.

Conclusively, we report the effectiveness of anti-norovirus (Norov-29) and the anti-HCV and flaviviruses (Bemnifosbuvir) against HMV. Based on our docking results, dynamics simulation, and calculated binding energies, we suggest these two drugs against the DdRp of HMV. This could help in fighting against the current outbreak that spreading worldwide during the last few months.

Declaration of Competing Interest

We declare that there is no conflict of interest regarding this paper's work or publication.

Acknowledgments

We are thankful to Bibliotheca Alexandrina for providing access to their High-Performance Computing facility.

References

1. Eva O., Anabel N., Oskar A., Ana V., Ana M.G., Sara M., et al. Monkeypox outbreak in Madrid (Spain): clinical and virological aspects. *J Infect* 2022. doi:10.1016/J.JINF.2022.07.005.
2. Jerome E., Diogo S.M., Tillack Andreas F., Stefano F.. AutoDock Vina 1.2.0: new docking methods, expanded force field, and python bindings. *J Chem Inf Model* 2021;**61**(8):3891–8. doi:10.1021/acs.jcim.1c00203.
3. Davis Ian W., Andrew L.F., Chen Vincent B., Block Jeremy N., Kapral Gary J., Xueyi W., et al. MolProbity: all-atom contacts and structure validation for proteins and nucleic acids. *Nucleic Acids Res* 2007;**35**(suppl_2):W375–83. doi:10.1093/nar/gkm216.
4. James A.M., Teemu M., Roland S., Szilárd P., Smith Jeremy C., Berk H., et al. GROMACS: high performance molecular simulations through multi-level parallelism from laptops to supercomputers. *SoftwareX* 2015;**1–2**:19–25. doi:10.1016/j.softx.2015.06.001.
5. Xuan-Yu M., Hong-Xing Z., Mihaly M., Meng C.. Molecular docking: a powerful approach for structure-based drug discovery. *Curr Comput Aided Drug Des* 2012;**7**(2):146–57. doi:10.2174/157340911795677602.
6. Tariq A., Philip Y., Jeffrey S., Pockros Paul J., Jacob L., Mitchell S., et al. Cardiac dysfunction associated with a nucleotide polymerase inhibitor for treatment of hepatitis C. *Hepatology* 2015;**62**(2):409–16. doi:10.1002/HEP.27488.
7. ClinicalTrials.gov. Study to evaluate the antiviral activity, clinical outcomes, safety, tolerability, and pharmacokinetics of orally administered lumicitabine regimens in adult participants hospitalized with respiratory syncytial virus - study results - ClinicalTrials.gov. Available at https://clinicaltrials.gov/ct2/show/results/NCT02935673. Accessed September 10, 2022.

Jameel M. Abduljalil
Department of Biological Sciences, Faculty of Applied Sciences, Thamar University, Dhamar, Yemen

Department of Botany and Microbiology, Faculty of Science, Cairo University, Giza, Egypt

Abdo A. Elfiky*
Biophysics Department, Faculty of Science, Cairo University, Giza, Egypt

*Corresponding author.
E-mail address: dr_abdo@cu.edu.eg (A.A. Elfiky)

Accepted 2 September 2022
Available online 8 September 2022

https://doi.org/10.1016/j.jinf.2022.09.002

CRISPR-Cas12a-based detection of monkeypox virus

Dear Editor,

We read with interest the recently published research in *Journal of Infection* by Dr. Usman Ayub Awan et al., who emphasized that the remerging monkeypox is a new threat to the world [1]. Monkeypox has been declared a public health emergency of international concern by the World Health Organization (WHO) on 23 July 2022. Between 1 January and 25 August 2022, it has resulted in more than 46,700 laboratory confirmed cases of monkeypox and 12 deaths worldwide in 75 countries [2]. Public health authorities are proactively identifying cases and tracing their contacts to contain its spread. As with COVID-19, PCR is the current method capable of being deployed at sufficient speed to provide timely feedback on any public health interventions [3]. However, standard RT-qPCR methods that require laboratory-based testing instruments such as a thermal cycler for DNA amplification have constraints, including high cost, detection time, and the need for trained experts, limiting their application in point-of-care (POC) testing and resource-limited areas. Thus, the development of novel detection strategies for monkeypox is still urgent needed.

CRIPSR-based detection strategies have been widely used to detect of various viruses [4,5]. In this study, we report the development and initial validation of a CRIPSR-Cas12a-based assay for detection of monkeypox virus. We designed the system that detect the monkeypox viral DNA by using fluorescence readout. In the presence of the DNA target analyte, the G-quadruplex oligonucleotide (Table 1), which is labeled with 6-fluorescein (6-FAM)

Table 1
Oligonucleotides in this study.

Name	Sequences (5′→3′)
Fluorescently-labeled G-quadruplex oligonucleotides	
P4-WT	BHQ-GGGTTAGGGTTAGGGTTAGGG-FAM
CRISPR Cas12a gRNA sequences	
F3L-gRNA	TCACAATGAAATATTATGTT
N3R-gRNA	TAACGGCGACGAATATACTG

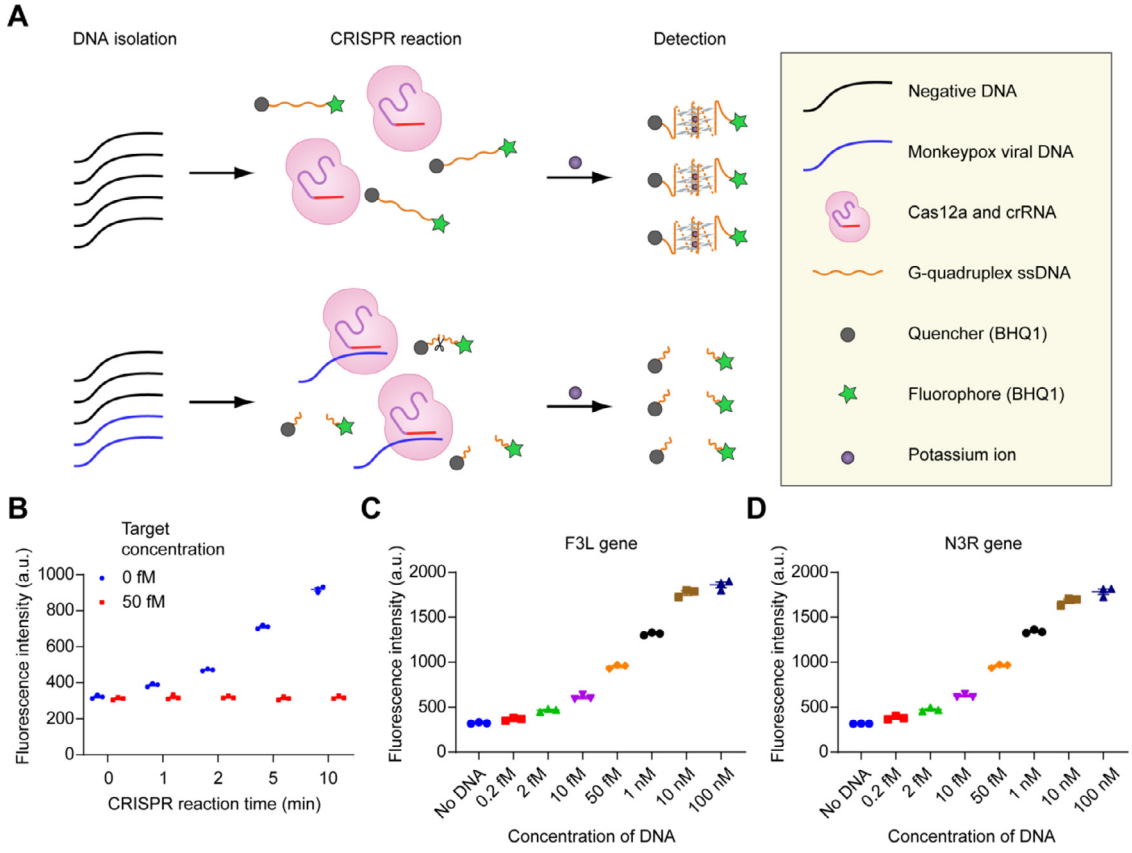

Fig. 1. The CRISPR-Cas12a-based system for detection of monkeypox virus. (A) Schematic of CRISPR-Cas12a-based system proposed in this study. (B) Fluorescence signal of CRISPR-Cas12a-based assay for target DNA saturates within 10 min. (C and D) The fluorescence intensity (λ_{em} = 520 nm) for the detection of the monkeypox viral F3L (C) and N3R (D) genes at various concentrations. The assay revealed a statistically significant detection of F3L and N3R DNAs, at a concentration as low as 2 fM ($^{**}P < 0.01$ vs. no RNA).

on the 3′-end and black hole-1 quencher (BHQ-1) on the 5′-end, gets degraded through Cas12a-mediated collateral cleavage resulting in fluorescent signal. While in the absence of the DNA target analyte, Cas12a cannot cleave the fluorescently-labeled G-quadruplex oligonucleotides and the oligonucleotides can formation G-quadruplex structures in 100 mM K^+condition, resulting in the fluorescence quenching (Fig. 1A). We found that the FAM fluorescent signal was detectable in 2 min and a strong signal was achieved within 10 min (Fig. 1B), suggesting the system is a potential rapid detection technology. In addition, we used the system to detect the F3L and N3R genes (Table 1). DNA samples of F3L and N3R genes in the same concentration range (from 0.2 fM to 100 nM) were subjected to the system, and the enhanced FAM fluorescence signal with monkeypox DNA was statistically significant ($P < 0.01$) at concentrations as low as 2 fM (Fig. 1C and 1D), indicating the high sensitivity of our system for monkeypox virus detection.

In summary, we develop a rapid, easy-to-implement and accurate CRISPR-Cas12a-based system for detection of monkeypox virus. Our CRISPR-based assay provides a visual and faster alternative to current PCR-based diagnosis for monkeypox virus.

Author contributions

J.Y.L. was the principal investigator who conceived and designed the study, obtained financial supports and approved the final version of the manuscript. Y.T.S. conducted the functional, mechanism and partial biophysical experiments, performed the statistical analyses, interpreted the results and drafted manuscript. Q.X. helped to conduct partial functional and mechanism experiments. M.S.L. and K.Y.Z. conducted data management. All the authors read and approved the final version of the manuscript.

Ethics approval and consent to participate

Not applicable.

Consent for publication

Not applicable.

Funding

Financial support was provided by the National Program of China (82073581).

Declaration of competing interest

The authors declare no conflict of interests.

Acknowledgments

Not applicable.

References

[1]. Li D., Liu Y., Li K., Zhang L.. Targeting F13 from monkeypox virus and variola virus by tecovirimat: molecular simulation analysis. *J. Infect.* 2022.
[2]. Alakunle E.F., Okeke M.I.. Monkeypox virus: a neglected zoonotic pathogen spreads globally. *Nat. rev. Microbiol.* 2022;**20**:507–8.
[3]. Huggett J.F., French D., O'Sullivan D.M., Moran-Gilad J., Zumla A.. Monkeypox: another test for PCR. Euro surveillance: bulletin Europeen sur les maladies transmissibles. *Eur. commun. dis. bull.* 2022:27.
[4]. Broughton J.P., Deng X., Yu G., et al. CRISPR-Cas12-based detection of SARS–CoV-2. *Nat. Biotechnol.* 2020;**38**:870–4.
[5]. Chen J.S., Ma E., Harrington L.B., et al. CRISPR-Cas12a target binding unleashes indiscriminate single-stranded DNase activity. *Science* 2018;**360**:436–9.

Yutong Sui[#]
Qi Xu[#]
Mingsheng Liu
Kuiyang Zuo
Xiaomei Liu[*]
Jinyu Liu[*]
Department of Toxicology, School of Public Health, Jilin University, Changchun, China
[*]Corresponding authors at: 1163 Xinmin Street.
E-mail addresses: liuxiaom@jlu.edu.cn (X. Liu), jy_liu@jlu.edu.cn (J. Liu)

[#] These authors contributed equally to this work.
Accepted 30 August 2022
Available online 7 September 2022

https://doi.org/10.1016/j.jinf.2022.08.043

The genomic epidemiology of *mcr*-positive *Salmonella enterica* in clinical patients from 2014 to 2017 in Sichuan, China and global epidemiological features

Dear Editor,

We read with interest the Wang et al. article in this journal describing the prevalence of *mcr* genes in 33, 205 *Salmonella enterica* isolated from England between 2014 and 2017.[1] This work highlights that *S. enterica* is an important carrier for *mcr* genes and majority of *S. enterica* were isolated from human-associated samples.[1] Recently, an international outbreak of multidrug-resistant (MDR) monophasic *S.* Typhimurium associated with chocolate products further indicated that *S. enterica* represent a serious public health hazard.[2,3] Meanwhile, the WHO has repeatedly advocated enhanced surveillance of *Salmonella* epidemics. In this study, we systematically studied the prevalence and genetic features of *mcr*-positive *S. enterica* identified from patients in Sichuan, China during 2014 to 2017 and the genomic characteristics of global *mcr-1*-positive *Salmonella*.

A total of 1046 *Salmonella* isolates were collected from patients from different hospitals from 2014 to 2017 in Sichuan, China. Among them, 12 *mcr*-positive (1.15%, 12/1046; ten *mcr-1* and two *mcr-3*) *S. enterica* isolates were detected using PCR (Table 1). Notably, all *mcr*-positive *S. enterica* isolates were isolated from children or infants. Antimicrobial susceptibility testing showed that the 12 *mcr*-positive *S. enterica* isolates were all resistant to colistin but sensitive to meropenem (Table S1). Complete genome sequences of the 12 isolates were successfully obtained by short-read and long-read sequencing platforms as our previous method.[4] The genomic features analysis revealed that ten isolates identified in 2016 and 2017 belonged to ST34 and the isolates SC2014107 and SC2014238 identified in 2014 were assigned as ST684 and ST463 respectively. The ten ST34 *S. enterica* isolates were serotyped as a monophasic variant of *S.* Typhimurium with the antigenic formula 4,[5],12:i:-. The serotype of isolates SC2014107 and SC2014238 were identified as *S.* Orion and *S.* Meleagridis (Table 1). Of note, ten *mcr*-positive *S. enterica* serovar 4,[5],12:i:- isolates were collected from different geographical locations of Sichuan province (Table 1), which indicated that the dominant *S. enterica* clones with serovar 4,[5],12:i:- had expanded throughout Sichuan since 2016.

IncHI2, IncX4, and IncI2 were common plasmid types carrying *mcr-1*, because they are self-transferable with high conjugation

Table 1
The basic information and genome information of *mcr*-positive *Salmonella* isolates investigated in this study.

Isolates	Geographical location	Collection data	Patient's age	Serovar	STs [a]	Chromosome and Plasmids	Accession number	Size (bp)	Plasmid replicon genes	Resistance Genes
SC2014107	Chengdu	2014.08.01	/	Orion	684	Chromosome	CP101365	4, 883, 488	/	/
						pSC2014107-mcr-62k	CP101366	62, 098	IncI2	*mcr-1.1*
SC2014238	Chengdu	2014.11.07	/	Meleagridis	463	Chromosome	CP101369	4, 920, 434	IncQ2	*fosA7.4*
						pSC2014238-90k	CP101371	90, 508	IncI1	$bla_{CTX-M-55}$
						pSC2014238-58k	CP101368	58, 878	IncR	*tet*(A), *qnrS1, dfrA12, aadA2, sul3*
						pSC2014238-mcr-33k	CP101370	33, 309	IncX4	*mcr-1.1*
SC2016025	Ya'an	2016.05.23	3 year	I 4,[5],12:i:-	34	Chromosome	CP101372	5, 245, 093	/	*aph(6)-Id, aph(3'')-Ib, sul2, tet*(B)
						PSC2016025-mcr-260k-c(chromosomally integrated plasmid)	CP101372	260, 012	IncHI2, IncHI2A, IncN	*mph(A), mcr-1.1, oqxB2, oqxA2, bleO, sul1, sul3, aadA1, cmlA1, aadA2, dfrA12, floR, sul2, aac(3)-IVa, fosA3,* $bla_{CTX-M-14}$
SC2016042	Chengdu	2016.06.12	1 year	I 4,[5],12:i:-	34	Chromosome	CP101373	4, 950, 959	/	bla_{TEM-1}, *aph(6)-Id, aph(3'')-Ib, sul2, tet*(B)
						pSC2016042-mcr-33k	CP101374	33, 309	IncX4	*mcr-1.1*
SC2016090	Chengdu	2016.07.15	4 month	I 4,[5],12:i:-	34	Chromosome	CP101375	5, 247, 576	/	*aph(6)-Id, aph(3'')-Ib, sul2, tet*(B)
						PSC2016090-mcr-261k-c(chromosomally integrated plasmid)	CP101375	261, 355	IncHI2, IncHI2A, IncN	*sul3, aadA1, cmlA1, aadA2, dfrA12, floR, sul2, aac(3)-IVa, fosA3,* $bla_{CTX-M-14}$, *mph(A), mcr-1.1, oqxB2, oqxA2, bleO, sul1*
SC2016091	Chengdu	2016.07.15	2 year	I 4,[5],12:i:-	34	Chromosome	CP101376	4, 999, 651	/	*tet*(B), *sul2, aph(3'')-Ib, aph(6)-Id,* bla_{TEM-1}
						pSC2016091-mcr-116k	CP101376	116, 686	IncFII, IncFIB	$bla_{CTX-M-55}$, *qnrS1, mcr-3.1, aac(3)-IId*
						pSC2016091-5k	CP101377	5, 632	Col(Ye4449)	/
SC2016290	Ya'an	2016.11.01	1 year	I 4,[5],12:i:-	34	Chromosome	CP101379	4, 999, 786	/	*sul2, aph(3'')-Ib, aph(6)-Id,* bla_{TEM-1}
						pSC2016290-mcr-147k	CP101380	147, 496	IncA/C2	*floR, tet*(A), *aph(6)-Id, aph(3'')-Ib, sul2, catA2,* $bla_{CTX-M-55}$, bla_{TEM-1}, *mcr-3.1*
						pSC2016290-3k	CP101381	3, 136	/	/
SC2017030	Chengdu	2017.03.29	1 year	I 4,[5],12:i:-	34	Chromosome	CP101382	4, 958, 087	/	*tet*(B), *sul2, aph(3'')-Ib, aph(6)-Id,* bla_{TEM-1}
						pSC2017030-mcr-257k	CP101383	257, 067	IncHI2, IncHI2A	*mcr-1, tet*(A), *fosA3,* $bla_{CTX-M-14}$, *aac(3)-IVa, aph(4)-Ia, sul2, floR, aadA2, oqxB2, oqxA2, bleO, sul1, aph(3')-Ia, sul3, aadA1, cmlA1*
						pSC2017030-6k	CP101384	6, 647	ColRNAI	/
						pSC2017030-4k	CP101385	4, 677	ColRNAI	/
SC2017057	Neijiang	2017.05.21	1 year	I 4,[5],12:i:-	34	pSC2017057-mcr-33k	JANDZX000000000	33, 309	IncX4	*mcr-1.1*
						Other contigs	JANDZX000000000	5, 033, 015	IncHI2, IncHI2A, ColRNAI	*tet*(B), *sul1, arr-3, catB3,* bla_{OXA-1}, *aac(6')-Ib-D181Y, aac(3)-IVa, aph(4)-Ia*
SC2017100	Bazhong	2017.05.31	10 month	I 4,[5],12:i:-	34	Chromosome	CP101386	4, 973, 602	/	*tet*(B)
						pSC2017100-mcr-218k	CP101387	218, 090	IncHI2, IncHI2A	*mcr-1.1, fosA3,* $bla_{CTX-M-14}$, *sul1, bleO, oqxA2, oqxB2*
SC2017167	Suining	2017.07.13	1 year	I 4,[5],12:i:-	34	Chromosome	CP101388	5, 002, 315	/	*tet*(B), *sul2, aph(3'')-Ib, aph(6)-Id,* bla_{TEM-1}
						pSC2017167-mcr-256k	CP101389	256, 591	IncHI2, IncHI2A, IncN	*mcr-1.1, sul2, floR, mph(A), aac(3)-IVa, fosA3,* $bla_{CTX-M-14}$, *dfrA12, aadA2, cmlA1, aadA1, sul3, aph(3')-Ia, sul1, bleO, oqxA2, oqxB2*
SC2017297	Panzhihua	2017.07.13	/	I 4,[5],12:i:-	34	Chromosome	CP101389	4, 978, 290	/	*tet*(B)
						pSC2017297-mcr-249k	CP101391	249, 573	IncHI2, IncHI2A	*mcr-1.1,* $bla_{CTX-M-14}$, *fosA3, aac(3)-IVa, sul2, floR, aadA2, cmlA1, aadA1, sul3, aph(3')-Ia, sul1, bleO, oqxA2, oqxB2*

[a] STs indicate sequence types.

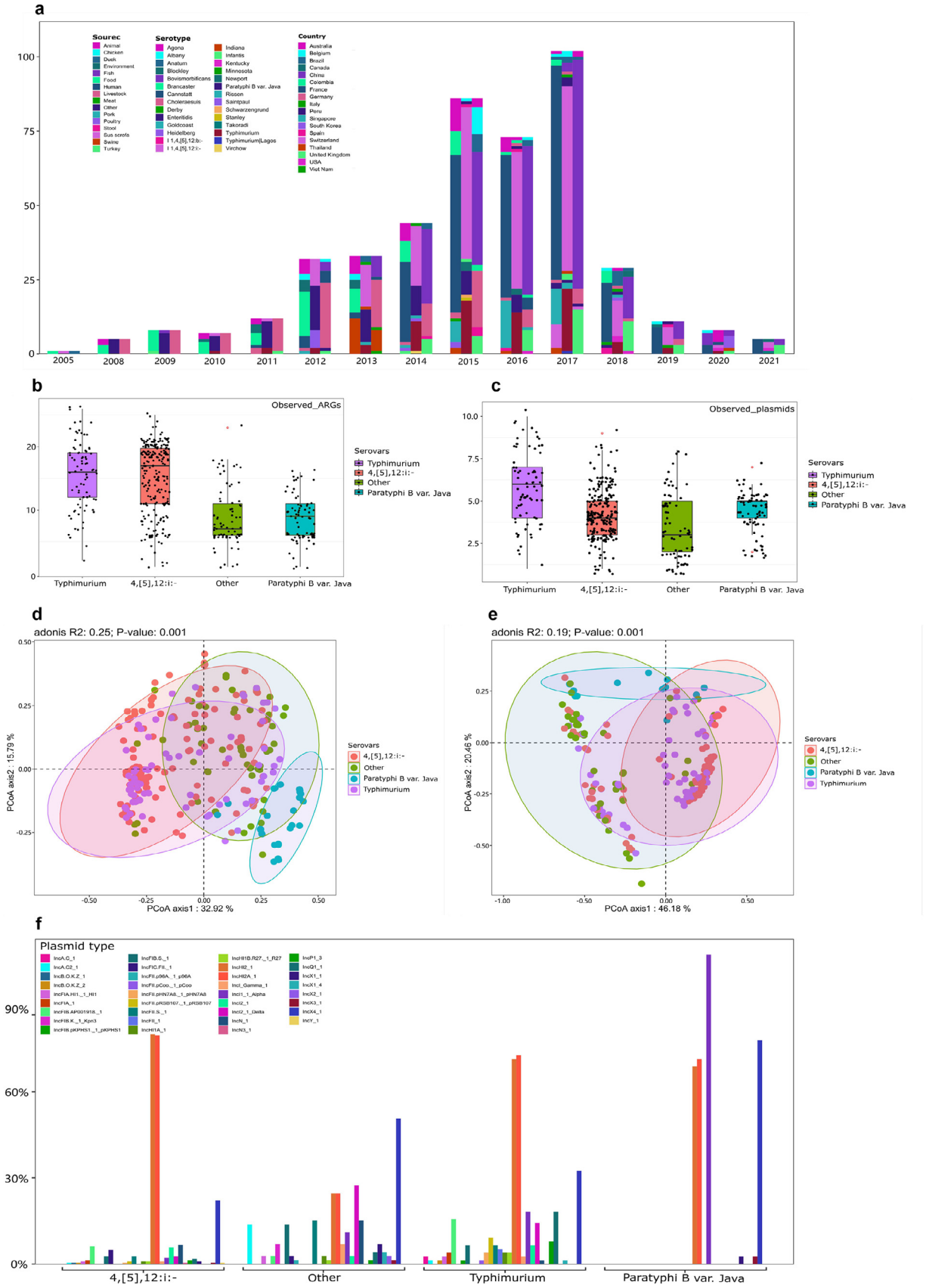

Fig. 1. The distribution of *mcr-1*-positive *Salmonella* isolates identified in different years and the ARGs and plasmids distribution features in *mcr-1*-positive *S. enterica* isolates. a) The ordinate indicates the number of isolates, the abscissa represents different years. The three bar charts from left to right represent the source, serotype and geographical location of *mcr-1*-positive *Salmonella* isolates, respectively. b) The number of ARGs in different serovars of *S. enterica* isolates. c) The number of plasmid replicon genes in different serovars of *S. enterica* isolates. d) Principal component analysis for resistance genes in different serovars of *Salmonella* isolates. e) Principal component analysis for plasmid types in different serovars of *Salmonella* isolates. f) The detection rate of different types of plasmids in different serovars of *Salmonella* isolates.

frequencies.[5,6,7] Whole genome sequencing showed that *mcr-1* in the ten *S. enterica* was mostly carried by IncHI2 plasmids, follow by IncX4 plasmids, and then IncI2 plasmid (Table 1). For the two *mcr-3*-harboring isolates, *mcr-3* was located on an IncA/C2 plasmid and an IncFIB plasmid, respectively (Table 1). According to the conjugation assay, the colistin resistance phenotype of the 12 *S. enterica* isolates could be transferred into *E. coli* C600. In addition, antimicrobial susceptibility testing showed that majority of transconjugants displayed resistance to other antimicrobials (Table S1). Further analysis found that most antimicrobial resistance genes (ARGs) in the *S. enterica* isolates were carried by conjugative plasmids.

In order to explore the epidemiological features of global *mcr-1*-positive *S. enterica* isolates, a total of 456 *mcr-1.1*-positive *S. enterica* isolates were downloaded from NCBI Pathogen database for further analysis (as of 2022.06.05) (Table S2). We found that *S.* paratyphi B var. Java was the predominant clone in 2008-2012 globally. Since 2013, the predominant clone has been replaced by *S.* 4,[5],12:i:-. The *mcr-1*-positive *S. enterica* was initially prevalent in Europe and then replaced by China, but this may be influenced by sampling bias. Further, most of *mcr-1*-positive *S. enterica* isolates were isolated from humans (244/456, 53.5%), which indicated that they have served as an important pathogen for humans (Fig. 1a). On the positive side, we found that *mcr-1*-positive *S. enterica* isolates were on the decrease since 2018, which might be the result of the withdrawal of colistin as an animal feed additive in many countries around the world.[8,9] Subsequently, we analyzed the distribution of ARGs and plasmid replicon genes in *mcr-1*-positive *S. enterica* isolates. The results showed that *S.* 4,[5],12:i:- and *S.* Typhimurium usually carry more ARGs compared with *S.* Paratyphi B var. Java and other *S. enterica* serovars (Fig. 1b). The number of plasmid replicon genes in different *S. enterica* serovars have no discernible difference (Fig. 1c). Principal coordinates analysis (PCoA) showed that the distribution of ARGs in *mcr-1*-positive *S.* 4,[5],12:i:- and *S.* Typhimurium were similar, but showed different with *S.* Paratyphi B var. Java and other *S. enterica* serovars (Fig. 1d). Meanwhile, the distribution of plasmid replicons in these *S. enterica* isolates was similar with ARGs, indicating plasmid played an important role in the distribution of ARGs in different *S. enterica* serovars (Fig. 1e). We further analyzed the distribution of plasmids in different serovars of *S. enterica* isolates in detail. In comparison to isolates of *S.* paratyphi B var. Java, we found that plasmid replicons in *S.* 4,[5],12:i:-, *S.* Typhimurium, and other *S. enterica* serovars are more diverse. IncHI2/HI2A and IncX4 plasmids have a large proportion in these *mcr-1*-positive *S. enterica* isolates (Fig. 1f), indicating that they play an important role in the dissemination of *mcr-1* in *S. enterica*.

S. Typhimurium and *S.* 4,[5],12:i:- were predominated *mcr-1*-bearing *Salmonella* serovars. In order to investigate the relationships of *mcr-1*-positive *S.* Typhimurium and *S.* 4,[5],12:i:- isolates, a phylogenetic tree was constructed. According to the phylogenetic tree, we found the eight *mcr-1*-positive *S.* 4,[5],12:i:- isolates in this study were distributed in three different Chinese clades (Figure S1). For the global *mcr-1*-positive *S. enterica* isolates, isolates from the same geographical location are usually located in the same clade. Of note, many closely related isolates were isolated from both humans and food. This reminds us that foodborne *mcr-1*-positive *S. enterica* has the potential risk to spread to humans.

In summary, the *mcr* genes were at a low prevalence level in clinical *S. enterica* in Sichuan, China. IncHI2 and IncX4 plasmids play an important role in the dissemination of *mcr-1* among *S. enterica*. The distinction of resistance phenotype in different serovars of *S. enterica* was associated with plasmids. *S.* 4,[5],12:i:- is a predominant serotype for *mcr-1*-harboring *S. enterica*. Global surveillance of *mcr-1*-bearing *S.* 4,[5],12:i:- in different settings as the One Health approach should be performed to curb the potential risk caused by high-risk MDR clones.

Transparency declarations

None to declare.

Data availability

The genome sequences in this study were deposited into the National Center for Biotechnology information under BioProject PRJNA855361.

Declaration of Competing Interest

The authors declare that there are no conflicts of interest.

Acknowledgments

This work was supported by the Key Research and Development Program of Sichuan Province (Major Science and Technology Projects) (2022ZDZX0017) and the Priority Academic Program Development of Jiangsu Higher Education Institutions (PAPD).

Supplementary materials

Supplementary material associated with this article can be found, in the online version, at doi:10.1016/j.jinf.2022.08.042.

References

1. Wang Y., Li Z., Lyu N., Ma S., Liu F., Hu Y., et al. Comparative genomic analysis of mobile colistin resistance gene mcr-9 in Salmonella enterica. *J Infect* Apr 2021;**82**(4):e15–17 PubMed PMID: 33406393Epub 2021/01/07. doi:10.1016/j.jinf.2020.12.029.
2. Samarasekera U.. Salmonella Typhimurium outbreak linked to chocolate. *Lancet Infect Dis* Jul 2022;**22**(7):947 PubMed PMID: 35636448Epub 2022/06/01. doi:10.1016/S1473-3099(22)00351-6.
3. Larkin L., Pardos de la Gandara M., Hoban A., Pulford C., Jourdan-Da Silva N., Valk H., et al. Investigation of an international outbreak of multidrug-resistant monophasic Salmonella Typhimurium associated with chocolate products, EU/EEA and United Kingdom, February to April 2022. *Euro Surveill* Apr 2022;**27**(15) PubMed PMID: 35426359Pubmed Central PMCID: PMC9012091Epub 2022/04/16. doi:10.2807/1560-7917.ES.2022.27.15.2200314.
4. Li R., Xie M., Dong N., Lin D., Yang X., Wong M., et al. Efficient generation of complete sequences of MDR-encoding plasmids by rapid assembly of MinION barcoding sequencing data. *Gigascience* Mar 1 2018;**7**(3):1–9 PubMed PMID: 29325009Pubmed Central PMCID: PMC5848804Epub 2018/01/13. doi:10.1093/gigascience/gix132.
5. Lu X., Zeng M., Xu J., Zhou H., Gu B., Li Z., et al. Epidemiologic and genomic insights on mcr-1-harbouring Salmonella from diarrhoeal outpatients in Shanghai, China, 2006-2016. *EBioMedicine* Apr 2019;**42**:133–44 PubMed PMID: 30905850Pubmed Central PMCID: PMC6491383Epub 2019/03/25. doi:10.1016/j.ebiom.2019.03.006.
6. Lu X., Xiao X., Liu Y., Huang S., Li R., Wang Z.. Widespread prevalence of plasmid-mediated colistin resistance gene mcr-1 in escherichia coli from pere David's deer in China. *mSphere* Dec 23 2020;**5**(6) PubMed PMID: 33361130Pubmed Central PMCID: PMC7763555Epub 2020/12/29. doi:10.1128/mSphere.01221-20.
7. Vazquez X., Garcia V., Fernandez J., Bances M., Toro M., Ladero V., et al. Colistin resistance in monophasic isolates of Salmonella enterica ST34 Collected from meat-derived products in Spain, with or without CMY-2 co-production. *Front Microbiol* 2021;**12**:735364 PubMed PMID: 35069462Pubmed Central PMCID: PMC8770973Epub 2022/01/25. doi:10.3389/fmicb.2021.735364.
8. Wang Y., Xu C., Zhang R., Chen Y., Shen Y., Hu F., et al. Changes in colistin resistance and mcr-1 abundance in Escherichia coli of animal and human origins following the ban of colistin-positive additives in China: an epidemiological comparative study. *Lancet Infect Dis* Oct 2020;**20**(10):1161–71 PubMed PMID: 32505232Epub 2020/06/09. doi:10.1016/S1473-3099(20)30149-3.
9. Shen C., Zhong LL., Yang Y., Doi Y., Paterson D., Stoesser N., et al. Dynamics of mcr-1 prevalence and mcr-1-positive Escherichia coli after the cessation of colistin use as a feed additive for animals in China: a prospective cross-sectional and whole genome sequencing-based molecular epidemiological study. *Lancet Microbe* May 2020;**1**(1):e34–43 PubMed PMID: 35538907Epub 2020/05/01. doi:10.1016/S2666-5247(20)30005-7.

Ruichao Li[1], Kai Peng[1]
Jiangsu Co-Innovation Center for Prevention and Control of Important Animal Infectious Diseases and Zoonoses, College of Veterinary Medicine, Yangzhou University, Yangzhou, Jiangsu Province, PR China
Institute of Comparative Medicine, Yangzhou University, Yangzhou, Jiangsu Province, PR China

Weifeng Huang[1]
Center for Disease Control and Prevention of Sichuan Province, Chengdu, Sichuan Province, PR China

Xinran Sun
Jiangsu Co-Innovation Center for Prevention and Control of Important Animal Infectious Diseases and Zoonoses, College of Veterinary Medicine, Yangzhou University, Yangzhou, Jiangsu Province, PR China
Institute of Comparative Medicine, Yangzhou University, Yangzhou, Jiangsu Province, PR China

Yulan Huang, Gaopeng Lei, Hong Lv
Center for Disease Control and Prevention of Sichuan Province, Chengdu, Sichuan Province, PR China

Zhiqiang Wang*
Jiangsu Co-Innovation Center for Prevention and Control of Important Animal Infectious Diseases and Zoonoses, College of Veterinary Medicine, Yangzhou University, Yangzhou, Jiangsu Province, PR China
Institute of Comparative Medicine, Yangzhou University, Yangzhou, Jiangsu Province, PR China

Xiaorong Yang**
Center for Disease Control and Prevention of Sichuan Province, Chengdu, Sichuan Province, PR China

*Corresponding author at: Jiangsu Co-Innovation Center for Prevention and Control of Important Animal Infectious Diseases and Zoonoses, College of Veterinary Medicine, Yangzhou University, Yangzhou, Jiangsu Province, PR China**Corresponding author.
E-mail addresses: zqwang@yzu.edu.cn (Z. Wang), yangyangxr@163.com (X. Yang)

[1] These authors contributed equally to this work.
Accepted 29 August 2022
Available online 5 September 2022

https://doi.org/10.1016/j.jinf.2022.08.042

Post-vaccination SARS-CoV-2 antibody kinetics and protection duration against Omicron in elderly population

Dear Editor,

Coronavirus disease 2019 (COVID-19) caused by the SARS-CoV-2 is particularly severe in older individuals because of an impaired immune response.[1] The vaccines presently available are less efficacious in older individuals, because of the senescence of their immune systems.[2] A recent letter in Journal of Infection showed the need of a third vaccine dose due to a waning antibody response against new SARS-CoV-2 variants in healthy and immunocompromised individuals.[3] In this study, we analysed the protection against Omicron provided by the immune responses of nursing home residents (NHRs) and a population of healthcare workers (HCWs).

We measured the antibody responses of 106 older adults (> 65 years old) living in 3 French nursing homes and vaccinated with 3 doses of BNT162b, matched with 106 HCWs for sex, past COVID-19 infection and vaccination status. Blood samples were taken 3-6 weeks after their third vaccine dose (12 September 2021- 13 October 2021 for HCWs, 8 November 2021-04 January 2022 for NHRs) before the Omicron epidemic wave erupted in France. The median follow-up was 179 days (IQR: 171-182) for HCWs, and 195 days (IQR: 167-195) for NHRs. Anti-S and anti-N antibodies were measured with an electrochemiluminescent assay (Alinity, Abbott, Sligo, Ireland). Neutralizing antibody titers were assessed by end-point dilution using Vero cells (ATCC, CCL-81^{TM}) and clinical SARS-CoV-2 Omicron BA.1 and BA.2 strains.[5] Infections were detected using a nucleic-acid amplification method (Aptima^{TM}, Hologic, USA)[4] and SARS-CoV-2 RNA was sequenced using single-molecule real-time sequencing (Pacific Biosciences, USA).[6] This study was approved by the French Research Ethics Committee Est-III (COVID BioToul, ID-RCB 2020-A01292-37, ClinicalTrials.gov Identifier: NCT04385108).

The 106 NHRs (81 (76.4%) women, median age: 89 years (range: 56–103)) included 53 (50%) who had been infected before vaccination (positive SARS-CoV-2 RNA or anti-N antibodies). The median age of the 106 paired HCWs was 41 years (range: 21–61). The median BA.1 neutralizing antibody (NAb) titer of the previously-uninfected, vaccinated NHRs was higher (8, IQR: 8-24) than that of the uninfected, vaccinated HCWs (2, IQR: 2-4), $p<0.01$ Wilcoxon signed-rank test). Similarly, the median BA.1 NAb titer in the infected-vaccinated NHRs was higher (16, IQR: 16-32) than that of the matched HCWs (8, IQR: 4-16, $p=0.03$ Wilcoxon). The anti-Omicron BA.2 NAb titers of uninfected NHR (32, IQR: 8-32) and uninfected HCWs (16, IQR:8- 32, $p>0.05$, Wilcoxon signed-rank test) were not significantly different. In contrast, the anti-Omicron BA.2 NAb titers of infected-vaccinated NHRs (32, IQR: 16-64) were significantly higher than those of the infected-vaccinated HCWs (16, IQR: 16-32, $p=0.04$, Wilcoxon signed-rank test). NHRs with no prior SARS-CoV-2 infection had a median binding antibody (BAb) concentration of 1959 BAU/ml (IQR 863-4,364) one month after their third dose of vaccine, not significantly different from that of their matched HCWs (1593 BAU/ml, IQR: 1125–2698 ; $p>0.05$, Wilcoxon signed-rank test, Fig. 1A). The median BAb concentrations of the NHRs who had been infected with SARS-CoV-2 before vaccination were significantly higher (3533 BAU/ml, IQR: 2151–5391) than those of the NHRs who had not been infected (1959 BAU/ml, IQR 863–4364 ; $p=0.03$ Wilcoxon, Fig. 1B). This concentration was also higher than that of infected-vaccinated HCWs (1,931 BAU/ml, IQR: 1202–3558, $p=0.03$, Wilcoxon signed-rank test).

None of the 106 NHR given the third dose of vaccine developed an Omicron BA.1 infection, but 33 (31.1%) were infected with Omicron BA.2 at least 1 month after the booster injection. Their median BA.2 NAb titer one month after the third dose of vaccine was 12 (IQR: 8-32); it was 32 (IQR 8-64) for those who did not become infected after the booster injection. A BA.2 NAb titer below 8 provided 19.2% protection against Omicron BA.2, titers of 16 or 32 gave 85.3% protection and an NAb titer of 64 or more provided 95.6% protection. Similarly, NHRs who were infected with BA.2 SARS-CoV-2 after their third dose of vaccine had median BAb concentration of 1959 BAU/ml (IQR 863–3707); it was 3339 BAU/ml (IQR: 1714–5836 ; $p=0.03$; Wilcoxon rank test) in those who did not subsequently become infected. Most (90%) of the Omicron BA.2 infections occurred in NHRs who had BAb concentrations below 6209 BAU/ml. A BAb concentration below 1000 BAU/ml provided only 25% protection against Omicron BA.2 ; 1000–6000 BAU/ml

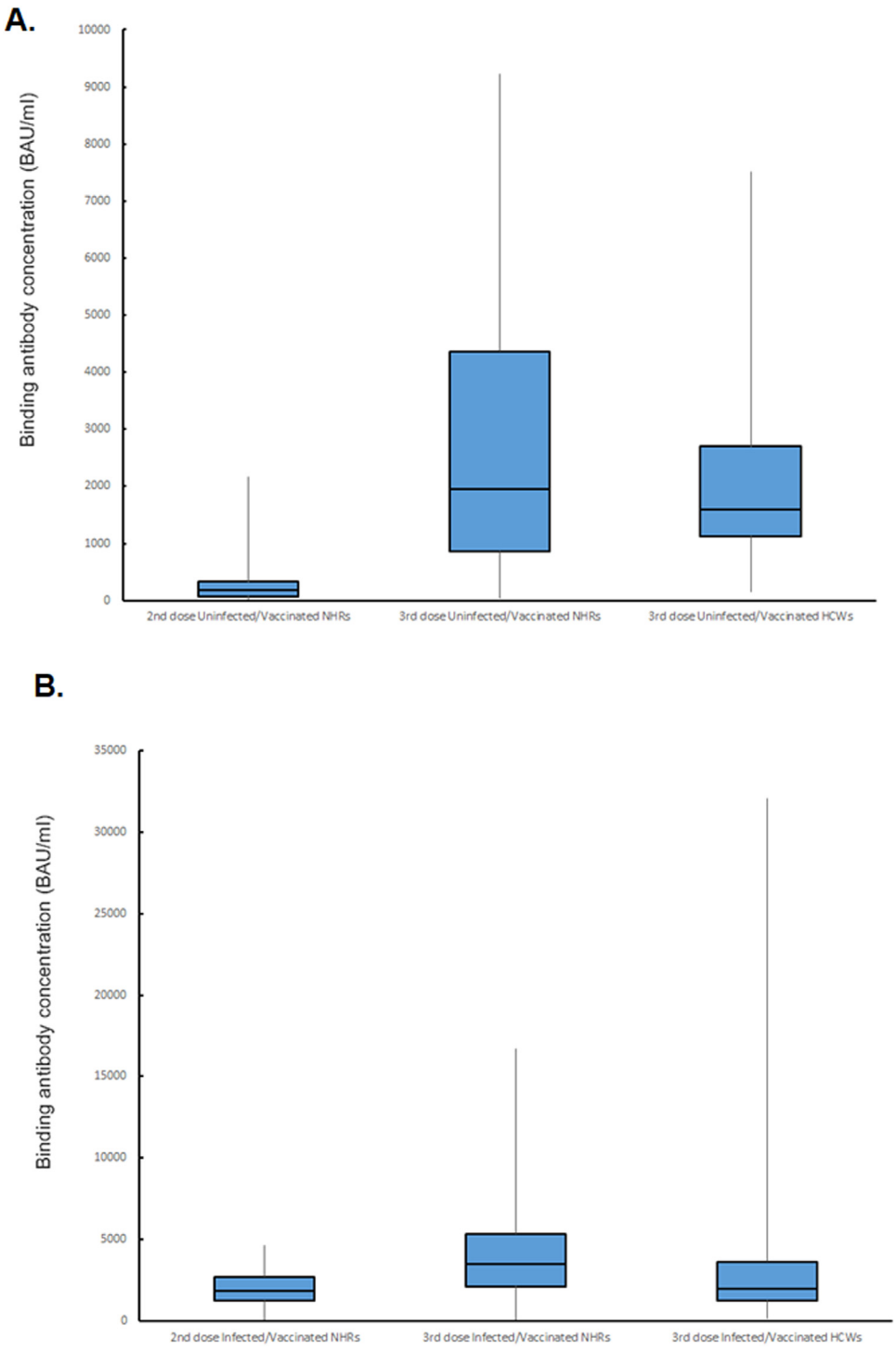

Fig. 1. A. Uninfected-Vaccinated NHRs and HCWs: binding antibody concentrations after 2/3 dose of vaccine. B. Infected-Vaccinated NHRs and HCWs: binding antibody concentrations after 2/3 dose of vaccine.

provided 77.9% protection; while >6000 provided 97.1% protection. Consequently, we set the average protection threshold against Omicron BA.2 at 5000 BAU/ml. The median BA.2 protection time for infected/vaccinated people with initial antibody concentrations > 10,000 BAU/ml was shorter in the NHRs (median 119 days, IQR: 61-223) than in the immunocompetent HCWs (189 days, IQR: 124–405, p <0.01, Wilcoxon signed rank test, Fig. 2 A&C). It was 48 days (IQR: 1-96) for uninfected-vaccinated HCWs and 30 days for uninfected-vaccinated NHRs (IQR: 0-40, p =0.13, Wilcoxon, signed rank test Fig. 2 B&D) whose total antibody concentrations were between 2000 BAU/ml and 10,000 BAU/ml one month after the third injection. There was no protection for the 89.2% of uninfected-vaccinated NHRs whose total antibody concentrations were below 2000 BAU/ml.

The 3-doses antibody responses against Omicron provided less protection than it did against the ancestral strain, although the anti-Omicron responses in NHRs after three doses were as good or better than those of younger adults. None of our NHRs acquired an Omicron BA.1 infection during follow-up, while 31.1% were infected with Omicron BA.2. The anti-BA.2 NAb concentra-

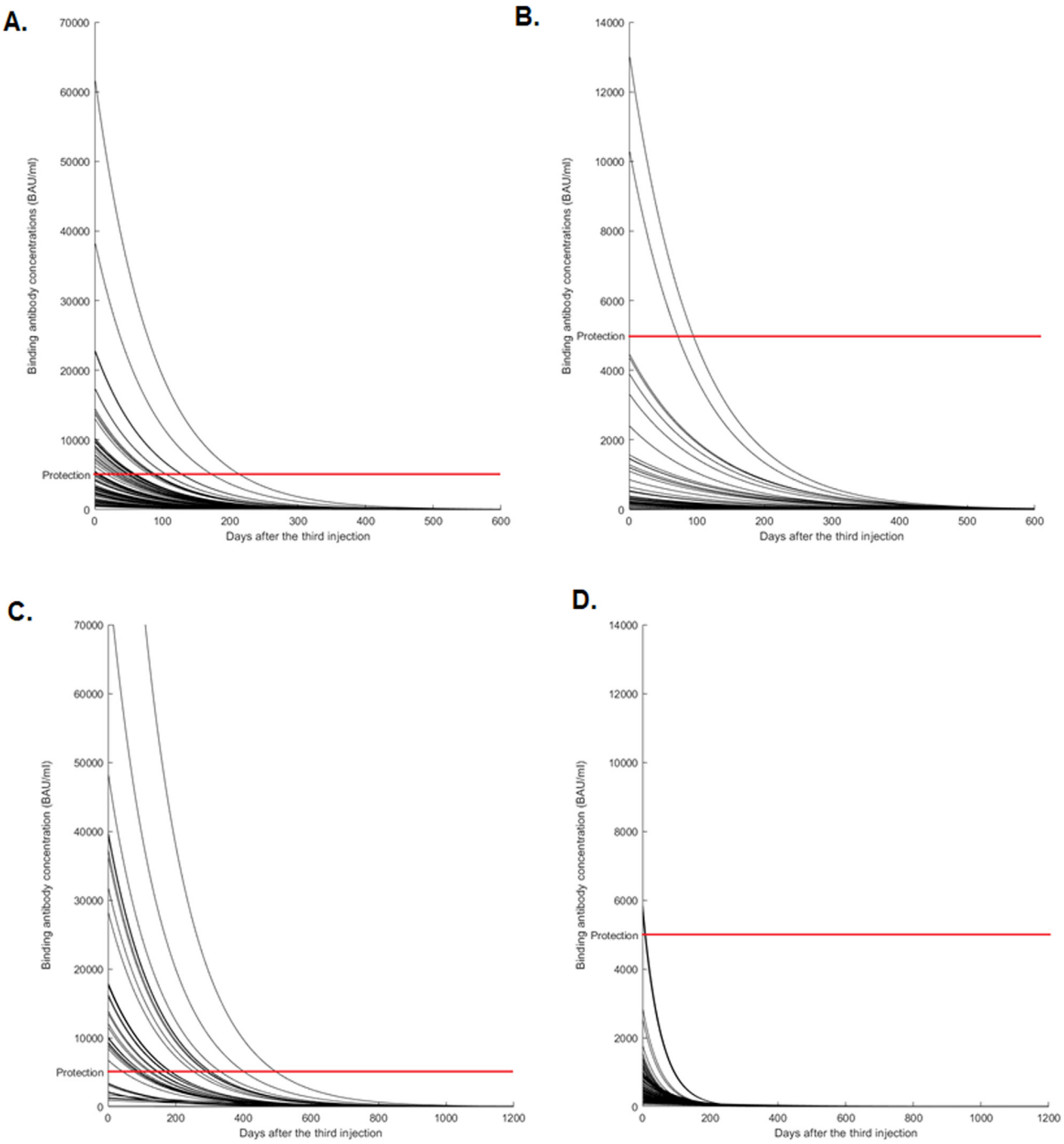

Fig. 2. Binding antibody kinetics after 3 doses of vaccine: A. Infected-vaccinated NHRs B. Uninfected-vaccinated NHRs. C. Infected-vaccinated HCWs. D. Uninfected-vaccinated HCWs.

tion providing at least 95.6% protection against Omicron BA.2 infection was 64 or higher. This is similar to that needed to protect younger populations against pre-Omicron strains.[7-8] The BAb concentration needed to protect against Omicron BA.2 was also high (about 5000 BAU/ml), the humoral responses of both uninfected-vaccinated HCWs and uninfected-vaccinated NHRs provided insufficient protection. These people could benefit from supplementary doses. On the other hand, the antibody protection decayed faster in NHRs than in HCWs, which may explain why NHRs were protected for a shorter time despite a high initial peak antibody concentration, in agreement with a previous report.[9]

Further studies on vaccination and protective immunity in the elderly should include other markers including T cells responses.

Funding

No specific funding

Declaration of Competing Interest

The authors declare no conflict of interest.

Acknowledgments

The English text was edited by Dr Owen Parkes.

References

1. Bartleson JM, Radenkovic D, Covarrubias AJ, Furman D, Winer DA, Verdin E.. SARS-CoV-2, COVID-19 and the ageing immune system. *Nat Aging* 2021;**1**(9):769–82. doi:10.1038/s43587-021-00114-7.
2. Collier DA, Ferreira IATM, Kotagiri P, Datir RP, Lim EY, Touizer E, et al. Age-related immune response heterogeneity to SARS-CoV-2 vaccine BNT162b2. *Nature* 2021;**596**(7872):417–22. doi:10.1038/s41586-021-03739-1.
3. Faustini S, Shields A, Banham G, Wall N, Al-Taei S, Tanner C, et al. Cross reactivity of spike glycoprotein induced antibody against Delta and Omicron variants before and after third SARS-CoV-2 vaccine dose in healthy and immunocompromised individuals. *J Infect* 2022;**84**(4):579–613. doi:10.1016/j.jinf.2022.01.002.
4. Trémeaux P, Lhomme S, Abravanel F, Raymond S, Mengelle C, Mansuy JM, et al. Evaluation of the Aptima™ transcription-mediated amplification assay (Hologic®) for detecting SARS-CoV-2 in clinical specimens. *J Clin Virol* 2020;**129**:104541. doi:10.1016/j.jcv.2020.104541.
5. Chapuy-Regaud S, Miédougé M, Abravanel F, Da Silva I, Porcheron M, Fillaux J, et al. Evaluation of three quantitative anti-SARS-CoV-2 antibody immunoassays. *Microbiol Spectr* 2021;**9**(3):e0137621. doi:10.1128/spectrum.01376-21.
6. Lhomme S, Latour J, Jeanne N, Trémeaux P, Ranger N, Migueres M, et al. Prediction of SARS-CoV-2 variant lineages using the S1-encoding region sequence obtained by pacbio single-molecule real-time sequencing. *Viruses* 2021;**13**(12):2544. doi:10.3390/v13122544.
7. Dimeglio C, Herin F, Martin-Blondel G, Miedougé M, Izopet J.. Antibody titers and protection against a SARS-CoV-2 infection. *J Infect* 2022;**84**(2):248–88. doi:10.1016/j.jinf.2021.09.013.
8. Dimeglio C, Herin F, Da-Silva I, Gernigon C, Porcheron M, Chapuy-Regaud S, et al. Decreased efficiency of neutralizing antibodies from previously infected or vaccinated individuals against the B.1.617.2 (Delta) SARS-CoV-2 variant. *Microbiol Spectr* 2022:e0270621. doi:10.1128/spectrum.02706-21.
9. Dan JM, Mateus J, Kato Y, Hastie KM, Yu ED, Faliti CE, et al. Immunological memory to SARS-CoV-2 assessed for up to 8 months after infection. *Science* 2021;**371**(6529) eabf4063. doi:10.1126/science.abf4063.

Chloé Dimeglio*, Pauline Trémeaux
CHU Toulouse, Hôpital Purpan, Virology Laboratory, 31300 Toulouse, France
INSERM UMR1291 – CNRS UMR5051, Toulouse Institute for Infectious and Inflammatory Diseases (INFINITy), 31300 Toulouse, France

Fabrice Herin
Occupational Diseases Department, Toulouse University Hospital, 31000 Toulouse, France
Inserm UMR 1295: Center for research in population health (CERPOP)- Department of Epidemiology and Public Health, Toulouse. University of Toulouse III F-31073, 37, allées Jules Guesde, 31073 Toulouse, France

Isabelle Da-Silva, Marion Porcheron
CHU Toulouse, Hôpital Purpan, Virology Laboratory, 31300 Toulouse, France

Guillaume Martin-Blondel
INSERM UMR1291 – CNRS UMR5051, Toulouse Institute for Infectious and Inflammatory Diseases (INFINITy), 31300 Toulouse, France
Infectious and Tropical Diseases Department, Toulouse University Hospital, 31300 Toulouse, France

Caroline Gernigon
Occupational Diseases Department, Toulouse University Hospital, 31000 Toulouse, France
Inserm UMR 1295: Center for research in population health (CERPOP)- Department of Epidemiology and Public Health, Toulouse. University of Toulouse III F-31073, 37, allées Jules Guesde, 31073 Toulouse, France

Sabine Chapuy-Regaud
CHU Toulouse, Hôpital Purpan, Virology Laboratory, 31300 Toulouse, France

Hélène Villars
Inserm UMR 1295: Center for research in population health (CERPOP)- Department of Epidemiology and Public Health, Toulouse. University of Toulouse III F-31073, 37, allées Jules Guesde, 31073 Toulouse, France
CHU Toulouse (Toulouse University Hospital) Geriatric Department, Hôpital Purpan Pavillon Leriche Place Baylac, 31300 Toulouse, France

Jacques Izopet
CHU Toulouse, Hôpital Purpan, Virology Laboratory, 31300 Toulouse, France
INSERM UMR1291 – CNRS UMR5051, Toulouse Institute for Infectious and Inflammatory Diseases (INFINITy), 31300 Toulouse, France

*Corresponding author at: 330 av de Grande Bretagne, 31052 Toulouse, France.
E-mail address: dimeglio.c@chu-toulouse.fr (C. Dimeglio)

Accepted 29 August 2022
Available online 3 September 2022

https://doi.org/10.1016/j.jinf.2022.08.040

Remdesivir reduced upper respiratory tract SARS-CoV-2 viral RNA concentration in COVID-19 patients who developed pneumonitis

Dear Editor,

We read with great interest the article by Yoon et al. describing the significant reduction of viable SARS-CoV-2 shedding with remdesivir treatment despite a non-significant reduction in viral load approximated by the cycle threshold value of real-time reverse-transcriptase polymerase chain reaction (RT-PCR).[1] Remdesivir was the earliest antiviral approved by the United States Food and Drug Administration of the treatment of COVID-19. Large scale clinical trials focused mainly on its clinical efficacy[2,3] and mortality.[3,4] Data on the effect of remdesivir on viral load changes is scanty and conflicting.[5–7] Here, we report an observational study on the effectiveness of remdesivir in reducing viral load a in real-world setting.

We performed a single-center prospective observational study between February 4, 2020 and February 22, 2021. Adult patients (age ≥18 years) admitted to Prince of Wales Hospital with laboratory confirmed COVID-19 and pneumonitis as documented by chest X-ray or computed tomography were identified. Patients with at least one respiratory sample collected during the early and late period of illness were included. We collected serial respiratory specimens including combined nasopharyngeal and throat swabs (NPSTS), combined nasopharyngeal aspirate and throat swabs (NPATS), nasopharyngeal swabs (NPS), and self-collected deep throat saliva (DTS) until discharge from hospital. Flocked swabs (FLOQSwabs, Copan, Italy) were used for nasopharyngeal and throat swabs collection. SARS-CoV-2 were detected using two separate RT-PCR platforms targeting different gene regions, and confirmed by the local reference laboratory.[8] The COVID-19 treatment strategy evolved over time and included the use of lopinavir, ribavirin, interferon-beta-1b, and remdesivir. For the purpose of analysis in this study, patients were classified into three different groups according to COVID-19 treatment regimens: (1) Remdesivir group who had received remdesivir as the only anti-COVID treatment, with a sub-group of early remdesivir treatment defined as remdesivir treatment started within 7 days after symptoms onset, (2) Other treatment group included those who had received lopinavir/ritonavir-based therapy, interferon-based therapy, or interferon-based therapy followed by remdesivir therapy, and;

Table 1
Patient characteristics.

	Overall (n = 208)	Remdesivir Group (n = 30)	Other treatment Group (n = 114)	No treatment Group (n = 64)	P value
Age, mean (SD) years	55.8 (16.0)	62.1 (13.3)	59.1 (14.9)	47.0 (15.6)	**<0.001**
Sex					**0.045**
Male	92 (44.2%)	12 (40.0%)	59 (51.8%)	21 (32.8%)	
Female	116 (55.8%)	18 (60.0%)	55 (48.2%)	43 (67.2%)	
Co-morbidities	140 (67.3%)	25 (83.3%)	83 (72.8%)	32 (50.0%)	**<0.001**
Received steroids treatment	66 (31.4%)	14 (46.7%)	50 (43.9%)	2 (3.1%)	<0.001
Log10 viral load on admission, mean (SD) in copies/ml	7.22 (2.17)	8.61 (1.55)	7.26 (2.07)	6.75 (2.40)	0.054
Severity					**<0.001***
Moderate	138 (66.3%)	14 (46.7%)	61 (53.5%)	63 (98.4%)	
Severe	38 (18.3%)	8 (26.7%)	29 (25.4%)	1 (1.6%)	
Critical	32 (15.4%)	8 (26.7%)	24 (21.1%)	0 (0.0%)	
Symptom					
Fever	136 (65.4%)	19 (63.3%)	88 (77.2%)	29 (45.3%)	**<0.001**
Cough	124 (59.6%)	24 (80.0%)	65 (57.0%)	25 (54.7%)	0.060
Sputum	64 (30.8%)	15 (50.0%)	32 (28.1%)	17 (26.6%)	0.055
Diarrhoea	46 (22.1%)	6 (20.0%)	26 (22.8%)	14 (21.9%)	0.940
Sore throat	45 (21.6%)	10 (33.3%)	20 (17.5%)	15 (23.4%)	0.162
Malaise	40 (19.2%)	5 (16.7%)	25 (21.9%)	10 (15.6%)	0.578
Shortness of breath	37 (17.8%)	10 (33.3%)	21 (18.4%)	6 (9.4%)	**0.021**
Myalgia	36 (17.3%)	8 (26.7%)	17 (14.9%)	11 (17.2%)	0.331
Runny nose	35 (16.8%)	4 (13.3%)	17 (14.9%)	14 (21.9%)	0.377
Headache	29 (13.9%)	4 (13.3%)	14 (12.2%)	11 (17.2%)	0.641*
Outcomes					0.261
Discharged	149 (71.6%)	21 (70.0%)	84 (73.7%)	44 (68.9%)	
Death	7 (3.4%)	1 (3.3%)	6 (5.3%)	0 (0.0%)	
Transferred to other hospital for convalescence care	52 (25.0%)	8 (26.7%)	24 (21.1%)	20 (31.2%)	
Sample collection time, mean (SD) days					
Days from admission to first sample collection	1 (1–3)	1 (1–2.75)	1 (1–2)	1 (1–3)	0.819
Days from onset to first sample collection	2 (5–8)	6 (4–8)	4.5 (2–7)	5.5 (3–8.25)	0.65
Days from admission to subsequent samples collection	9 (6–13)	9 (6–13)	9 (6–14)	8.5 (5–12)	0.253
Days from admission to last sample collection	13 (9–17)	13 (10–16.8)	13 (8–17)	12 (9–17)	0.826

Age and timing of sample collection were reported in the format of mean (SD). Hemoptysis (n = 1) and Vomiting (n = 7) were removed from the list because of too few samples. Timing of sample collection was reported in the format of median (IQR). P-values in bold indicate the significant difference among groups. chi-square test was used for proportional variables; ANOVA was used for age.

* Fisher exact test was used.

(3) No treatment group. Clinical severity was classified as mild (no pneumonitis), moderate (with pneumonitis), severe (required oxygen supplement), and critical (required mechanical ventilation) as previously described.[9] The longitudinal measurements of viral load were compared between treatment groups in a log scale. Univariate analyses were performed with chi-square test or fisher exact test for categorical variables as appropriate. Analysis of variance (ANOVA) was used for comparing the age between groups. *T*-test was used for comparing the change in viral load between treatment groups and adjusted with Benjamini-Hochberg procedure for multiple comparisons.

We recruited 208 patients, 30 (14.4%) received remdesivir alone, 17 of whom received remdesivir within 7 days after symptom onset, 114 (54.8%) received other treatments, and 64 (30.8%) had no specific therapeutic interventions. The mean (±standard deviation [SD]) age of the entire cohort was 55.8 (±16) years, and 92 (44.2%) were male. 138 (66.3%) had moderate, 38 (18.3%) had severe, and 32 (15.4%) had critical disease. Seven patients did not survive the hospital admission with one from remdesivir group, and six from other treatment group. For patients who had received remdesivir treatment, those with moderate severity received remdesivir earlier (mean 6.67, SD: 2.82 days) than those with severe (mean 9.52 SD: 2.96 days) and critical disease (mean 8.94: SD 4.37), respectively ($P < 0.001$ for both comparisons). The duration of remdesivir treatment was significantly longer in patients with critical disease (mean 6.4, SD 2.73 days) as compared to patients with moderate (mean 4.80, SD 2.32 days) and severe disease (mean 4.67, SD 1.85) ($P = 0.013$). A total of 849 samples collected from 208 patients, with a median of 4 (IQR: 2–5) samples from each patient (Fig. S1). The median collection time was 1 (IQR: 1–3) day from admission for baseline samples and 9 (IQR: 6–13) days from admission for follow up samples with no significant difference observed between treatment groups. The baseline viral load for the three treatment groups were not significantly different from each other (Table 1, Fig. 1A). The median log transformed viral load for early remdesivir group dropped from 6.77 copies/ml (IQR 6.28–8.59) at day 2–4, to 6.12 copies/ml (IQR 4.92–7.30) at day 5–7, and to 4.00 copies/ml (IQR 3.21–4.34) at day 8 onwards. We found a significant difference in viral load decrease in early remdesivir group as compared to patients who had received other treatment ($P = 0.029$), but not to patients with no treatment at day 8 onwards (Fig. 1A). A similar result was observed when using day from onset instead of day from admission, though differences were not statistically significant (Fig. 1B). Patients with moderate severity had a significantly faster decrease in viral load from baseline when compared to patients with severe disease ($P = 0.018$) and critical disease ($P = 0.039$) respectively at days 5–7 from admission. The difference remained significant from day 8 onwards for those with severe disease ($P = 0.003$) (Fig. S2).

In this single-center prospective observational study, we found patients receiving early remdesivir monotherapy had a faster reduction in viral load as compared to those receiving other treatment, suggesting remdesivir may be effective in reducing SARS-CoV-2 viral load in upper respiratory tract of COVID-19 patients when prescribed early in the disease course. There are however limitations in our study. Firstly, in this observational study, there could be treatment assignment bias. This is reflected by our findings that patients who received no treatment were younger, with less comorbidities, less presented with fever, and with less severe disease. However, the two groups received remdesivir or other

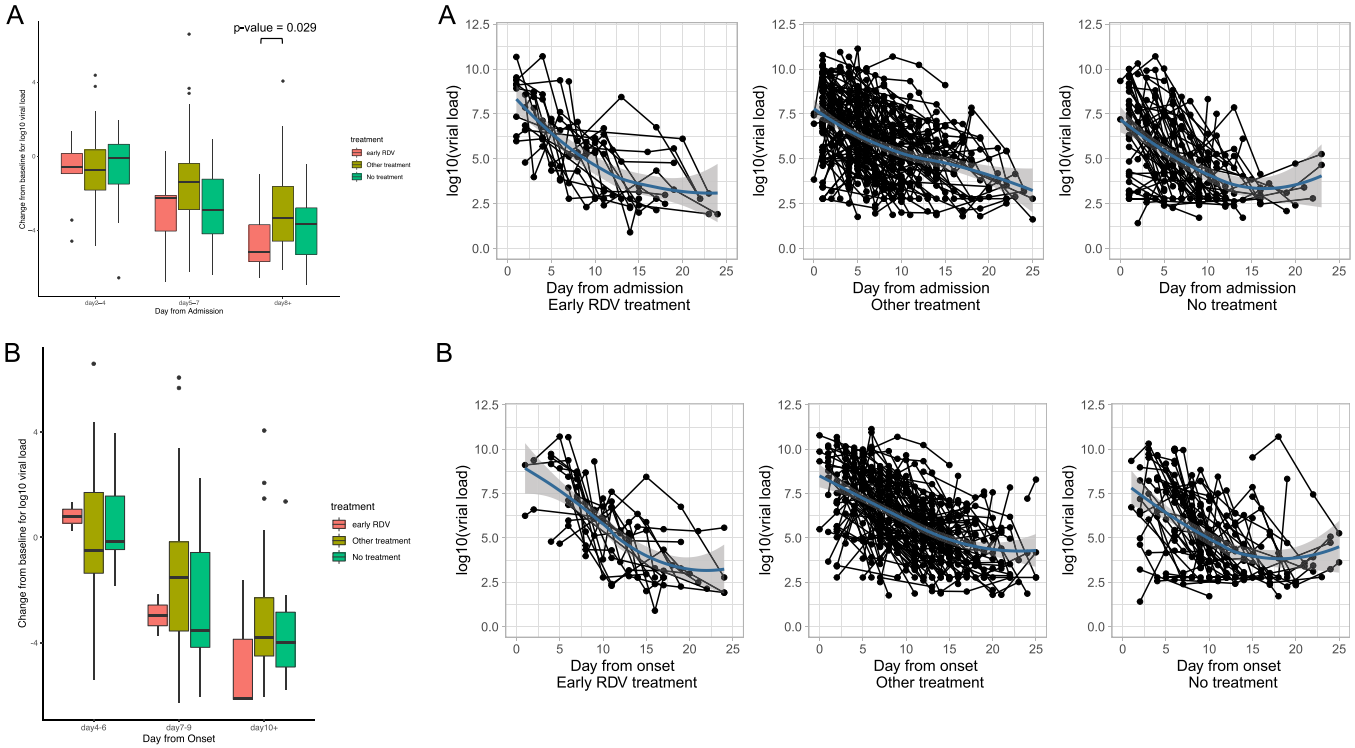

Fig. 1. Comparison of viral load response between treatment groups. (A) Comparison by treatment group and day from admission. Left panel: Box plot for change of log10 viral load (in copies/ml) from baseline to day 2–4, day 5–7, and day >7. *t*-test was used for comparing of the viral load change between early remdesivir group and other treatment group. Right panel: Change of log10 viral load (in copies/ml) over time. Each black dot represents a single sample. Early RDV, early remdesivir group. Other treatment, other treatment group. No treatment, no treatment group. (B) Comparison by treatment group and day from onset. Left panel: Box plot for change of log10 viral load (in copies/ml) from baseline to day 2–4, day 5–7, and day >7. Right panel: Change of log10 viral load (in copies/ml) over time. Each black dot represents a single sample. Early RDV, early remdesivir group. Other treatment, other treatment group. No treatment, no treatment group.

treatments were similar and did not differ significantly. Secondly, we could not use the length of hospital stay as a clinical end point, since during the first year of COVID-19 pandemic, hospitalization also served the purpose of isolation. Thirdly, the study spanned over 12-months and the treatment protocol evolved over time as more evidence emerged. In conclusion, we found early treatment with remdesivir for hospitalized patients could accelerate the decline in SARS-CoV-2 viral concentration in upper respiratory tract, supporting further investigations to maximize the clinical benefits of remdesivir administration.

Ethical statement

All patients provided a written consent, and the study was approved by The Joint Chinese University of Hong Kong – New Territories East Cluster Clinical Research Ethics Committee. (CREC Ref. No.: 2020.076).

Financial support

The study was supported by the Health and Medical Research Fund - Commissioned Research on the Novel Coronavirus Disease (COVID-19) (reference no. COVID190107 and COVID19F06) from the Food and Health Bureau, Hong Kong SAR Government.

Declaration of Competing Interest

All authors declare no conflict of interest.

Supplementary materials

Supplementary material associated with this article can be found, in the online version, at doi:10.1016/j.jinf.2022.08.031.

References

[1]. Yoon J.G., Yoo J.S., Lee J., Hyun H.J., Seong H., Noh J.Y., et al. Viable SARS-CoV-2 shedding under remdesivir and dexamethasone treatment. *J Infect* 2022;**84**(6):834–72 Jun. doi:10.1016/j.jinf.2022.03.022.

[2]. Beigel J.H., Tomashek K.M., Dodd L.E., Mehta A.K., Zingman B.S., Kalil A.C., et al. ACTT-1 study group members. remdesivir for the treatment of COVID-19 - final report. *N Engl J Med* 2020;**383**(19):1813–26 Nov 5. doi:10.1056/NEJMoa2007764.

[3]. Gottlieb R.L., Vaca C.E., Paredes R., Mera J., Webb B.J., Perez G., et al. GS-US-540-9012 (PINETREE) investigators. Early remdesivir to prevent progression to severe COVID-19 in outpatients. *N Engl J Med* 2022;**386**(4):305–15 Jan 27. doi:10.1056/NEJMoa2116846.

[4]. W.H.O. Solidarity Trial Consortium Remdesivir and three other drugs for hospitalised patients with COVID-19: final results of the WHO Solidarity randomised trial and updated meta-analyses. *Lancet* 2022;**399**(10339):1941–53 May 21. doi:10.1016/S0140-6736(22)00519-0.

[5]. Joo E.J., Ko J.H., Kim S.E., Kang S.J., Baek J.H., Heo E.Y., et al. Clinical and virologic effectiveness of remdesivir treatment for severe coronavirus disease 2019 (COVID-19) in Korea: a nationwide multicenter retrospective cohort study. *J Korean Med Sci* 2021;**36**(11):e83 Mar 22. doi:10.3346/jkms.2021.36.e83.

[6]. Goldberg E., Ben Zvi H., Sheena L., Sofer S., Krause I., Sklan E.H., et al. A real-life setting evaluation of the effect of remdesivir on viral load in COVID-19 patients admitted to a large tertiary centre in Israel. *Clin Microbiol Infect* 2021;**27**(6):917.e1–917.e4 Jun. doi:10.1016/j.cmi.2021.02.029.

[7]. Biancofiore A., Mirijello A., Puteo M.A., Di Viesti M.P., Labonia M., Copetti M., et al. CSS-COVID-19 Group. Remdesivir significantly reduces SARS-CoV-2 viral load on nasopharyngeal swabs in hospitalized patients with COVID-19: a retrospective case-control study. *J Med Virol* 2022;**94**(5):2284–9 May. doi:10.1002/jmv.27598.

[8]. Lui G., Ling L., Lai C.K., Tso E.Y., Fung K.S., Chan V., et al. Viral dynamics of SARS-CoV-2 across a spectrum of disease severity in COVID-19. *J Infect* 2020;**81**(2):318–56 Aug. doi:10.1016/j.jinf.2020.04.014.
[9]. Wu J., Liu J., Zhao X., Liu C., Wang W., Wang D., et al. Clinical characteristics of imported cases of coronavirus disease 2019 (COVID-19) in Jiangsu province: a multicenter descriptive study. *Clin Infect Dis* 2020;**71**(15):706–12 Jul 28. doi:10.1093/cid/ciaa199.

Christopher KC Lai[1]
Department of Microbiology, Faculty of Medicine, The Chinese University of Hong Kong, 1/F, Clinical Sciences Building, Prince of Wales Hospital, 30-32 Ngan Shing Street, N.T., Shatin, China Hong Kong Special Administrative Region

Grace CY Lui[1]
Department of Medicine and Therapeutics, Faculty of Medicine, The Chinese University of Hong Kong, China Hong Kong Special Administrative Region
Stanley Ho Centre for Emerging Infectious Diseases, The Chinese University of Hong Kong, China Hong Kong Special Administrative Region

Yuchen Wei[1], Ka Chun Chong
School of Public Health and Primary Care, Faculty of Medicine, The Chinese University of Hong Kong, China Hong Kong Special Administrative Region

Zigui Chen
Department of Microbiology, Faculty of Medicine, The Chinese University of Hong Kong, 1/F, Clinical Sciences Building, Prince of Wales Hospital, 30-32 Ngan Shing Street, N.T., Shatin, China Hong Kong Special Administrative Region

Lowell Ling
Department of Anaesthesia and Intensive Care, Faculty of Medicine of Medicine, The Chinese University of Hong Kong, China Hong Kong Special Administrative Region

Rita WY Ng, Siaw SS Boon, Wendy CS Ho, Apple CM Yeung
Department of Microbiology, Faculty of Medicine, The Chinese University of Hong Kong, 1/F, Clinical Sciences Building, Prince of Wales Hospital, 30-32 Ngan Shing Street, N.T., Shatin, China Hong Kong Special Administrative Region

David SC Hui
Department of Medicine and Therapeutics, Faculty of Medicine, The Chinese University of Hong Kong, China Hong Kong Special Administrative Region
Stanley Ho Centre for Emerging Infectious Diseases, The Chinese University of Hong Kong, China Hong Kong Special Administrative Region

Paul KS Chan*
Department of Microbiology, Faculty of Medicine, The Chinese University of Hong Kong, 1/F, Clinical Sciences Building, Prince of Wales Hospital, 30-32 Ngan Shing Street, N.T., Shatin, China Hong Kong Special Administrative Region
Stanley Ho Centre for Emerging Infectious Diseases, The Chinese University of Hong Kong, China Hong Kong Special Administrative Region

*Corresponding author at: Department of Microbiology, Faculty of Medicine, The Chinese University of Hong Kong, 1/F, Clinical Sciences Building, Prince of Wales Hospital, 30-32 Ngan Shing Street, N.T., Shatin, China Hong Kong Special Administrative Region.
E-mail address: paulkschan@cuhk.edu.hk (P.K. Chan)

[1] These author contributed equally to this work.
Accepted 25 August 2022
Available online 31 August 2022

https://doi.org/10.1016/j.jinf.2022.08.031